NOVA SCHOOL OF SCIENCE & TECHNOLOGY

DEPARTMENT OF CHEMISTRY

Daniel Ascenso Galrito

Bachelor in Applied Chemistry

# DEVELOPMENT OF QUINONE-BASED COMPOUNDS AND ZWITTERIONIC PYRIDINIUM PHENOLATES AS ORGANIC REDOX MEDIATORS

MASTER'S DEGREE IN BIOORGANIC CHEMISTRY

Universidade NOVA de Lisboa

August, 2023

DEPARTMENT OF CHEMISTRY

# DEVELOPMENT OF QUINONE-BASED COMPOUNDS AND ZWITTERIONIC PYRIDINIUM PHENOLATES AS ORGANIC REDOX MEDIATORS

**DANIEL ASCENSO GALRITO**

Bachelor in Applied Chemistry

**Advisor:** Paula Cristina de Sério Branco,
Associate Professor with Aggregation, Universidade NOVA de Lisboa

**Joint supervisor:** Hugo Gonçalo da Silva Cruz,
Researcher, Universidade NOVA de Lisboa

**Jury:**

**President:** João Montargil Aires de Sousa, Associate Professor with Habilitation, NOVA University Lisbon

**Arguer:** António Jorge Dias Parola, Full Professor, NOVA University Lisbon

MASTER'S DEGREE IN BIOORGANIC CHEMISTRY

Universidade NOVA de Lisboa
August, 2023

**Development of quinone-based compounds and zwitterionic pyridinium phenolates as organic redox mediators**

# ACKNOWLEDGEMENTS

I would first like to thank Professor Paula Branco and Dr. Hugo Cruz for accepting me under this project, and constantly guiding me through the difficulties that appeared during its development, and for introducing to the technique of cyclic voltammetry, vital for this work.

I also want to give a special thanks to Flávia Leitão, she helped me more than anyone else. I thank her for her help, patience and answering all my dumb questions.

Thanks to Professor Luís Branco for the assistance with certain reactions and procedures, and for the time to discuss various questions.

Also, to all the members of the labs. 202 and 205, for helping with any questions I had.

And finally, I want to thank my parents, who always supported me, for constantly encouraging and motivating me to continue studying and follow my interest in chemistry.

We thank FCT – Fundação para a Ciência e a Tecnologia I. P, this work was performed under the project PTDC/QUI-QOR/7450/2020 "Organic Redox Mediators for Energy Conversion", http://doi.org/10.54499/PTDC/QUI-QOR/7450/2020. This work was supported by the Associate Laboratory for Green Chemistry - LAQV financed by national funds from FCT/MCTES (UIDB/50006/2020 and UIDP/50006/2020). FCT/MCTES is also acknowledged for the National NMR Facility Network (ROTEIRO/0031/2013-PINFRA/22161/2016, co-financed by FEDER through COMPETE 2020, POCI, PORL, and FCT through PIDDAC).

# ABSTRACT

The need to decrease our dependency on fossil fuels requires alternative renewable energy sources, such as solar and wind energy. However, these energy sources have an intermittent nature that proves to be a challenge and reveals the importance of developing energy storage systems with higher efficiency.

Redox flow batteries present themselves as an option for energy storage systems, these rely on the electrochemical reaction between two redox mediators to reversibly store and release electrical energy.

Some batteries are dependent on scarce or toxic elements, such as lithium or cobalt, which increases the difficulty in their deployment on large scale. Replacing these with organic redox mediators, ORMs, would prove to have lower costs and be a highly tunable alternative.

This work aims to study several new potential organic redox mediators form the classes of compounds diphenoquinone, hydrodiphenoquinone, hydrobenzoquinone, and zwitterionic pyridinium phenolates. Diphenoquinones and benzoquinones were synthesized from commercially available disubstituted phenols, through oxidation with ceric ammonium nitrate, or (diacetoxyiodo)benzene, respectively. Hydrobenzoquinones and hydrodiphenoquinones were then produced through the reduction of the respective quinones with zinc in acetic acid.

Zwitterionic pyridinium phenolates were produced by the coupling of 2,6-di-*tert*-phenol with pyridine derivatives in a 11 step total synthesis. This synthesis involved from one side the methylation and *p*-bromination of 2,6-di-*tert*-butylphenol to allow the Suzuki cross-coupling of the compound with a *p*-bromopyridine-*N*-oxide derivative, which was in turn prepared through the activation of a pyridine ring, followed by nitration and subsequent bromination.

The electrochemical properties of these compounds were studied by cyclic voltammetry (CV) to access their upcoming applicability as organic redox mediators. The diphenoquinones presented two reversible electron transfers (ET), however the hydrobenzoquinones showed a chemical irreversible electron transfer and the hydrodiphenoquinones presented either chemical irreversible or quasi-reversible electron transfers. Representative cases are: tetra-*tert*-butyldiphenoquinone, that presented ETs at $E^0$= -0.53 V and $E^0$= -0.92 V; the respective hydrodiphenoquinone presented irreversible ETs at $E_{pc}$= 0.64 V and $E_{pa}$= 1.04 V vs. SCE; and di-*tert*-butylbenzoquinone presented two irreversible Ets at $E_{pc}$= 0.31 V and $E_{pa}$= 1.00 V vs. SCE.

The zwitterionic pyridinium phenolates are a class of compounds with unexplored potential as ORMs for redox flow batteries, whose CV measurements revealed a reversible electron transfer, at $E^0$= -1.47 V vs. SCE.

**Keywords:** Redox flow batteries, diphenoquinones, hydrobenzoquinones, zwitterionic pyridinium phenolates, cyclic voltammetry

# RESUMO

A necessidade de diminuir a nossa dependência em combustíveis fósseis requer fontes de energia renováveis como alternativa, tais como energia solar e eólica. No entanto, a natureza intermitente destas fontes de energia prova ser um desafio e revela a importância de desenvolver sistemas de armazenamento de energia com maior eficiência.

Baterias redox de caudal apresentam-se como uma opção para sistemas de armazenamento de energia, estas dependem na reação eletroquímica entre dois mediadores redox para armazenar e libertar energia elétrica de forma reversível.

Algumas baterias são dependentes de elementos escassos ou tóxicos, como lítio ou cobalt, o que aumenta a dificuldade da sua aplicação em grande escala. A sua substituição por mediadores redox orgânicos, ORMs, poderia oferecer custos reduzidos, assim como uma alternativa altamente ajustável.

Este trabalho tem como objetivo estudar vários novos potenciais mediadores redox orgânicos, das classes de compostos difenoquinona, hidrodifenoquinona, hidrobenzoquinona, e fenolatos de piridínio zwitteriónicos. As difenoquinonas e benzoquinonas foram sintetizadas a partir de fenóis disubstituidos comerciais, através da sua oxidação com nitrato de amónio cérico, ou (diacetoxiiodo)benzeno, respetivamente. Hidroquinonas e hidrodifenoquinonas foram então produzidas pela redução das respetivas quinonas com zinco em ácido acético.

Fenolatos de piridínio zwitteriónicos foram produzidos pelo acoplamento de 2,6-di-*terc*-butilfenol com derivados de piridinas numa síntese total de 11 passos. Esta síntese envolveu a metilação e p-bromação do 2,6-di-*terc*-butilfenol para permitir o acoplamento de Suzuki do compost com um derivado de N-óxido de p-bromopiridina, que por sua vez foi preparado a partir da ativação de um anel de piridina, seguido de nitração e subsequente bromação.

As propriedades eletroquímicas destes compostos foram estudadas por voltametria cíclica (VC) de forma a avaliar a sua possível aplicação como mediadores redox orgânicos em baterias redox de caudal. As difenoquinonas revelaram duas transferências eletrónicas (TE) reversíveis, no entanto as hidroquinonas apresentam uma transferência eletrónica quimicamente irreversível, e as hidrodifenoquinonas apresentaram transferências eletrónicas quimicamente irreversíveis ou quasi-reversíveis. Casos representativos são: tetra-*terc*-butildifenoquinona, que apresentou TEs a $E^0$= -0.53 V e $E^0$= -0.92 V; a respetiva hidrodifenoquinona, que apresentou TEs a $E_{pc}$= 0.64 V e $E_{pa}$= 1.04 V vs. SCE; e di-*terc*-butilbenzoquinona, que apresentou TEs a $E_{pc}$= 0.31 V e $E_{pa}$= 1.00 V vs. SCE.

Os fenolatos de piridínio zwitteriónicos são uma classe de compostos com potencial, mas ainda inexplorados como ORMs para baterias redox de caudal, cujas medições de VC revelaram uma transferência mono-eletrónica reversível, a $E^0$= -1.47 V vs. SCE.

**Palavras-chave**: Baterias redox de caudal, difenoquinonas, hidrobenzoquinonas, fenolatos de piridínio zwitteriónicos, voltametria cíclica.

# INDEX

# FIGURE INDEX

# TABLE INDEX

# SCHEME INDEX

# GRAPHIC INDEX

# LIST OF ABBREVIATIONS

| | |
|---|---|
| $^{1}$H NMR | Proton nuclear magnetic resonance |
| $^{13}$C NMR | Carbon 13 nuclear magnetic resonance |
| ACN | Acetonitrile |
| BQ | Benzoquinone |
| CAN | Ceric ammonium nitrate |
| CV | Cyclic voltammetry |
| DCM | Dichloromethane |
| DIB | (Diacetoxyiodo)benzene |
| DMF | Dimethylformamide |
| DQ | Diphenoquinone |
| ET | Electronic transfer |
| FTIR | Fourier-transform infrared |
| HBQ | Hydrobenzoquinone |
| HDQ | Hydrodiphenoquinone |
| iPr | Isopropyl |
| OCV | Open circuit voltage |
| ORM | Organic redox mediator |
| Ph | Phenyl |
| RFB | Redox flow battery |
| SCE | Saturated calomel electrode |
| tBu | *Tert*-butyl |
| TLC | Thin layer chromatography |

# 1. INTRODUCTION

## 1.1 Redox flow batteries

The need to decrease our dependency on fossil fuels requires alternative renewable energy sources, such as solar and wind energy. However, these energy sources have an intermittent nature that proves to be a challenge and reveals the importance of developing energy storage systems with higher efficiency.[1,2]

A proposed solution is the development of redox flow batteries. This kind of battery relies on the electrochemical reaction between two fluids containing redox flow mediators, the chemical species that will be either reduced or oxidized.

A redox flow battery (RFB), as exemplified by **Figure 1.1**, is constituted by two half-cells, separated by a membrane that prevents the fluids from mixing, allowing passage only to specific ions. An electrode on each half cell, connected to the power grid, allows for its respective half-cell reaction to occur on its surface. Each half-cell is connected to a storage tank from which the fluid with its respective redox mediator can be pumped in. There are, however, RFBs that exhibit variations from this design. Some batteries, to avoid the cost of expensive membranes, rely on laminar flow of the electrolytes to avoid mixing. Or in the case of hybrid RFBs, not all of the redox-active species are soluble, and are instead deposited on the surface of the electrode.[3] Due to their structure, these batteries allow for the decoupling of energy storage and power output. Storage capability depends on tank size and electrolyte

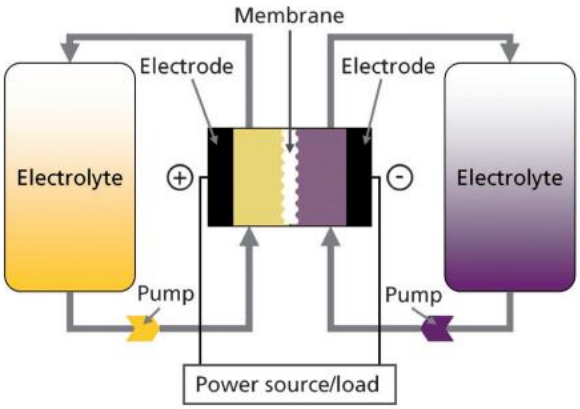


**Figure 1.1 -** Structure of a liquid-liquid RFB, ilustrating the half-cells, electrodes, electrolyte tanks and connections to the power grid. Figure taken from Noack, J., Roznyatovskaya, N., Herr, T. & Fischer, P. The Chemistry of Redox-Flow Batteries. *Angew. Chemie - Int. Ed.* **54**, 9776–9809 (2015).

concentration, while power output depends on the electrode size and reaction kinetics.[4] This decoupling leads to advantages as a flexible modular design, excellent scalability, moderate maintenance costs and long-life cycling.[1]

The first design of a flow battery was patented in the US by John Doyle in 1879, this was a galvanic cell based on the redox reaction between zinc and bromine. Although not rechargeable, it could have become so by adding pumps to its design.[5] Zinc-bromine hybrid RFBs have undergone continued development over the last 50 years, including research in how to reduce the hazards associated with bromine, so far as to become one of the RFB designs with the most commercial potential, with some designs reaching open circuit voltages (OCV) of 1.58 V.[1,5]

Vanadium RFBs also present some of the greatest success in commercialization, these batteries were first developed by Skyllas-Kazacos et al. in the late 1980s, and rely on the electrochemical reactions among the multiple oxidation states of vanadium, from +2 to +5,[6] in aqueous solution with sulfuric acid as supporting electrolyte, exhibiting an OCV ranging between 1.1 and 1.6 V. These are the most studied and developed RFBs, and as a result are part of the state of the art in the field of flow batteriess.[1,2,5]

Although the most developed RFBs use water as the solvent, this choice has its limitations, as water has an electrochemical window of 1.23 V, beyond which it starts decomposing, presents a fundamental limit on the cell voltage of aqueous RFBs. An alternative, then, is the use of organic solvents, such as acetonitrile or propylene carbonate, that can have wider electrochemical windows, allow higher redox mediator concentrations, as well as lead redox mediators to present new electrochemical behavior in said solvents.[7] Organic solvents also come with their faults, however, as they can be volatile and require constant replacement, as well as present toxicity or fire hazards. Regardless, there is a great variety of organic solvents, some of which could be fit for RFBs while reducing the hazards associated with organic solvents.[8]

## 1.2 Redox mediators

Redox flow batteries rely on the electrochemical reactions of redox mediators, these are compounds capable of changing their oxidation state in a reversible manner (**Figure 1.2**). A redox couple

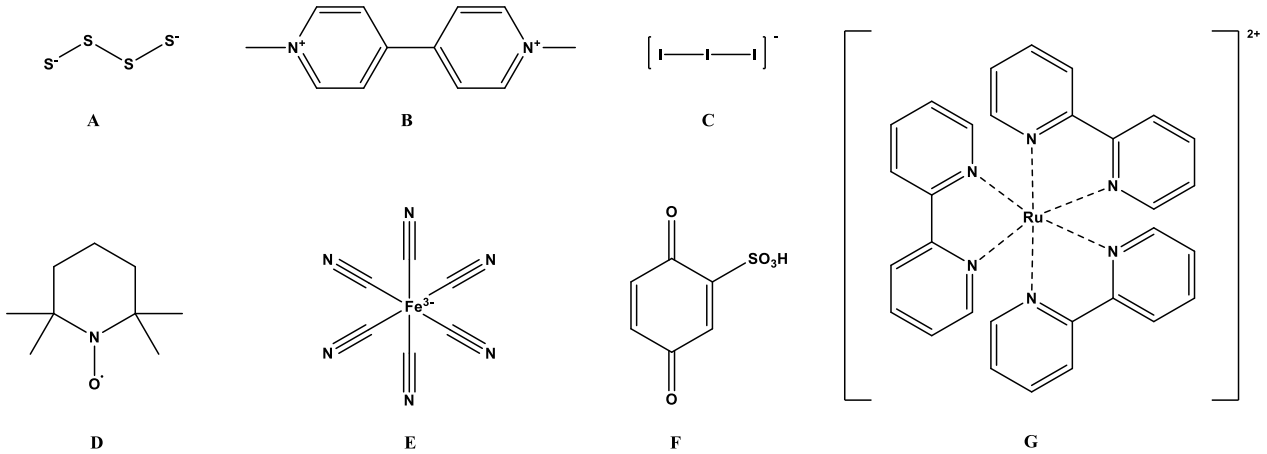


**Figure 1.2** - Structures of multiple redox mediators. **A** - polysulfide; **B** - methyl viologen; **C** - triiodide; **D** – TEMPO; **E** – hexacyanoferrate; **F** – 1,4-benzoquinone-2-sulfonic acid; **G** – tris(bipyridine)ruthenium (II).

happens in each half-cell of the battery, the reducing mediator constituting the catholyte and the oxidizing mediator constituting the anolyte, with their respective half-cell potential, and the difference in potential between these redox couples dictates the OCV of the battery, one of the factors that defines its energy density.[3]

There is a great variety of redox mediators, with a seemingly infinite number of possible structures. These can range from simple metallic ions, complexed with water or halide ions, to polysulfides or polyhalides, to organic compounds and organometallic complexes.

Two of the most developed RFBs are vanadium RFBs and zinc-bromine RFBs. Vanadium RFBs rely on the stability and solubility in water of its compounds in oxidation states from +2 to +5, with its redox mediators forming the redox couples $V^{2+}/V^{3+}$ and $VO^{2+}/VO_2^{+}$. Zinc-bromine RFBs in turn rely on the mediators that form the couples $Zn/Zn^{2+}$ and $Br^{-}/Br_2$.

Organic redox mediators (ORMs) are a subset of redox mediators, organic compounds capable of undergoing reversible redox reactions. The application of these could lead to a reduced dependence on scarce or toxic metals such as lithium or cobalt.[1] ORMs offer great tunability, as their properties can be modified with change to the molecule's structure, such as adding hydroxyl or acid groups to increase its solubility in water, or adding groups that change the molecule's electron density to change its half-cell potentials.[9] Some classes of compounds belonging to this group are viologens,[10] nitroxyl radicals such as TEMPO[10], quinones,[11] and certain polycyclic aromatic hydrocarbons such as naphthalene[12] or anthracene.[2]

## 1.3 Quinone-based redox mediators

Quinones are compounds containing a cyclohexadiene ring with two carbonyl groups as their core structure. These are a focus of research on redox mediators for RFBs, as they can be stable in two redox states, the oxidized form, quinone, and aromatic reduced form, hydroquinone. In aqueous media, tend to exhibit a $2e^- + 2H^+$ reduction, however, in aprotic media they can exhibit two $1e^-$ transfers, forming an intermediary semiquinone radical followed by formation of a dianion (**Figure 1.3**).[13]

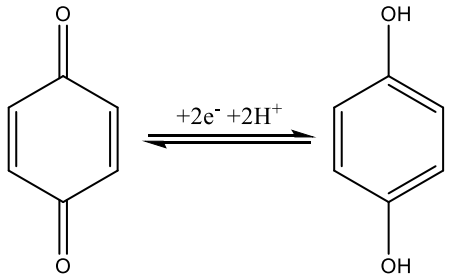


**Quinone reduction in protic media**

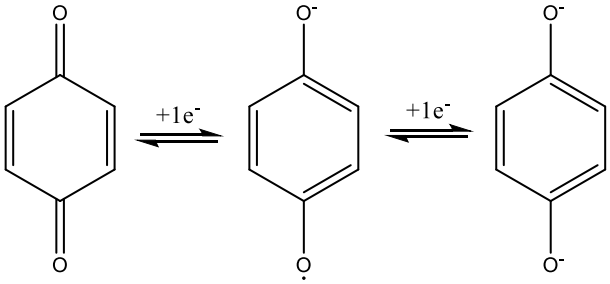


**Quinone reduction in aprotic media**

**Figure 1.3** - Reduction steps of quinones in protic and aprotic media.

Quinones are incredibly common in nature (**Figure 1.4**), even being used by living beings for their redox properties, as is the case for ubiquinone and plastoquinone, that participate in the electron transport chains of oxidative phosphorylation and photosynthesis, respectively.[14] Other biological quinones include vitamin K, hypericin, and phoenicin. This last one presents a recent case of a biological quinone with a fungal origin being studied for application in RFBs, as developed by Wilhelmsem et al. in 2023, in which phoenicin is used as a anolyte paired against hexacyanoferrate(II) in an aqueous RFB, showing an OCV of 0.87 V.[15]

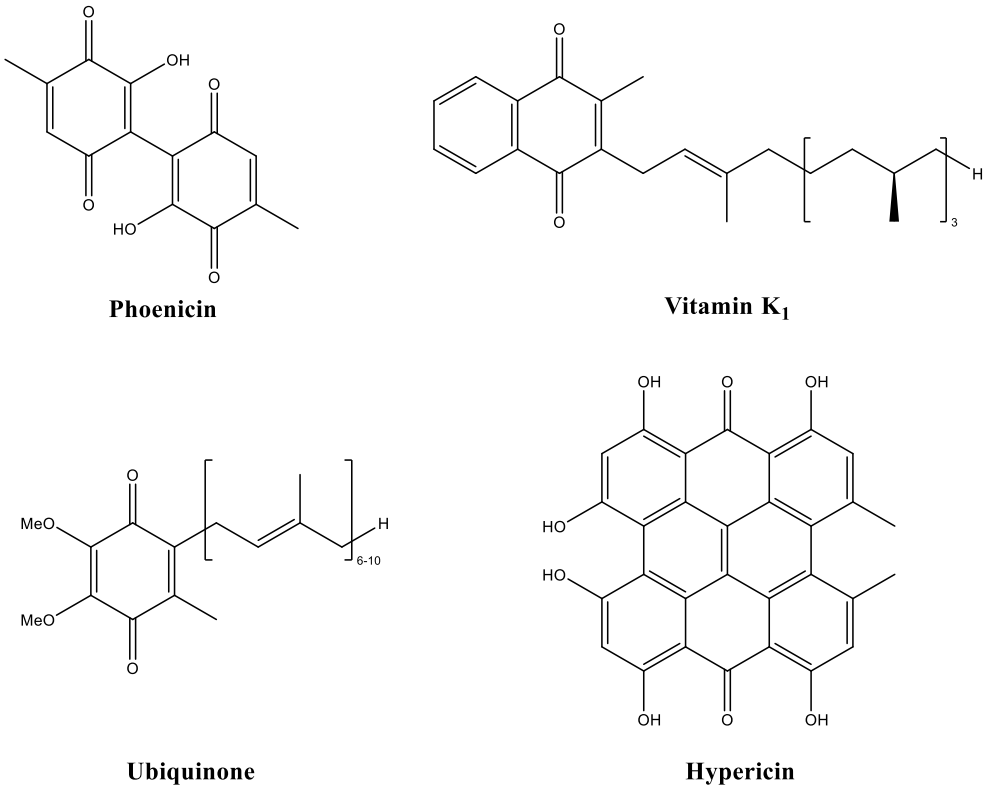


**Figure 1.4** - Examples of biological quinones.

Synthetic quinones developed for use in RFBs include 2,5-dimethoxy-1,4-benzoquinone, chloranil, 1,2-benzoquinone-3,5-disulfonic acid, among others (**Figure 1.5**).

One such quinone, 9,10-anthraquinone-2,7-disulfonic acid, was developed by Huskinson et al. in 2014 as an ORM in aqueous RFBs, used against bromine/bromide as the catholyte, presenting an OCV of 0.8 V and reaching high power densities, becoming one of the most notable cases of a quinone being used in a RFB.[1,11]

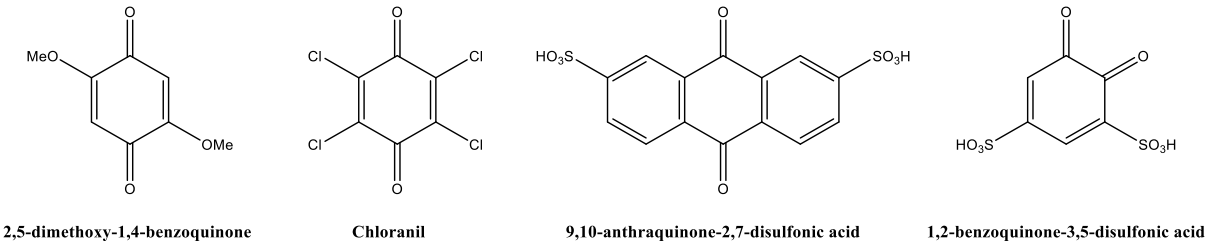


**Figure 1.5** - Examples of quinones being developed for use in RFBs.

## 1.4 Zwitterionic pyridinium phenolates

Zwitterionic pyridinium phenolates are a class of compounds with unexplored potential as ORMs. These have a core structure comprised of a pyridinium ring attached at its C-4 position to a phenolate group at its respective 4 position. These compounds have been mostly studied for optoelectronic applications, as their asymmetric π system, along with an increased interplanar angle between the two rings for sterically hindered derivatives, leads to enhanced non-linear optics properties.[16]

The conjugation between the two charged centers allows the molecule to have two major resonance forms (**Figure 1.6**), a zwitterion with two aromatic rings, and a quinonoid form, that could allow the compound to have redox properties similar to quinones.

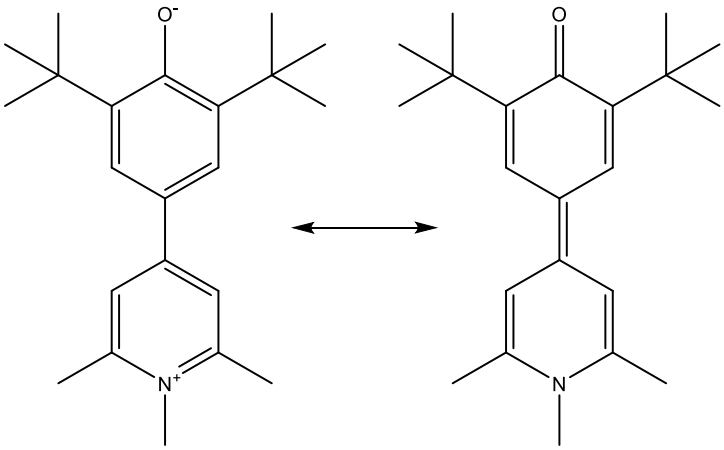


**Figure 1.6** - Resonance structures of zwitterionic pyridinium phenolate, exhibiting zwitterionic and quinonoid traits.

These compounds have not been previously considered for application in RFBs, and voltammetric studies of said compounds are scarce. There is, however, an article by Emel Ay et al., where cyclic voltammetry was performed for such compounds, exhibiting a reversible electron transfer at positive potentials, likely associated with the oxidation of the phenolate.[17] This reveals the potential of these compounds to have reversible electron transfers that could be useful for applications in organic RFBs.

# 2. RESULTS AND DISCUSSION

## 2.1 Preamble

In this work, several benzoquinone derivatives, along with three pyridinyl-phenol derivatives, were synthesized from commercial reagents to have their electrochemical properties studied by cyclic voltammetry. All compounds synthesized in this work were also characterized by $^{1}H$ and $^{13}C$ NMR, FTIR spectroscopy and mass spectrometry.

In the first part, several quinones and respective reduced forms, hydrobenzoquinones and hydrodiphenoquinones, were synthesized from commercial phenols to be studied by cyclic voltammetry in acetonitrile or dimethylformamide. Benzoquinones (**1**) were synthesized by oxidation of phenols with (diacetoxyiodo)benzene (**Scheme 2.1**). Diphenoquinones (**3**) were synthesized by oxidation with ceric ammonium nitrate (CAN) in the presence of $HClO_4$. The respective hydrobenzoquinones (**2**) and hydrodiphenoquinones (**4**) were produced by reduction of the **(1)** and (**3)** with zinc in acetic acid at 70ºC (**Scheme 2.1**).

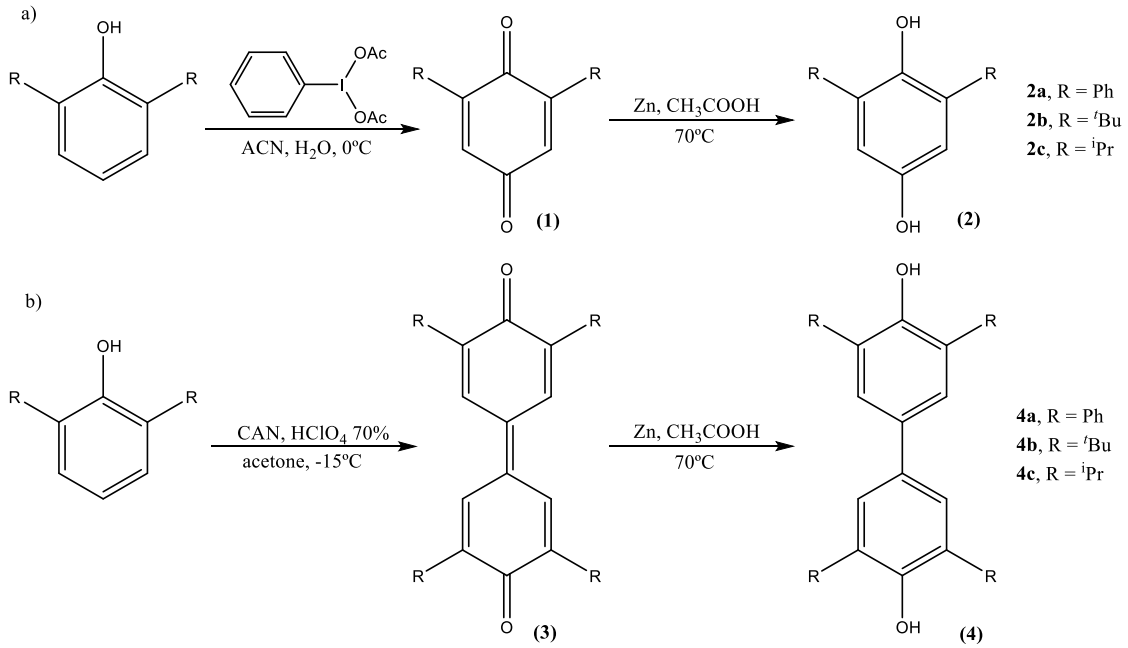


**Scheme 2.1** - Synthetic pathway for benzoquinones, diphenoquinones, and respective hydrobenzoquinones and hydrodiphenoquinones.

In the second part, the zwitterionic pyridinium phenolates were synthesized by the coupling of di-*tert*-butylphenol to pyridines, mostly following a previously reported procedure.[16] This synthesis involved three major segments, which were from one side the protection of the phenol, bromination followed by its borylation, and from another the nitration and subsequent bromination of the pyridines. In the final part, the two compounds were joined by Suzuki-Miyaura coupling. Following this, the resulting compound had its N-oxide functionality reduced and replaced by a methyl group, whereas the phenol was deprotected and deprotonated (**Scheme 2.2**). The synthesis will be described in more detail later. The zwitterion was studied by cyclic voltammetry in acetonitrile, along with some intermediates of the synthetic pathway that were also studied in the same conditions. The target zwitterion **15**a has not been previously reported in the literature, to the best of our knowledge, however zwitterion **15b** and several similar compounds have been reported by Diemer et al.[16] This group has reported several derivatives, with the intent of increasing the interplanar angle between the two rings to observe the effect this would have on the compound's non-linear optics. Of interest to this work, the interplanar angle could likely also have an effect on the electrochemical properties of the zwitterions. Unfortunately, the synthesis of two such compounds was attempted, with only one reaching the final step of the synthesis and subsequent cyclic voltammetry studies, so no conclusion could be drawn from the effect of the interplanar angle.

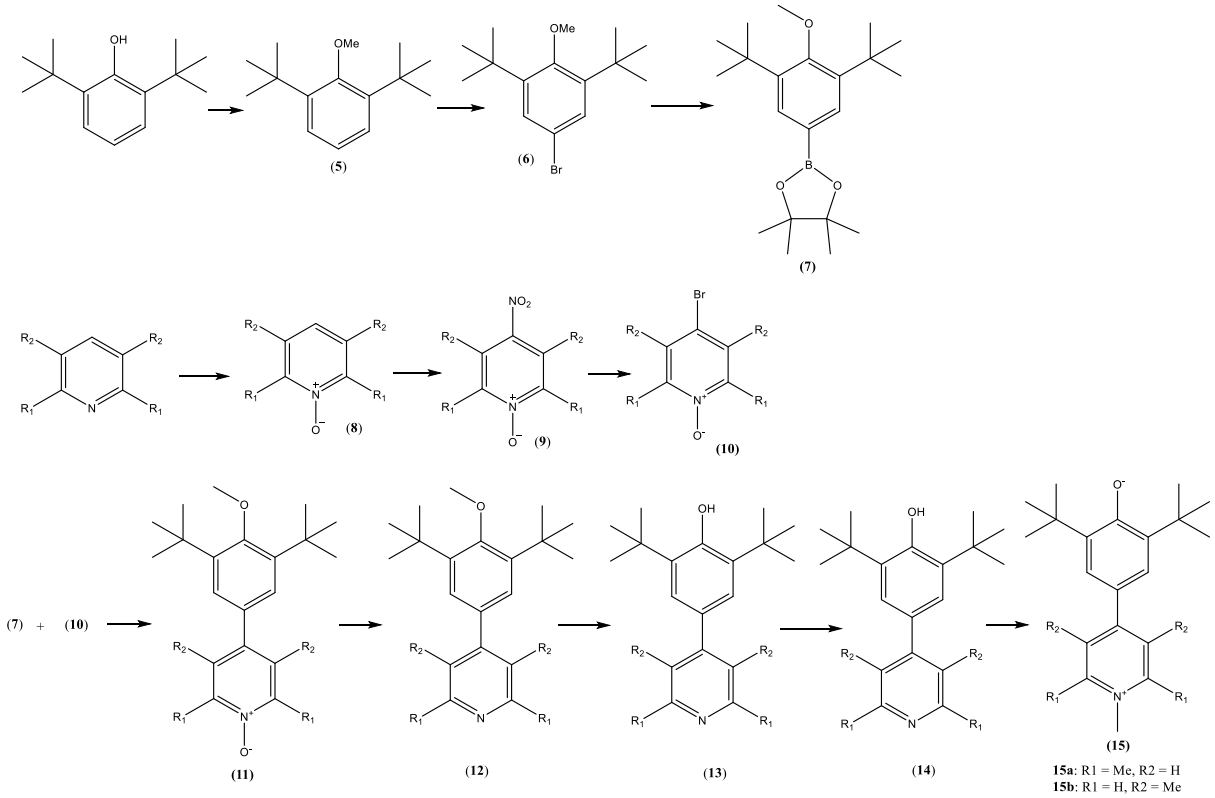


**Scheme 2.2** – Compounds involved in the pathway towards zwitterionic pyridinium phenolates.

## 2.2 Preparation of benzoquinones, diphenoquinones and their reduction

## 2.2.1 Preparation of benzoquinones

Benzoquinones, also named as cyclohexadienediones, are generally synthesized from substituted phenols through their oxidation. Several processes exist to perform this oxidation, such as reaction with lead dioxide and 70% $HClO_4$ in acetic acid. The lead dioxide acts as the oxidizer, and in the presence of a strong acid leads to the formation of benzoquinones with good yield.[18]

Another example is the use of oxygen in the presence of a cobalt catalyst to perform the oxidation. Oxygen can coordinate with cobalt salen complexes or analogues, forming a superoxide complex capable of oxidizing the phenol to benzoquinone.[19]

Electrochemical oxidation has also been used, presenting itself as a green alternative, avoiding the use of stoichiometric oxidizers or expensive catalysts while still achieving yields of 99%.[20]

In this work, 1,4-benzoquinones were synthesized by the oxidation of 2,6-disubstituted phenols with (diacetoxyiodo)benzene (DIB) in a mixture of water and acetonitrile at 0 ºC following the procedure

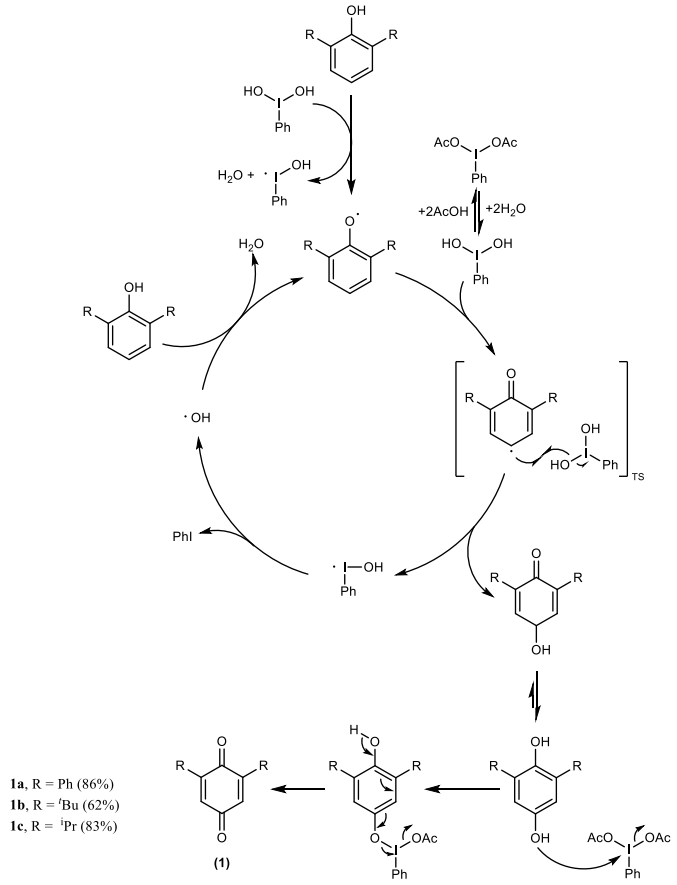


**Scheme 2.3** – Mechanism of the formation of benzoquinones by oxidation with DIB.

developed by N. Scheiber at al.[21] The reaction gave good yields, upwards of 60%, however a small amount of the diphenoquinone was also produced, and had to be separated by flash chromatography.

The mechanism of the oxidation of phenols by DIB is still under debate, however there is strong evidence that it involves a radical chain starting with the formation of phenoxyl radicals that react with the hydrolyzed form of DIB, $PhI(OH)_2$, to produce the hydrobenzoquinones (**2**) that is in turn oxidized by DIB to the benzoquinone (**1**) (**Scheme 2.3**).[22]

A possible side reaction might occur, however, through the dimerization of the phenoxyl radical to form hydrodiphenoquinone (**4**), that is quickly oxidized to the diphenoquinone (**3**), requiring separation. The 1,4-benzoquinones (**2**) and diphenoquinones (**3**) can be told apart by their $^1H$ NMR spectra. The 1,4-benzoquinones have two protons attached to the core structure, with a typical chemical shift between 6.0 and 7.0 ppm, whereas the protons attached to the core structure of diphenoquinones have typical chemical shifts between 7.5 and 8.5 ppm (**Figure 2.1**).


**Figure 2.1** – $^1H$ NMR spectra comparison between diphenoquinone and benzoquinone, focusing the alkene hydrogens of the core structure.

The spectroscopy data obtained for the benzoquinones are in accordance with the article by Fiona Sprang et al.[20] The yields obtained were 86%, 62% and 83% for the diphenyl, di-*tert*-butyl and diisopropyl benzoquinones. In the work developed by N. Scheiber, the same method was used to produce naphthoquinones, giving yields between 71% and 87%.

## 2.2.2 Preparation of diphenoquinones

Preparation of diphenoquinones usually requires the oxidation of either phenols or 4,4'-dihydroxybyphenyls, in this works referred to as hydrodiphenoquinones. The synthesis of diphenoquinones has been reported previously using manganese(III) acetate as the oxidizer. Performing this reaction in glacial acetic acid with $Mn(OAc)_3$ produces the diphenoquinone with good yield, while using $Mn(acac)_3$ instead produces the hydrodiphenoquinone.[23] These compounds have also been prepared by the oxidation of hydrodiphenoquinones, using an oxidizer such as (diacetoxyiodo)benzene.[24]

In this work, diphenoquinones were synthesized by the oxidation of phenols with CAN in the presence of $HClO_4$ at -15ºC, following a procedure adapted from the work of Domagala et al.,[25] giving yields above 60%. This reaction, too, produced small amounts of the benzoquinone, but it was easily separated by flash chromatography.

The mechanism of this reaction starts with the oxidation of the phenol to form a radical cation that then deprotonates to form a phenoxyl radical. After dimerization, this tautomerizes to a hydrodiphenoquinone (**4**), which is then also oxidized by the $Ce^{4+}$ ions to the diphenoquinone (**3**) (**Scheme 2.4**).[25]

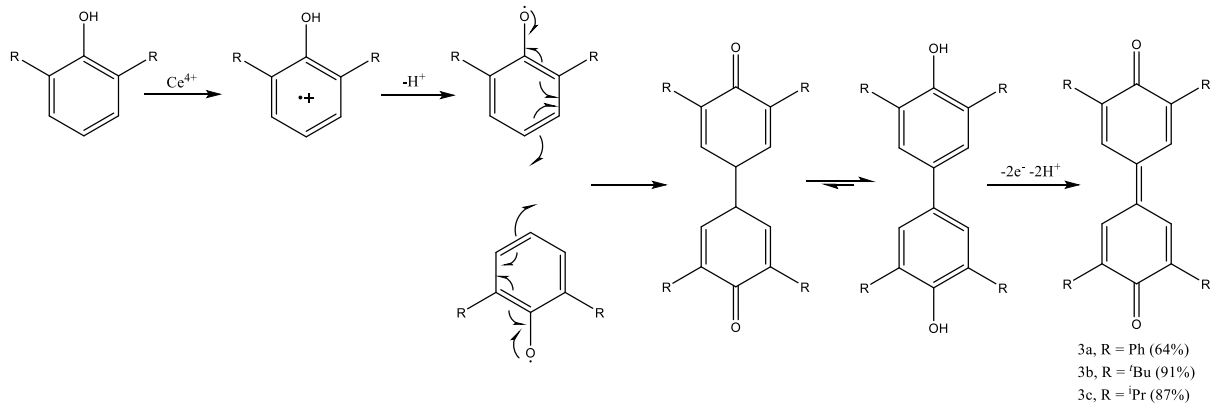


**Scheme 2.4** – Mechanism of oxidation of phenol to diphenoquinone by CAN.

## 2.2.3 Reduction of quinones

Hydrobenzoquinones are usually prepared via the reduction of benzoquinones. This reduction can be done using common reduction procedures, such as hydrochloric acid and tin(II) chloride[26], or reduction with hydrogen over Raney nickel,[27] or acetic acid with zinc dust.[28]

Hydrodiphenoquinones can both be prepared via the oxidation of phenols, stopping the oxidation before forming the quinones, or via the reduction of the respective quinones. These could be prepared in glacial acetic acid using as oxidizer $Mn(acac)_3$, from the coupling of two phenol molecules,[23] as well as reduction of the diphenoquinone with hydrogen over ruthenium.[29]

However, the method used in this work was that employed by Coffield et al. The reduction of both benzoquinones (**1**) and diphenoquinones (**3**) was performed in acetic acid at 70ºC, using zinc dust as reductant (**Scheme 2.5**), producing the respective hydrobenzoquinones and hydrodiphenoquinones (**2** and **4**) with high yield, around 90%. Coffield et al. attained a yield of 76%, however their method of purification was recrystallization, whereas this work used preparative TLC.

Whereas the studied quinones present a color, ranging from red to yellow, their reduced forms were colorless, and the lack of coloration of the reaction mixture could be a sign that the reaction was complete. However, the hydrobenzoquinones and hydrodiphenoquinones were sensitive to light, and after even a short amount of time of exposure, would already start developing color, due to formation of the respective quinone.

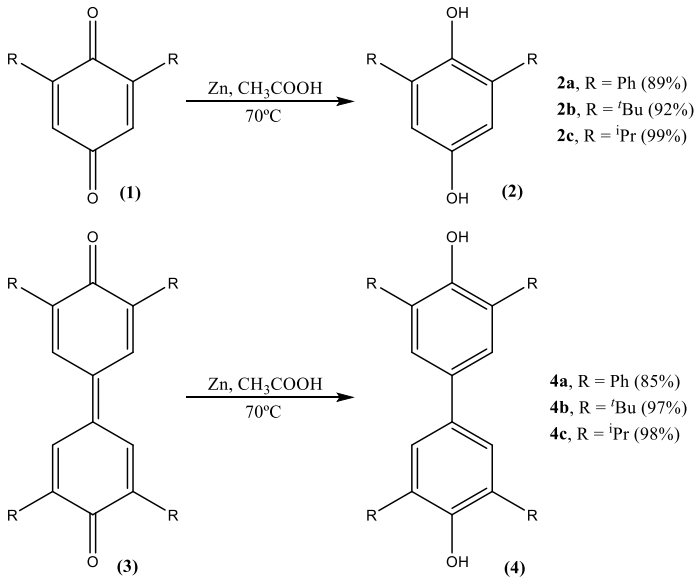


**Scheme 2.5** – Reduction reaction to produce the hydrobenzoquinones and hydrodiphenoquinones.

The occurrence of the reaction could be confirmed by the $^{13}C$ and FTIR spectra. After the reaction, the carbonyl groups were reduced, so the $^{13}C$ chemical shifts of these groups, usually between 180 and 190 ppm for these compounds, shifted to higher field. The appearance of hydroxyl groups is also visible in FTIR spectroscopy, as a band appeared near 3500 $cm^{-1}$.

## 2.3 Preparation of zwitterionic pyridinium phenolates

We prepared zwitterionic pyridinium phenolates following the methodology established by Diemer et al.,[16] presented resumed in **Scheme 2.2**. The synthesis process is outlined in the subsequent sections, and each step will be discussed separately.

## 2.3.1 Synthesis of the boronic ester (7)

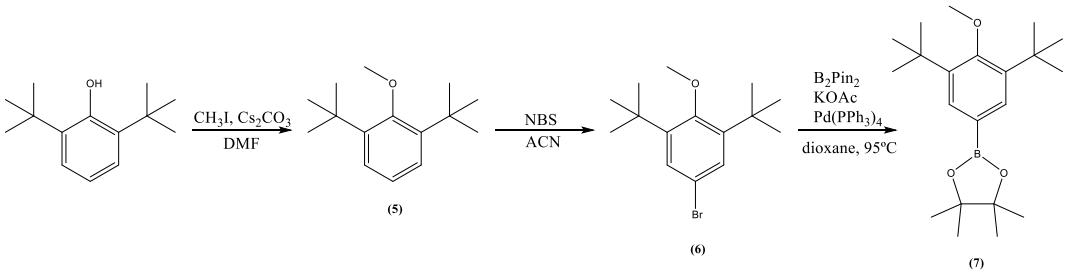


**Scheme 2.6** – Preparation of the anisole boronic acid pinacol ester (**7**) from 2,6-di-*tert*-butylphenol.

The procedure towards the synthesis of the boronic ester (**7**) (**Scheme 2.6**) begins with the protection of the phenol, as its acidic proton could cause issues during the Suzuki reaction. Sterically hindered arylboronic acids have been previously reported to suffer protonolysis of the C-B bond to a significant extent, greatly reducing the yield of Suzuki reactions. Therefore, it is advantageous to perform the Suzuki reaction using arylboronate esters, as well as ensuring anhydrous conditions are used.[30]

The methoxy group was chosen as the protection group due to the steric hindrance caused by the *tert*-butyl groups in the neighbouring positions, which would block bigger protection groups.[16] This protection was achieved reacting the phenol with iodomethane and cesium carbonate in DMF.[31] Compound **5** was successfully synthesized with an yield of 89% as can be observed in the $^{1}$H NMR spectrum, by the appearance of a signal at 3.71 ppm with an integral of 3 for the methoxyl group (Appendix, **Figure 6.37**), as well as in the FTIR spectrum by the absence of a band associated with the O-H bond of the phenol in the 3000-4000 $cm^{-1}$ range. The mechanism involved the deprotonation of the phenol, followed by nucleophilic attack towards the iodomethane in an $S_N2$ reaction.

The next step was the bromination of the anisole by *N*-bromosuccinimide in acetonitrile. In this process, the aromatic compound goes through an electrophilic aromatic substitution, replacing the hydrogen in the *para* position with a bromine. The reaction produced compound **6** with a yield of 63%. This substitution could be observed in the $^{1}$H NMR spectra, as the signal of the hydrogen in the *para* position disappeared, and the hydrogens in the *meta* positions changed to a singlet spin multiplicity (Appendix, **Figure 6.40**).

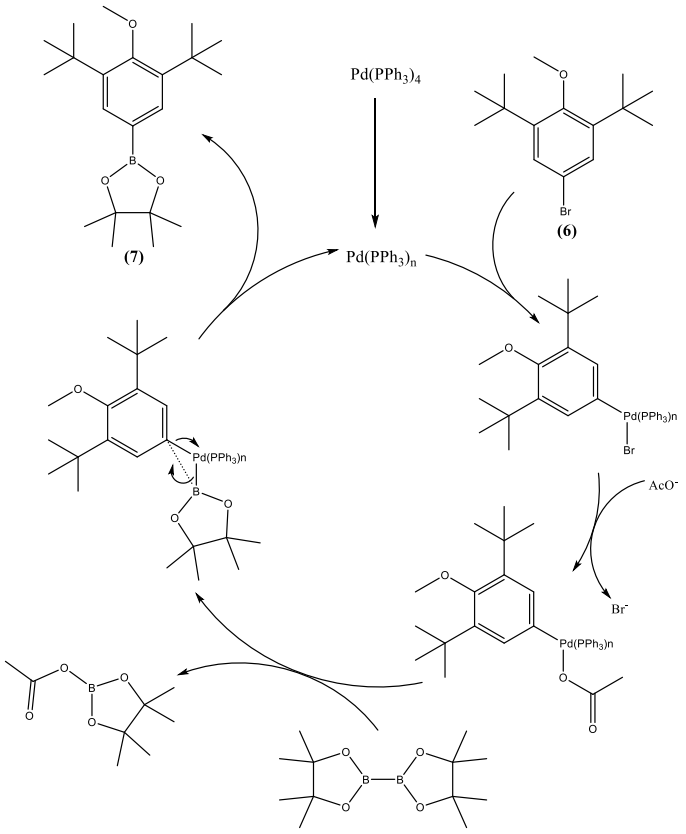


**Scheme 2.7** – Mechanism of the Miyaura borylation of the bromoanisole **6**.

As the final step of this sequence was the Miyaura borylation of the bromoanisole, forming the boronic ester (**6**). The reaction was performed in dioxane at 95ºC, using tetrakis(triphenylphosphine)palladium(0) as catalyst, potassium acetate as base and bis(pinacolato)diboron as a source of the boron pinacol ester group, following a procedure adapted from the work of Wu et al,[32] resulting in a good yield of 83%. The replacement of bromine by the boron pinacol group could be confirmed in the $^{1}$H NMR spectrum, as a signal appeared at 1.33 ppm with an integral of 12, and the hydrogens in the *para* positions relative to the oxygen moved to a higher chemical shift, from 7.33 ppm in compound **6** to 7.71 ppm in compound **7**. The mechanism of this borylation is similar to that of Suzuki-Miyaura couplings, differing in that the aryl boronic ester is replaced with bis(pinacolato)diboron (**Scheme 2.7**).[33] It begins with the dissociation of triphenylphosphine ligands from the palladium catalyst, followed by the oxidative addition of the bromoanisole. This forms a aryl(bromo)palladium(II) complex, in which the bromide ion is quickly replaced by an acetate ion. Transmetalation then occurs with bis(pinacolato)diboron, forming a complex that decomposes by reductive elimination, restoring the catalyst and producing the boronic ester (**7**).

## 2.3.2 Synthesis of the 4-bromopyridine N-oxides (10a) and (10b)

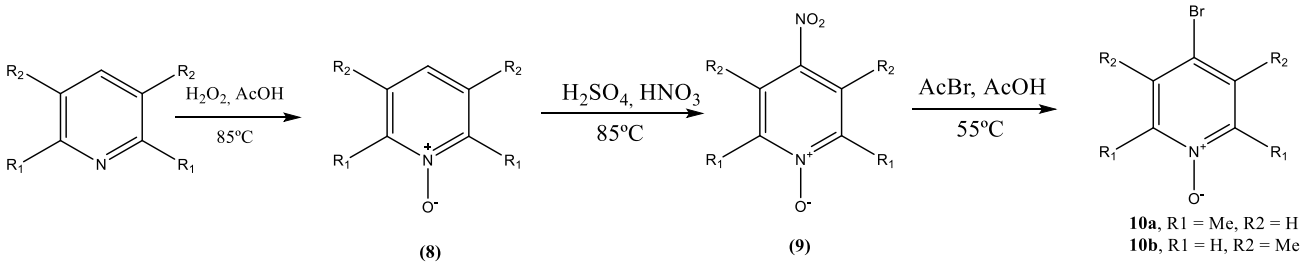


**Scheme 2.8** – Reactions performed to produce the 4-bromopyridine N-oxides (**7**).

In order to perform the nitration of the pyridine easily, it first had to be activated. Pyridines generally have lower reactivity in electrophilic aromatic substitutions due to the decrease in electron density of the ring, resulting from the higher electronegativity of the nitrogen. Not only that, the pyridine can delocalize partial positive charges by resonance to the *ortho* and *para* positions of the ring, further inhibiting the reaction with electrophiles in these positions and favoring reaction in the *meta* positions.[34]

This can be averted by forming the N-oxide, as the electrons can be delocalized through the pyridine ring, the electron density increases, enhancing the reactivity towards electrophilic aromatic substitutions. The delocalized partial negative charge in the *ortho* and *para* positions also greatly favours reaction in these positions.[34]

The pyridine N-oxide (**8b**) was prepared by reaction with acetic acid and hydrogen peroxide (**Scheme 2.8**), as pyridine N-oxides are nitrated more easily due to increased electron density. The 2,6-dimethylpyridine N-oxide (**8a**) was available commercially.

Following this, the pyridine N-oxide was nitrated successfully using concentrated sulfuric acid and nitric acid at high temperature. In the case of 3,5-dimethylpyridine N-oxide, it was possible to isolate both isomers of the nitration, nitrated either in the *para* position or *ortho* position, with an approximate ratio of 7 to 1 of *para* to *ortho* substituted compounds. Compound **9a** was produced with a yield of 98%, while compound **9b** only have a yield of 65%. The nitration could be observed in the $^{1}H$ spectra by the disappearance of the signal of the hydrogen in the *para* position for both compounds, and in the case of the 2,6-dimethylpyridine **9b**, the hydrogens in *meta* positions becoming singlets.

The final step of this sequence was the *para*-bromination of pyridine-N-oxide through reaction of the nitropyridine N-oxide with acetyl bromide in acetic acid, following a procedure reported previously

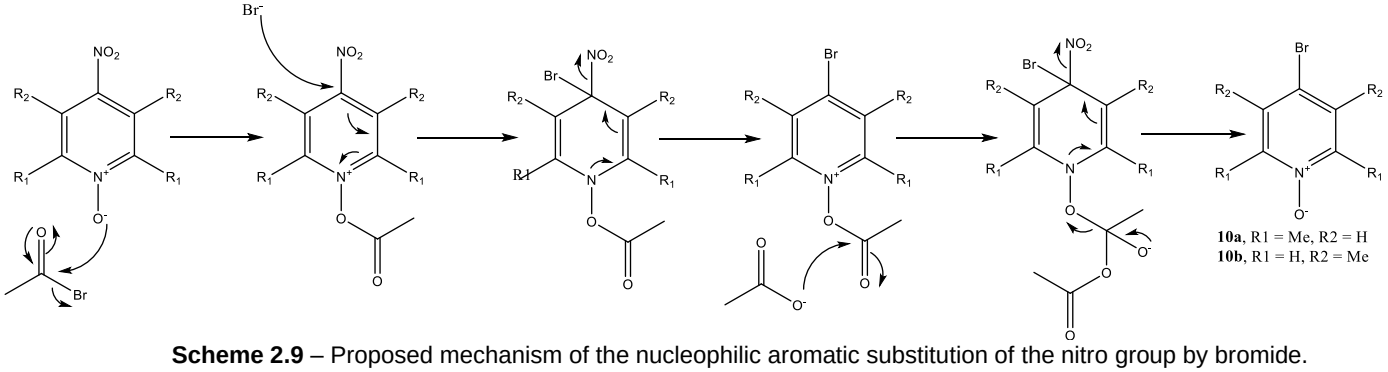


**Scheme 2.9** – Proposed mechanism of the nucleophilic aromatic substitution of the nitro group by bromide.

by Ma F. H. et al.[35] The reaction gave compound **10a** in a low yield of 49% and compound **10b** in a yield of 94%. This substitution could be confirmed in the $^1$H spectra, as the chemical shifts of the hydrogens in the *meta* positions changed to lower values, as the bromine is a weaker electron withdrawing group.

In a proposed mechanism presented in **Scheme 2.9**, the N-oxide would attack the acetyl bromide, forming an N-acetoxy pyridine, making the aromatic ring more electron deficient, and therefore more prone to nucleophilic aromatic substitution by the bromide ion. A nitrogen dioxide molecule would then be released, restoring the aromaticity of the ring. Then, another acetate ion would attack the acetoxy group, in turn forming the N-oxide again.

## 2.3.3 Preparation of compound 11 by a Suzuki-Miyaura coupling

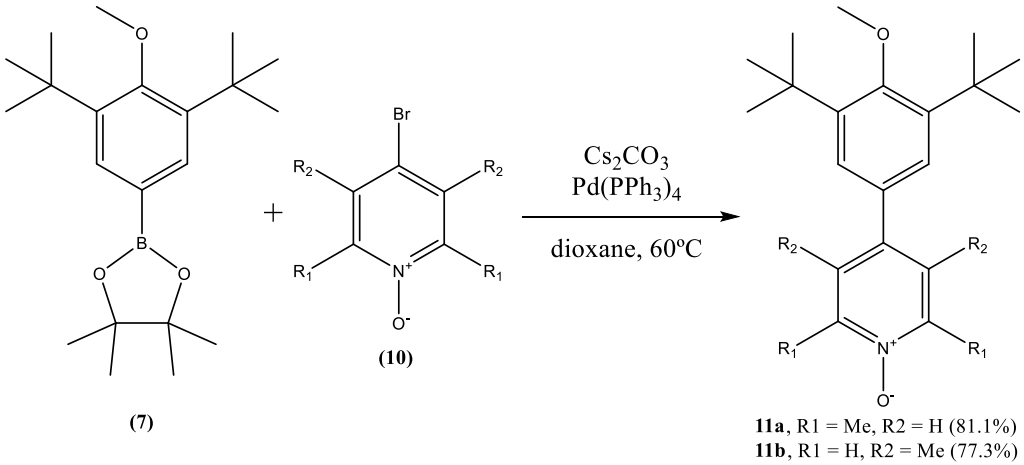


**Scheme 2.10** – Suzuki-Miyaura coupling reaction.

The preparation of the (methoxyphenyl)pyridine-*N*-oxide **11** involved the coupling reaction of the boronic ester **7** and the *p*-bromopyridine-N-oxide **10** by a Suzuki-Miyaura palladium coupling reaction (**Scheme 2.10**).

This reaction was performed in dioxane at 60ºC, using tetrakis(triphenylphosphine)palladium(0) as catalyst and cesium carbonate as base, using a slight excess of the bromopyridine N-oxide **7**.

The compounds were produced with a yield of 81% for the 2,6-dimethyl compound (**11a**) and 77% for the 3,5-dimethyl compound (**11b**). Although compound **11a** hasn't been reported previously, **11b** has been prepared by Diemer et al., with a yield of 71%, who have also prepared several other similar compounds with yields ranging between 70% and 85%. The change in position of the methyl groups from *ortho* to *meta* positions could be expected to influence the yield due to steric effects, however the small yield difference of 4% is not enough to say with certainty if that is the case.

In the $^1$H NMR spectra it is possible to observe for both compounds a peak near 1.48 ppm with an integral of 18 and a peak at 3.73 ppm with integral of 3. These two peaks correspond, respectively, to the *tert*-butyl and methoxy groups of the anisole part of the structure. The methyl groups of the

pyridine correspond to a peak of integral 6 at 2.58 ppm for compound **11a**, which move to 2.01 ppm in compound **11b**, due to the increased distance to the nitrogen atom. Compound **11a** also presents two peaks both of integral 2, at 7.46 and 7.12 ppm. In compound **11b** one peak moves to 6.93 ppm, while the other moves to 8.01 ppm, likely being the protons attached to the carbons neighboring the nitrogen atom.

The mechanism of this reaction (**Scheme 2.11**) starts with the dissociation of triphenylphospine ligands from the palladium catalyst, allowing the oxidative insertion into the bromopyridine bond. A carbonate ion then replaces the bromide ion in the complex, forming a carbonate complex that facilitates the reaction with the boronic ester by transmetalation. This final intermediate then decomposes by reductive elimination, releasing the initial palladium complex and restarting the cycle, and producing the coupled product.

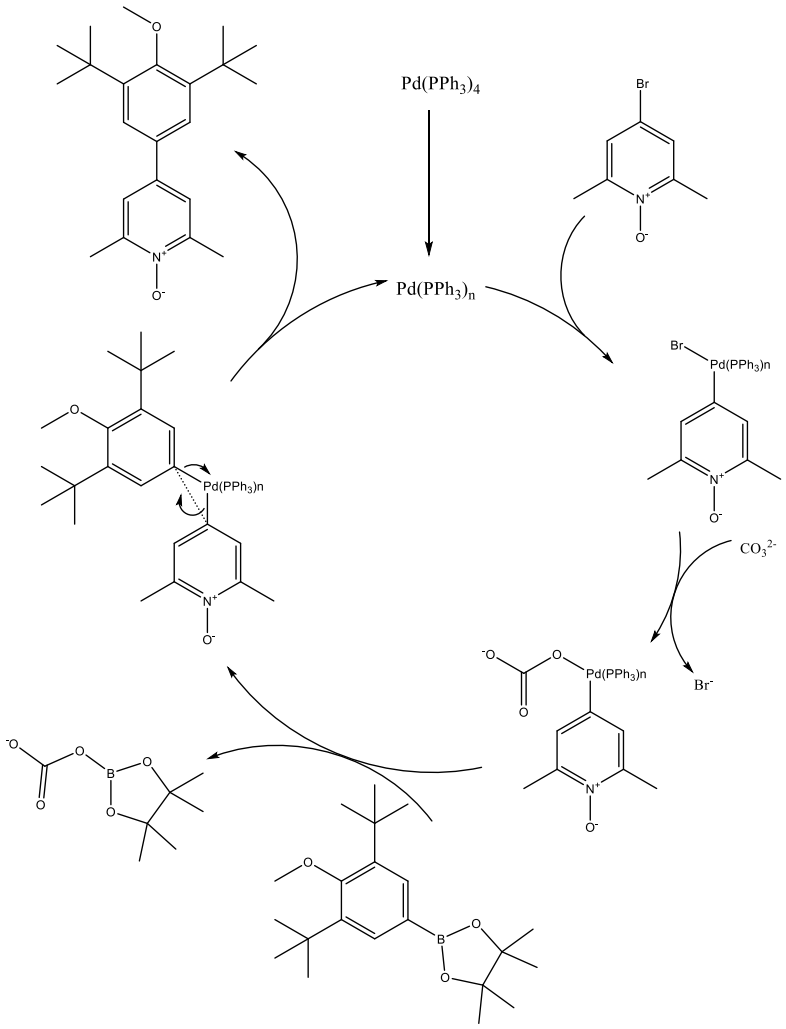


**Scheme 2.11** – Mechanism of the Suzuki-Miyaura coupling between the boronic este rand the bromopyridine N-oxide.

## 2.3.4 Preparation of the zwitterionic pyridinium phenolates

Following the coupling reaction, the next step was the reduction of the N-oxide to form the (methoxyphenyl)pyridine (**12**) (**Scheme 2.12**), however these steps were only performed for compound **11a**, with compound **11b** not progressing further in the synthesis.

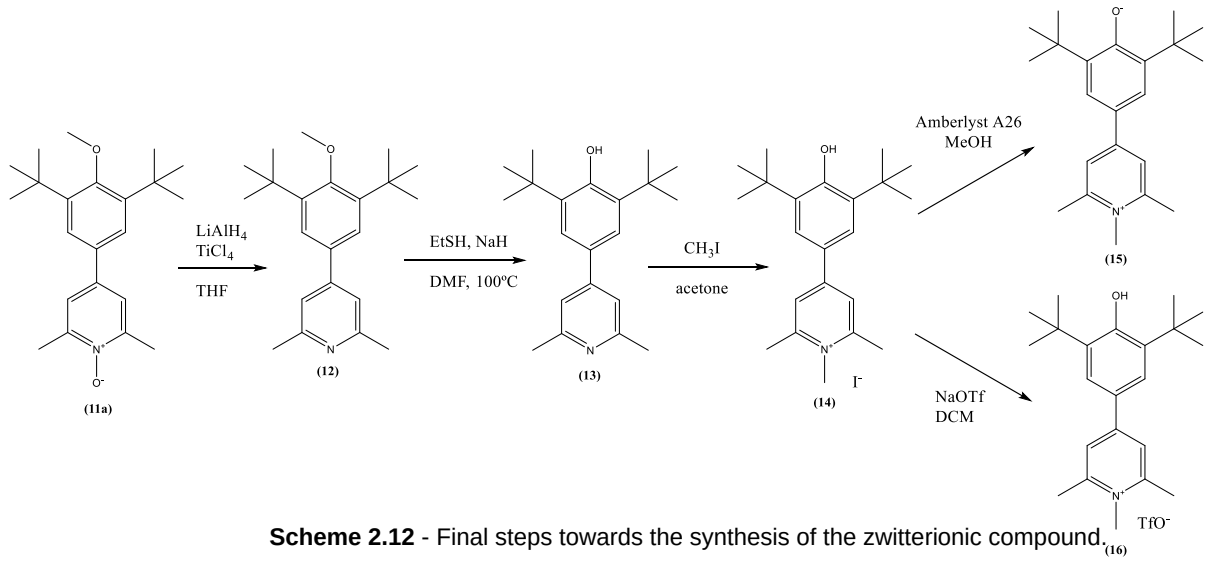


**Scheme 2.12** - Final steps towards the synthesis of the zwitterionic compound, (16).

This was achieved by reacting titanium tetrachloride and lithium aluminium hydride, which forms the reducing species that in turn reduces the N-oxide. The product was recovered with a good yield of 83%, which was slightly below the yield of 90% reported by Diemer et al. for the analogous 3,5-dimethyl compound.[16] Other similar compounds produced by this group, disubstituted at the 3,5-positions presented yields between 84% and 94%. During the reaction, the oxygen of the N-oxide coordinates to a titanium center, so steric hindrance could influence the reaction, however the 2,6-dimethyl compound **12** did not present a significantly decreased yield, likely due to the small size of the methyl groups.

The mechanism (**Scheme 2.13**), as proposed by Malinowski et al.,[36] starts with the reduction of $TiCl_4$, forming a low oxidation state titanium complex that contains chemisorbed hydrogen chloride. Upon addition of the N-oxide, the titanium complex is attacked by the oxygen atom, transferring one electron to the nitrogen and forming an anion radical, that immediately reacts with the HCl to form the pyridine hydrochloride, and a $Ti^{II}$=O species.

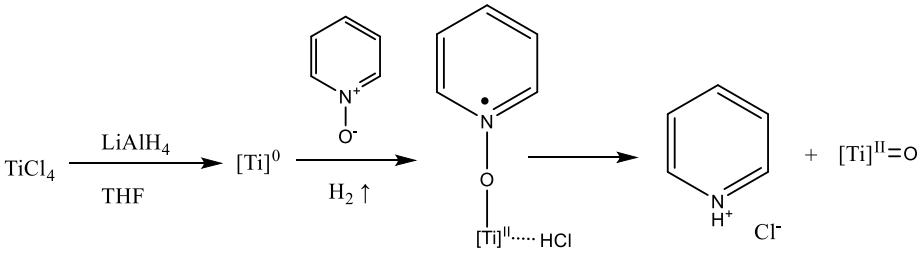


**Scheme 2.13** – Mechanism for the reduction of N-oxide by a titanium(0) complex. Proposed by Malinowski et al.

The next step involved the deprotection of the phenol performed, in a first attempt, in acetic acid containing HBr. It was expected that the bromide ion would attack the methyl group, in a nucleophilic reaction, to form the phenol, however, the target compound could not be obtained, as $^{1}H$ spectra did not correspond to the expected. A possible explanation is that, as the reaction was performed in acidic conditions at high temperature, the harsh conditions were capable of causing the dealkylation of the *tert*-butyl groups of the phenol.

A different reaction was tried instead. By adding ethanethiol to a sodium hydride slurry, sodium ethanethiolate formed, which proved capable of deprotecting the phenol (**Scheme 2.12**). The thiolate anions, being strongly nucleophilic, were capable of attacking the methyl group by nucleophilic substitution, freeing the phenol. Compound **13** was obtained with a yield of 93%, close to the analogous 3,5-dimethyl compound prepared Diemer et al., with a yield of 96%. The other similar 3,5-disubstituted compounds produced by this group gave yields as low as 89%. Following this step, FTIR spectra now presented a band near 3600 $cm^{-1}$, associated with a O-H bond (Appendix, **Figure 6.72**), while the $^{1}H$ spectra no longer presented a signal caused by a methoxy group at 3.73 ppm, and the remaining signals indicated that the structure didn't suffer further degradation through the reaction (Appendix, **Figure 6.70**).

Another methyl group was added to the structure, this time to the pyridine, by methylation with iodomethane (**Scheme 2.12**). This reaction was performed in acetone, in the absence of base, to ensure the oxygen of the phenol would not be methylated, only the nitrogen of the pyridine. This strategy was successful, as the FTIR spectra of compound **14** still presented a band near 3600 $cm^{-1}$, associated with a hydroxyl group, while the $^{13}C$ spectra of the methylpyridinium, as opposed to the anisole, presented no peak associated with the methoxy carbon (Appendix, **Figures 6.73** and **6.75**), as it appeared for the anisole **12**, at 64.50 ppm (Appendix, **Figure 6.68**). The yield of this reaction was 98%, similarly to the yield of 97% reported for the 3,5-dimethyl analogue.

The final step of the synthesis was the deprotonation of the phenol to form the zwitterionic compound (**15**). This was first attempted using as base $(n\text{-}Bu)_4NOH$ in methanol, as similar compounds were reported to have comparable solubilities to NaOH and KOH[37]. However, this base was also too difficult to separate, and the pure product could not be recovered. As alternative to using a soluble base, Amberlyst A26 OH resin was used. As a basic resin, it could be used to perform the deprotonation, and due to its insolubility, the compound could be separated easily by filtering the resin. The deprotonation was observed by a color change to a deeper red color, as well as the disappearance of the band near 3600 $cm^{-1}$ in the FTIR spectra. This procedure resulted in a yield of 91%, differing significantly from that of the previously reported 3,5-dimethyl analogue, with a yield of 56%. However, similar compounds present yield that vary greatly, 56% being the lowest and going up to 93% for the 3,5-diethyl. Also important to note, Diemer et al. used the procedure previously mentioned, of $(n\text{-}Bu)_4NOH$ in methanol to deprotonate the iodide salts, followed by recrystallization, whereas the procedure used here involved the usage of a resin, without further purification

In order to study this zwitterion by cyclic voltammetry, both in its neutral as well as protonated state, the triflate salt **16** was prepared from the iodide salt **14**. As iodine is electrochemically active in electrochemical window used to study these compounds, it had to be replaced with an inert ion such as

triflate. This ion exchange was performed in DCM as the reaction would produce sodium iodide, which is highly insoluble in this solvent, and therefore could be easily separated. This reaction gave a yield of 79%, likely resulting from a loss of product still dissolved in the removed solvent. The presence of the triflate ion was confirmed by $^{19}F$ NMR, with a signal at -80.06 ppm as well as by FTIR spectra, by the appearance of a band at 1260 $cm^{-1}$, associated with the C-F bond, and by mass spectrometry in negative mode, as it displayed a peak caused by triflate anions, with m/z value of 149.0. However, not all iodide ions were removed, as the MS spectra in negative mode presented a peak at 126.9, as well as the CV of this compound exhibiting electron transfers associated with iodine. Results to be presented in the following section.

## 2.4 Cyclic Voltammetry studies

Cyclic voltammetry studies were performed for all diphenoquinones (**3**), hydrodiphenoquinones (**4**) and hydrobenzoquinones (**2**), as well as the zwitterionic pyridinium phenolate (**15**), 4-(4-pyridinyl)phenol (**13**), and 4-(4-hydroxyphenyl)methylpyridinium triflate (**16**). The measurements were made in a 3 electrode cylindrical electrochemical cell, the working electrode used was a glassy carbon electrode with diameter of 3 mm, the counter-electrode used was a platinum wire, and the reference electrode was a saturated calomel electrode. All measurements were done using as supporting electrolyte 0.1 M tetrabutylammonium hexafluorophosphate and a concentration of 1 mM of the compound to be studied, in acetonitrile, except for tetraphenyl diphenoquinone (**3a**) due to its low solubility in this solvent. This diphenoquinone (**3a**) was instead studied in DMF, along with its respective hydrodiphenoquinone (**4a**), and the other diphenoquinones (**3b** and **3c**), to allow these compounds' properties to be compared.

The standard potential (potential for the reversible electron transfers) was calculated as the average set by the peak cathodic and peak anodic voltages (**Table 2.1**). The number of electrons associated with an electron transfer was calculated by comparison to the standard ferrocene electrochemical probe in the same experimental conditions. The reversibility of reversible ETs was calculated using the formula $i_{pa}/i_{pc}$, $i_{pa}$ being peak anodic current and $i_{pc}$ peak cathodic current.

**Table 2.1** – Potentials of the most significant electron transfers for all compounds studied. These potentials were measured at a scan rate of 0.100 V/s.

| Compound | Solvent | Potential (V vs. SCE) | | | | | |
|---|---|---|---|---|---|---|---|
| | | $E^0_1$ | $E^0_2$ | $E_{pa1}$ | $E_{pc1}$ | $E_{pa2}$ | $E_{pc2}$ |
| Ph DQ (**3a**) | DMF | -0.09 | -0.47 | -0.06 | -0.13 | -0.43 | -0.51 |
| tBu DQ (**3b**) | ACN | -0.53 | -0.92 | -0.49 | -0.56 | -0.88 | -0.96 |
| | DMF | -0.35 | -0.87 | -0.31 | -0.39 | -0.81 | -0.92 |
| iPr DQ (**3c**) | ACN | -0.46 | -0.81 | -0.42 | -0.50 | -0.76 | -0.85 |
| | DMF | -0.32 | -0.75 | -0.28 | -0.35 | -0.70 | -0.79 |
| Ph HDQ (**4a**) | ACN | - | - | 0.98 | 0.73 | 1.13 | 0.99 |
| | DMF | - | - | 0.78 | 0.32 | - | - |
| tBu HDQ (**4b**) | ACN | - | - | 1.06 | 0.64 | - | - |
| iPr HDQ (**4c**) | | - | - | 1.05 | 0.75 | - | - |
| Ph HBQ (**2a**) | | - | - | 0.76 | 0.34 | 1.04 | 0.65 |
| tBu HBQ (**2a**) | | - | - | 1.00 | - | - | - |
| iPr HBQ (**2a**) | | - | - | 1.00 | 0.63 | 1.84 | 0.88 |
| Pyridinylphenol (**13**) | | - | - | 1.63 | -1.42 | - | - |
| Zwitterionic pyridinium phenolate (**15**) | | -1.48 | - | -1.44 | -1.51 | 1.64 | - |
| Phenolpyridinium triflate (**16**) | | -1.41 | - | -1.37 | -1.46 | 1.70 | - |

## 2.4.1 Diphenoquinones

All diphenoquinones presented two reversible mono-electronic electron transfers (ET), the first one being associated with first reduction of the diphenoquinones leading the formation of the semiquinone radical anion, and the second reductions leading to the formation of the dianion (see **Table 2.2** and **Graphic 2.1**). These compounds in the oxidation displayed chemical irreversible ET at potentials near 1.82 V vs. SCE in ACN and near 1.67 V vs. SCE in DMF, as shown in **Graphic 2.1**. Tetraphenyl diphenoquinone (**3a**) also displayed several smaller chemical irreversible ET. A possible explanation for these ETs is that these transfers are somehow related to the extended conjugation system of the compound, as reactions might occur on the phenyl rings.

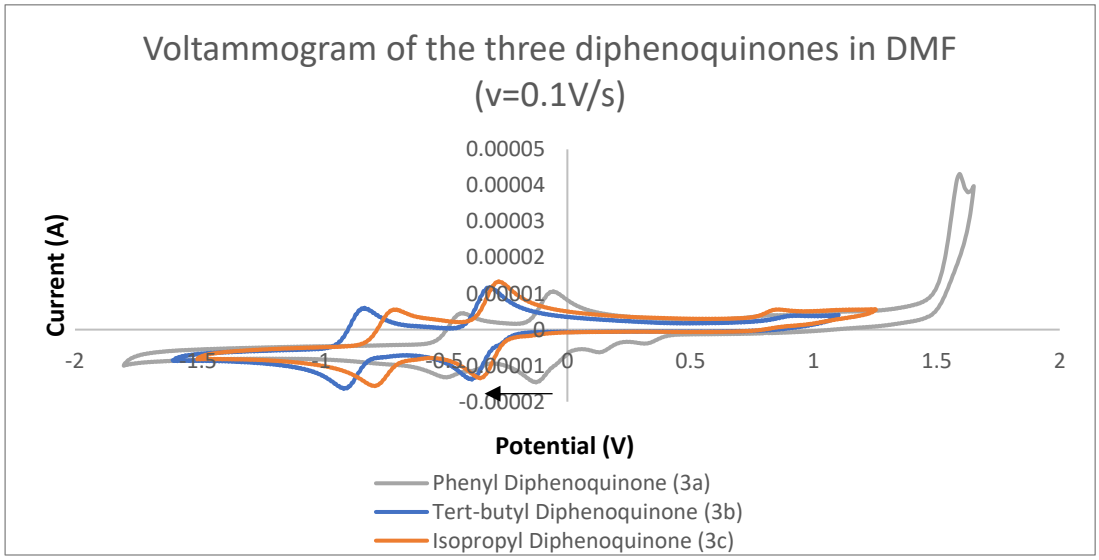


**Graphic 2.1** – Voltammograms of the three diphenoquinones in DMF, at a scan rate of 0.100 V/s.

**Table 2.2** – Potentials of the most significant electron transfers of diphenoquinones. These potentials were measured at a scan rate of 0.100 V/s.

| Solvent | R Group | Standard Potential (V vs. SCE) | |
|---|---|---|---|
| | | $E^0_1$ | $E^0_2$ |
| DMF | Ph (**3a**) | -0.09 | -0.47 |
| | tBu (**3b**) | -0.35 | -0.87 |
| | iPr (**3c**) | -0.32 | -0.75 |
| ACN | tBu (**3b**) | -0.53 | -0.92 |
| | iPr (**3c**) | -0.46 | -0.81 |

Tetraphenyl diphenoquinone (**3a**) was studied in DMF rather than ACN, unlike all the other compounds, due to its insolubility in this solvent. Also in this electrolyte reduction of the diphenoquinones leading the formation of the semiquinone radical anion, and the second reduction leading to the formation of the dianion are both stable at all studied scan rates, with standard potential for the ETs at $E^0$= -0.09 V and $E^0$= -0.47 V vs. SCE, see **Table 2.2**. The first and second reversible ETs have, respectively, approximate reversibilities of 80% and 100%.

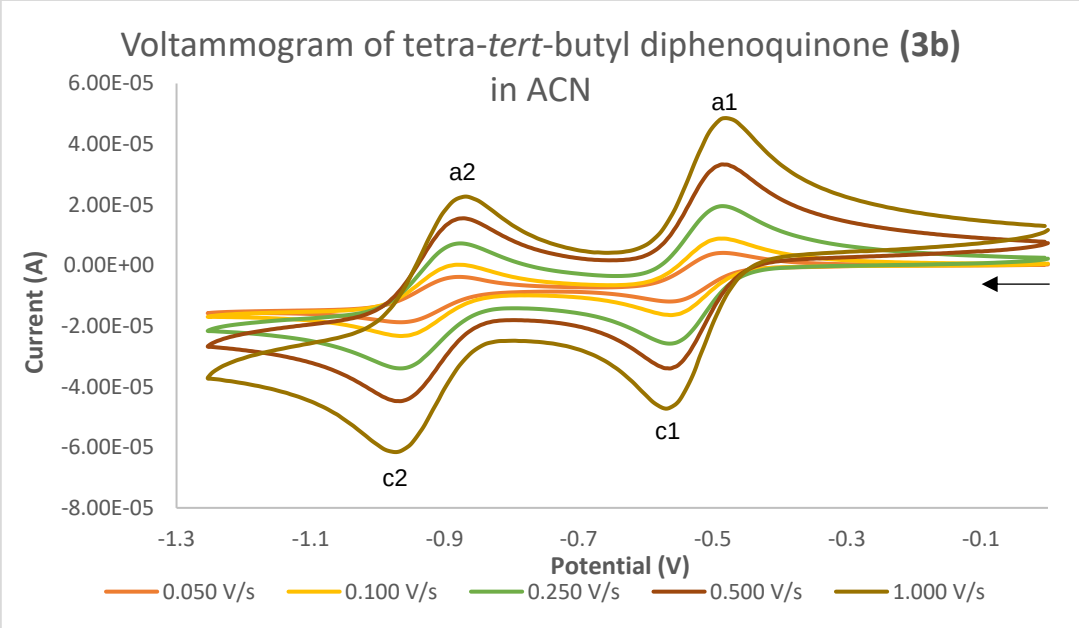


**Graphic 2.2** – Voltammograms of tetra-*tert*-butyl diphenoquinone (**3b**) in ACN, at multiple scan rates.

Tetra-*tert*-butyl diphenoquinone (**3b**) was studied in ACN, as well as DMF, so that it could be compared to tetraphenyl diphenoquinone. In both solvents it exhibited two mono-electronic ETs that were reversible at all studied scan rates, as seen in **Graphic 2.2**. In ACN, these ETs occurred at $E^0$= -0.53 V and $E^0$= -0.92 V vs. SCE, while in DMF they occurred at $E^0$= -0.35 V and $E^0$= -0.87 V vs. SCE. Both ETs presented, in both solvents, reversibilities of approximately 100%. It's more difficult to form the radical anion and dianion in ACN than in DMF, that's why the shift to more negative potentials occurs. Of all the diphenoquinones studied, this one presented the lowest potentials, as such it would be the most fit as an anolyte in RFBs, leading to increased cell voltages.

Tetraisopropyl diphenoquinone (**3c**) was also studied in both ACN and DMF. In both solvents two mono-electronic ETs were presented, being reversible, the radical anion and dianion formed are stable in both electrolyte at all studied scan rates. In ACN then ETs occur at $E^0$= -0.46 V and $E^0$= -0.81 V vs. SCE, while in DMF they occur at $E^0$= -0.32 V and $E^0$= -0.75 V vs. SCE following the same trend observed for the tetra-*tert*-butyl diphenoquinone that is harder to form the radical anion in acetonitrile. The first ET presented a reversibility of approximately 75% in ACN and 90% in DMF, while for the second ET it was approximately 100% in both solvents.

The three diphenoquinones presented two reversible mono-electronic ETs in all scan rates studied. Of these compounds, the tetra-*tert*-butyl diphenoquinone (**3b**) presented ETs at lowest potentials. As cell voltage is the difference between the standard potentials of the two redox pairs used in an RFB,

using an anolyte with lower reduction potentials leads to higher cell voltage, and as a result compound **3b** would be the studied diphenoquinone most fit to be used in an RFB.

## 2.4.2 Hydrodiphenoquinones

The hydrodiphenoquinones studied here presented either irreversible or quasi-reversible mono-electronic ET (**Table 2.3**). The irreversibility is associated to a chemical reaction of the species formed by the oxidation step, occurring faster than the reduction process. A possible explanation is the loss of an electron, forming a radical cation that then deprotonates, in turn forming a radical that reacts further. When moving to more negative potentials, the species being reduced is no longer the same as the one formed from the oxidation the cathodic peak is further away from the anodic peak.

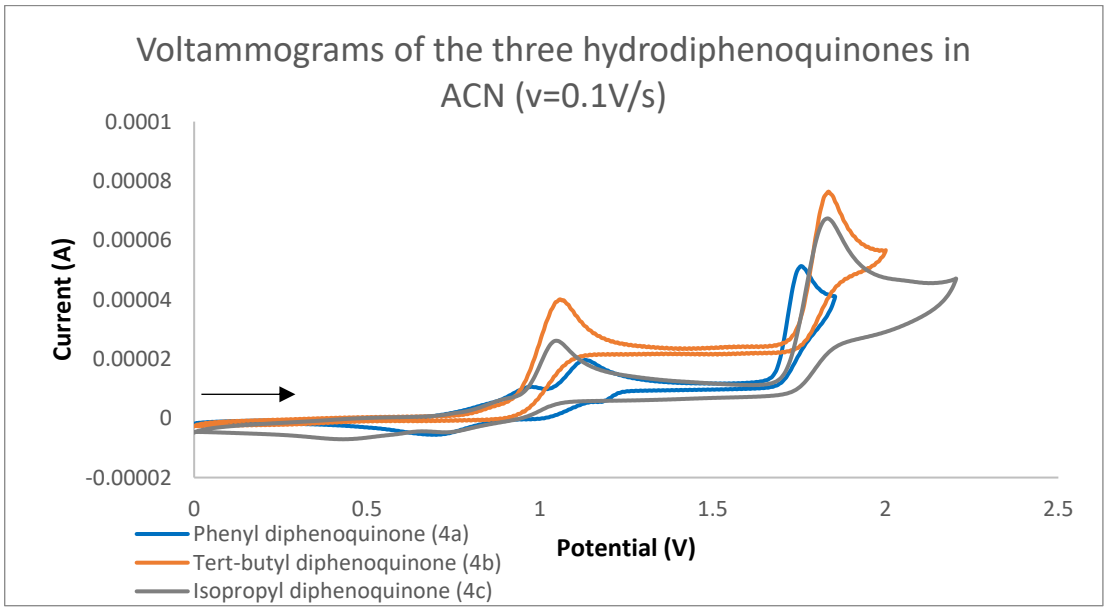


**Graphic 2.3** - Voltammograms of the three hydrodiphenoquinones in ACN, at a scan rate of 0.100 V/s

The hydrodiphenoquinones, like the respective diphenoquinones, also displayed an anodic peak near 1.8 V vs. SCE, as seen in **Graphic 2.3**. A possible explanation is related to the diphenoquinones, because part of them could be formed from the oxidation of the hydrodiphenoquinones.

**Table 2.3** – Potentials of the most significant electron transfers of hydrodiphenoquinones. These potentials were measured at a scan rate of 0.100 V/s.

| Solvent | R Group | Potential (V vs. SCE) | | | |
|---|---|---|---|---|---|
| | | $E_{pa1}$ | $E_{pa2}$ | $E_{pc1}$ | $E_{pc2}$ |
| DMF | Ph (**4a**) | 0.78 | - | 0.32 | - |
| ACN | Ph (**4a**) | 0.98 | 1.13 | 0.73 | 0.99 |
| | tBu (**4b**) | 1.06 | - | 0.64 | - |
| | iPr (**4c**) | 1.05 | - | 0.75 | - |

Tetraphenyl hydrodiphenoquinone (**4a**), in ACN, displayed multiple ETs (**Graphic 2.4**). At scan rates of 0.250 V/s and lower, it displayed three anodic peaks, the first of which disappears at higher scan rates, a possible explanation is the overlapping by the second and third anodic peaks. These three transfers occurred approximately at $E_{pa}$= 0.87 V, $E_{pa}$= 0.98 V and $E_{pa}$= 1.13 V vs. SCE, presenting a slight displacement to higher potentials as the scan rate increased. It also observed two cathodic peaks, approximately at $E_{pc}$= 0.73 V and $E_{pc}$= 0.99 V vs. SCE. The two peaks a2 and c2 presented a reversibility of approximately 50%. In DMF, however, in this electrolyte it is observed only one anodic peak at $E_{pa}$= 0.78 V and one cathodic peak at $E_{pc}$= 0.32 V vs. SCE.

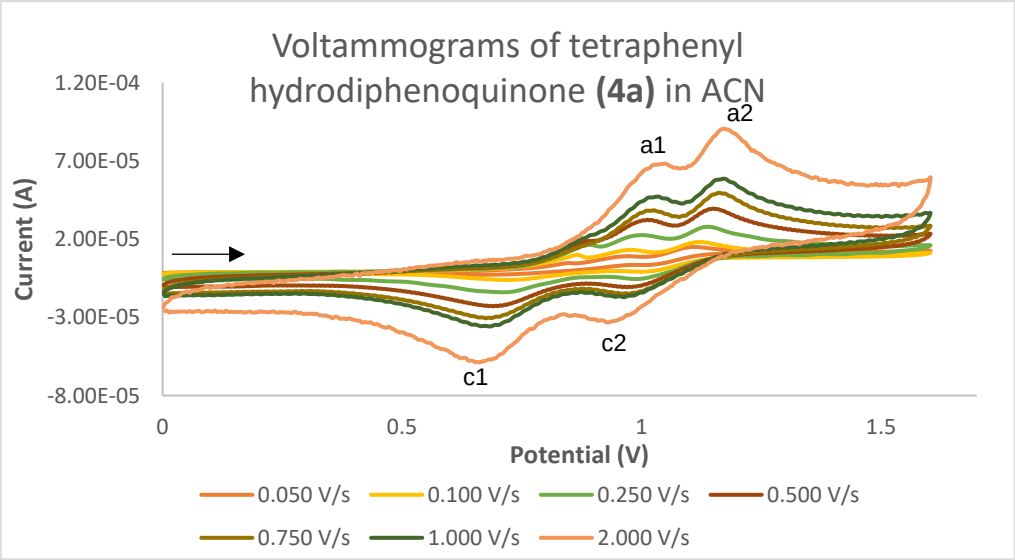


**Graphic 2.4** – Voltammograms of tetraphenyl hydrodiphenoquinone (**4a**) in ACN, at multiple scan rates

Tetra-*tert*-butyl hydrodiphenoquinone (**4b**) presented a chemical irreversible ET, with an anodic peak at $E_{pa}$= 1.06 V vs. SCE and a cathodic peak $E_{pc}$= 0.64 V vs. SCE. This cathodic ET is absent at scan rates lower than 0.250 V/s, and steadily becoming bigger at higher scan rates see **Graphic 2.4**.

Tetraisopropyl diphenoquinone (**4c**) displayed an ET with quasi-reversible behavior. An anodic peak occurs at $E_{pa}$= 1.05 V vs. SCE and a cathodic peak at $E_{pc}$= 0.75 V vs. SCE.

No hydrodiphenoquinones presented fully reversible ETs, however compound **2a** was the closest. It presented the highest standard potentials, as well as highest reversibility, so, of this group, it would be the most useful in an RFB

## 2.4.3 Hydrobenzoquinones

Hydrobenzoquinones behaved similarly to the hydrodiphenoquinones (**Graphic 2.5**). These presented chemical irreversible mono-electronic ETs **(Table 2.4).** As described for the hydrodiphenoquinones a possible explanation for the irreversibility is that it is associated to a chemical reaction of the species formed by the oxidation step faster than the redox process.

It is possible that the species formed is a radical cation, which immediately loses a proton to form a semiquinone radical.

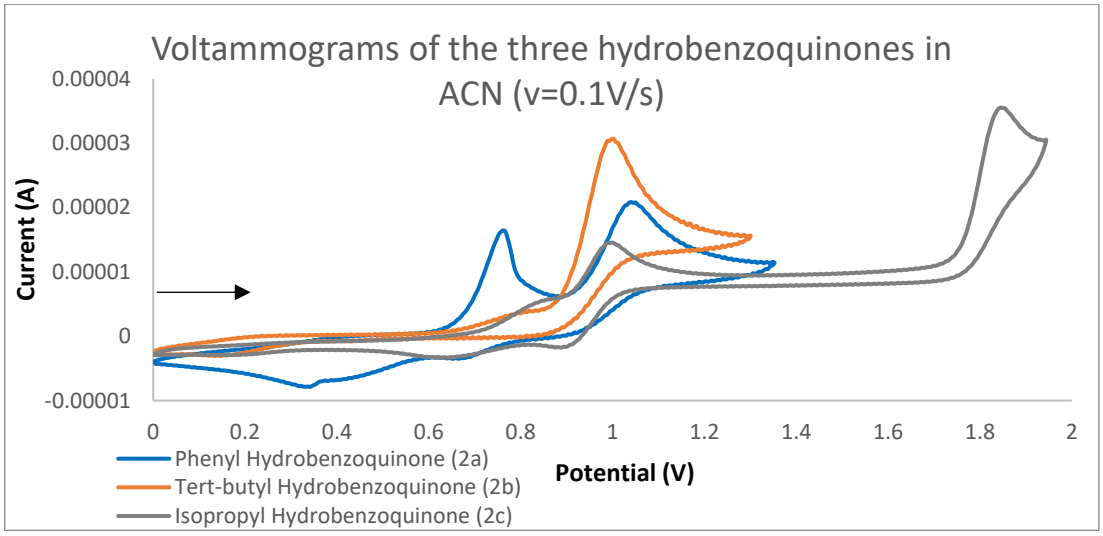


**Graphic 2.5** - Voltammograms of the three hydrobenzoquinones in ACN, at a scan rate of 0.100 V/s.

**Table 2.4** – Potentials of the most significant electron transfers of hydrobenzoquinones. These potentials were measured at a scan rate of 0.100 V/s.

| R Group | Potential(V vs. SCE) | | | |
|---|---|---|---|---|
| | $E_{pa1}$ | $E_{pa2}$ | $E_{pc1}$ | $E_{pc2}$ |
| Ph (**2a**) | 0.76 | 1.04 | 0.34 | 0.65 |
| tBu (**2b**) | 1.00 | - | - | - |
| iPr (**2c**) | 1.00 | 1.84 | 0.63 | 0.88 |

The diphenyl hydrobenzoquinone presented several chemical irreversible ETs (**Graphic 2.6**). The first anodic peak appears at $E_{pa}$= 0.76 V vs. SCE, at scan rates lower than 0.500 V/s. The second anodic peak is presented at approximately $E_{pa}$= 1.04 V vs. SCE. Two cathodic peaks are also present, the first of which is located at $E_{pc}$= 0.34 V and the second at $E_{pc}$= 0.65 V vs. SCE, the second one appearing only at scan rates equal or higher than 0.500 V/s.

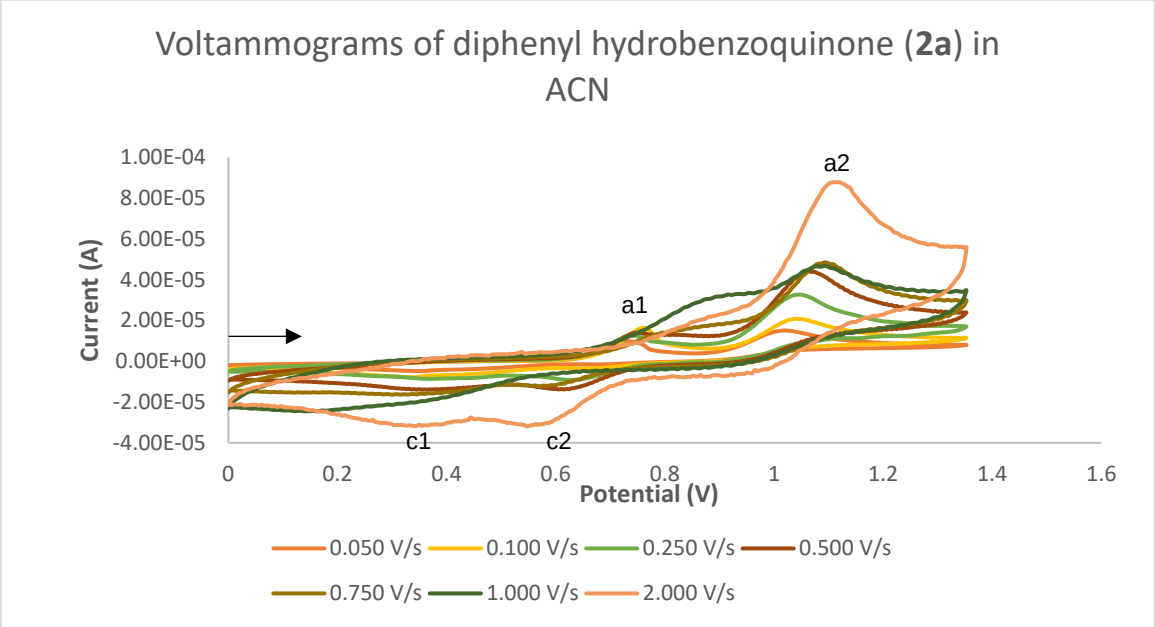


**Graphic 2.6** - Voltammograms of diphenyl hydrobenzoquinone (**2a**) in ACN, at multiple scan rates.

The di-*tert*-butyl hydrobenzoquinone presents only one chemical irreversible mono-electronic ET, with an anodic peak $E_{pa}$= 1.00 V vs. SCE, and a small cathodic peak $E_{pc}$= 0.34 V vs. SCE.

The diisopropyl hydrobenzoquinone presents two chemical irreversible ETs, displaying two anodic peaks at $E_{pa}$= 1.00 V and $E_{pa}$= 1.89 V vs. SCE, and two cathodic peaks at $E_{pc}$= 0.63 V and $E_{pc}$= 0.88 V vs. SCE. The anodic peak at 1.89 V vs. SCE appears to be unique among the studied hydrobenzoquinones, however it is similar to that presented by the diphenoquinones and hydrodiphenoquinones.

No hydrobenzoquinone stands out, as the three present an irreversible ET at $E_{pa}$~ 1.00 V vs. SCE, with compound **2c** presenting an ET at $E_{pa}$= 1.84 V vs. SCE as well, although it is completely irreversible, so these compounds may not be fit for use in RFBs.

## 2.4.4 Zwitterionic pyridinium phenolates

The zwitterionic pyridinium phenolate, as well as the pyridinyl phenol and pyridinium phenol triflate were studied in ACN (**Graphic 2.7**). The pyridinyl phenol revealed a chemical irreversible ETs at $E_{pc}$ = -1.42V while the zwitterion and the triflate salt revealed one ET at $E^0$= -1.48 and 1.41 V vs. SCE, respectively (**Table 2.5**).

The pyridinylphenol **13** presented two chemical irreversible ETs, with a cathodic peak at $E_{pc}$= -1.42 V vs. SCE and an anodic peak at $E_{pa}$= 1.63 V vs. SCE. This compound is analogous to the triflate salt **16**, with a cathodic peak at $E_{pc}$= -1.46 V vs. SCE and an anodic peak at $E_{pa}$= 1.37 V vs. SCE, that makes the compound 1**6** harder to reduce and easier to oxidize than compound **13**. Their structures differ by the lack of a methyl group bonded to the nitrogen in the pyridine, as well as having no positive charge in that nitrogen. Probably, the lack of these traits may be enough to cause the ET at -1.42 V vs. SCE to be irreversible, whereas it is reversible in the zwitterion and the triflate salt.

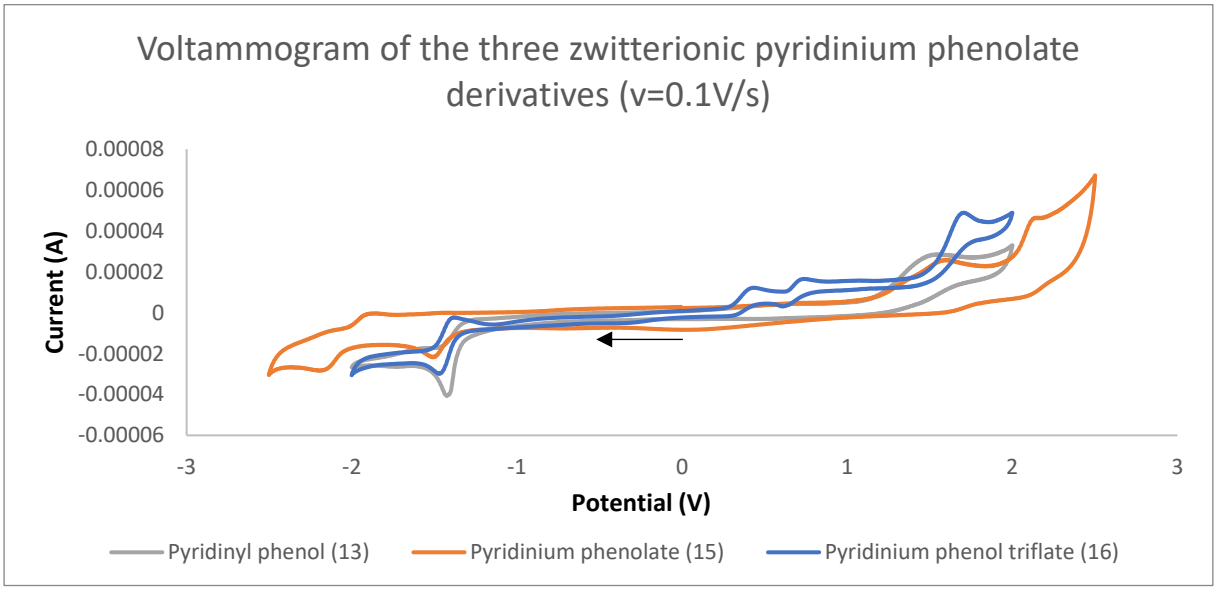


**Graphic 2.7** - Voltammograms of the three zwitterionic pyridinium phenolate derivatives in ACN, at a scan rate of 0.100 V/s.

**Table 2.5** – Potentials of the most significant electron transfers of zwitterionic pyridinium phenolate derivatives. These potentials were measured at a scan rate 0.100 V/s

| Compound | Potential (V vs. SCE) | | | | |
|---|---|---|---|---|---|
| | $E^0$ | $E_{pa1}$ | $E_{pc1}$ | $E_{pa2}$ | $E_{pc2}$ |
| Pyridinylphenol (**13**) | - | 1.63 | -1.42 | - | - |
| Pyridinium phenolate (**15**) | -1.48 | -1.44 | -1.51 | 1.64 | - |
| Triflate salt (**16**) | -1.41 | -1.37 | -1.46 | 1.70 | - |

The zwitterion **15** presented a chemical irreversible ET with an anodic peak at $E_{pa}$= 1.64V vs. SCE, as well as a reversible mono-electronic ET (**Graphic 2.8**), with a reversibility of approximately 70%, at $E_{pc}$= - 1.51 V ($E^0$= -1.48 V vs. SCE). This presents the most negative potential of all the compounds studied here and, therefore, could be the most effective anolyte studied here.

The triflate salt **16** presented a chemical irreversible ET at $E_{pa}$= 1.70 V vs. SCE, as well as a reversible mono-electronic ET, with a reversibility of approximately 50%, at $E_{pc}$= -1.37 V ($E^0$= -1.41 V vs. SCE). This value is similar to that of the zwitterion's reversible ET, despite the compound being protonated in its oxygen atom and having a positive charge. The voltammogram also presented ETs at $E_{pc}$~ 0.48 V and $E_{pc}$~ 0.77 V vs. SCE, caused by the presence of iodide ions, revealing that the synthetic procedure for this compound failed to remove all iodine.

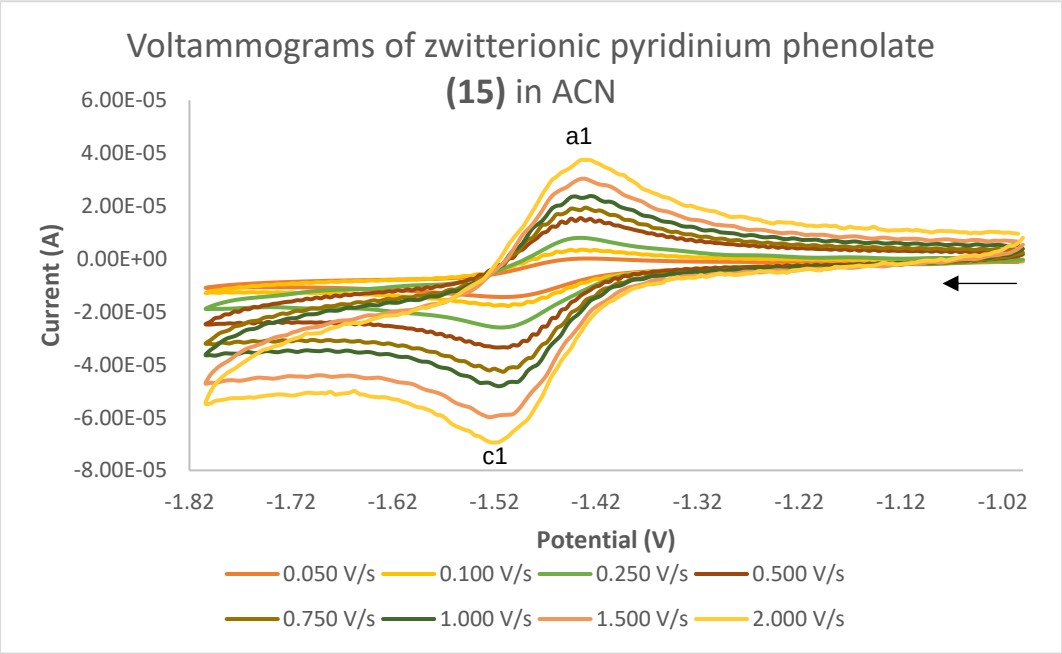


**Graphic 2.8** - Voltammograms of the zwitterionic pyridinium phenolate in ACN, at multiple scan rates.

Among the pyridine phenol derivatives, the zwitterion **15** presented the lowest standard potential, of $E^0$= -1.48 V vs. SCE, which makes it the best option of this group to be used as an anolyte in RFBs, with the triflate salt **16** a second-best alternative because its $E^0$= -1.41 V vs. SCE.

Comparing the zwitterion **15** with the tetra-*tert*-butyl diphenoquinone **3b**, however is somewhat more difficult, as the diphenoquinone, despite having two ETs at higher potentials of $E^0_1$= -0.53 V and $E^0_2$= -0.92 V vs. SCE, can transfer two electrons per molecule, and could have higher solubility, so the energy densities achievable by each anolyte are more difficult to compare.

# 3. CONCLUSIONS

Several compounds to be studied by cyclic voltammetry were synthesized in this work, namely diphenoquinones (**3**), hydrodiphenoquinones (**4**), hydrobenzoquinones (**2**) and zwitterionic pyridinium phenolates (**15**). Benzoquinones (**1**) were also prepared, however these were not studied by CV.

Benzoquinones (**1**) were produced by oxidation of phenols with DIB, giving moderate (60%) to high yields as 85%, while diphenoquinones (**3**) were producing by oxidation with CAN, giving yields varying between 60% and 90%. Both reaction procedures revealed to produce both benzoquinone (**1**) and diphenoquinone (**3**), however the procedure with DIB favored the benzoquinones (**1)**, while the one with CAN favored the diphenoquinones (**3**). The unfavored quinones was produced in small amounts that were easy to separate without a significant decrease in yield.

Hydrobenzoquinones (**2**) and hydrodiphenoquinones (**4**) were produced by the reduction of the benzoquinones (**1**) and diphenoquinones (**3**), respectively, with zinc in acetic acid, producing high yields of 90%.

One zwitterionic pyridinium phenolate compound (**15**) was produced, after a longer synthesis pathway, following the protection of the phenol by methylation (**5**), and then bromination (**6**) followed by a Miyaura borylation to produce the anisole boronic acid pinacol ester (**7**). The pyridine moiety was in turn prepared by nitration (**9**) of a commercial disubstituted pyridine N-oxide followed by substitution of the nitro group by bromine (**10**). The boronic ester (**7**) and bromopyridine N-oxide (10) were then successfully coupled in a palladium catalyzed Suzuki-Miyaura coupling reaction, forming a biaryl (**11**) that would then be reduced and deprotected.

The initial attempt to do the demethoxylation of anisole with HBr in AcOH failed, possibly due to the removal of a *tert*-butyl group of the compound. A second procedure was then attempted, using sodium thiolate as nucleophile to deprotect the phenol, which happened successfully, forming a pyridinyl phenol (**13**). After methylation with iodomethane formed the iodide salt, a sample of this salt was deprotonated to form the zwitterion. The first attempt at deprotonation was done with $NH_4OH$ in methanol, however it proved too difficult to separate from the product. Instead, a successful procedure was appliyed, using Amberlyst A26 to deprotonate the iodide salt.

A part of this iodide salt was also used in the preparation of the triflate salt, by ion exchange, so that the zwitterion could be studied in neutral and protonated forms. These two compounds, along with the pyridinyl phenol, had their electrochemical properties studied by cyclic voltammetry.

The diphenoquinones (**3**) exhibited two reversible ETs, each involving one electron, at negative potentials. The tetra-*tert*-butyldiphenoquinone (**3b**) revealed the most negative redox potentials, of -0.52 V vs. SCE for the first transfer, and -0.92 V vs. SCE for the second, with both ETs being fully reversible. This could lead to higher differences between the half-cell potentials, that is, higher cell voltages. As a result, this diphenoquinone is the most suited for use in RFBs.

The anodic behavior of the tetraphenyl hydrodiphenoquinone, (**4a**) displayed multiple ETs each involving one electron with peak anodic potentials at $E_{pa}$= 0.87 V, $E_{pa}$= 0.98 V and $E_{pa}$= 1.13 V vs. SCE, and cathodic peak potentials $E_{pc}$= 0.73 V and $E_{pc}$= 0.99 V vs. SCE, with a reversibility between the second pair of ETs of approximately 50%. As a result, the tetraphenyl hydrodiphenoquinone is the most suited for use in RFBs.

The hydrobenzoquinones (**2**) all exhibited either irreversible or quasi-reversible electron transfers, which would lead to power losses, so they are not fit for use in RFBs.

The pyridinyl phenol (**13**) only showed irreversible electron transfers, so it has no applications in RFBs. The zwitterion (**15**) and triflate salt (**16**), however, both showed a reversible one-electron transfer.

The zwitterion and the triflate salt exhibit transfers at -1.46 V and -1.39 V vs. SCE, respectively, although, these aren't entirely reversible, with a reversibility around 70% for the zwitterion and 50% for the triflate salt. Depending on other factors, such as solubility and cost, of all the compounds studied in this work, these ones might be the most promising for use in RFBs.

There are still challenges to deal with, however, as these compounds were only studied by cyclic voltammetry, the first step in the study of their applicability for RFBs. Further ahead, it would be necessary to try using these compounds in a RFB prototype, for which much greater quantities of the compounds would be needed, quantities that the procedures followed in this work might not be capable of producing, so a way to upscale their production is likely necessary.

The solubilities of the studied compounds should also be tested in other RFB-compatible solvents. As concentration of the ORM is directly proportion to power capacity, using solvents in which the compounds can reach higher concentrations would lead to more powerful RFBs.

Future work should also involve other zwitterionic pyridinium phenolates. We successfully completed the synthesis of a zwitterionic pyridinium phenolate. Although we initiated the synthesis of another compound, time constraints prevented us from completing the entire synthesis. It would be interesting to find out what effect other substituents on the rings could have, or even to see what an increase in the interplanar angle of the two aromatic rings would do to these compounds' electrochemical properties.

# 4. EXPERIMENTAL PROCEDURE

## 4.1 General Information

All reagents and solvents were obtained commercially from TCI, Sigma-Aldrich, Scharlau and Honeywell without further purification. When dry solvents were required, these were dried by addition of the solvent to 3Å molecular sieves from Carlo Erba that had been previously activated by exposure to microwaves for 8 minutes, stopping every minute to stir the sieves to ensure no sintering would occur. Afterwards, the sieves were allowed to cool down under vacuum for a few hours. Then, the solvent could be added to the sieves and could be used after drying for 24 hours.

Nuclear magnetic Resonance (NMR) spectra were acquired by a Bruker Avance III 400 spectrometer, $^{1}H$, $^{13}C$ and $^{19}F$ spectra were measured at frequencies 400 MHz, 101 MHz and 376 MHz, respectively. 1H NMR spectra were described by frequency, in MHz, deuterated solvent used, chemical shift, δ, in ppm, multiplicity, coupling constants, J, in Hz, number of protons, and corresponding protons. $^{13}C$ and $^{19}F$ spectra were described by frequency, in MHz, deuterated solvent used, and chemical shift, δ, in ppm.

Infrared spectroscopy (IR) was done using a PerkinElmer Spectrum Two FT-IR Spectrometer, spectra data was acquired by the Spectrum 10 software. The spectra were obtained in ATR mode between 400 and 4000 $cm^{-1}$ over 4 scans, data is presented as: sample holder, wavenumber of peak, and identification of functional group.

LC-MS spectrometry data was acquired using a LC Agilent 1200 Series with Binary pump and MS Agilent 6130B Single Quadrupole with an API-ES ionization source. A G1316A column was used, with three 30 cm columns, with an injection volume of 1 µL and flow of 0.400 mL/min. The mass spectrometer conditions used were: drying gas temperature of 350ºC, drying gas flow rate of 12 L/min, VCap of 4000 V for both positive and negative mode.

Cyclic voltammetry was performed using a Autolab PGSTAT12 Potentiostat/Galvanostat Electrochemical System, the data was collected using the software GPES Manager 4.9. The measurements were made in a glass cylinder electrochemical cell, the working electrode used was a glassy carbon electrode with diameter of 3 mm, the counter-electrode used was a platinum wire, and the reference electrode was a saturated calomel electrode. The samples were prepared by dissolving the compound (1 mM) and supporting electrolyte (1 M) in dry solvent (ACN or DMF), followed by the addition of 3Å molecular sieves. The solution was then degassed with argon for 10 minutes. Following this, the CV measurements were done at multiple scan rates. Between each measurement, the working electrode was washed with ethanol and polished in 1.0 mm and 0.3 mm alumina polishings and washed again, while the solution was kept being degassed with argon in the downtime.

## 4.2 Synthesis of benzoquinones

Benzoquinones were produced by adding to a round bottom flask ACN (6.5 mL/mmol), $H_2O$ (2 mL/mmol), the respective phenol, and the oxidizer DIB by slow addition. The reaction was kept stirring at 0ºC in an ice bath until completion. Upon completion, the flask temperature was allowed to reach RT, and the solution was then diluted with water and extracted with DCM. The organic phase was then dried with anhydrous $Na_2SO_4$ and evaporated under reduced pressure. The compounds were purified by flash chromatography using a mixture of solvents petroleum ether and DCM.

### 4.2.1 Synthesis of 2,6-diphenyl-1,4-benzoquinone (1a)

Following the procedure described above, 2.73 mL ACN, 0.82 mL $H_2O$, 100 mg of 2,6-diphenylphenol (0.41 mmol), and 264.12 mg DIB (0.82 mmol) were added to a round bottom flask and left to react at 0ºC for 1 hour. After the workup, the crude product was purified by flash chromatography, using as eluent a mixture of 6:4 petroleum ether and DCM, to give 91.9 mg of the product (yield of 86%).

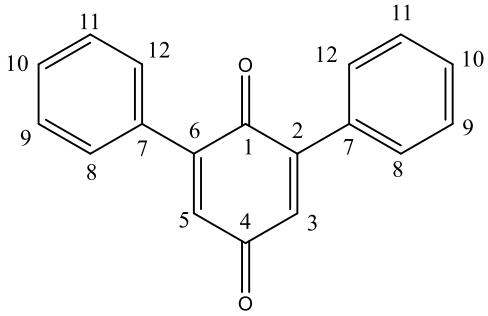

**1a**

**IR (ATR) $\nu_{max}$ ($cm^{-1}$):** 3057.7 (C-H Ar), 3036.6 (C-H alkene), 1659.2 (C=O conjugated ketone), 1646.5 (C=C conjugated alkene), 1591.5, 1494.4, 1447.9, 1304.2, 1109.9, 911.3, 750.7, 691.6.
**$^1$H NMR (400 MHz, $CDCl_3$) δ** 7.54-7.45 (m, 10H, H-8/9/10/11/12), 6.93 (s, 2H, H-3/5).
**$^{13}$C NMR (101 MHz, $CDCl_3$) δ** 187.72, 186.25, 146.63, 133.31, 132.76, 130.17, 129.53, 128.62.

### 4.2.2 Synthesis of 2,6-tert-butyl-1,4-benzoquinone (1b)

Following the procedure described above, 3.2 mL ACN, 0.96 mL $H_2O$, 100 mg of 2,6-di-*tert*-butylphenol (0.48 mmol), and 309.21 mg DIB (0.96 mmol) were added to a round bottom flask and left to react at 0ºC for 2 hours. After the workup, the crude product was purified by flash chromatography, using as eluent a mixture of 7:3 petroleum ether and DCM, to give 66.0 mg of the product (yield of 62%).

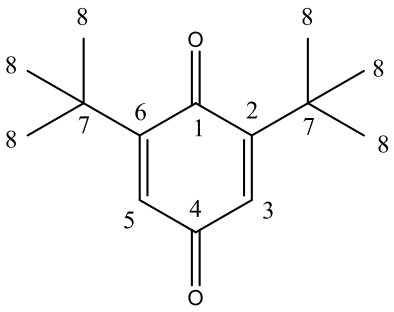

**1b**

**IR (ATR) $\nu_{max}$ ($cm^{-1}$):** 2956.7 (C-H aliphatic), 1667.3 (C=O conjugated ketone), 1655.8 (C=C conjugated alkene), 1600.1, 1457.4, 1362.6 (C-H gem dimethyl), 1318.8, 1245.2, 1156.7, 1074.7, 917.8, 880.1.
**$^1$H NMR (400 MHz, $CDCl_3$) δ** 6.50 (s, 2H, H-3/5), 1.28 (s, 18H, H-8).
**$^{13}$C NMR (101 MHz, $CDCl_3$) δ** 189.23, 187.94, 158.05, 130.28, 35.71, 29.52.

#### 4.2.3 Synthesis of 2,6-isopropyl-1,4-benzoquinone (1c)

Following the procedure described above, 3.73 mL ACN, 1.12 mL $H_2O$, 100 mg of 2,6-diisopropylphenol (0.56 mmol), and 361.36 mg DIB (1.12 mmol) were added to a round bottom flask and left to react at 0ºC for 1 hour. After the workup, the crude product was purified by flash chromatography, using as eluent a mixture of 6:4 petroleum ether and DCM, to give 89.2 mg of the product (yield of 83%).

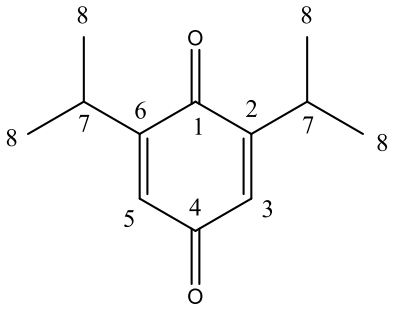


**1c**

**IR (ATR) $\nu_{max}$ ($cm^{-1}$):** 2965.6 (C-H alkene), 2934 (C-H aliphatic), 2875 (C-H aliphatic), 1653.2 (C=O conjugated ketone), 1642.6 (C=C conjugated alkene), 1610, 1466.0, 1385.3 (C-H gem dimethyl), 1307.4, 1288.6, 1198.78, 1066.2, 916.5, 821.9, 442.0.

**$^1$H NMR (400 MHz, $CDCl_3$) δ** 6.46 (s, 2H, H-3/5), 3.06 (septet, J=6.8 Hz, 2H, H-7), 1.12 (d, J=6.8 Hz, 12H, H-8).

**$^{13}$C NMR (101 MHz, $CDCl_3$) δ** 188.87, 187.00, 155.51, 129.91, 27.04, 21.61.

## 4.3 Synthesis of hydrobenzoquinones

Hydrobenzoquinones were produced by adding to a round bottom flask the respective benzoquinones followed by 5 mL/mmol acetic acid and 5 eq. zinc dust. The reaction proceeded at 70ºC with stirring for 1 hour. Upon completion, the mixture was left to reach room temperature, after which it was poured over cold water. It was then extracted several times with ethyl acetate, and the organic phase was dried with anhydrous $Na_2SO_4$ and evaporated under reduced pressure. The product was then kept for a few hours in a round bottom flask connected to a vacuum line, and immersed in a hot water bath to evaporate remaining traces of acetic acid.

#### 4.3.1 Synthesis of 2,6-diphenyl-1,4-hydrobenzoquinone (2a)

To a round bottom flask, 84.32 mg of 2,6-diphenyl-1,4-benzoquinone (0.32 mmol) were added, followed by 1.62 mL of acetic acid and 105.92 mg and the addition of zinc dust (1.62 mmol). The reaction proceeded at 70ºC for 1 hour. After the workup and removal of remaining acetic acid, 75.8 mg of the product were obtained (yield of 89%).

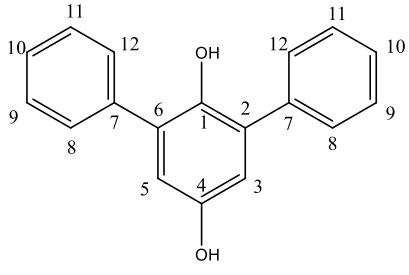


**2a**

**IR (ATR) $\nu_{max}$ ($cm^{-1}$):** 3315.7 (O-H), 3083.9 (C-H alkene), 3061 (C-H alkene), 3030.4 (C-H alkene), 1596.2 (C=C Ar), 1456.3 (C=C Ar), 1429.9 (C=C Ar), 1294.5, 1274.7, 1182.7, 863.9, 750.7, 696.3.
**$^1$H NMR (400 MHz, $CDCl_3$) δ** 7.55 (d, J=7.8 Hz, 4H, H-8/12), 7.47 (t, J=7.7 Hz, 4H, H-9/11), 7.38 (t, J=7.2 Hz, 2H, H-10), 6.79 (s, 2H, H-3/5).
**$^{13}$C NMR (101 MHz, $CDCl_3$) δ** 149.24, 143.43, 137.58, 129.72, 129.40, 128.97, 127.89, 116.64.

### 4.3.2 Synthesis of 2,6-di-tert-butyl-1,4-hydrobenzoquinone (2b)

To a round bottom flask, 68.73 mg of 2,6-di-*tert*-butyl-1,4-benzoquinone (0.312 mmol) were added, followed by 1.56 mL of acetic acid and 101.99 mg and the addition of zinc dust (1.56 mmol). The reaction proceeded at 70ºC for 1 hour. After the workup and removal of remaining acetic acid, 63.8 mg of the product were obtained (yield of 92%).

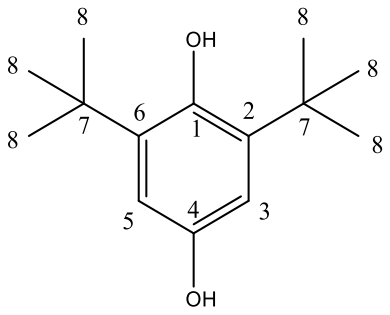

**2b**

**IR (ATR) $\nu_{max}$ ($cm^{-1}$):** 3646 (O-H), 3321.4 (O-H), 2958.4 (C-H Ar), 2913 (C-H aliphatic), 2874.5 (C-H aliphatic), 1652.7, 1598.7 (C=C) Ar, 1429.3 (C=C Ar), 1302.7 (O-H), 1199.5, 1151.9, 966.7, 863.4, 781.1.
**$^1$H NMR (400 MHz, $CDCl_3$) δ** 6.68 (s, 2H, H-3/5), 1.42 (s, 18H, H-8).
**$^{13}$C NMR (101 MHz, $CDCl_3$) δ** 148.28, 147.80, 111.91, 34.58, 30.32.

### 4.3.3 Synthesis of 2,6-diisopropyl-1,4-hydrobenzoquinone (2c)

To a round bottom flask, 62.37 mg of 2,6-di-*tert*-butyl-1,4-benzoquinone (0.324 mmol) were added, followed by 1.62 mL of acetic acid and 105.92 mg and the addition of zinc dust (1.62 mmol). The reaction proceeded at 70ºC for 1 hour. After the workup and removal of remaining acetic acid, 62.3 mg of the product were obtained (yield of 99%).

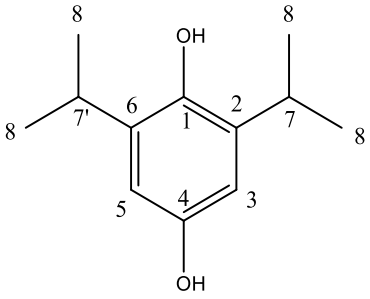

**2c**

**IR (ATR) $\nu_{max}$ ($cm^{-1}$):** 3569.9 (O-H), 2960.7 (C-H Ar), 2931.2 (C-H aliphatic), 2870.3 (C-H aliphatic), 1450.5 (C=C Ar), 1440.4 (C=C Ar), 1304.5 (O-H phenol), 1196.2, 1149.6, 1109.6, 870.7.
**$^1$H NMR (400 MHz, $CDCl_3$) δ** 7.19 (s, H2, H-3/5), 3.21 (sept, J=6.8 Hz, 2H, H-7), 1.33 (d, J=6.8 Hz, 12H, H-8).
**$^{13}$C NMR (101 MHz, $CDCl_3$) δ** 149.12, 134.75, 133.77, 122.44, 27.44, 22.80.

## 4.4 Synthesis of diphenoquinones

Diphenoquinones were prepared by adding to a round bottom flask acetone (14.3 mL/mmol), perchloric acid 70% (0.86 ml/mmol, 10 eq.) and CAN (2.5 eq.), followed by placing the bottle in an ice bath at -15ºC and then adding the phenol. The reactions proceeded with stirring at -15ºC for an hour and, upon completion, the mixture was diluted with water and the acetone was evaporated under reduced pressure. The mixture was extracted with DCM, then this phase was washed with water several times, and the resulting aqueous phase was in turn also extracted with DCM. The organic phases were then combined, dried with anhydrous $Na_2SO_4$ and evaporated under reduced pressure. These crude products were further purified by flash chromatography using a mixture of solvents petroleum ether and DCM.

### 4.4.1 Synthesis of 3,3',5,5'-tetraphenyl-4,4'-diphenoquinone (3a)

To a round bottom flask were added 5.9 mL acetone, 0.35 mL $HClO_4$ 70% and 561.93 mg CAN (1.025 mmol). Then 100 mg of 2,6-diphenylphenol (0.406 mmol) were added and the reaction proceeded at -15ºC for an hour. The crude compound was purified by flash chromatography, with a mixture of 1:1 petroleum ether and DCM, to give 68.1 mg of the product (yield of 64%).

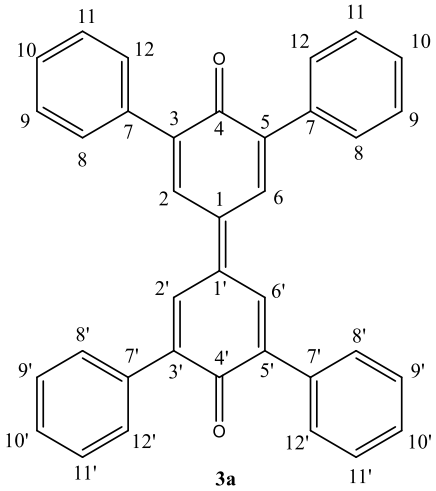

**3a**

**IR (ATR) $\nu_{max}$ ($cm^{-1}$):** 3058.2 (C-H Ar), 3029.7 (C-H alkene), 1627.2 (C=O conjugated ketone), 1582.3 (C=C Ar), 1488.6 (C=C Ar), 1443.7 (C=C Ar), 1341.8, 1280.6, 987.1, 901.5, 689.5.
**$^1$H NMR (400 MHz, $CDCl_3$) δ** 8.12 (s, 4H, H-2/2'/6/6'), 7.62 (d, J=7.8 Hz, 8H, H-8/8'/12/12'), 7.46 (m, 12H, H-9/9'/10/10'/11/11').
**$^{13}$C NMR (101 MHz, $CDCl_3$) δ** 184.50, 140.85, 137.82, 135.96, 129.93, 129.58, 129.10, 128.38.

### 4.4.2 Synthesis of 3,3',5,5'-tetra-tert-butyl-4,4'-diphenoquinone (3b)

To a round bottom flask were added 6.93 mL acetone, 0.42 mL $HClO_4$ 70% and 664.28 mg CAN (1.212 mmol). Then 100 mg of 2,6-di-tert-butylphenol (0.485 mmol) were added and the reaction proceeded at -15ºC for an hour. The crude was purified by flash chromatography, with a mixture of 1:1 petroleum ether and DCM, to give 95.5 mg of the product (yield of 91%).

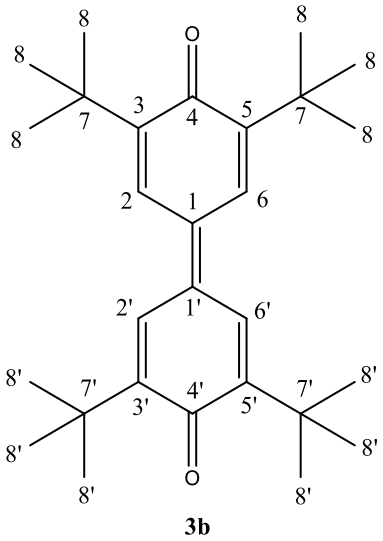

**3b**

**IR (ATR) $\nu_{max}$ ($cm^{-1}$):** 3005.2 (C-H alkene), 2956.3 (C-H aliphatic), 2903.3 (C-H aliphatic), 2866.6 (C-H aliphatic), 1639.4 (C=O conjugated ketone), 1606.8 (C=C conjugated alkene), 1566, 1456, 1358, 1260.2, 1089, 1044.2, 897.4.

**$^1$H NMR (400 MHz, $CDCl_3$) δ** 7.70 (s, 4H, H-2/2'/6/6'), 1.36 (s, 36H, H-8/8').

**$^{13}$C NMR (101 MHz, $CDCl_3$) δ** 186.49, 150.47, 136.15, 126.02, 36.04, 29.60.

### 4.4.2 Synthesis of 3,3',5,5'-tetraisopropyl-4,4'-diphenoquinone (3c)

To a round bottom flask were added 8.01 mL acetone, 0.48 mL $HClO_4$ 70% and 664.28 mg CAN (1.212 mmol). Then 100 mg of 2,6-di-tert-butylphenol (0.10 mL, 0.485 mmol) were added and the reaction proceeded at -15ºC for an hour. The crude product was purified by flash chromatography, using as eluent a mixture of 6:4 petroleum ether and DCM, to give 85.8 mg of the product (yield of 87%).

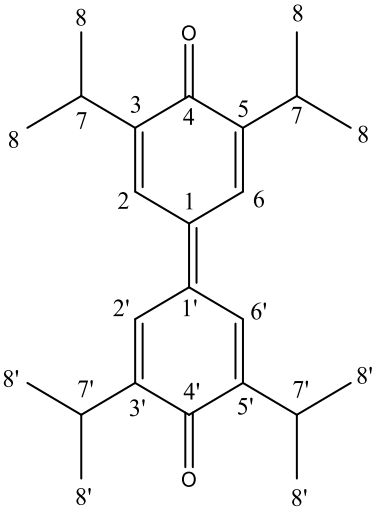

**3c**

**IR (ATR) $\nu_{max}$ ($cm^{-1}$):** 3054.1 (C-H alkene), 2960.4 (C-H aliphatic), 2931.8 (C-H aliphatic), 2874.7 (C-H aliphatic), 1631.3 (C=O conjugated ketone), 1586.4 (C=C conjugated alkene), 1464, 1382.6, (C-H gem dimethyl), 1268.4, 1076.8, 897.4, 734.3, 701.7.

**$^1$H NMR (400 MHz, $CDCl_3$) δ** 7.65 (s 4H, H-2/2'/6/6'), 3.24 (sept, J=6.8 Hz, 4H, H-7/7'), 1.21 (d, J=6.8 Hz, 24H, H-8/8').

**$^{13}$C NMR (101 MHz, $CDCl_3$) δ** 185.45, 148.54, 136.40, 125.61, 27.72, 22.02.

## 4.5 Synthesis of hydrodiphenoquinones

Hydrodiphenoquinones were produced following the same procedure as hydrobenzoquinones, as mentioned in 4.3. That is to say, they were produced by adding to a round bottom flask the respective benzoquinones followed by 5 mL/mmol acetic acid and 7 eq. zinc dust. The reaction proceeded for 1 hour with stirring at 70ºC. Upon completion, the mixture was left to cool down to room temperature, after which it was poured over cold water. It was then extracted with ethyl acetate several times, and the organic phase was dried with anhydrous $Na_2SO_4$ and evaporated under reduced pressure. The product was then kept in a round bottom flask connected to a vacuum line for a few hours, and immersed in a hot water bath to evaporate remaining traces of acetic acid.

### 4.5.1 Synthesis of 3,3',5,5'-tetraphenyl-4,4'-hydrodiphenoquinone (4a)

To a round bottom flask, 54.8 mg of 3,3',5,5'-tetraphenyl-4,4'-diphenoquinone (0.11 mmol) were added, followed by 0.55 mL of acetic acid and the addition of 50.34 mg of zinc dust (0.77 mmol). The reaction proceeded at 70ºC for 1 hour. After the workup and removal of remaining acetic acid, 45.6 mg of the product were obtained (yield of 85%).

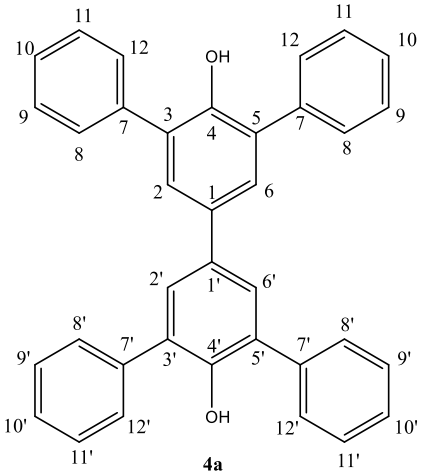

**4a**

**IR (ATR) $\nu_{max}$ ($cm^{-1}$):** 3531.8 (O-H), 3082 (C-H Ar), 3052.3 (C-H Ar), 3031 (C-H Ar), 1601.8 (C=C Ar), 1575.5, 1494.8, 1458.2, 1422.0, 1324.5 (O-H phenol), 1263.2, 1222.4, 1119.9, 776.3, 735.2, 698.1, 572.2.

**$^1$H NMR (400 MHz, $CDCl_3$) δ** 7.63 (d, J=7.6 Hz, 8H, H-8/8'/12/12'), 7.57 (s, 4H, H-2/2'/6/6'), 7.51 (t, J=7.6 Hz, 8H, H-9/9'/11/11'), 7.42 (t, J=7.6 Hz, 4H, H-10/10').

**$^{13}$C NMR (101 MHz, $CDCl_3$) δ** 148.76, 137.67, 133.26, 129.52, 129.33, 129.04, 128.35, 127.93.

### 4.5.2 Synthesis of 3,3',5,5'-tetra-tert-butyl-4,4'-hydrodiphenoquinone (4b)

To a round bottom flask, 75.21 mg of 3,3',5,5'-tetra-*tert*-butyl-4,4'-diphenoquinone (0.18 mmol) were added, followed by 0.90 mL of acetic acid and the addition of 82.38 mg of zinc dust (1.26 mmol). The reaction proceeded at 70ºC for 1 hour. After the workup and removal of remaining acetic acid, 71.8 mg of the product were obtained (yield of 97%).

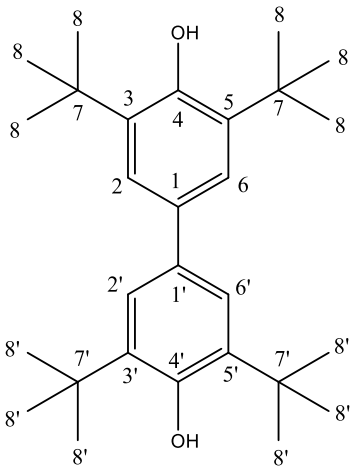

**4b**

**IR (ATR) $\nu_{max}$ ($cm^{-1}$):** 3643.7 (O-H), 3000.4 (C-H Ar), 2957.11 (C-H aliphatic), 2913 (C-H aliphatic), 2871.1 (C-H aliphatic), 1480 (C=C Ar), 1426.1 (C=C Ar), 1391.6, 1361.2, 1312.2, 1231.8, 1155.9, 1106.9, 871.0.
**$^{1}$H NMR (400 MHz, $CDCl_3$) δ** (7.30 (s, 4H, H-2/2'/6/6'), 1.50 (s, 36H, H-8/8').
**$^{13}$C NMR (101 MHz, $CDCl_3$) δ** 152.95, 136.09, 134.07, 124.23, 34.59, 30.50.

### 4.5.3 Synthesis of 3,3',5,5'-tetraisopropyl-4,4'-hydrodiphenoquinone (4c)

To a round bottom flask, 132.8 mg of 3,3',5,5'-tetraisopropyl-4,4'-diphenoquinone (0.376 mmol) were added, followed by 1.88 mL of acetic acid and the addition of 172.08 mg of zinc dust (2.63 mmol). The reaction proceeded at 70ºC for 1 hour. After the workup and removal of remaining acetic acid, 130.5 mg of the product were obtained (yield of 98%).

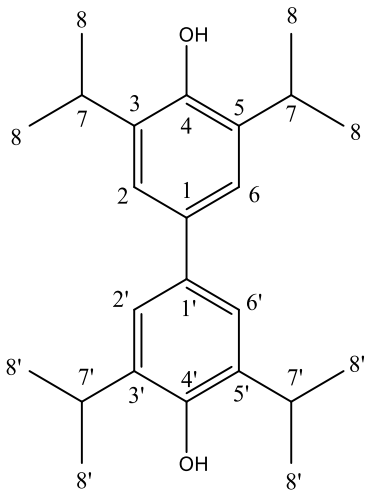

**4c**

**IR (ATR) $\nu_{max}$ ($cm^{-1}$):** 3570.4 (O-H), 2961.7 (C-H Ar), 2931.2 (C-H aliphatic), 2874 (C-H aliphatic), 1460.4 (C=C Ar), 1440.8 (C=C Ar), 1305.8 (O-H phenol), 1197.4, 1150.4, 871.
**$^{1}$H NMR (400 MHz, $CDCl_3$) δ** 7.19 (s, 4H, H-2/2'/6/6'), 3.21 (sept, J=6.9 Hz, 4H, H-7/7'), 1.33 (d, J=6.9 Hz, 24H, H-8/8').
**$^{13}$C NMR (101 MHz, $CDCl_3$) δ** 149.25, 134.89, 133.90, 122.57, 27.58, 22.93.

## 4.6 Synthesis of the anisole boronic acid pinacol ester

### 4.6.1 Synthesis of 1,3-di-tert-butyl-2-methoxybenzene (5)

In a round bottom flask, 500 mg of 2,6-di-*tert*-butylphenol (2.42 mmol) were added to in 7.45 mL of dry DMF (0.325 M), then 0.91 mL of $CH_3I$ (14.54 mmol, 6 eq.) were added, followed by 909.04 mg of $Cs_2CO_3$ (2.79 mmol, 1.15 eq.).[31] The mixture was then kept stirring for 2 days. Upon completion, cold brine was added to the solution and the product was extracted with diethyl ether. This organic phase was dried with anhydrous $Na_2SO_4$ and evaporated under reduced pressure. Toluene was then added to the product to aid in the evaporation of remaining DMF under reduced pressure, giving 473.4 mg of an oily product (yield of 89%).

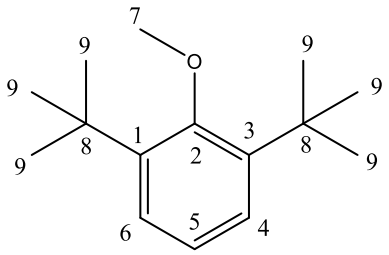

**5**

**IR (ATR) $\nu_{max}$ ($cm^{-1}$):** 2954 (C-H Ar), 2923.3 (C-H alkane), 2853.71 (C-H alkane), 1663.9 (C=C Ar), 1637.2, 1463.6 (C-H methyl), 1408.1, 1377.64, 1259.2 (C-O alkyl aryl ether), 1217.3, 1099, 1018.8, 805, 766.8, 721.0.

**$^1$H NMR (400 MHz, $CDCl_3$) δ** 7.26 (d, J=7.8 Hz, 2H, H-4/6), 6.99 (t, J=7.8 Hz, 1H, H-5), 3.71 (s, 1H, H-7), 1.45 (s, 18H, H-9).

**$^{13}$C NMR (101 MHz, $CDCl_3$) δ** 159.63, 143.79, 126.66, 123.03, 64.36, 35.87, 32.27.

### 4.6.2 Synthesis of 5-bromo-1,3-di-tert-butyl-2-methoxybenzene (6)

In a round bottom flask, 473.4 mg of 1,3-di-*tert*-butyl-2-methoxybenzene (2.15 mmol) were added to 10.75 mL of acetonitrile (0.2 M), followed by addition of 535.75 mg of N-Bromosuccinimide (3.01 mmol, 1.4 eq.). The reaction proceeded with stirring for 5 days. Upon completion, the acetonitrile was evaporated under reduced pressure, and the resulting solid was then washed with n-hexane and filtered. The organic phase was evaporated, giving an oily crude product. This product was further purified by flash chromatography, using as eluent a mixture of 9:1 n-hexane:DCM, resulting in 406.5 mg of product (yield of 63%).

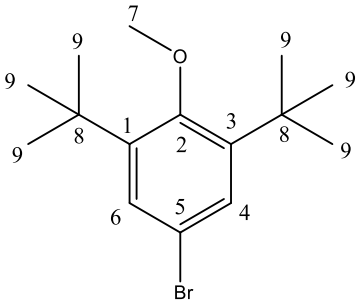

**6**

**IR (ATR) $\nu_{max}$ ($cm^{-1}$):** 3011.8 (C-H Ar), 2961.4 (C-H alkane), 2870.0 (C-H alkane), 1563.9 (C=C Ar), 1447.2 (C-H methyl), 1405.7, 1362.1, 1253.7 (C-O alkyl aryl ether), 1219.6, 1115.0, 1009.6, 866.8, 852.0, 672.9 (C-Br), 573.2.

**$^1$H NMR (400 MHz, $CDCl_3$) δ** 7.33 (s, 2H, H-4/6), 3.68 (s, 3H, H-7), 1.41 (s, 18H, H-9).

**$^{13}$C NMR (101 MHz, $CDCl_3$) δ** 158.91, 146.18, 129.67, 116.53, 64.54, 36.09, 32.03.

### 4.6.3 Synthesis of 2-(3,5-di-tert-butyl-4-methoxyphenyl)-4,4,5,5-tetramethyl-1,3,2-dioxaborolane (7)

To a round bottom flask, was added 325.08 mg of 5-bromo-1,3-di-*tert*-butyl-2-methoxybenzene (1.086 mmol), 4.46 mL of dioxane (0.24 M), 413.67 mg of bis(pinacolato)diboron (1.629 mmol, 1.5 eq.), 319.77 mg of $KCH_3COO$ (3.258 mmol, 3 eq.). The flask was then placed in ice to freeze the mixture and allow the removal of the air and replacement with nitrogen. Then the catalyst was added, 62.40 mg of $Pd(PPh_3)_4$ (0.054 mmol, 0.05 eq.) under nitrogen flow. The reaction proceeded at 95ºC with stirring under a nitrogen atmosphere for one day. Upon completion, the solution was left to cool down to room temperature, then the dioxane was evaporated under reduced pressure and to the solid residue was added cold brine. The mixture was washed several times with ethyl acetate, dried with anhydrous $Na_2SO_4$ and was then evaporated under reduced pressure, giving 686.2 mg of crude. This was then purified by flash chromatography, with a mixture of 7:3 petroleum ether and DCM as eluent, giving 308.7 mg of the pure product (yield of 83%).

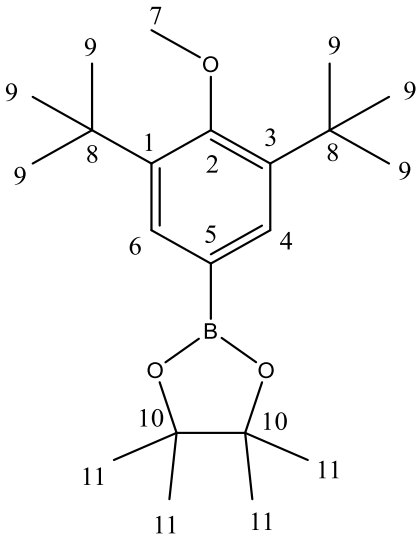


**7**

**IR (ATR) $\nu_{max}$ ($cm^{-1}$):** 2963.5 (C-H Ar), 2869.4 (C-H alkane), 1596.8 (C=C Ar), 1468.1 (C-H methyl), 1378.7, 1353.3 (C-H gem dimethyl), 1307.7, 1255.2 (C-O alkyl aryl ether), 1217.8, 1144.7, 1128.3, 1116.6, 1005.5, 965.0, 853.72, 693.3.

**$^1$H NMR (400 MHz, $CDCl_3$) δ** 7.71 (s, 2H, H-4/6), 3.69 (s, 3H, H-7), 1.45 (s, 18H, H-9), 1.33 (s, 12H, H-11).

**$^{13}$C NMR (101 MHz, $CDCl_3$) δ** 162.66, 143.09, 133.45, 83.63, 64.36, 35.82, 32.27, 25.03.

### 4.7 Synthesis of 3,5-dimethylpyridine-1-oxide (8)

In a round bottom flask, 0.11 mL of 3,5-lutidine (100 mg, 0.93 mmol) were dissolved in 0.11 mL acetic acid, followed by the dropwise addition of 0.3 mL of 30% hydrogen peroxide. The reaction occurred with stirring at 85ºC. When the reaction seemed to have stopped without full consumption of the starting material, more hydrogen peroxide was added, leading to full conversion after 5 days. Upon completion, the mixture was left to reach room temperature, and was neutralized with a saturated solution of $Na_2CO_3$. The solution was extracted several times using DCM, which was then dried with anhydrous $Na_2SO_4$ and evaporated under reduced pressure, obtaining 213.9 mg of product that was used without further purification.

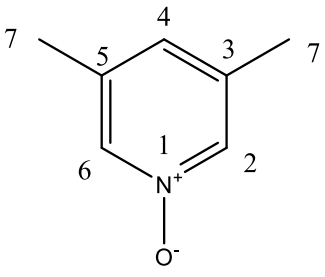


**8**

**IR (ATR) $\nu_{max}$ ($cm^{-1}$):** 3378.1 (O-H intermolecular), 3088.5 (C-H Ar), 2966.7 (C-H aliphatic), 2927.2, 1653.7, 1601 (C=C Ar), 1588.7 (C=C Ar), 1456, 1309.3, 1158.4, 1049.3, 1028.5, 1012, 846.9.

**$^{1}$H NMR (400 MHz, $CDCl_3$) δ** 7.88 (s, 2H, H-2/6), 6.89 (s, 1H, H-4), 2.24 (s, 6H, H-7).
**$^{13}$C NMR (101 MHz, $CDCl_3$) δ** 136.71, 136.10, 128.74, 18.29.

## 4.8 Synthesis of 4-nitropyridine-1-oxides

Nitro pyridine oxides were produced by adding the pyridine oxide to a round bottom flask, followed by placing this flask in ice and then adding dropwise sulfuric acid 98% (0.32 mL/mmol) and nitric acid 65% (0.17 mL/mmol). The reaction occurred with stirring at 85ºC for 1 day. Upon completion, the mixture was allowed to cool down, and was then added dropwise to cold water and neutralized with a solution saturated with $Na_2CO_3$. The product was then extracted using DCM several times. The organic phase was dried with anhydrous $Na_2SO_4$ and evaporated under reduced pressure.

### 4.8.1 Synthesis of 4-nitro-2,6-dimethylpyridine-1-oxide (9a)

To a round bottom flask were added 0.09 mL of 2,6-dimethylpyridine-1-oxide (100 mg, 0.812 mmol), followed by dropwise addition of 0.24 mL of sulfuric acid and 0.13 mL of nitric acid. The reaction proceeded at 85ºC with stirring for 1 day, and after the workup, 133.7 mg of product were obtained (yield of 98%). The product was not purified further.

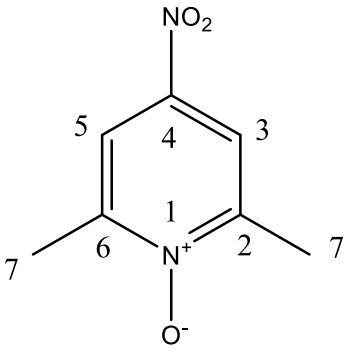

**9a**

**IR (ATR) $\nu_{max}$ ($cm^{-1}$):** 3073.7 (C-H Ar), 1614.7, 1518.4 (N-O nitro), 1461.6, 1339.7, 1272.8, 1107.5, 943.6, 747.8, 543.53.
**$^{1}$H NMR (400 MHz, $CDCl_3$) δ** 8.01 (s, 2H, H-3/5), 2.57 (s, 6H, H-7).
**$^{13}$C NMR (101 MHz, $CDCl_3$) δ** 150.46, 140.83, 118.04, 18.67.

### 4.8.2 Synthesis of 4-nitro-3,5-dimethylpyridine-1-oxide (9b)

To a round bottom flask were added 197.3 mg of 3,5-dimethylpyridine-1-oxide (1.602 mmol), followed by dropwise addition of 0.51 mL of sulfuric acid and 0.27 mL of nitric acid. The reaction proceeded at 85ºC with stirring for 3 days, and after the workup, 218.7 mg of product were obtained. This was then purified by flash chromatography using as eluent a mixture of 98:2 ethyl acetate and methanol, giving 175.5 mg of product (yield of 65%).

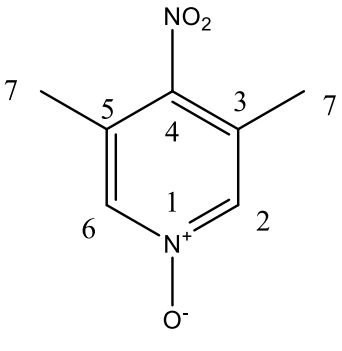

**9b**

**IR (ATR) $\nu_{max}$ ($cm^{-1}$):** 3096.82 (C-H Ar), 3056.4, 2997 (C-H aliphatic), 1595 (C=C Ar), 1571.7, 1515.3 (N-O nitro), 1467.7, 1391.4, 1356.3, 1325.1 (N-O nitro), 1190.2, 1108, 866.2, 639.7.
**$^{1}$H NMR (400 MHz, $CDCl_3$) δ** 7.98 (s, 2H, H-2/6), 2.30 (s, 6H, H-7).
**$^{13}$C NMR (101 MHz, $CDCl_3$) δ** 146.60, 138.81, 129.45, 15.53.

## 4.9 Synthesis of 4-bromopyridine-1-oxides

Bromo pyridine oxides were produced by adding to a round bottom flask the nitro pyridine oxide, followed by addition of acetic acid (0.24 mL/mmol) and dropwise addition of acetyl bromide (3.2 eq.).
The reaction proceeds with stirring at 55ºC for 1 day. Once the reaction was complete, and the mixture was allowed to cool down, the mixture was diluted with water and $Na_2CO_3$ was added to raise the pH of the solution to 10. The product was extracted several times using ethyl acetate, this phase was then dried with anhydrous $Na_2SO_4$ and evaporated under reduced pressure.

### 4.9.1 Synthesis of 4-bromo-2,6-dimethylpyridine-1-oxide (10a)

To a round bottom flask, 453.7 mg of 4-nitro-2,6-dimethylpyridine (2.698 mmol) was added, followed by 0.64 mL of glacial acetic acid and dropwise addition of 0.63 mL of acetyl bromide (8.58 mmol, 3.2 eq.). The reaction proceeded at 55ºC for 1 day. After the workup, 401.9 mg of crude were obtained, which were further purified by flash chromatography with eluent a mixture of 98:2 DCM and methanol, giving 269.38 mg of product (yield of 49%).

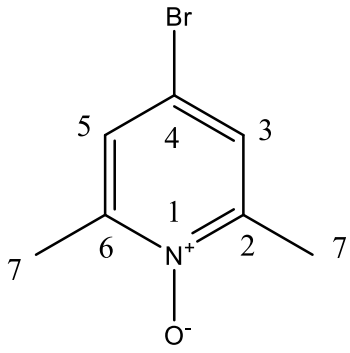

**10a**

**IR (ATR) $\nu_{max}$ ($cm^{-1}$):** 3410.7 (O-H intermolecular), 3045.3 (C-H Ar), 2957.5 (C-H aliphatic), 1607.9 (C=C Ar), 1554.4, 1454.4, 1369.8, 1239.3, 1034.3, 993.4, 858.0, 751.20, 539.5 (C-Br).
**$^1$H NMR (400 MHz, $CDCl_3$) δ** 7.29 (s, 2H, H-3/5), 2.49 (s, 6H, H-7).
**$^{13}$C NMR (101 MHz, $CDCl_3$) δ** 150.25, 127.00, 117.71, 18.28.

### 4.9.2 Synthesis of 4-bromo-3,5-dimethylpyridine-1-oxide (10b)

To a round bottom flask, 175.5 mg of 4-nitro-3,5-dimethylpyridine (1.044 mmol) was added, followed by 0.25 mL of glacial acetic acid and dropwise addition of 0.25 mL of acetyl bromide (3.32 mmol, 3.2eq.). The reaction proceeded quickly at 55ºC for 4 hours. After the workup, 198.5 mg of product were obtained (yield of 94%).

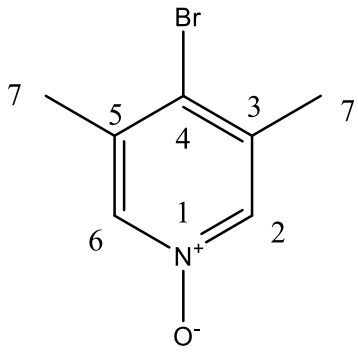

**10b**

**IR (ATR) $\nu_{max}$ ($cm^{-1}$):** 3074.6 (C-H Ar), 2990.9 (C-H aliphatic), 2950.8 (C-H aliphatic), 1731.8, 1590.1 (C=C Ar), 1544.4, 1462.1, 1428.2, 1388.1, 1320.8, 1174, 874, 732.2, 689.7, 630.9 (C-Br).
**$^1$H NMR (400 MHz, $CDCl_3$) δ** 7.94 (s, 2H, H-2/6), 2.33 (s, 6H, H-7).
**$^{13}$C NMR (101 MHz, $CDCl_3$) δ** 137.41, 136.84, 125.50, 20.66.

## 4.10 Suzuki-Miyaura Coupling Reactions

To a round bottom flask was added the boronic ester **7** (1 eq.) and dioxane (10 mL/mmol), followed by addition of 4-bromopyridine oxides **10a** or **10b** (1.2 eq.) and $Cs_2CO_3$ (1.2 eq.). The flask was placed in ice to freeze the mixture and allow the removal of the air and replacement with nitrogen and then the catalyst was added under nitrogen flow, $Pd(PPh_3)_4$ (0.08 eq.). The reaction proceeded with stirring in nitrogen atmosphere at 60ºC for 3 days. Upon completion, the mixture was left to cool down to room temperature, then the dioxane was evaporated under reduced pressure and cold brine was added to the resulting solid. The mixture was washed with ethyl acetate several times, and the resulting organic phase was then dried with anhydrous $Na_2SO_4$ and evaporated under reduced pressure.

### 4.10.1 Synthesis of 4-(3,5-di-tert-butyl-4-methoxyphenyl)-2,6-dimethylpyridine-1-oxide (11a)

To a round bottom flask were added 150 mg of the boronic ester (0.433 mmol), 4.3 mL of dioxane, 105.07 mg of 4-bromo-2,6-dimethylpyridine-1-oxide (0.520 mmol), 169.43 mg of $Cs_2CO_3$ (0.520 mmol) and 40.45 mg of $Pd(PPh_3)_4$ (0.035 mmol). After the workup, 254.1 mg of crude product were obtained. The compound was further purified by flash chromatography, with a mixture 95:5 ethyl acetate and methanol as eluent, giving 119.9 mg of (yield of 81%).

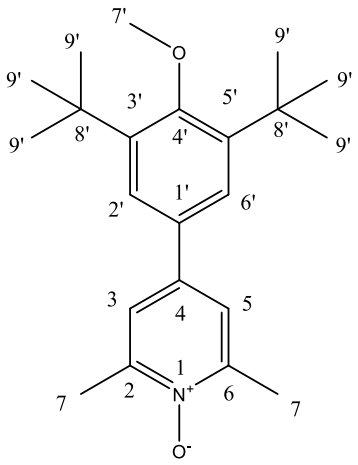

**11a**

**IR (ATR) $\nu_{max}$ ($cm^{-1}$):** 2958.2 (C-H Ar), 2920 (C-H aliphatic), 2873.5 (C-H aliphatic), 1555.6 (C-H Ar), 1454.5, 1419.7, 1394.5, 1376.9 (C-H methyl), 1252.7 (C-O alkyl aryl ether), 1226.2, 1099.5, 1010.6, 865.5, 520.3.

**$^1$H NMR (400 MHz, $CDCl_3$) δ** 7.42 (s, 2H, H-3/5), 7.30 (s, 2H, H-2'/6'), 3.73 (s, 3H, H-7'), 2.60 (s, 6H, H-7), 1.48 (s, 18H, H-9').

**$^{13}$C NMR (101 MHz, $CDCl_3$) δ** 160.50, 148.79, 144.76, 138.28, 131.53, 125.03, 121.77, 64.55, 36.12, 32.19, 18.67.

### 4.10.2 Synthesis of 4-(3,5-di-tert-butyl-4-methoxyphenyl)-3,5-dimethylpyridine-1-oxide (11b)

To a round bottom flask was added 200 mg of the boronic ester (0.578 mmol), 5.8 mL of dioxane, 140.02 mg of 4-bromo-3,5-dimethylpyridine-1-oxide (0.693 mmol), 225.79 mg of $Cs_2CO_3$ (0.693 mmol) and 53.39 mg of $Pd(PPh_3)_4$ (0.046 mmol). After the workup, 360.4 mg of crude product were obtained. The compound was further purified by flash chromatography, using as eluent a mixture 9:1 ethyl acetate and methanol, giving 152.5 mg of (yield of 77%).

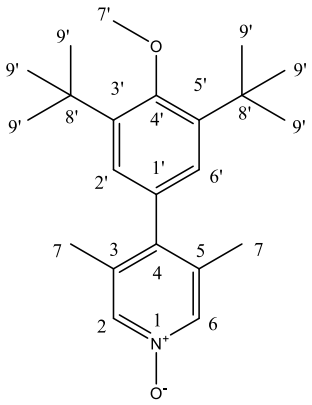

11b

**IR (ATR) $\nu_{max}$ ($cm^{-1}$):** 2960.7 (C-H Ar), 2870.7 (C-H aliphatic), 1462.8, 1408.5, 1362 (C-H methyl), 1313.1, 1222.1 (C-O alkyl aryl ether), 1163.7, 1077.4, 1011.8, 887, 604.8.
**$^1$H NMR (400 MHz, $CDCl_3$) δ** 8.01 (s, 2H, H-2/6), 6.93 (s, 2H, H-2'/6'), 3.73 (s, 3H, H-7'), 2.01 (s, 6H, H-7), 1.42 (s, 18H, H-9').
**$^{13}$C NMR (101 MHz, $CDCl_3$) δ** 159.21, 144.32, 142.14, 137.01, 134.96, 130.51, 126.83, 64.44, 36.03, 32.27, 18.01.

### 4.11 Synthesis of 4-(3,5-di-tert-butyl-4-methoxyphenyl)-2,6-dimethylpyridine (12)

The reaction was performed in a two neck round bottom flask, one neck was attached to a take-off with a nitrogen filled balloon, the other had a rubber septum to allow the injection of reactants.

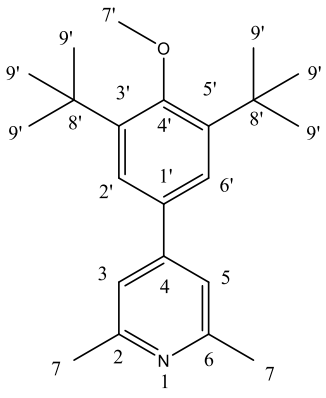

12

To a two neck round bottom flask was added 9.07 mg of $LiAlH_4$ (0.239 mmol, 0.72 eq.) followed by addition of 0.8 mL of dry THF (2.5 mL/mmol). The flask was then closed with a take-off and a rubber septum. 0.03 mL of $TiCl_4$ (0.329 mmol, 0.1 mL/mmol, 0.99 eq.) was injected and allowed to react with the $LiAlH_4$ for 15 minutes. The flask was then placed in ice to allow the injection at low temperature of 113.4 mg of 4-(3,5-di-*tert*-butyl-4-methoxyphenyl)-2,6-dimethylpyridine-1-oxide (0.332 mmol, 1 eq.), dissolved in dry THF. The mixture was allowed to reach room temperature, and the reaction proceeded at this temperature for 90 minutes. Once complete, 0.8 mL of water was added (2.5 mL/mmol), along with 0.8 mL of $NH_4OH$ 33% (2.5 mL/mmol). The aqueous phase was extracted with diethyl ether several times, and the resulting organic phase was dried with anhydrous $Na_2SO_4$ and evaporated under reduced pressure. The mass obtained of product was 89.7 mg (yield of 83%).

**IR (ATR) $\nu_{max}$ ($cm^{-1}$):** 3013 (C-H Ar), 2958.7 (C-H Ar), 2923.9 (C-H aliphatic), 2869.7 (C-H aliphatic), 1605.9 (C=C Ar), 1553.9, 1448, 1418, 1392.2, 1361.9 (C-H methyl), 1261.2, 1224.7 (C-O alkyl aryl ether), 1207.3, 1117, 1011.2, 856.7.
**$^1$H NMR (400 MHz, $CDCl_3$) δ** 7.46 (s, 2H, H-3/5), 7.12 (s, 2H, H-2'/6'), 3.73 (s, 3H, H-7'), 2.58 (s, 6H, H-7), 1.48 (s, 18H, H-9').

**$^{13}$C NMR (101 MHz, $CDCl_3$) δ** 160.53, 158.09, 149.87, 144.46, 133.07, 125.50, 118.48, 64.50, 36.09, 32.22, 24.73.
**LCMS(+)** m/z: calculated 326.5, found 326.4 for $C_{22}H_{32}NO$ $[M+H]^+$.

### 4.12 Synthesis of 2,6-di-tert-butyl-4-(2,6-dimethylpyridin-4-yl)phenol (13)

**Method A – demethylation with HBr in $CH_3COOH$:**
To a round bottom flask 52.9 mg of 4-(methoxyphenyl)pyridine (0.163 mmol, 1 eq.) was added, followed by addition of 0.5 mL of 33% HBr in $CH_3COOH$. The reaction proceeded under reflux with stirring for 24 hours. Once the mixture was allowed to cool down to room temperature, a solution saturated with $Na_2S_2O_3$ was added, followed by $NH_4OH$ 25%. The product was then extracted several times using ethyl acetate, that in turn was dried with anhydrous $Na_2SO_4$ and dried under reduced pressure, giving 46.4 mg of crude product. This product was further purified by elution in a preparative TLC, using a mixture of 9:1 petroleum ether and ethyl acetate as eluent. Several fractions were produced, however none matched the desired product.

**Method B – demethylation with NaSEt:**
To a round bottom flask was added 44.9 mg of NaH 60% dispersion in mineral oil (1.123 mmol, 8 eq.), followed by the addition of 1.96 mL of dry DMF (14 mL/mmol) and 0.07 mL of EtSH (0.983 mmol, 7 eq.). Once the release of $H_2$ had stopped, 43.61 mg of 4-(methoxyphenyl)pyridine (0.140 mmol, 1 eq.) were added to the mixture and the reaction proceeded with stirring at 100ºC for 3 days. Once allowed to cool down to room temperature, to the mixture were added 0.35 mL water (2.5 mL/mmol), 1.12 mL of 1 M HCl (8 mL/mmol) and 1.12 mL of a 0.5 M (pH 7.2) phosphate buffer solution, (8 mL/mmol). The solution was extracted several times with diethyl ether, that was in turn washed with water several times. The organic phase was dried with anhydrous $Na_2SO_4$ and dried under reduced pressure, giving 77.9 mg of crude product. This product was further purified by elution in a preparative TLC, being eluted twice with a mixture 99:1 of DCM and methanol. One fraction of 40.7 mg of the target product was obtained (yield of 93%).

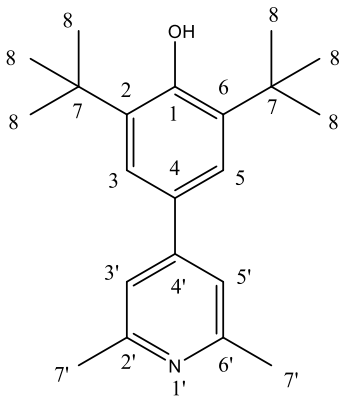

**13**

**IR (ATR) $\nu_{max}$ ($cm^{-1}$):** 3634.9 (O-H), 2956.2 (C-H Ar), 2916.1 (C-H aliphatic), 2873.5 (C-H aliphatic), 1733.8, 1605.9 (C=C Ar), 1556.6, 1437.8, 1390.3 (O-H phenol), 1236.4, 1207.0, 1156.9, 857.6, 732.8.
**$^1$H NMR (400 MHz, $CDCl_3$) δ** 7.41 (s, 2H, H-3/5), 7.11 (s, 2H, H-3'/5'), 2.57 (s, 6H, H-7'), 1.50 (s, 18H, H-8).
**$^{13}$C NMR (101 MHz, $CDCl_3$) δ** 158.02, 154.86, 150.13, 136.60, 129.95, 124.01, 118.26, 34.63, 30.43, 24.73.
**LCMS(+)** m/z: calculated 312.5, found 312.4 for $C_{21}H_{30}NO$ $[M+H]^+$; **LCMS(-)** m/z: calculated 310.5, found 310.4 for $C_{21}H_{28}NO$ $[M-H]^-$.

### 4.13 Synthesis of 4-(3,5-di-tert-butyl-4-hydroxyphenyl)-1,2,6-trimethylpyridinium iodide (14)

To a round bottom flask were added 21 mg of the 4-(pyridine-4-yl)phenol (0.067 mmol, 1 eq.), followed by dissolution in 1.1 mL of acetone (16 mL/mmol) and addition of 0.02 mL of $CH_3I$ (0.269 mmol, 4 eq.). The reaction proceeded with stirring for 2 days at room temperature. Once complete, the acetone was evaporated under reduced pressure, and the product was washed first with diethyl ether followed by ethyl acetate, leaving behind the iodide salt as a solid, giving, after drying, 29.94 mg of product (yield of 98%).

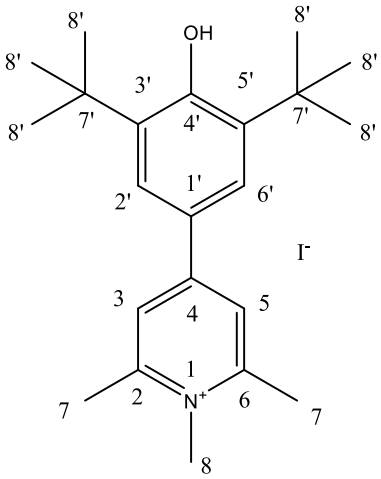

**14**

**IR (ATR) $\nu_{max}$ ($cm^{-1}$):** 3436.5 (O-H), 2955.5 (C-H Ar), 2916.1 (C-H aliphatic), 2873.5 (C-H aliphatic), 1631.2 (C=C Ar), 1594.7, 1566.4, 1438.7 (C-H methyl), 1338.1 (O-H phenol), 1218.8, 1179.5, 1121.5, 866.6.

**$^1$H NMR (400 MHz, $CD_3OD$) δ** 8.01 (s, 2H, H-3/5), 7.71 (s, 2H, H-2'/6'), 4.07 (s, 3H, H-8), 2.87 (s, 6H, H-7), 1.50 (s, 18H, H-8').

**$^{13}$C NMR (101 MHz, $CD_3OD$) δ** 158.25, 157.37, 141.13, 126.93, 124.91, 40.83, 36.70, 31.37, 22.72.

**LCMS(+)** m/z: calculated 326.5, found 326.4 for $C_{22}H_{32}NO$ $[M]^+$; **LCMS(-)** m/z: 126.9 $[I]^-$, 380.6 $[I_3]^-$.

### 4.14 Synthesis of 2,6-di-tert-butyl-4-(1,2,6-trimethylpyridinium-4-yl)phenolate (15)

**Method A – deprotonation with $NBu_4OH$ 20% in water:**

To a round bottom flask were added 20.23 mg of the iodide salt **14** (0.045 mmol, 1 eq.), followed by addition of 0.06 mL of 20% $NBu_4OH$ in water (1.05 eq.) and 0.5 mL of methanol. The reaction proceeded with stirring at room temperature for 1 hour. The mixture was then dried under reduced pressure, however, after washing the solid with n-hexane, 8:2 n-hexane:DCM, and water, and trying to purify with a C18 sep-pak column, the product could not be separated from the $NBu_4I$ and $NBu_4OH$.

**Method B – deprotonation with Amberlyst A26 resin:**

To a 5 mL polytop vial were added 20.84 mg of the iodide salt **14** (0.046 mmol), along with 2 mL of methanol. Then, 40.1 mg of Amberlyst A26 OH resin were added to the solution and the reaction proceeded with stirring for 20 minutes. Afterwards, the resin was filtered and washed with methanol, and the filtered solution was evaporated under reduced pressure, giving 13.64 mg of the zwitterionic compound (yield of 91%).

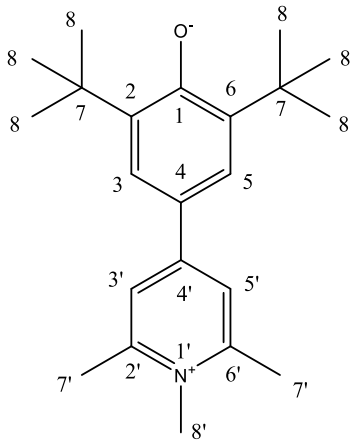

**15**

**IR (ATR) $\nu_{max}$ ($cm^{-1}$):** 3368.1 (O-H), 2942.1 (C-H aliphatic), 2855.2 (C-H aliphatic), 1639.7 (C=C Ar), 1579.5, 1524.1, 1480.0, 1445.63 (C-H methyl), 1350.0, 1326.0, 1225.4, 1182.4, 939.9, 652.5.

**$^{1}$H NMR (400 MHz, $CDCl_3$) δ** 7.43 (s, 2H, H-3/5), 7.04 (s, 2H, H-3'/5'), 3.60 (s, 3H, H-8'), 2.47 (s, 6H, H-7'), 1.43 (s, 18H, H-8).

**$^{13}$C NMR (101 MHz, $CDCl_3$) δ** 147.53, 141.60, 124.52, 115.29, 36.24, 35.39, 29.92, 21.82.

**LCMS(+)** m/z: calculated 326.5, found 326.2 for $C_{22}H_{32}NO$ $[M+H]^+$; **LCMS(-)** m/z: calculated 324.5, found 324.2 for $C_{22}H_{30}NO$ $[M-H]^-$.

**4.15 Synthesis of 4-(3,5-di-tert-butyl-4-hydroxyphenyl)-1,2,6-trimethylpyridinium triflate (16)**

In a 5 mL polytop vial, 20.54 mg of the iodide salt **14** (0.045 mmol) were dissolved in 2 mL of DCM, followed by adding 13.33 mg of sodium triflate (unknown level of hydration, 6 water molecules of hydration were assumed, 0.0476 mmol, 1.05 eq.). The reaction proceeded with stirring for 24 hours at room temperature. This vial was left to stand for an hour at 0ºC to further precipitate NaI. Then the dichloromethane was pipetted and was passed through compacted cotton inside a Pasteur pipette to filter remaining NaI. After evaporating the DCM, 17.07 mg of the triflate salt were obtained (yield of 79%).

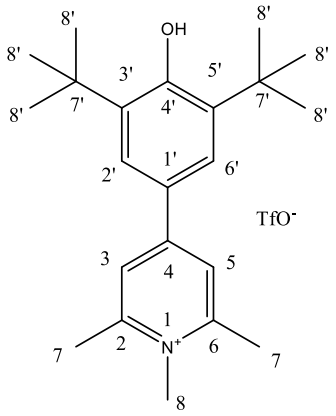

**16**

**IR (ATR) $\nu_{max}$ ($cm^{-1}$):** 3434.8 (O-H), 2954.8 (C-H Ar), 2923.9 (C-H aliphatic), 2858 (C-H aliphatic), 1727.7, 1632.4 (C=C Ar), 1596.1, 1569, 1441.3 (C-H methyl), 1260.9 (C-F), 1220.6, 1182, 1120, 1031, 872.3, 636.1.

**$^{1}$H NMR (400 MHz, $CD_3OD$) δ** 8.01 (s, 2H, H-3/5), 7.71 (s, 2H, H-2'/6'), 4.07 (s, 3H, H-8), 2.87 (s, 6H, H-7), 1.51 (s, 18H, H-8').

**$^{19}$F NMR (376MHz, $CD_3OD$) δ** -80.06 ($CF_3$).

**LCMS(+)** m/z: calculated 326.5, found 326.4 for $C_{22}H_{32}NO$ [M]+; **LCMS(-)** m/z: 126.9 $[I]^-$, 149.0 $[CF_3SO_3]^-$

.

# 5. REFERENCES


1. Sánchez-Díez, E., Ventosa, E., Guarnieri, M., Trovò, A., Flox, C., Marcilla, R., Soavi, F., Mazur, P., Aranzabe, E. & Ferret, R. Redox flow batteries: Status and perspective towards sustainable stationary energy storage. *J. Power Sources* **481**, (2021). doi.org/10.1016/j.jpowsour.2020.228804.
2. Soloveichik, G. L. Flow Batteries: Current Status and Trends. *Chem. Rev.* **115**, 11533–11558 (2015). doi.org/10.1021/cr500720t.
3. Noack, J., Roznyatovskaya, N., Herr, T. & Fischer, P. The Chemistry of Redox-Flow Batteries. *Angew. Chemie - Int. Ed.* **54**, 9776–9809 (2015). doi.org/10.1002/anie.201410823.
4. Chen, R., Kim, S. & Chang, Z. Redox Flow Batteries: Fundamentals and Applications. *Redox - Princ. Adv. Appl.* (2017). doi.org/10.5772/intechopen.68752.
5. Tolmachev, Y. V. Review—Flow Batteries from 1879 to 2022 and Beyond. *J. Electrochem. Soc.* **170**, 030505 (2023). doi.org/10.32388/G6G4EA.
6. Rychcik, M. & Skyllas-Kazacos, M. Characteristics of a new all-vanadium redox flow battery. *J. Power Sources* **22**, 59–67 (1988). doi.org/10.1016/0378-7753(88)80005-3.
7. Zhang, J., Corman, R. E., Schuh, J. K., Ewoldt, R. H., Shkrob, I. A. & Zhang, L. Solution Properties and Practical Limits of Concentrated Electrolytes for Nonaqueous Redox Flow Batteries. *J. Phys. Chem. C* **122**, 8159–8172 (2018). doi.org/10.1021/acs.jpcc.8b02009.
8. Gong, K., Fang, Q., Gu, S., Li, S. F. Y. & Yan, Y. Nonaqueous redox-flow batteries: Organic solvents, supporting electrolytes, and redox pairs. *Energy Environ. Sci.* **8**, 3515–3530 (2015). doi.org/10.1039/C5EE02341F.
9. Arenas, L. F., Ponce de León, C. & Walsh, F. C. Redox flow batteries for energy storage: their promise, achievements and challenges. *Curr. Opin. Electrochem.* **16**, 117–126 (2019). doi.org/10.1016/j.coelec.2019.05.007.
10. Liu, T., Wei, X., Nie, Z., Sprenkle, V. & Wang, W. A Total Organic Aqueous Redox Flow Battery Employing a Low Cost and Sustainable Methyl Viologen Anolyte and 4-HO-TEMPO Catholyte. *Advanced Energy Materials.* **6**, 1501449-1501456 (2016). doi.org/10.1002/aenm.201501449.
11. Huskinson, B., Marshak, M. P., Suh, C., Er, S., Gerhardt, M. R., Galvin, C. J., Chen, X., Aspuru-Guzik, A., Gordon, R. G. & Aziz, M. J. A metal-free organic-inorganic aqueous flow battery. *Nature* **505**, 195–198 (2014). doi.org/10.1038/nature12909.
12. Bugga, R. V.; West, W. C.; Kindler, A.; Smart, M. C. Lithium based high energy density flow batteries. US 8889300 B2, 2014.
13. Quan, M., Sanchez, D., Wasylkiw, M. F. & Smith, D. K. Voltammetry of quinones in unbuffered aqueous solution: Reassessing the roles of proton transfer and hydrogen bonding in the aqueous electrochemistry of quinones. *J. Am. Chem. Soc.* **129**, 12847–12856 (2007). doi.org/10.1021/ja0743083.
14. Nohl, H., Jordan, W. & Youngman, R. J. Quinones in Biology: Functions in electron transfer and oxygen activation. *Adv. Free Radic. Biol. Med.* **2**, 211–279 (1986). doi.org/10.1016/S8755-9668(86)80030-8.
15. Wilhelmsen, C. O., Kristensen S. B., Nolte, O., Volodin, I. A., Christiansen, J. V., Isbrandt, T., Sørensen, T., Petersen, C., Sondergaard, T. E., Nielsen, K. L., Larsen, T. O., Frisvad, J. C., Hager, M. D., Schubert, U. S., Muff, J. & Sørensen, J. L. Demonstrating the Use of a Fungal Synthesized Quinone in a Redox Flow Battery. *Batteries and Supercaps* **6**, e202200365 (2023). doi.org/10.1002/batt.202200365.
16. Diemer, V., Chaumeil, H., Defoin, A., Fort, A., Boeglin, A. & Carré, C. Syntheses of sterically hindered zwitterionic pyridinium phenolates as model compounds in nonlinear optics. *European J. Org. Chem.* 1767–1776 (2008) doi.org/10.1002/ejoc.200701023.
17. Ay, E., Hobeika, N., Chaumeil, H., Tschamber, T., Jin, M., Versace, D. L. & Malval, J. P. Rotamerism-driven large magnitude host-guest binding change in a crown ether derivatized pyridinium-phenolate series. *Chem. Commun.* **52**, 4652–4654 (2016). doi.org/10.1039/C6CC00684A.
18. Omura, K. Rapid conversion of phenols to p-benzoquinones under acidic conditions with lead dioxide. *Synthesis (Stuttg).* 1145–1148 (1998) doi.org/10.1055/s-1998-2118.
19. Yamada, M., Araki, K. & Shiraishi, S. Oxygenation of 2,6-Di-t-butylphenol catalysed by a new

cobalt(II) complex [Co(babp)]: A salen analogue having higher catalytic activity, selectivity, and durability. *J. Chem. Soc. Perkin Trans. 1* 2687–2690 (1990) doi.org/10.1039/p19900002687.
20. Sprang, F., Herszman, J. D. & Waldvogel, S. R. Electrochemical oxidation of phenols in flow: a versatile and scalable access to para-benzoquinones. *Green Chem.* **24**, 5116–5124 (2022). doi.org/10.1039/D2GC01296K.
21. Scheiber, N., Blaser, G., Pferschy-Wenzig, E. M., Kaiser, M., Mäser, P. & Presser, A. Efficient Oxidative Dearomatisations of Substituted Phenols Using Hypervalent Iodine (III) Reagents and Antiprotozoal Evaluation of the Resulting Cyclohexadienones against T. b. rhodesiense and P. falciparum Strain NF54. *Molecules* **27**, 1–19 (2022). doi.org/10.3390/molecules27196559.
22. Kraszewski, K., Tomczyk, I., Drabinska, A., Bienkowski, K., Solarska, R. & Kalek, M. Mechanism of Iodine(III)-Promoted Oxidative Dearomatizing Hydroxylation of Phenols: Evidence for a Radical-Chain Pathway. *Chem. - A Eur. J.* **26**, 11584–11592 (2020). doi.org/10.1002/chem.202002026.
23. Nishino, H., Itoh, N., Nagashima, M. & Kurosawa, K. Choice of manganese(iii) complexes for the synthesis of 4,4′-biphenyldiols and 4,4′-diphenoquiones. *Bulletin of the Chemical Society of Japan* vol. **65** 620–622 (1992). doi.org/10.1246/bcsj.65.620.
24. Pelter, A. & Elgendy, S. M. A. Phenolic oxidations with phenyliodonium diacetate. *J. Chem. Soc. Perkin Trans. 1* 1891–1896 (1993) doi.org/10.1039/p19930001891.
25. Domagała, S., Steglińska, V. & Dziegieć, J. Oxidative coupling of some 2,6-disubstituted phenol derivatives in perchloric acid mediated by cerium(IV) ions. *Monatshefte fur Chemie* **129**, 761–768 (1998). doi.org/10.1007/PL00013485.
26. James, T. H., Snell, J. M. & Weissberger, A. Oxidation Processes. XII. The Autoxidation of Hydroquinone and of the Mono-,Di- and Trimethylhydroquinones. *J. Am. Chem. Soc.* **60**, 2084–2093 (1938). doi.org/10.1021/ja01276a020.
27. Tsukayama, M., Kawamura, Y., Ishizuka, T., Hayashi, S. & Torii, F. Improved, Rapid and Efficient Synthesis of Polymethoxyflavones under Microwave Irradiation and Their Inhibitory Effects on Melanogenesis. Heterocycles **60**, 2775–2784 (2003). doi.org/10.3987/COM-03-9891.
28. Coffield, T. H., Filbey, A. H., Ecke, G. G. & Kolka, A. J. Some Reactions of 2,6-Dialkylphenols 1. *J. Am. Chem. Soc.* **79**, 5019–5023 (1957). doi.org/10.1021/ja01575a051.
29. Maeno, Z., Mitsudome, T., Mizugaki, T. & Jitsukawa, K. A dual-functional heterogeneous ruthenium catalyst for the green one-pot synthesis of biphenols. *Catal. Sci. Technol.* **7**, 3205–3209 (2017). doi.org/10.1039/C7CY00919D.
30. Chaumeil, H., Signorella, S. & Le Drian, C. Suzuki cross-coupling reaction of sterically hindered aryl boronates with 3-iodo-4-methoxybenzoic acid methylester. *Tetrahedron* **56**, 9655–9662 (2000). doi.org/10.1016/S0040-4020(00)00928-5.
31. Adams, A. D.; Santini, C. Pyridine, Pyrimidine and Pyrazine Derivatives as Cxcr3 Receptor Modulators. US 2009/0030012 A1, 2009.
32. Wu, Y., Zhang, Y., Guo, Y., Pan, Z., Zhong, S., Jin, X., Zhuang, W., Chen, S., Gao, J., Huang, W., Dong, X. & Che, J. Discovery of phenyl-linked symmetric small molecules as inhibitors of the programmed cell death-1/programmed cell death-ligand 1 interaction. *Eur. J. Med. Chem.* **223**, 113637 (2021). doi.org/10.1016/j.ejmech.2021.113637.
33. Ishiyama, T., Murata, M. & Miyaura, N. Palladium(0)-Catalyzed Cross-Coupling Reaction of Alkoxydiboron with Haloarenes: A Direct Procedure for Arylboronic Esters. *J. Org. Chem.* **60**, 7508–7510 (1995). doi.org/10.1021/jo00128a024.
34. Clayden, J., Greeves, N. & Warren, S. Organic Chemistry, p. 725-731, Second Edition, Volume **7**, Oxford University Press, Oxford, 2012.
35. Ma, F. H., Chen, J. L., Li, Q. F., Zuo, H. H., Huang, F. & Su, X. C. Kinetic assay of the michael addition-like thiol-ene reaction and insight into protein bioconjugation. *Chem. - An Asian J.* **9**, 1808–1816 (2014). doi.org/10.1002/asia.201402095.
36. Malinowski, M., Kaczmarek, Ł. & Rozpłoch, F. Reductive properties of low-valent titanium reagents. Mechanistic studies. *J. Chem. Soc. Perkin Trans. 2* 879–883 (1991) doi.org/10.1039/p29910000879.
37. Diemer, V., Chaumeil, H., Defoin, A., Fort, A., Boeglin, A. & Carré, C. Syntheses of sterically hindered pyridinium phenoxides as model compounds in nonlinear optics. *European J. Org. Chem.* 2727–2738 (2006) doi.org/10.1002/ejoc.200600030.

# 6. APPENDIX

## Appendix 1 – Diphenyl benzoquinone (1a)

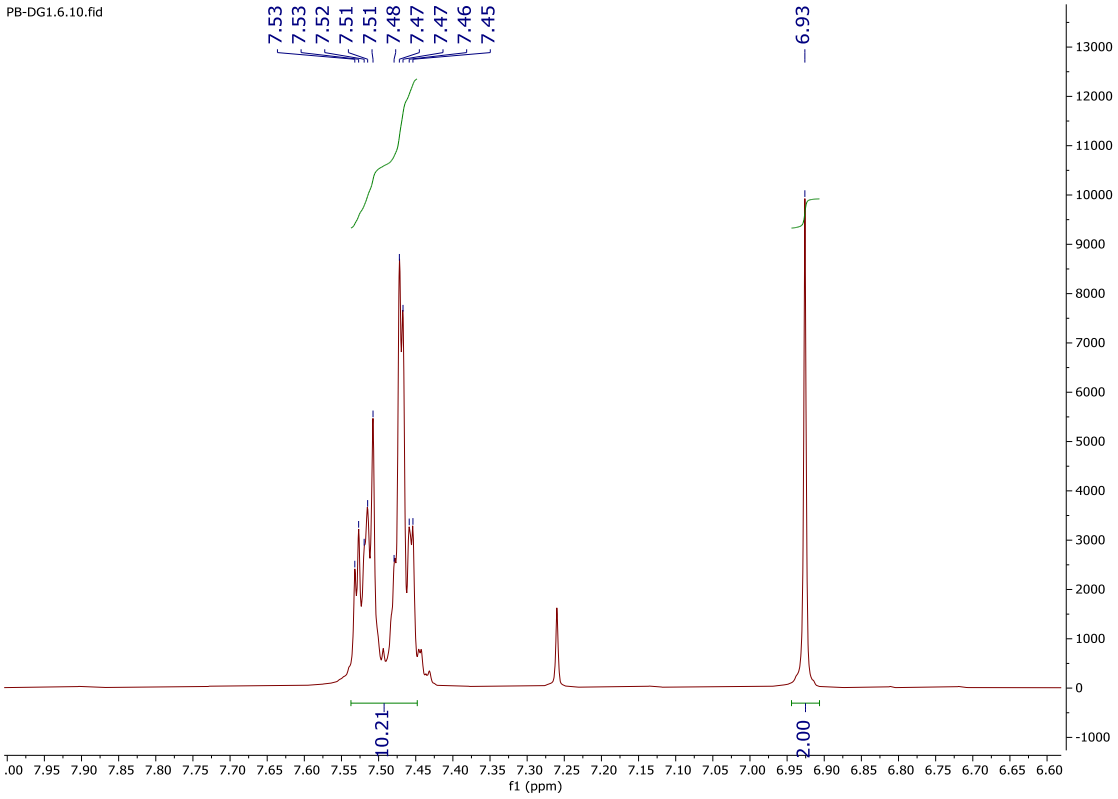


**Figure 6.1** – $^{1}H$ NMR spectrum of diphenyl benzoquinone (**1a**) in $CDCl_3$.

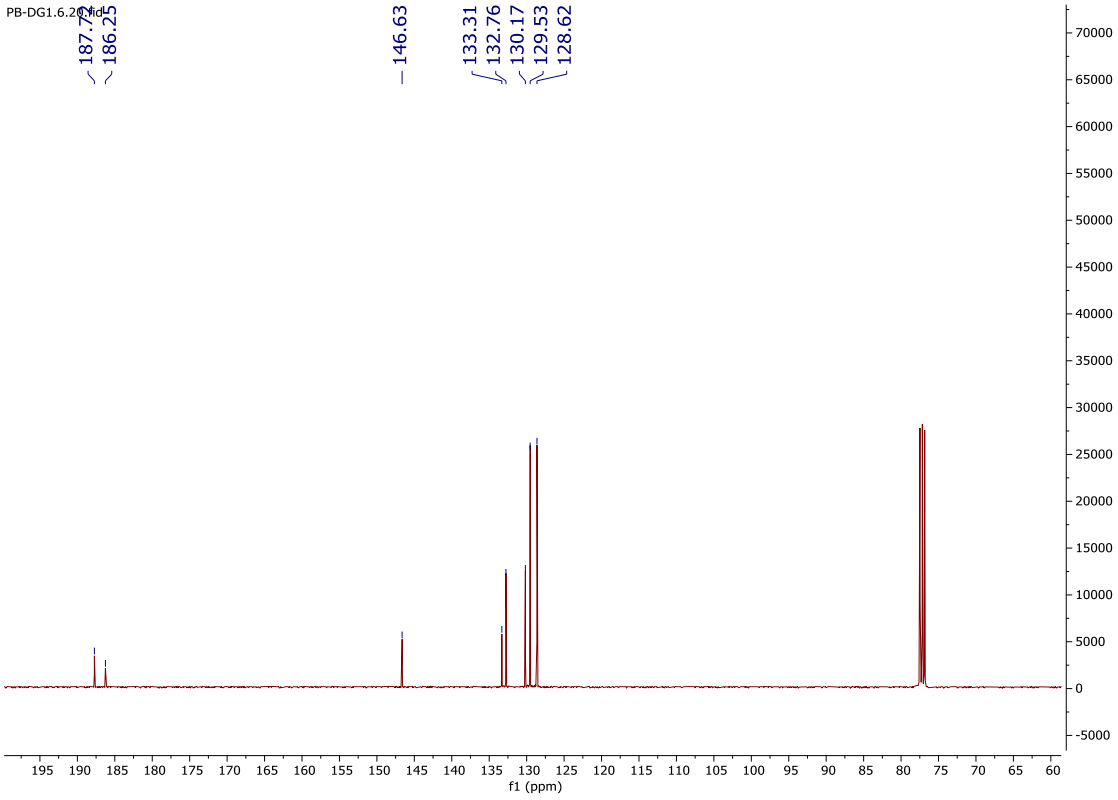


**Figure 6.2** – $^{13}C$ NMR spectrum of diphenyl benzoquinone (**1a**) in $CDCl_3$.

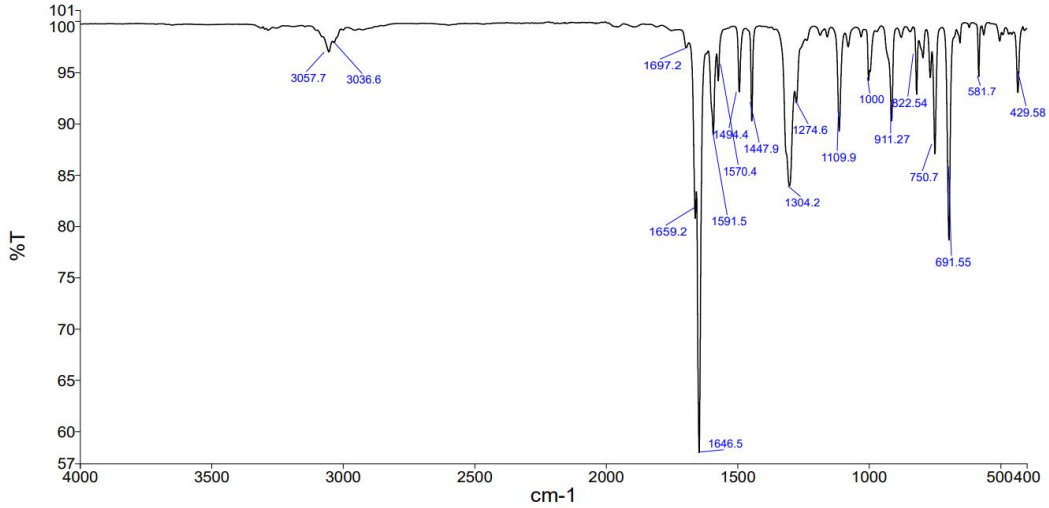


**Figure 6.3** – IR spectrum of diphenyl benzoquinone (**1a**).

## Appendix 2 – Di-*tert*-butyl benzoquinone (1b)

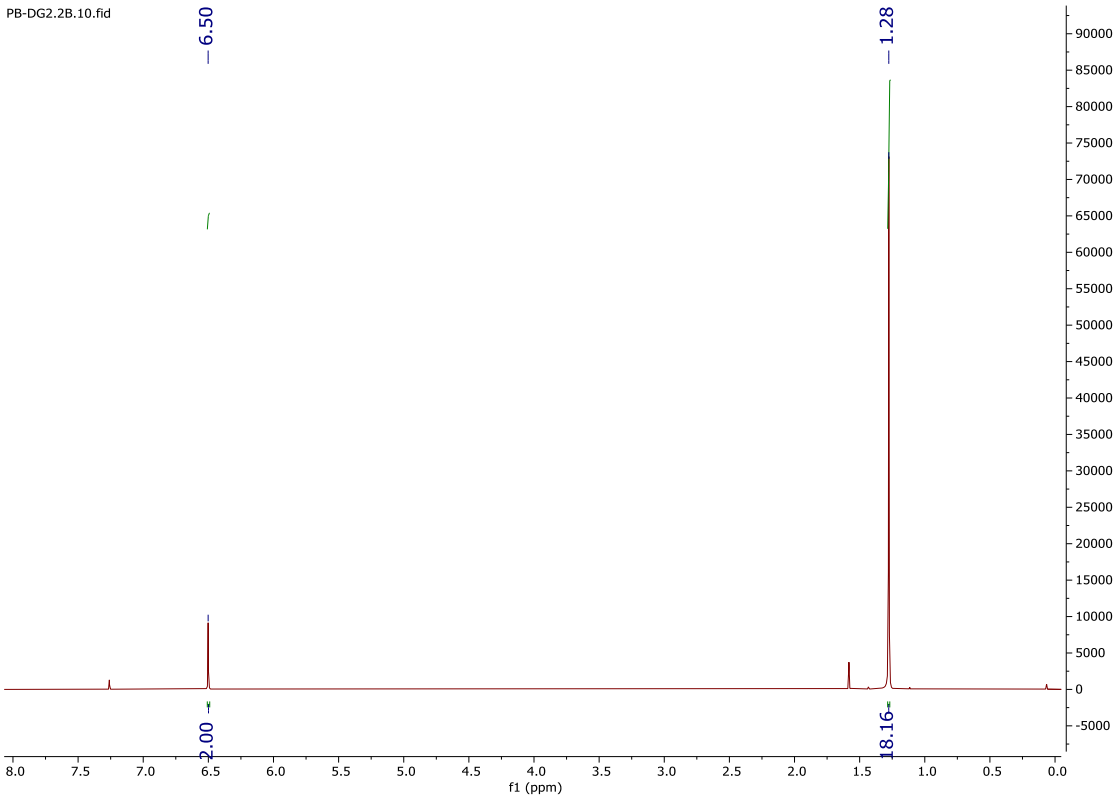


**Figure 6.4** – $^{1}H$ NMR spectrum of di-*tert*-butyl benzoquinone (**1b**) in $CDCl_3$.

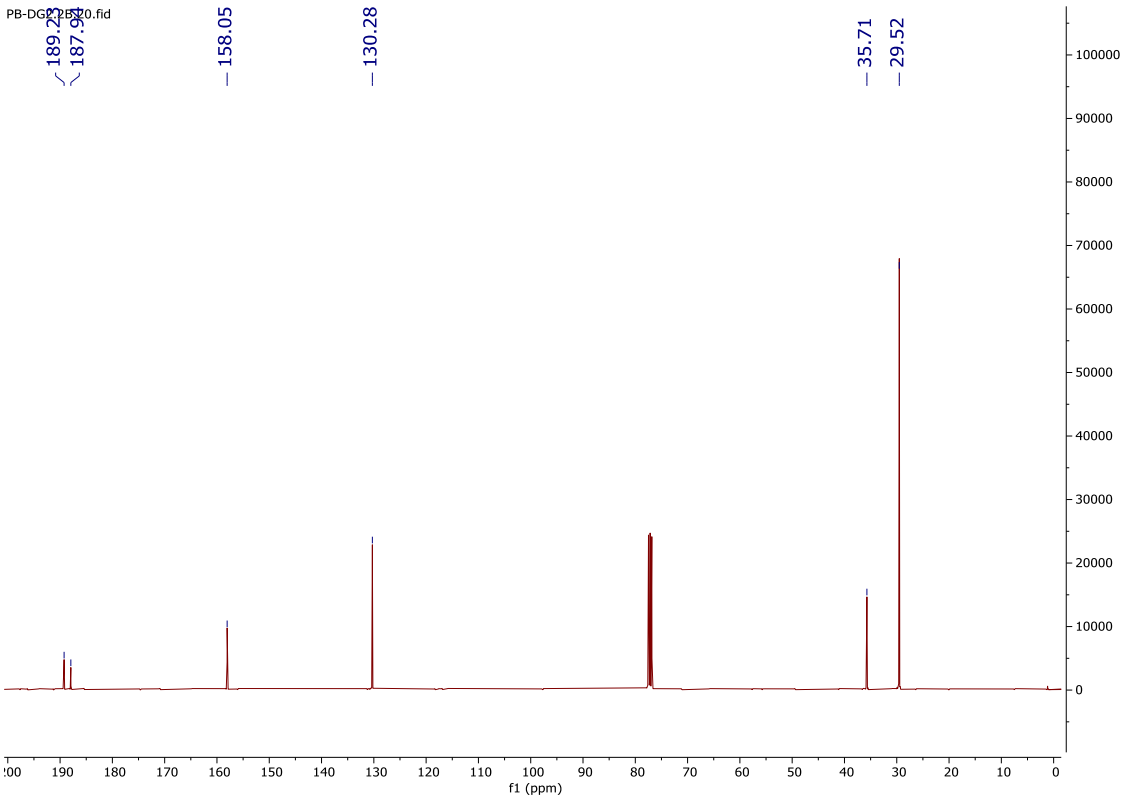


**Figure 6.5** – $^{13}C$ NMR spectrum of di-*tert*-butyl benzoquinone (**1b**) in $CDCl_3$.

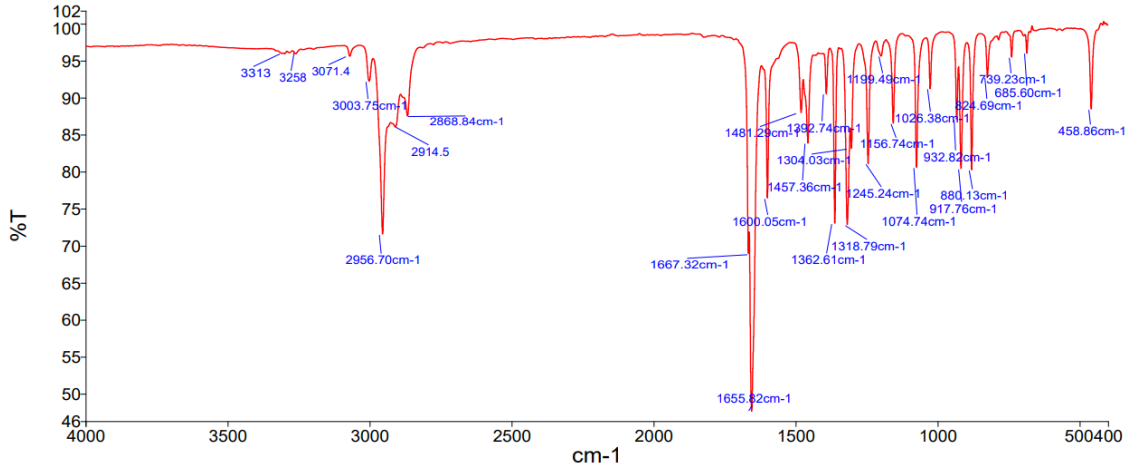


**Figure 6.6** – IR spectrum of di-*tert*-butyl benzoquinone (**1b**).

## Appendix 3 – Diisopropyl benzoquinone (1c)

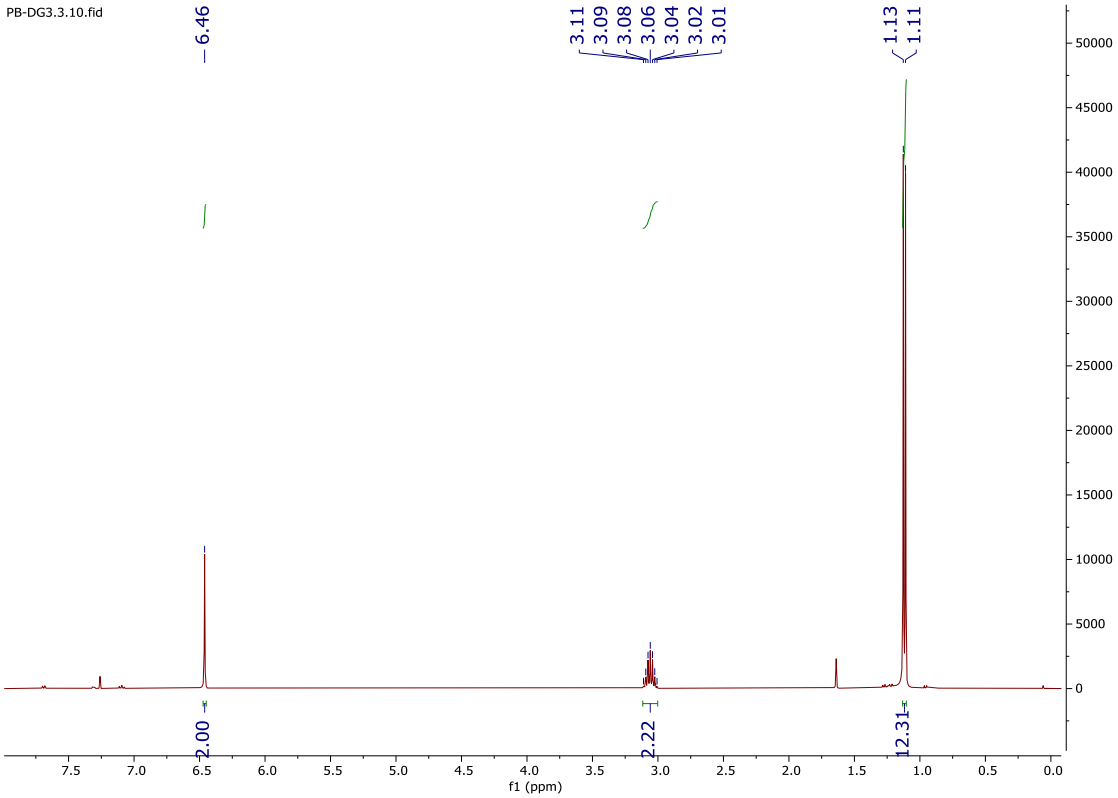


**Figure 6.7** – $^{1}H$ NMR spectrum of diisopropyl benzoquinone (**1c**) in $CDCl_3$.

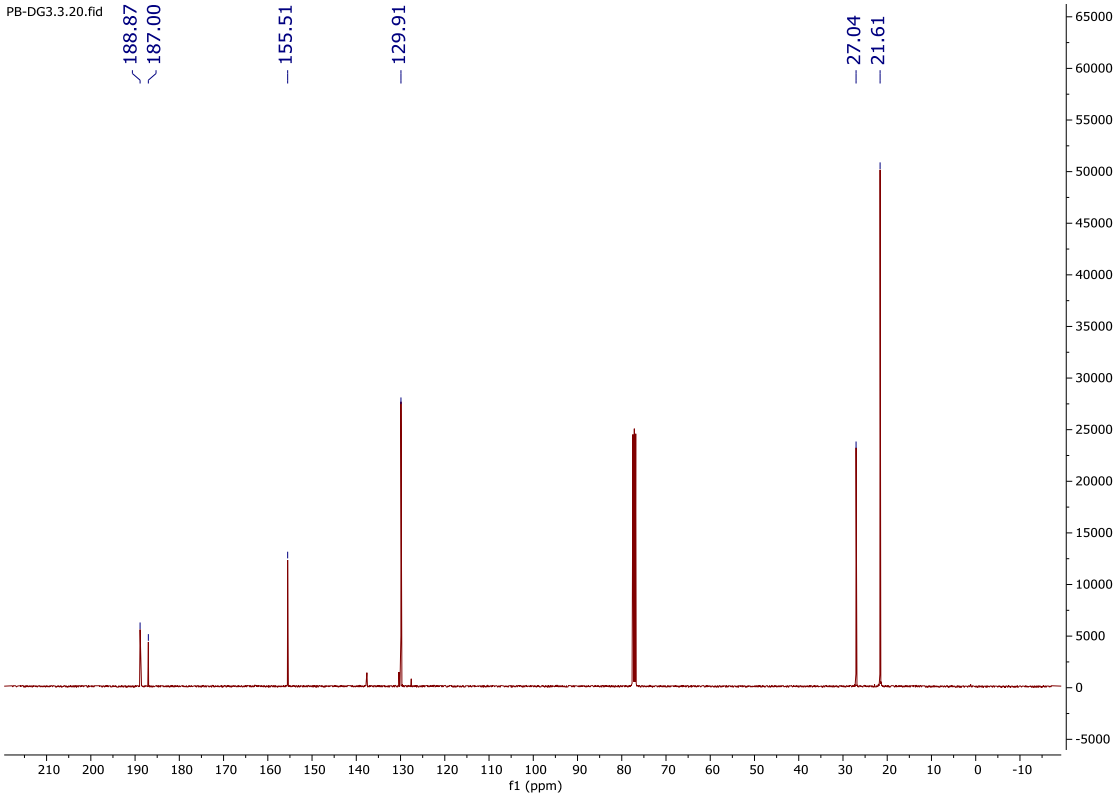


**Figure 6.8** – $^{13}C$ NMR spectrum of di-*tert*-butyl benzoquinone (**1c**) in $CDCl_3$.

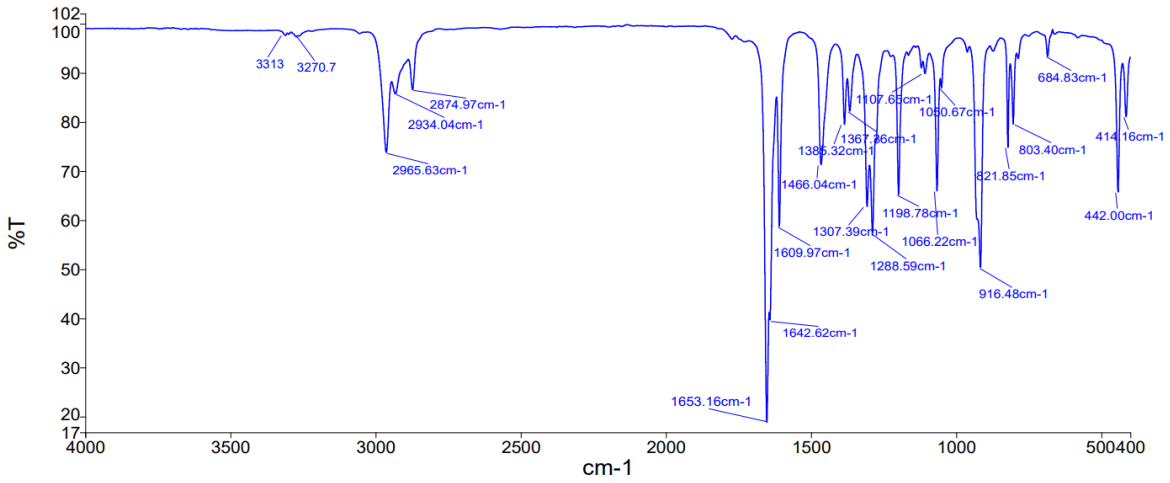


**Figure 6.9** – IR spectrum of diisopropyl benzoquinone (**1c**).

## Appendix 4 – Diphenyl hydrobenzoquinone (2a)

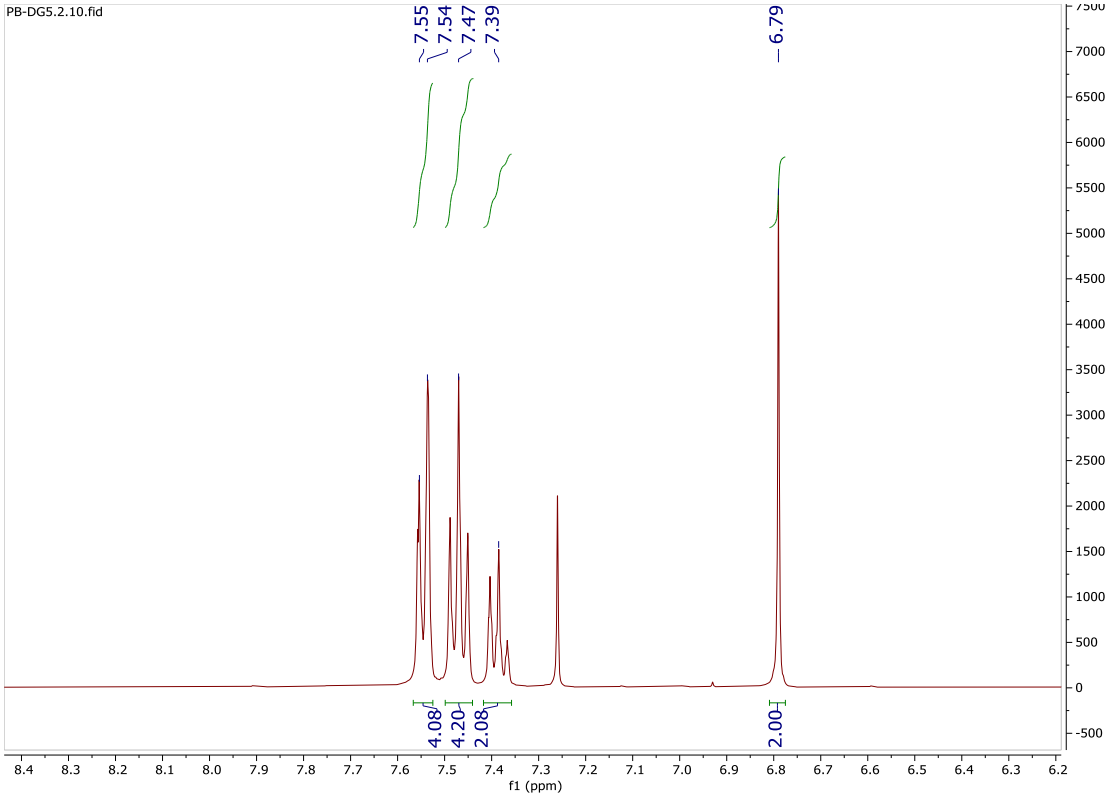


**Figure 6.10** – $^{1}H$ NMR spectrum of diphenyl hydrobenzoquinone (**2a**) in $CDCl_3$.

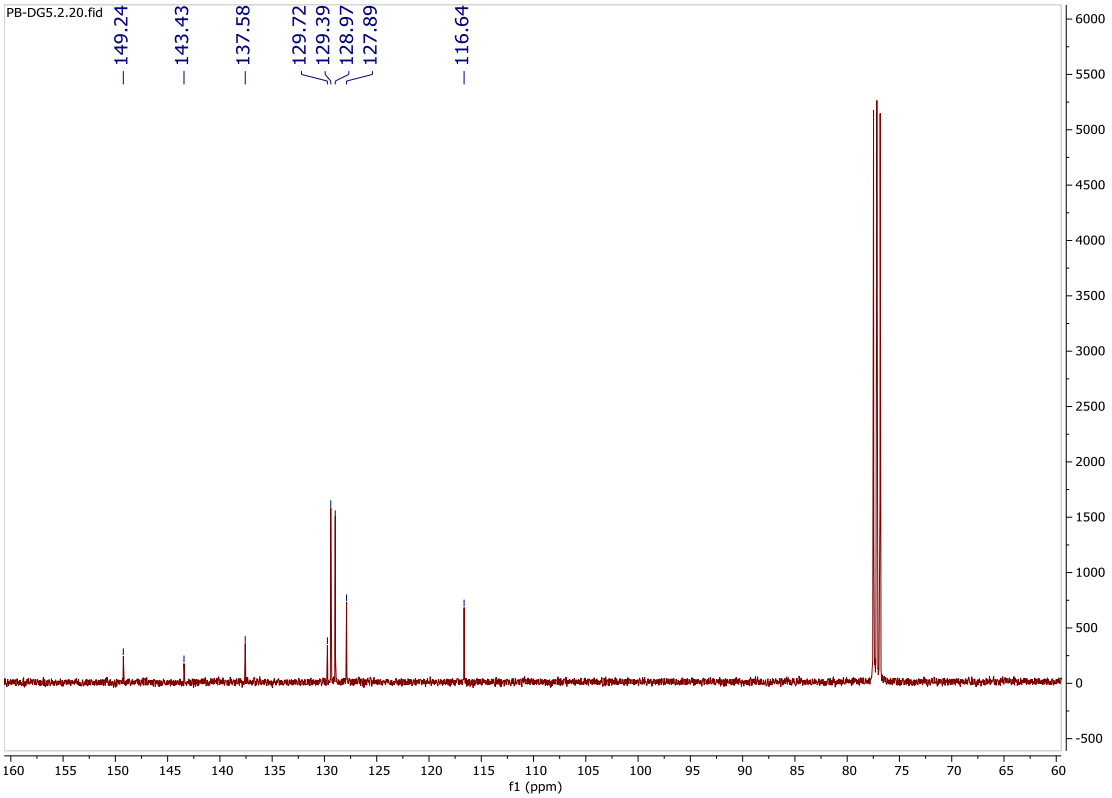


**Figure 6.11** – $^{13}C$ NMR spectrum of diphenyl hydrobenzoquinone (**2a**) in $CDCl_3$.

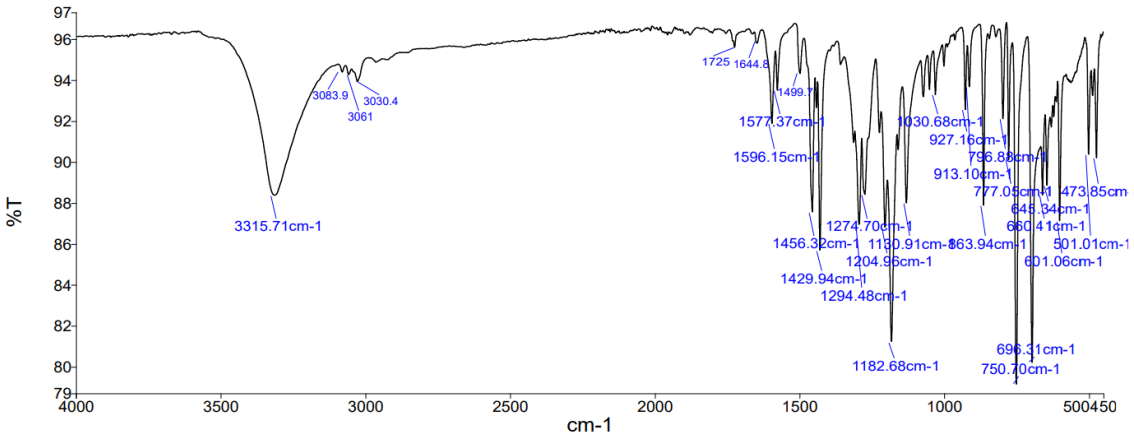


**Figure 6.12** – IR spectrum of diphenyl hydrobenzoquinone (**2a**).

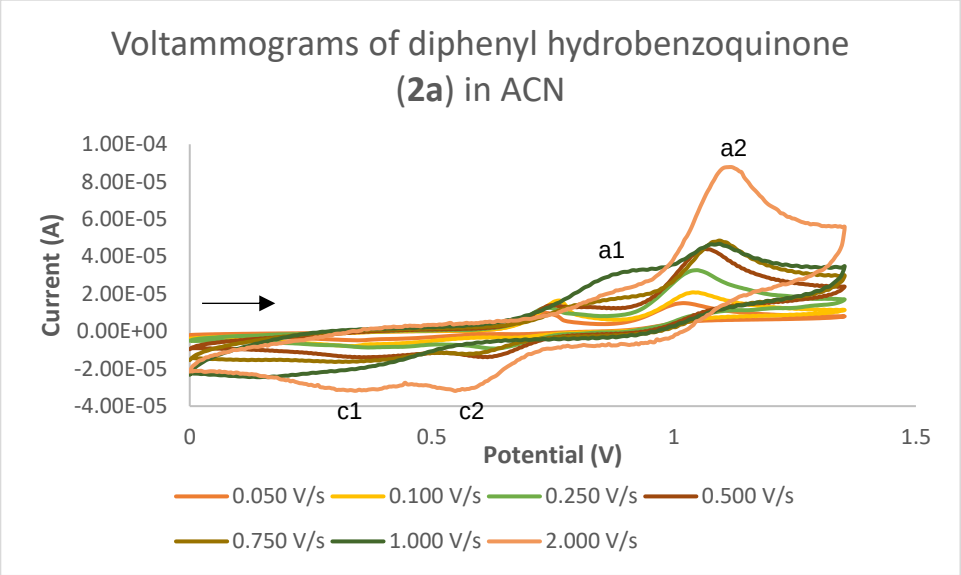


**Graphic 6.1** – Voltammograms of diphenyl hydrobenzoquinone (**2a**) in ACN, at multiple scan rates.

## Appendix 5 – Di-*tert*-butyl hydrobenzoquinone (2b)

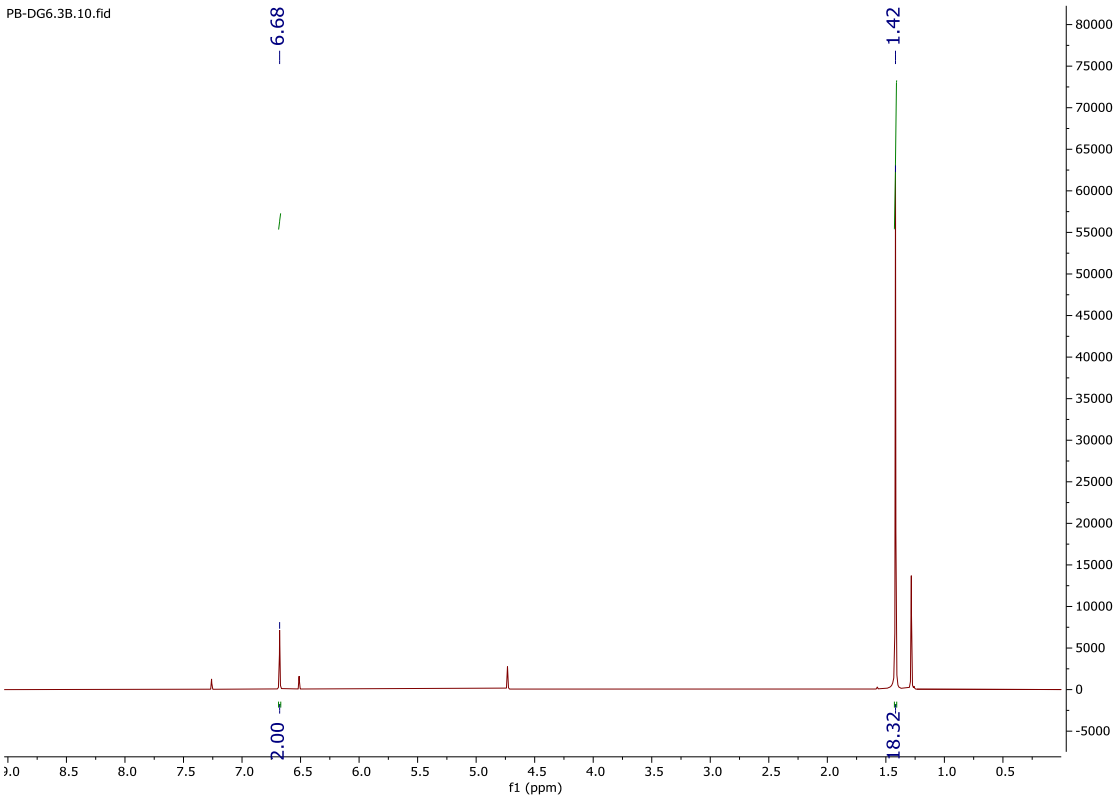


**Figure 6.13** – $^{1}H$ NMR spectrum of di-*tert*-butyl hydrobenzoquinone (**2b**) in $CDCl_3$.

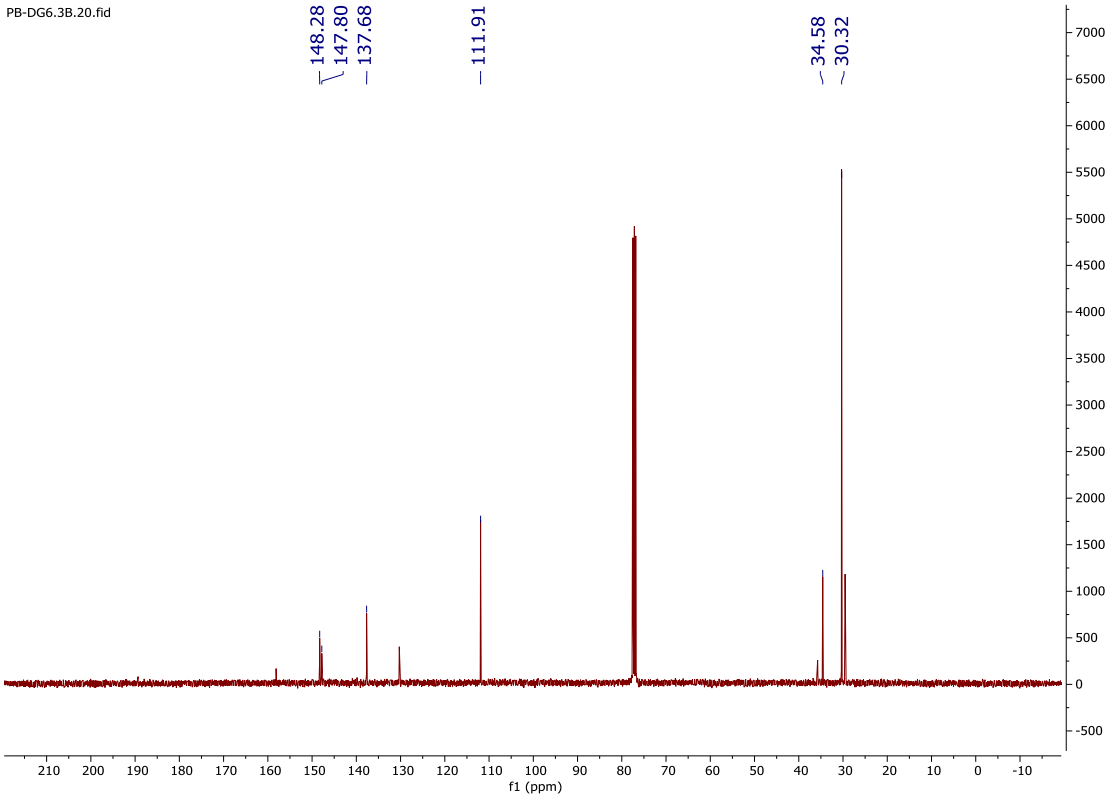


**Figure 6.14** – $^{13}C$ NMR spectrum of di-*tert*-butyl hydrobenzoquinone (**2b**) in $CDCl_3$.

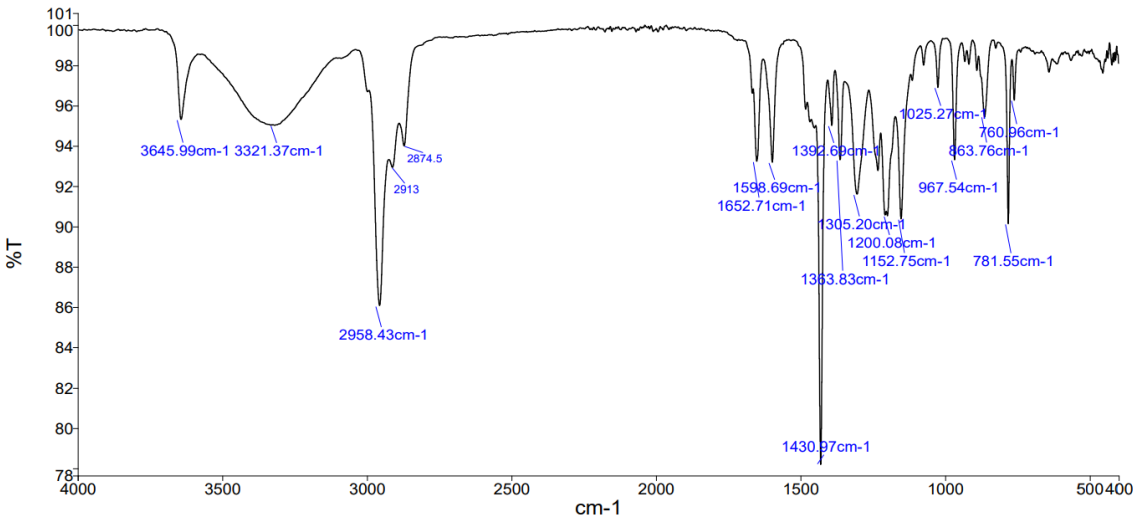


**Figure 6.15** – IR spectrum of di-*tert*-butyl hydrobenzoquinone (**2b**).

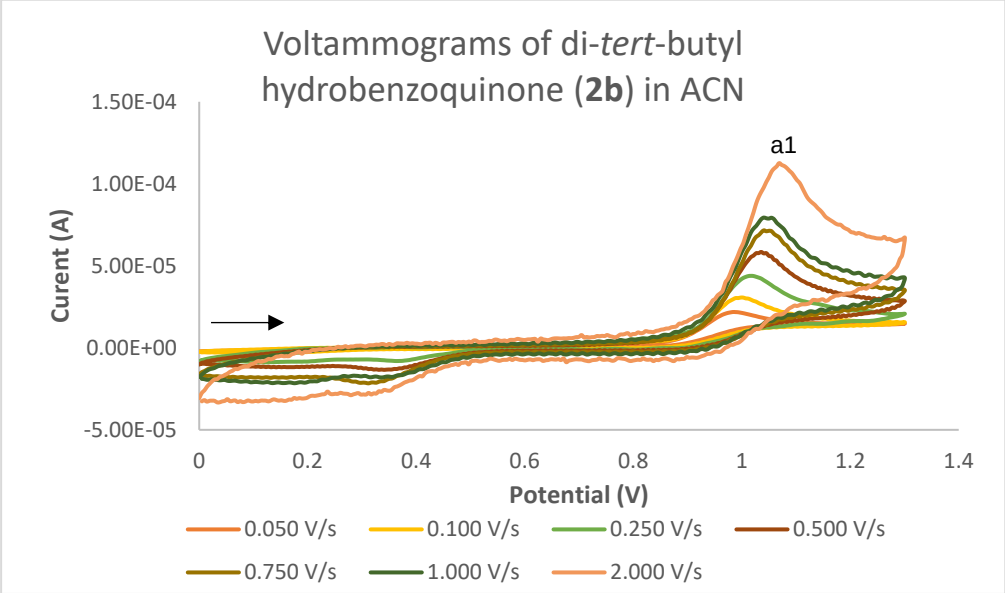


**Graphic 6.2** – Voltammograms of di-*tert*-butyl hydrobenzoquinone (**2b**) in ACN, at multiple scan rates.

## Appendix 6 – Diisopropyl hydrobenzoquinone (2c)

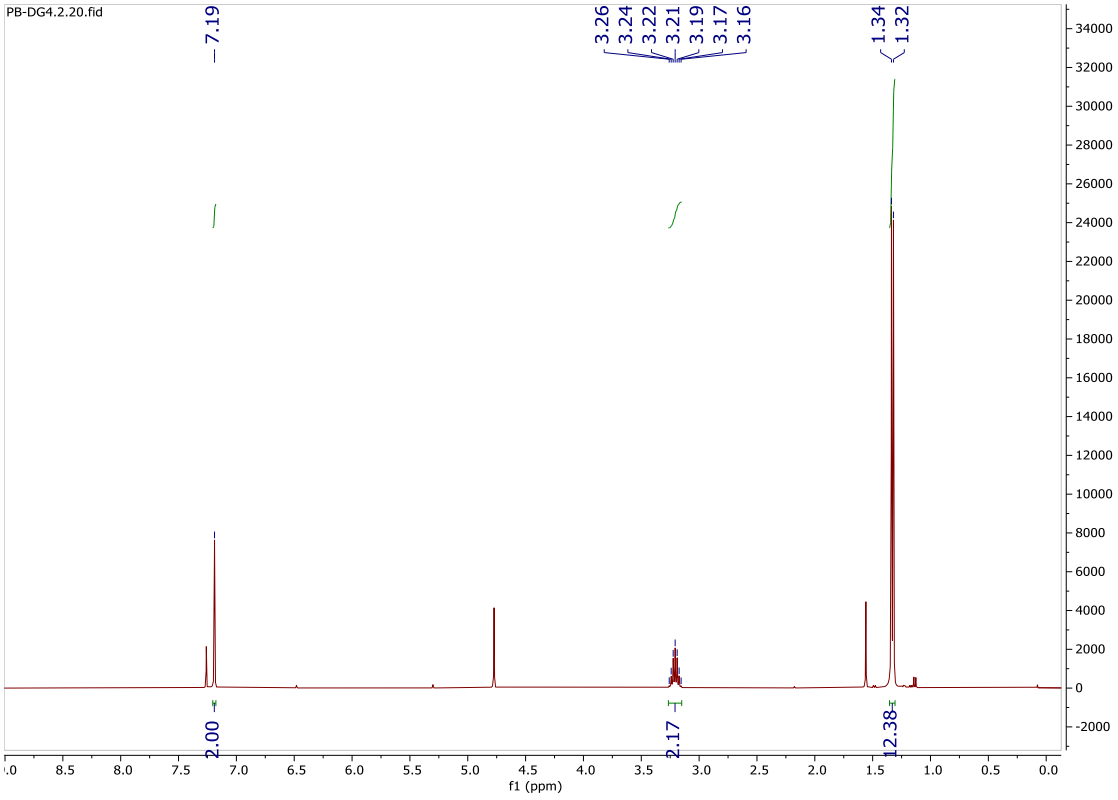


**Figure 6.16** – $^{1}H$ NMR spectrum of diisopropyl hydrobenzoquinone (**2c**) in $CDCl_3$.

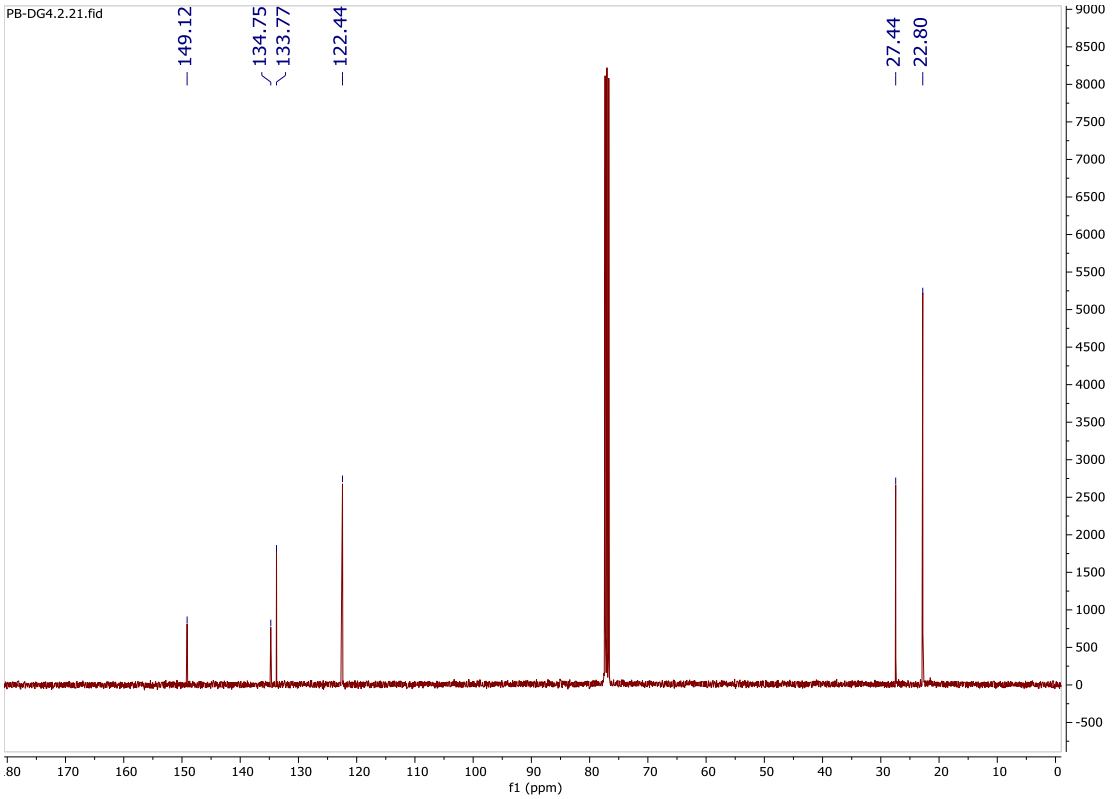


**Figure 6.17** – $^{13}C$ NMR spectrum of diisopropyl hydrobenzoquinone (**2c**) in $CDCl_3$.

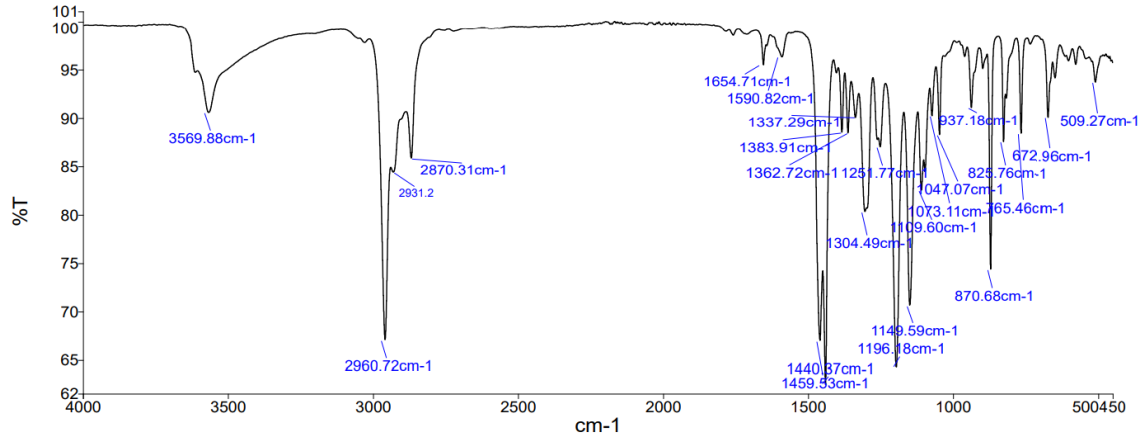


**Figure 6.18** – IR spectrum of diisopropyl hydrobenzoquinone (**2c**).

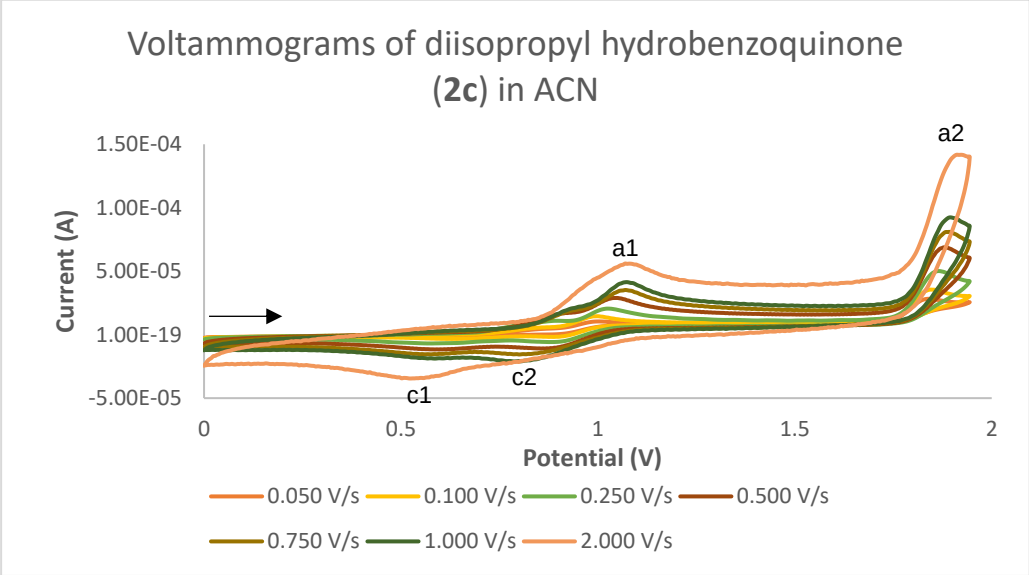


**Graphic 6.3** – Voltammograms of diisopropyl hydrobenzoquinone (**2c**) in ACN, at multiple scan rates.

## Appendix 7 – Tetraphenyl diphenoquinone (3a)

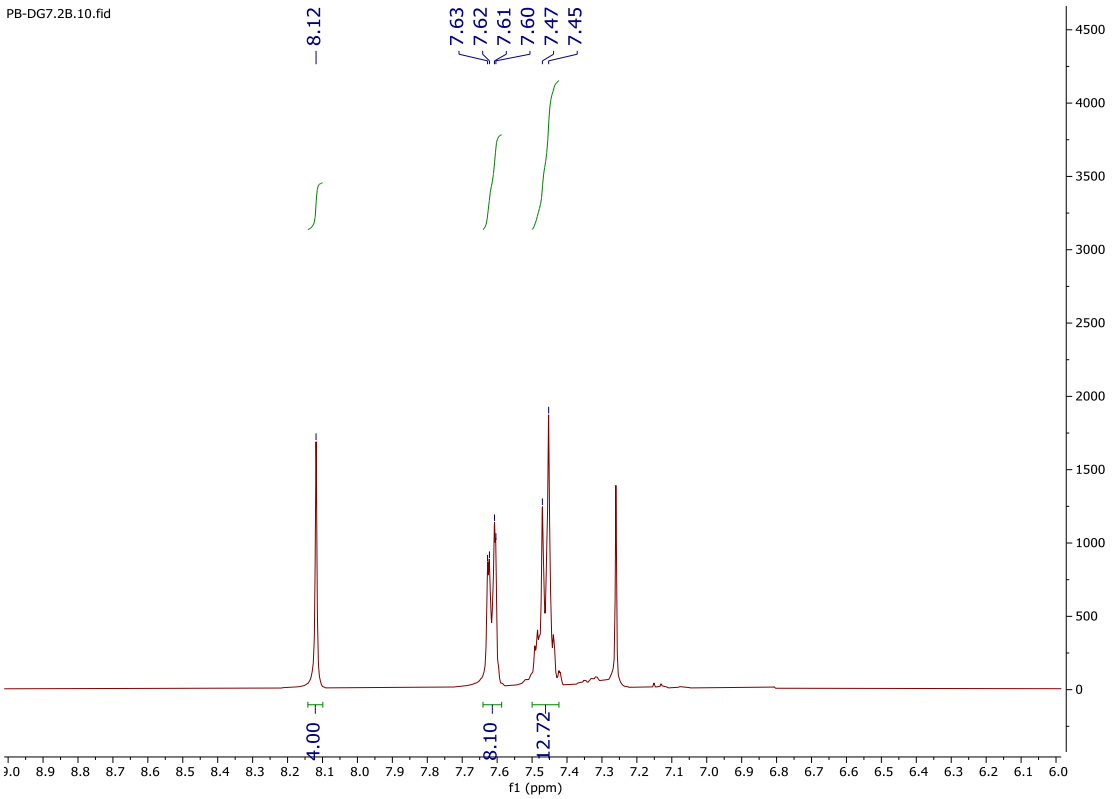


**Figure 6.19** – $^{1}H$ NMR spectrum of tetraphenyl diphenoquinone (**3a**) in $CDCl_3$.

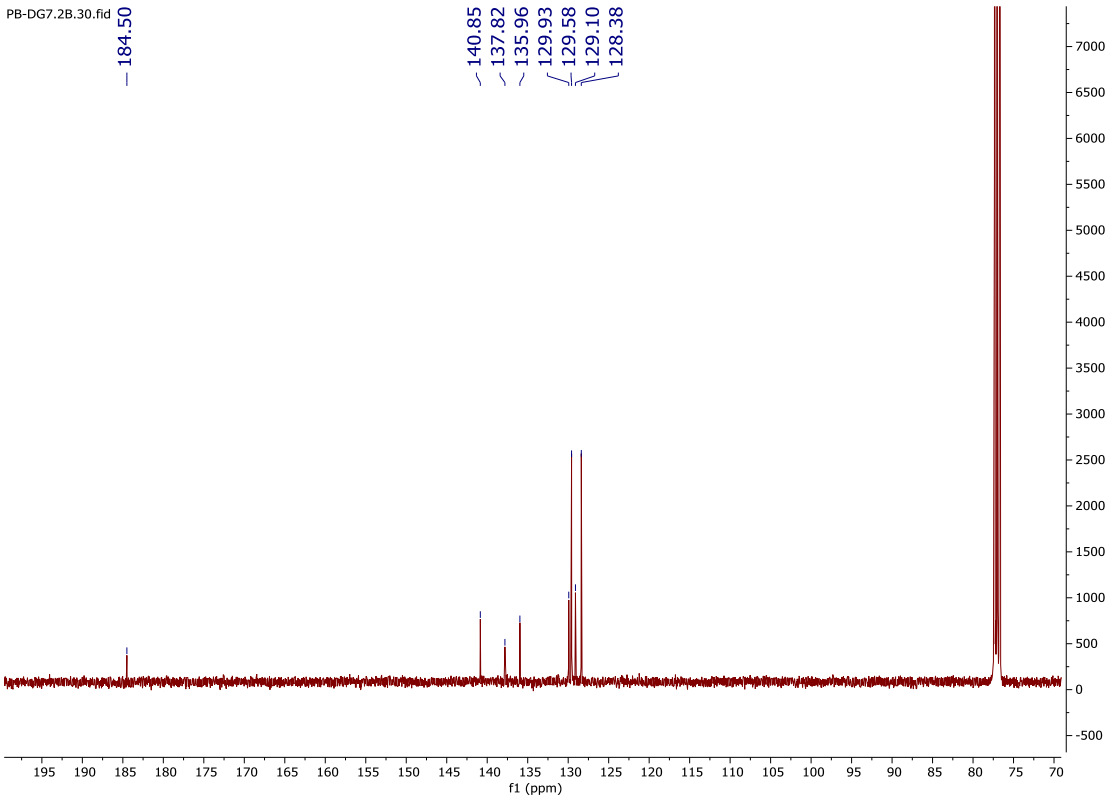


**Figure 6.20** – $^{13}C$ NMR spectrum of tetraphenyl diphenoquinone (**3a**) in $CDCl_3$.

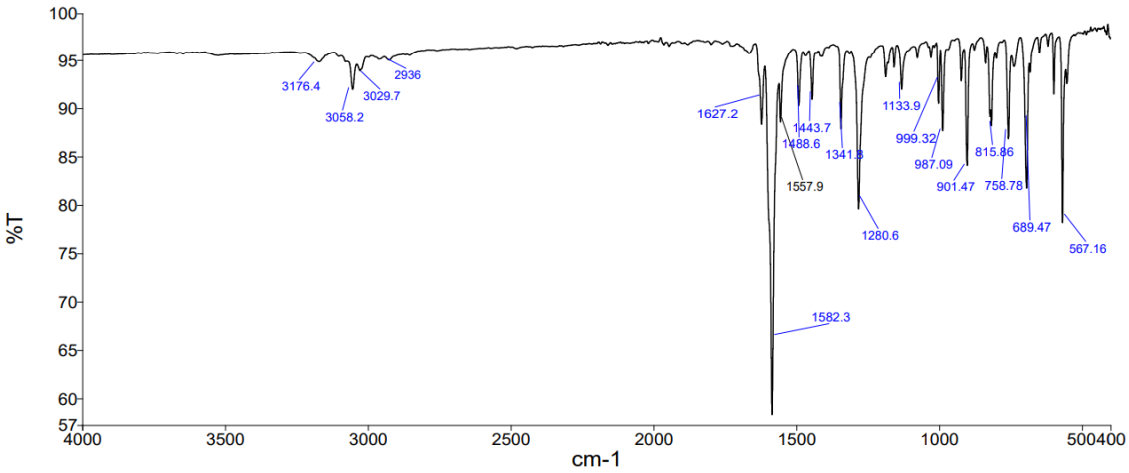


**Figure 6.21** – IR spectrum of tetraphenyl diphenoquinone (**3a**).

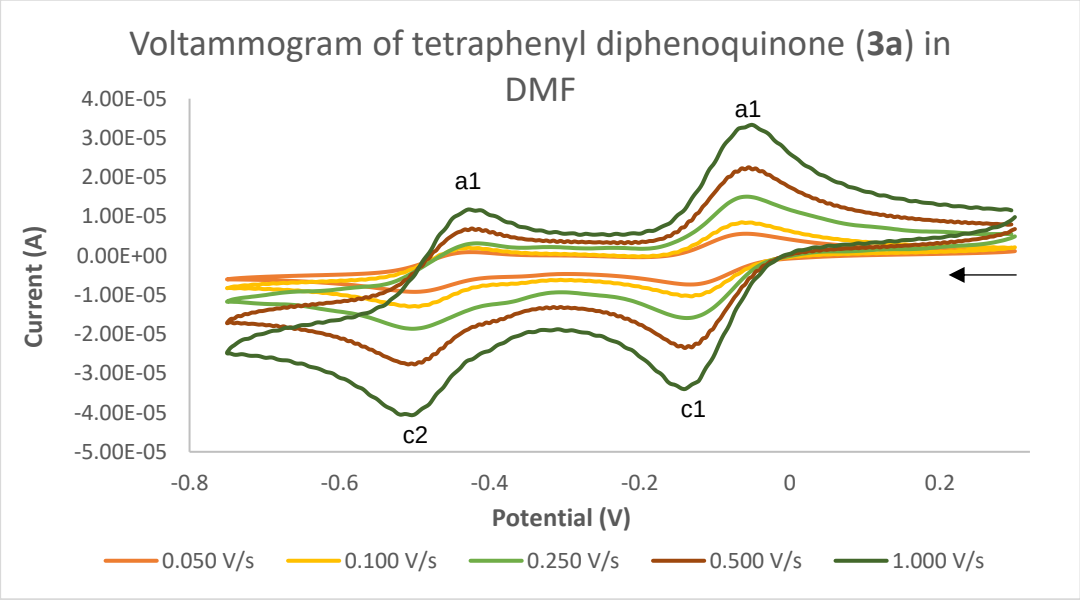


**Graphic 6.4** - Voltammograms of tetraphenyl diphenoquinone (**3a**) in DMF, at multiple scan rates.

## Appendix 8 – Tetra-*tert*-butyl diphenoquinone (3b)

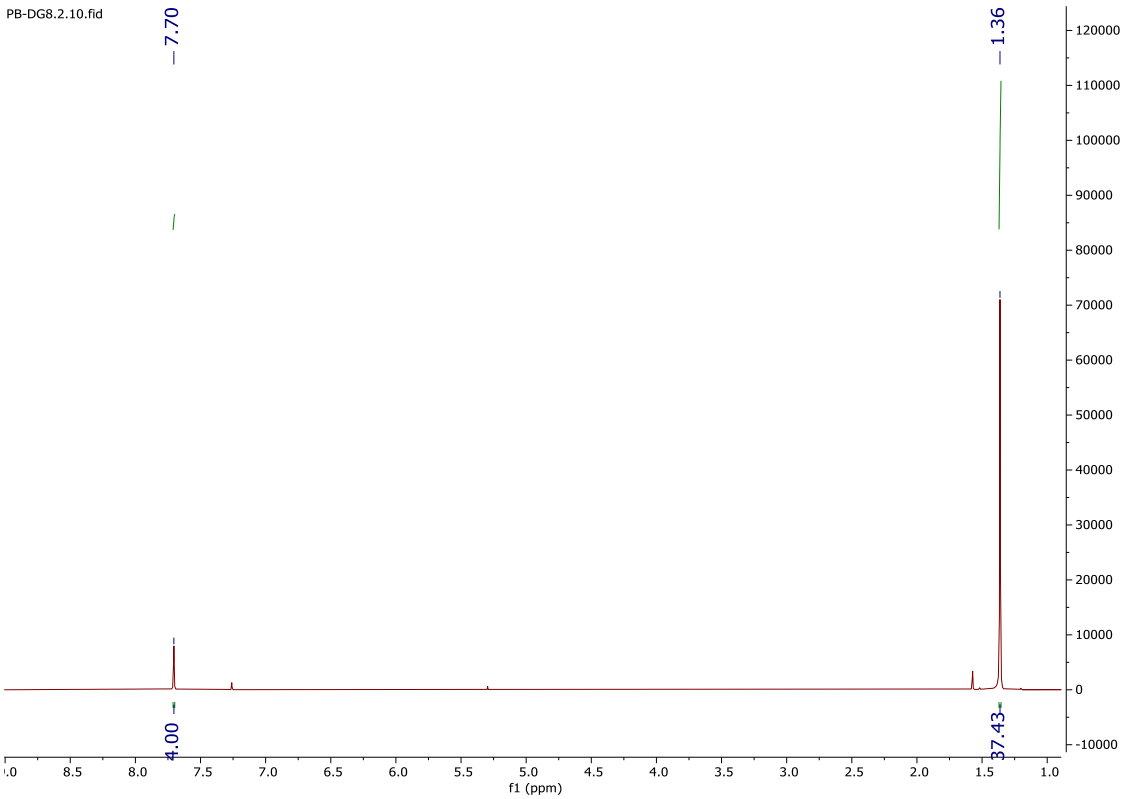


**Figure 6.22** – $^{1}$H NMR spectrum of tetra-tert-butyl diphenoquinone (**3b**) in $CDCl_3$.

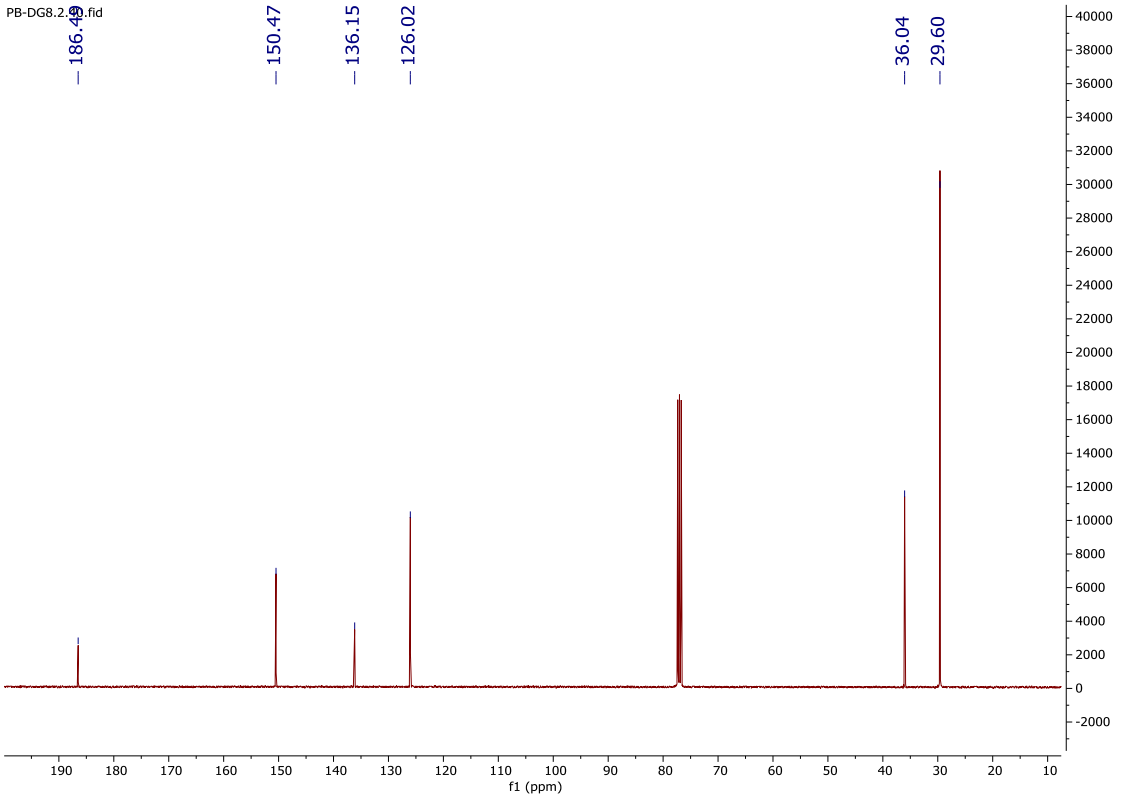


**Figure 6.23** – $^{13}C$ NMR spectrum of tetra-tert-butyl diphenoquinone (**3b**) in $CDCl_3$.

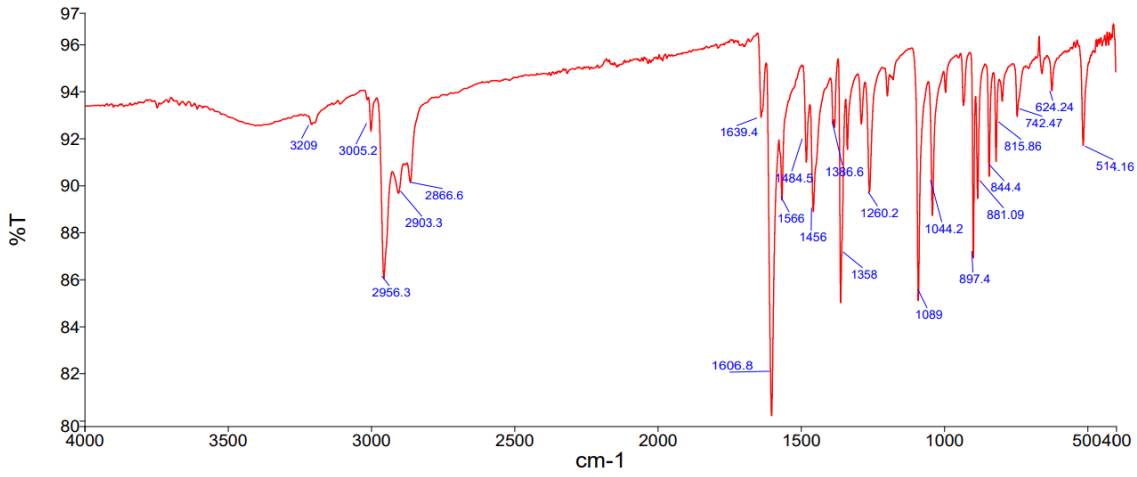


**Figure 6.24** – IR spectrum of tetra-tert-butyl diphenoquinone (**3b**).

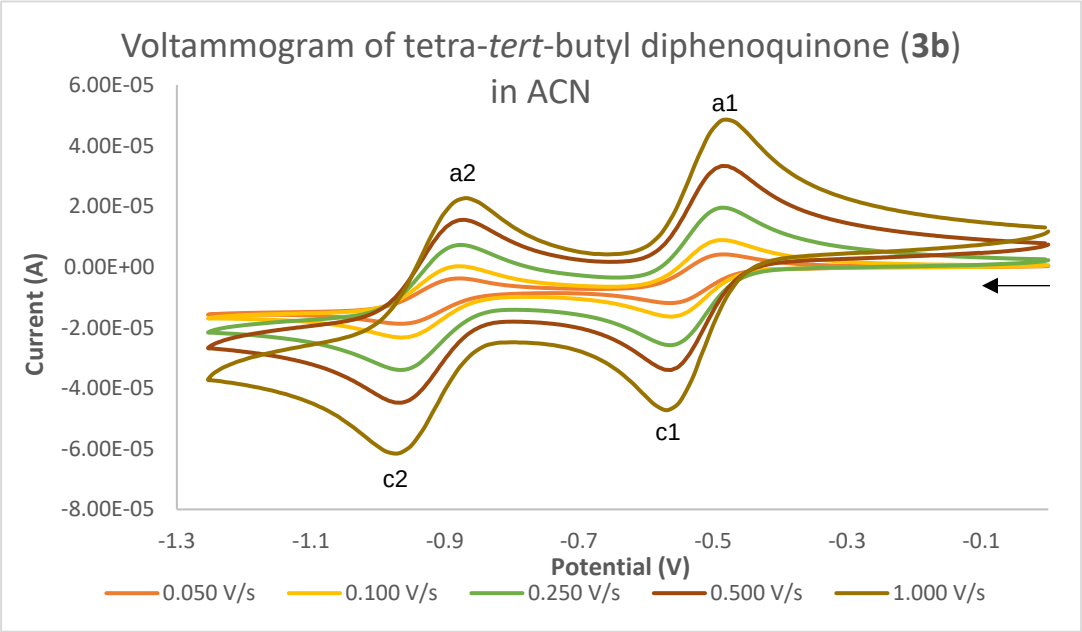


**Graphic 6.5** – Voltammograms of tetra-*tert*-butyl diphenoquinone (**3b**) in ACN, at multiple scan rates.

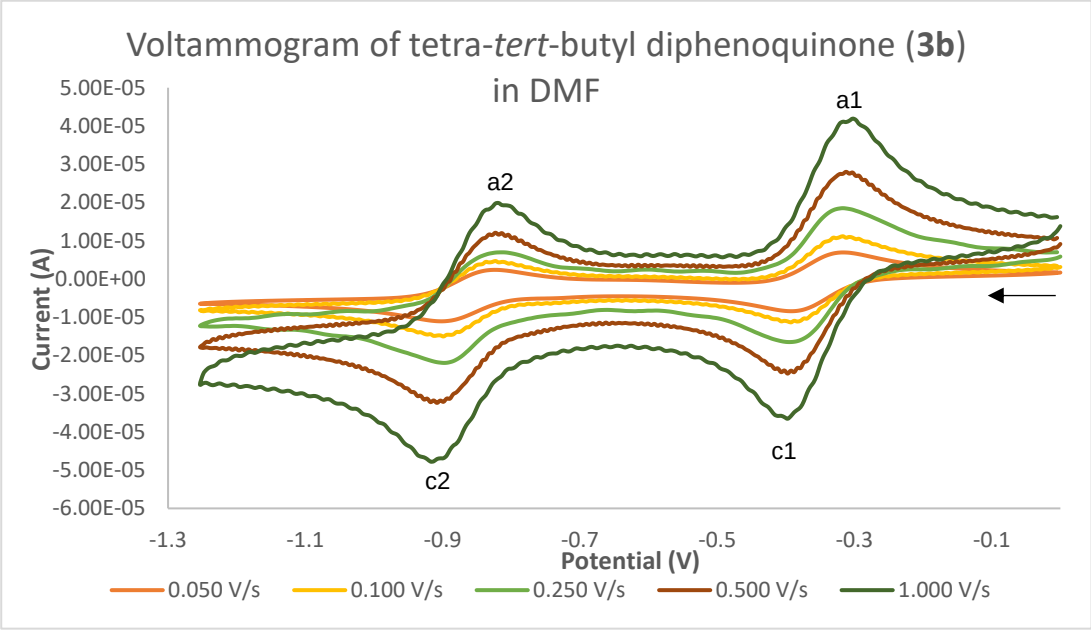


**Graphic 6.6** – Voltammograms of tetra-*tert*-butyl diphenoquinone (**3b**) in DMF, at multiple scan rates.

## Appendix 9 – Tetraisopropyl diphenoquinone (3c)

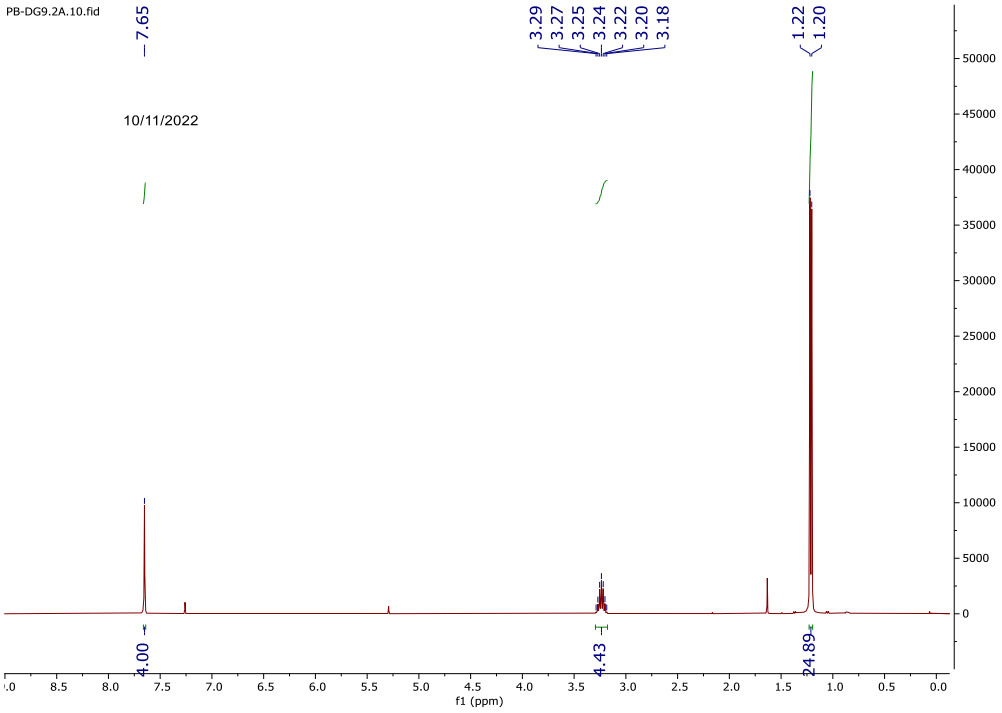


**Figure 6.25** – $^{1}H$ NMR spectrum of tetraisopropyl diphenoquinone (**3c**) in $CDCl_3$.

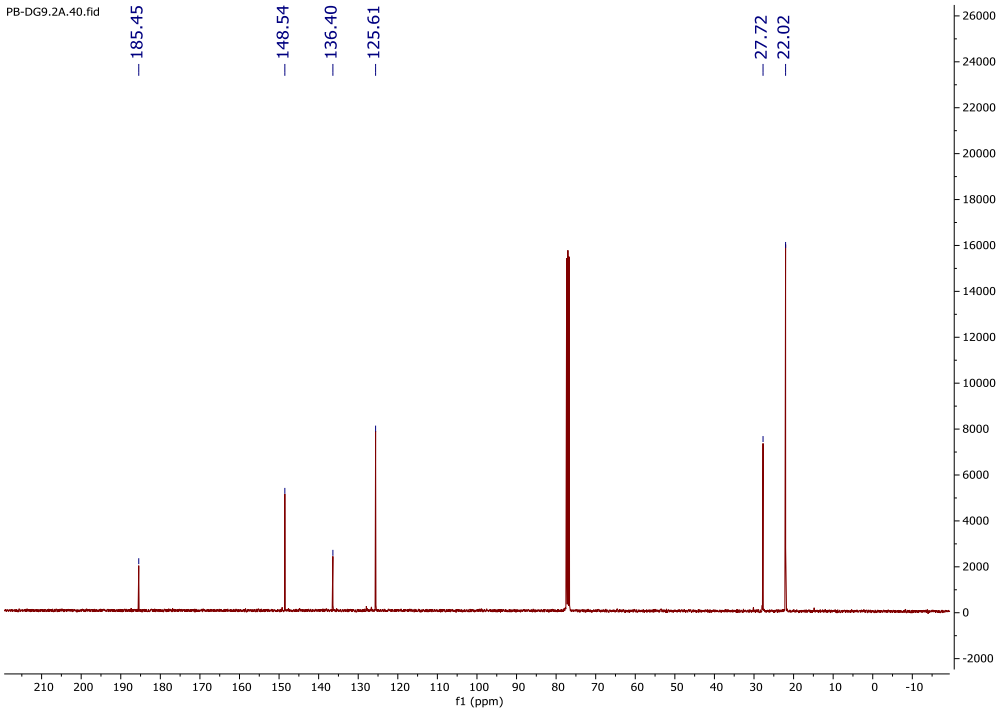


**Figure 6.26** – $^{13}C$ NMR spectrum of tetraisopropyl diphenoquinone (**3c**) in $CDCl_3$.

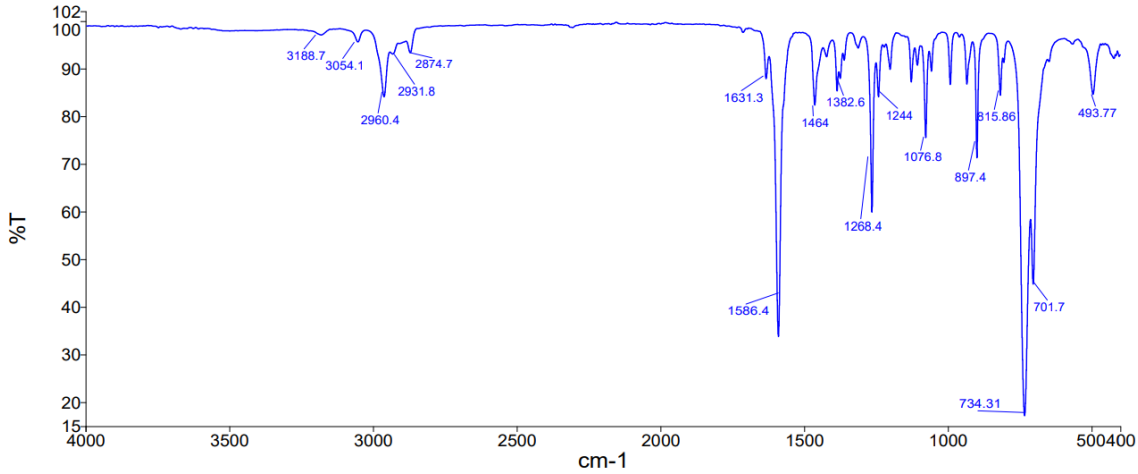


**Figure 6.27** – IR spectrum of tetraisopropyl diphenoquinone (**3c**).

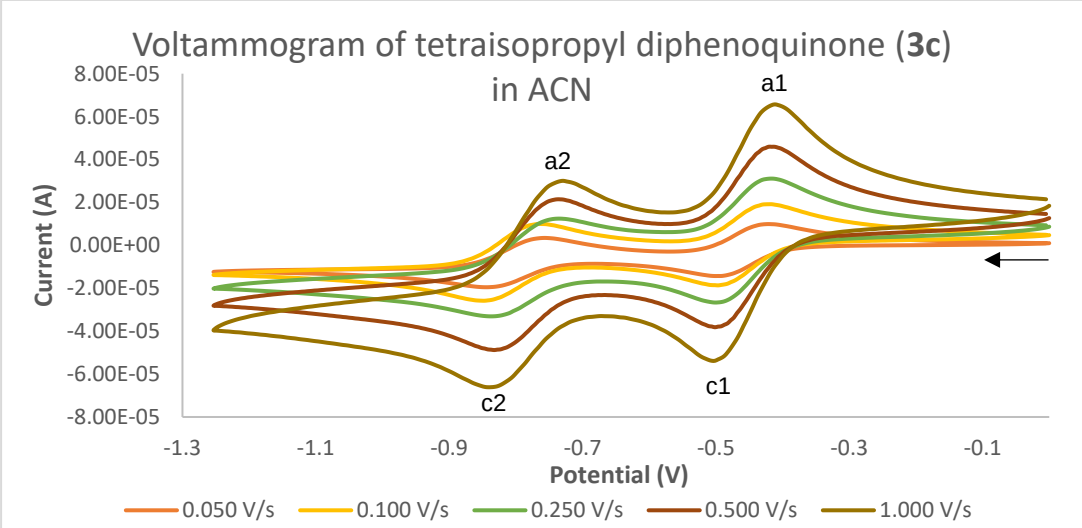


**Graphic 6.7** - Voltammograms of tetraisopropyl diphenoquinone (**3c**) in ACN, at multiple scan rates.

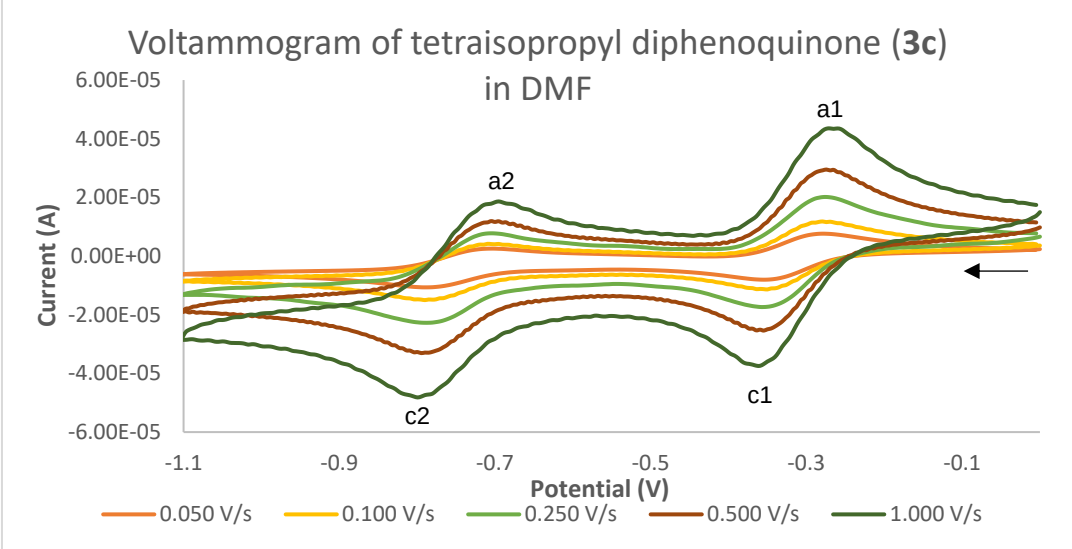


**Graphic 6.8** - Voltammograms of tetraisopropyl diphenoquinone (**3c**) in DMF, at multiple scan rates.

## Appendix 10 – Tetraphenyl hydrodiphenoquinone (4a)

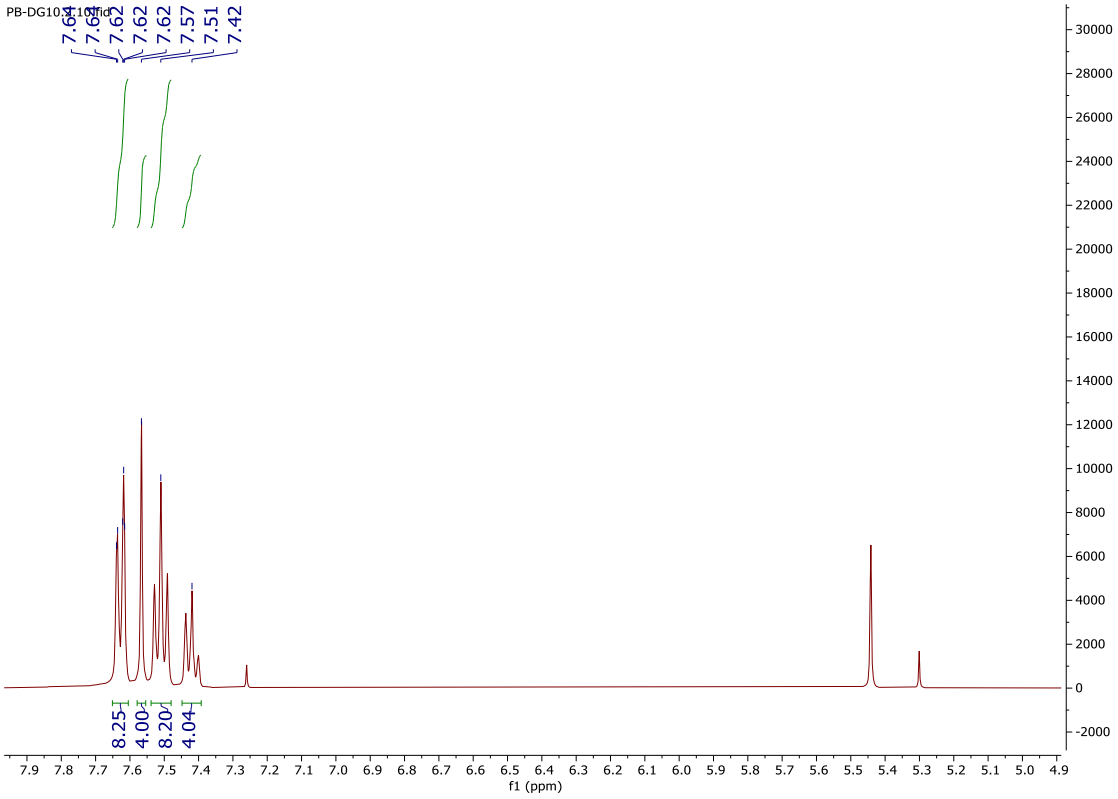


**Figure 6.28** – $^{1}H$ NMR spectrum of tetraphenyl hydrodiphenoquinone (**4a**) in $CDCl_3$.

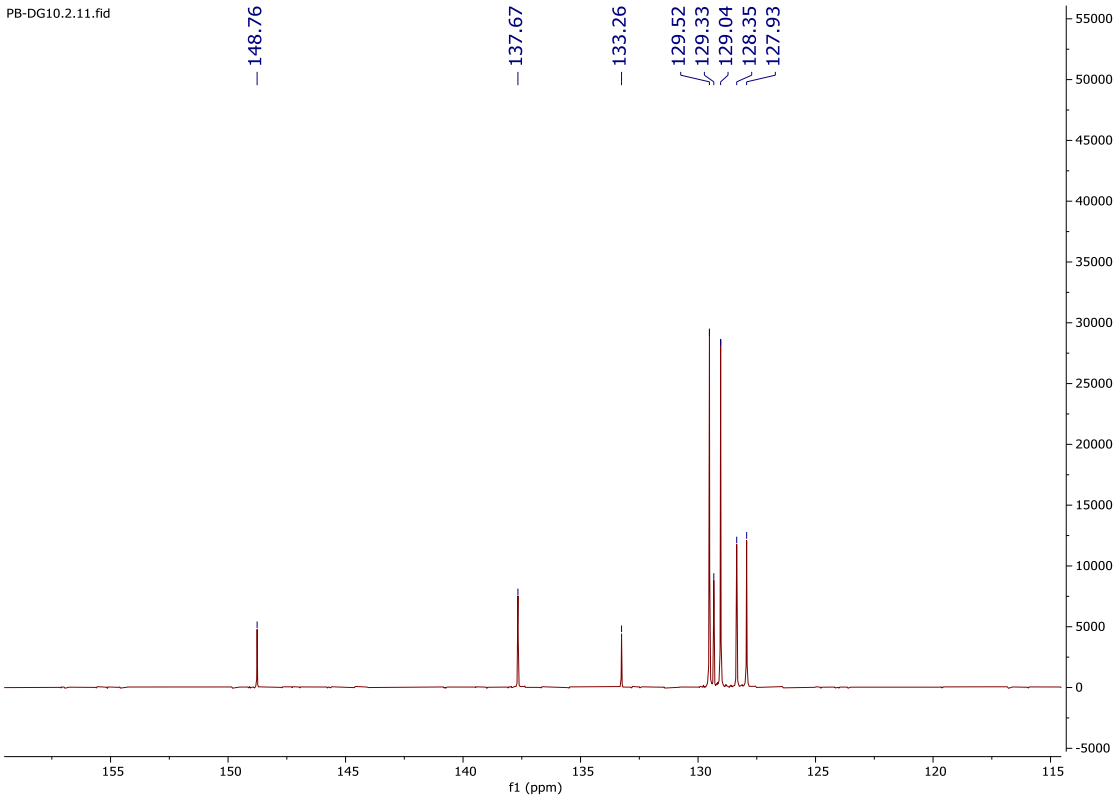


**Figure 6.29** – $^{13}C$ NMR spectrum of tetraphenyl hydrodiphenoquinone (**4a**) in $CDCl_3$.

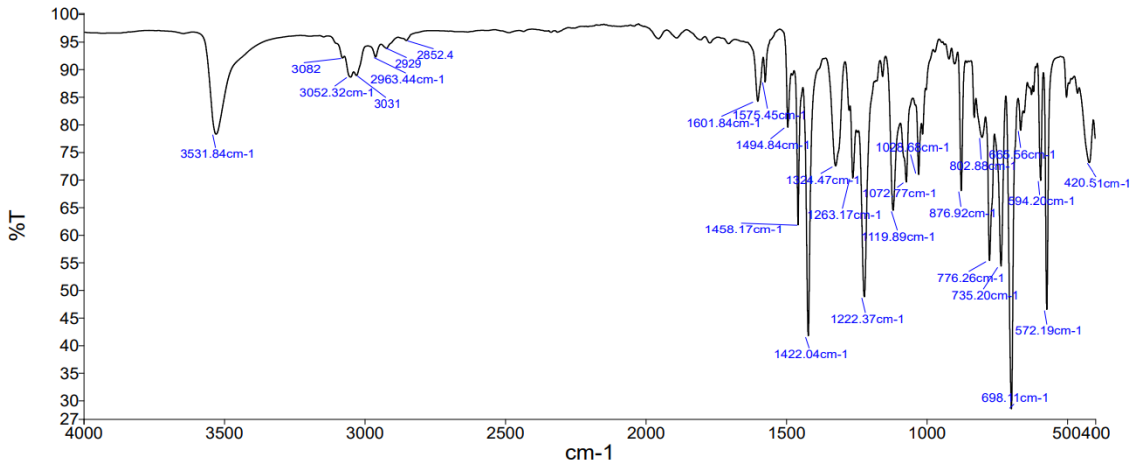


**Figure 6.30** – IR spectrum of tetraphenyl hydrodiphenoquinone (**4a**).

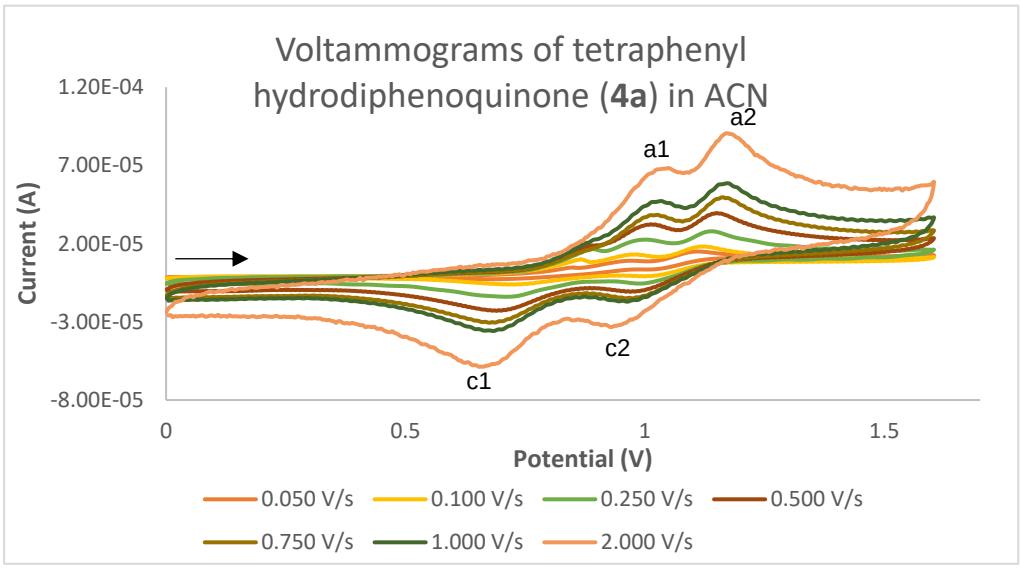


**Graphic 6.9** – Voltammograms of tetraphenyl hydrodiphenoquinone (**4a**) in ACN, at multiple scan rates.

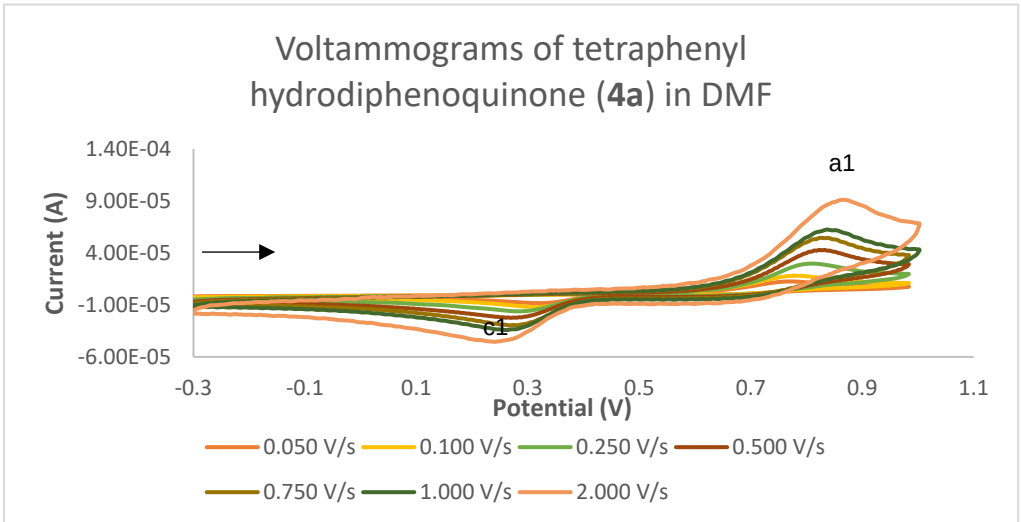


**Graphic 6.10** – Voltammograms of tetraphenyl hydrodiphenoquinone (**4a**) in DMF, at multiple scan rates.

## Appendix 11 – Tetra-*tert*-butyl hydrodiphenoquinone (4b)

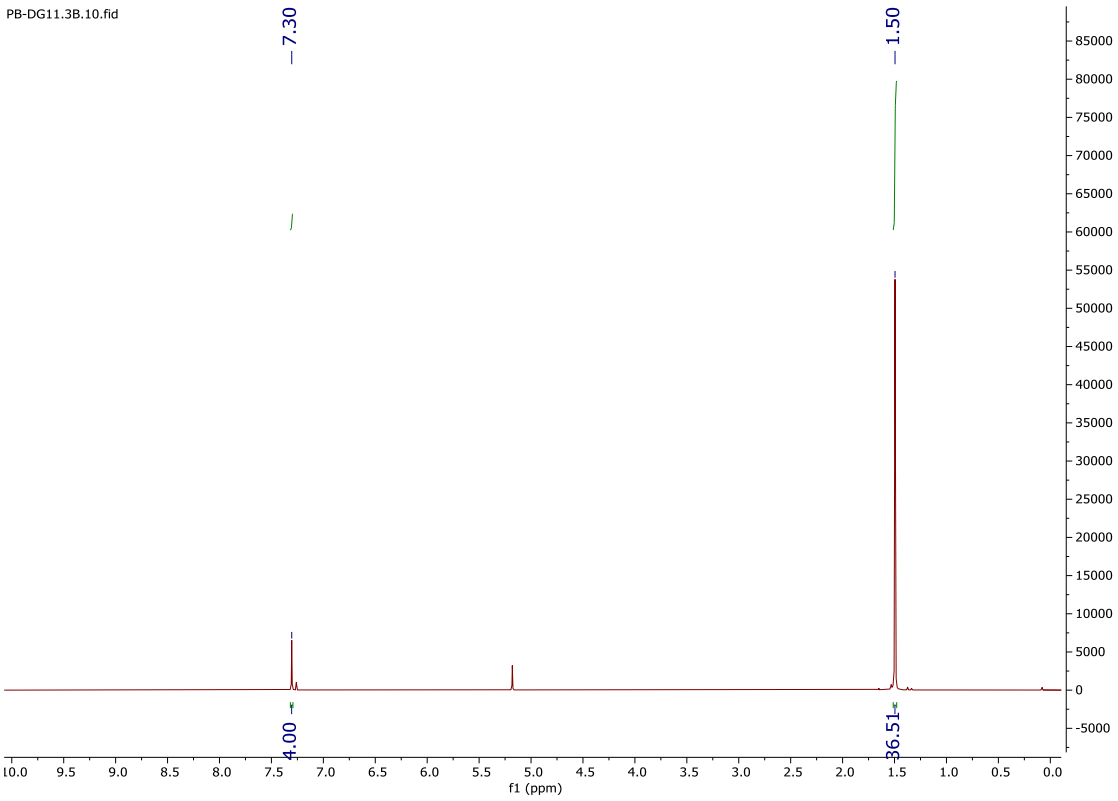


**Figure 6.31** – $^{1}$H NMR spectrum of tetra-*tert*-butyl hydrodiphenoquinone (**4b**) in $CDCl_3$.

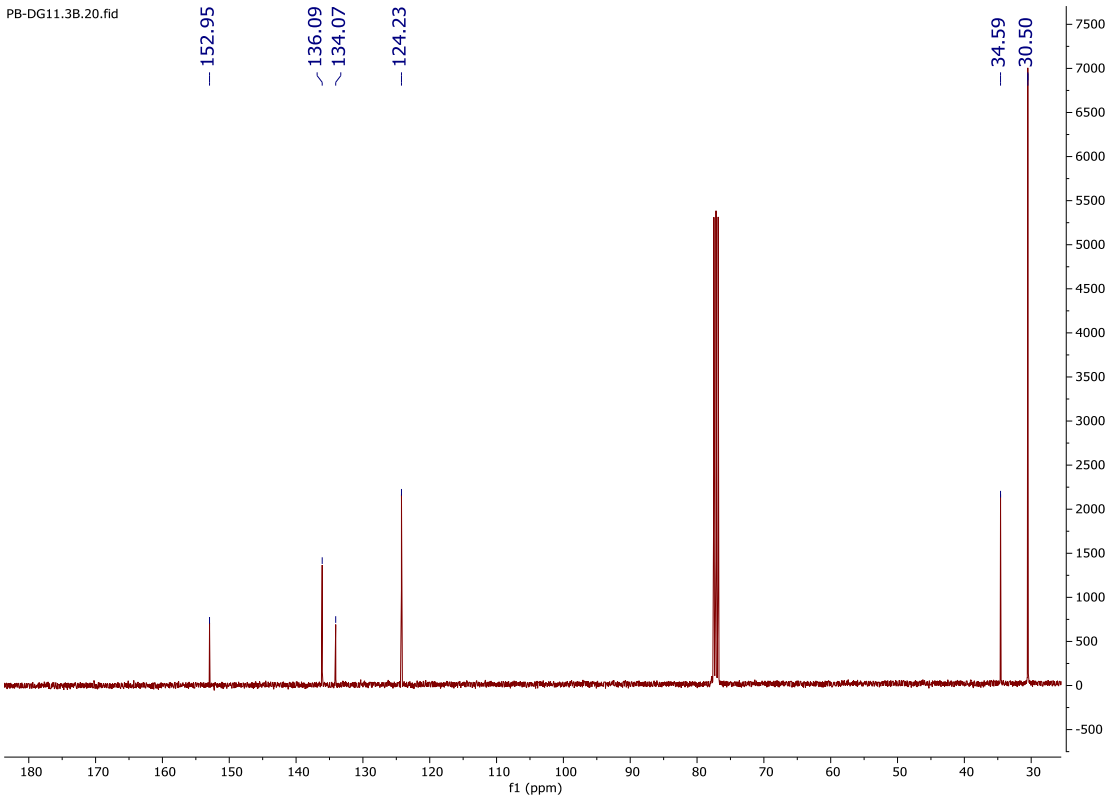


**Figure 6.32** – $^{13}$C NMR spectrum of tetra-*tert*-butyl hydrodiphenoquinone (**4b**) in $CDCl_3$.

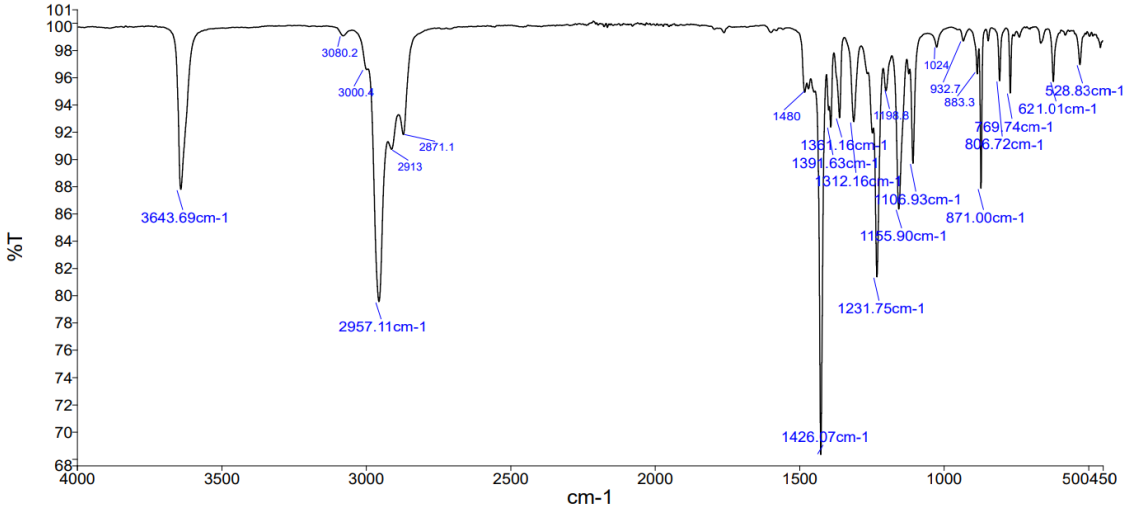


**Figure 6.33** – IR spectrum of tetra-*tert*-butyl hydrodiphenoquinone (**4b**).

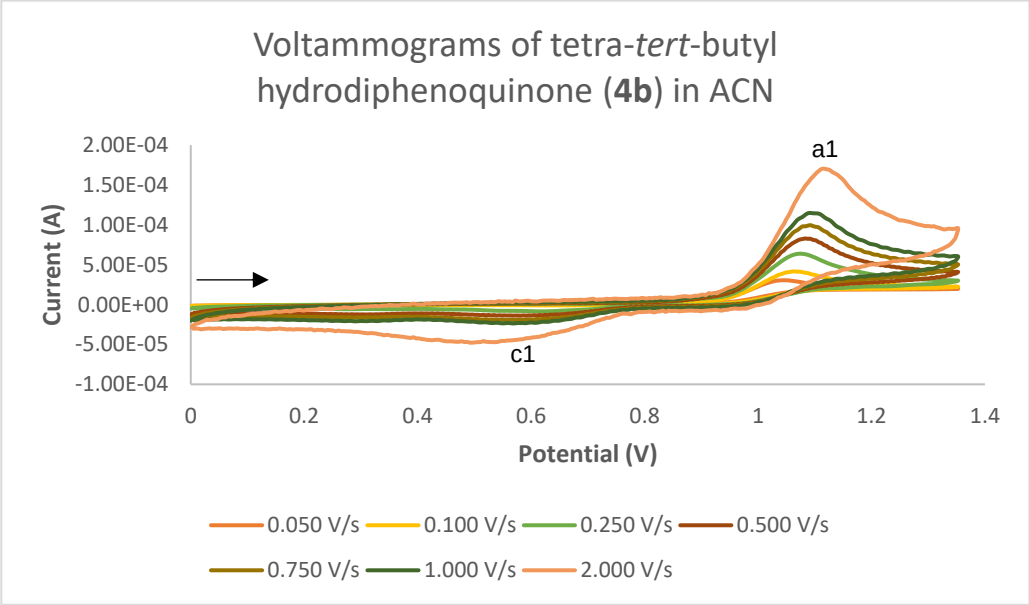


**Graphic 6.11** – Voltammograms of tetra-*tert*-butyl hydrodiphenoquinone (**4b**) in ACN, at multiple scan rates.

## Appendix 12 – Tetraisopropyl hydrodiphenoquinone (4c)

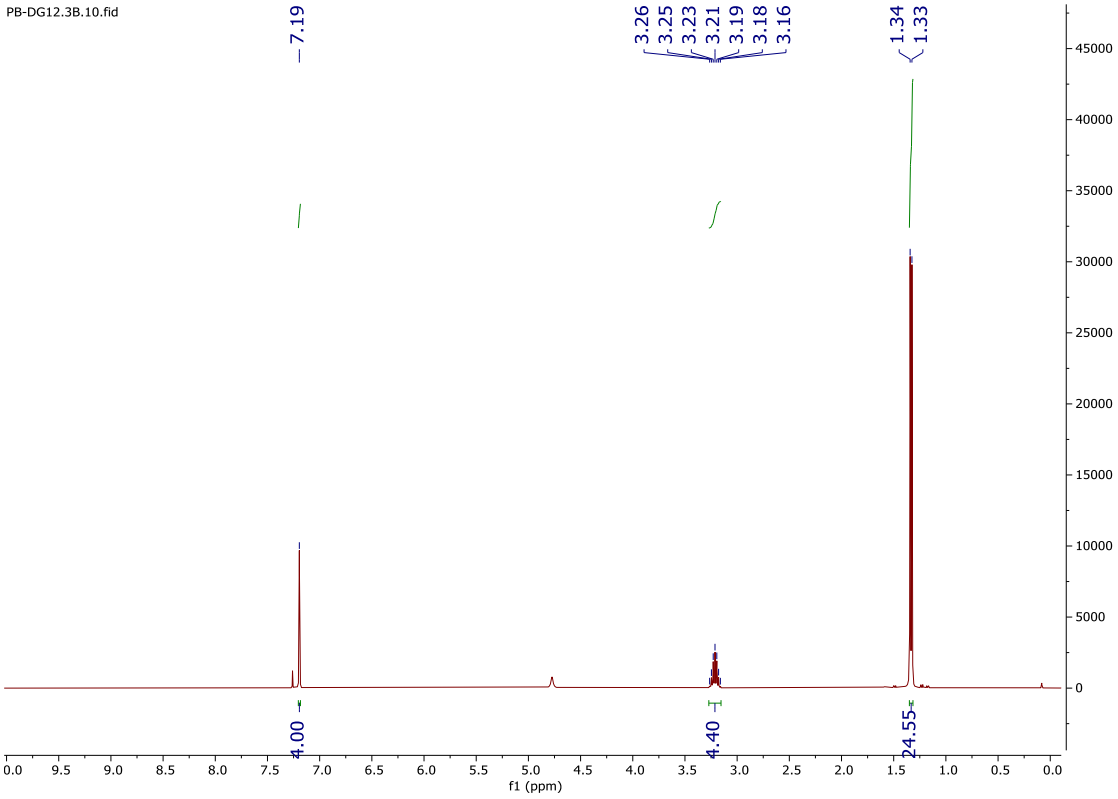


**Figure 6.34** – $^{1}H$ NMR spectrum of tetraisopropyl hydrodiphenoquinone (**4c**) in $CDCl_3$.

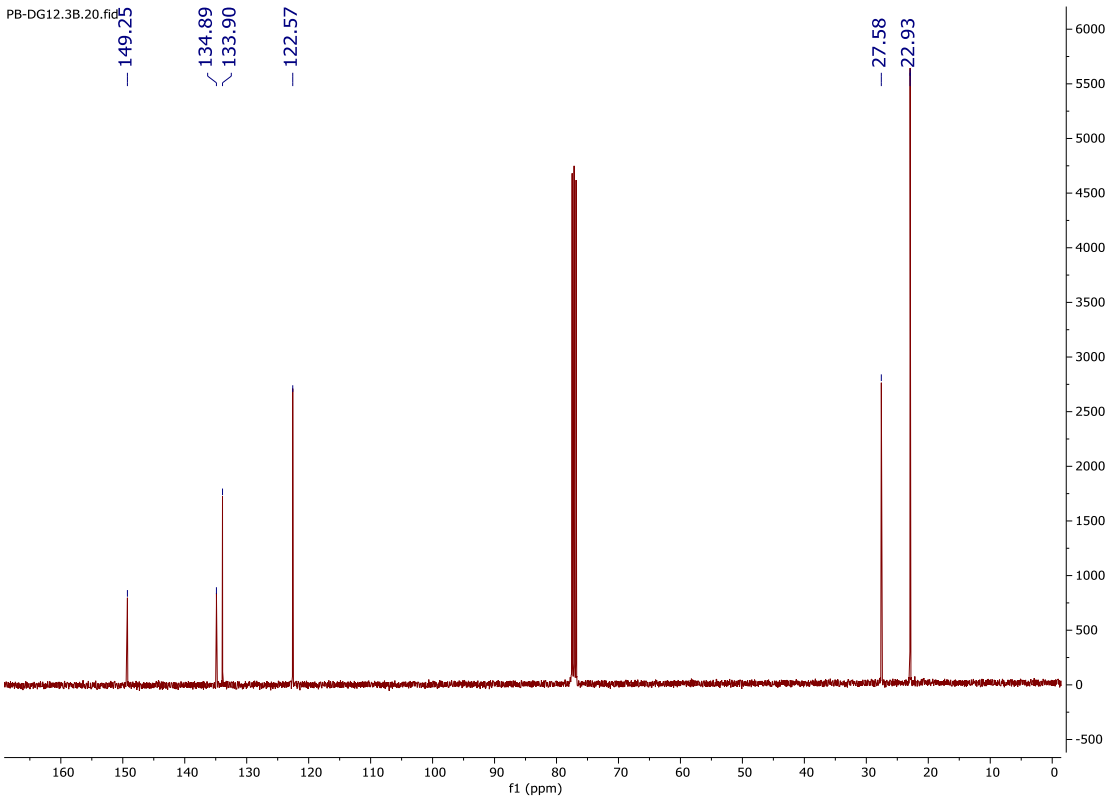


**Figure 6.35** – $^{13}C$ NMR spectrum of tetraisopropyl hydrodiphenoquinone (**4c**) in $CDCl_3$.

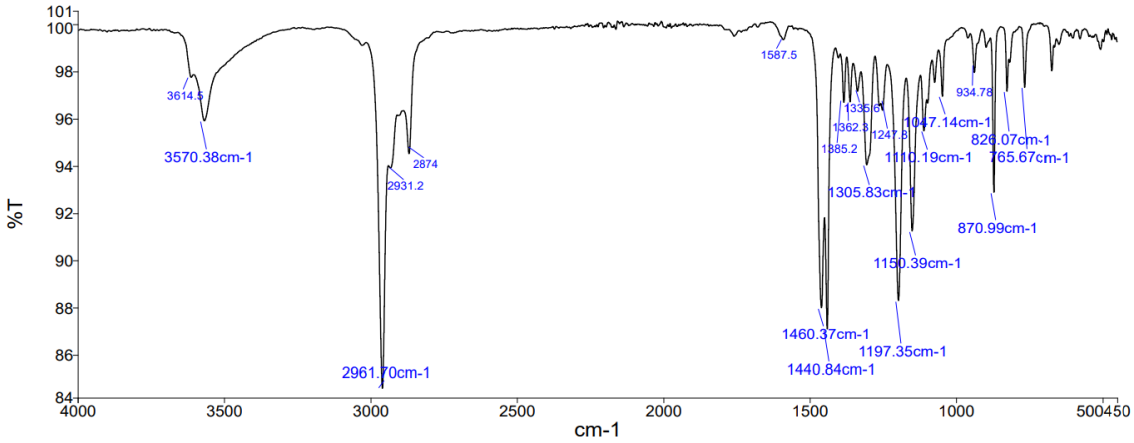


**Figure 6.36** – IR spectrum of tetraisopropyl hydrodiphenoquinone (**4c**).

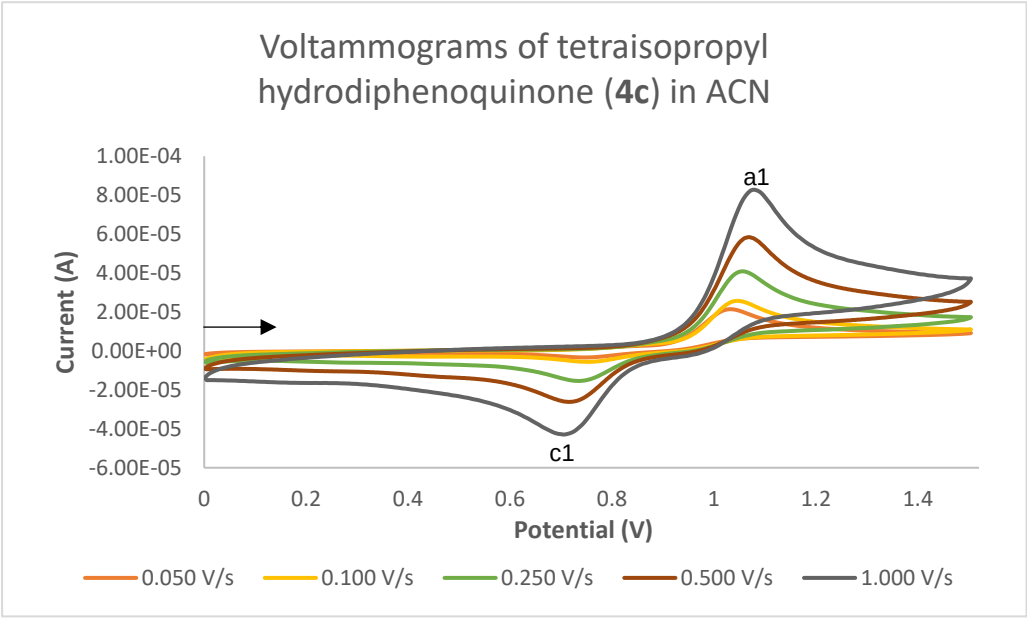


**Graphic 6.12** – Voltammograms of tetraisopropyl hydrodiphenoquinone (**4c**) in ACN, at multiple scan rates.

## Appendix 13 – 1,3-di-*tert*-butyl-2-methoxybenzene (5)

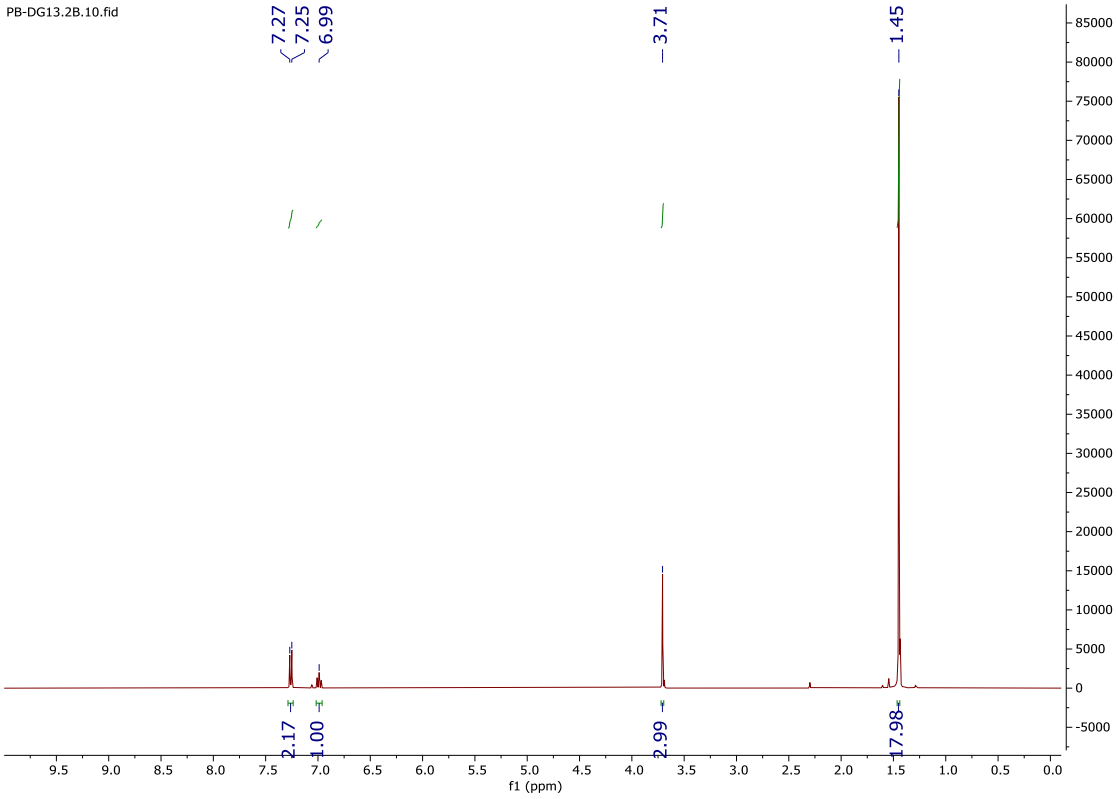


**Figure 6.37** – $^{1}$H NMR spectrum 1,3-di-*tert*-butyl-2-methoxybenzene (**5**) in $CDCl_3$.

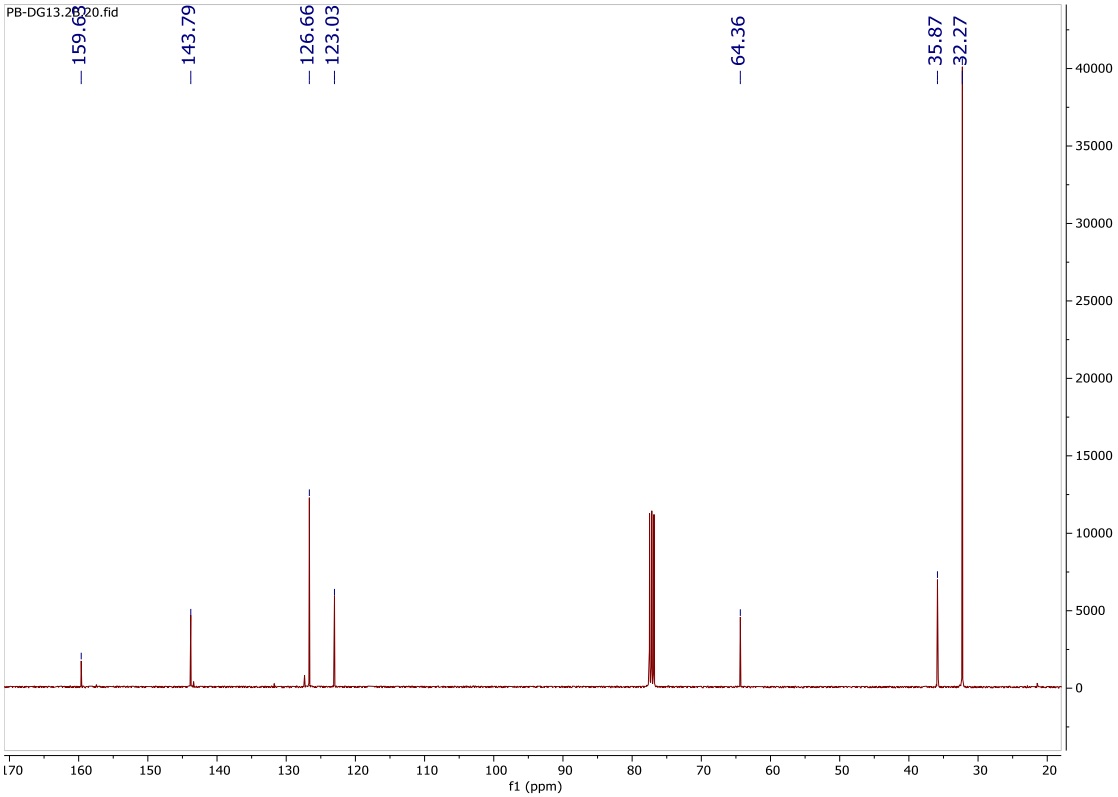


**Figure 6.38** – $^{13}$C NMR spectrum 1,3-di-*tert*-butyl-2-methoxybenzene (**5**) in $CDCl_3$.

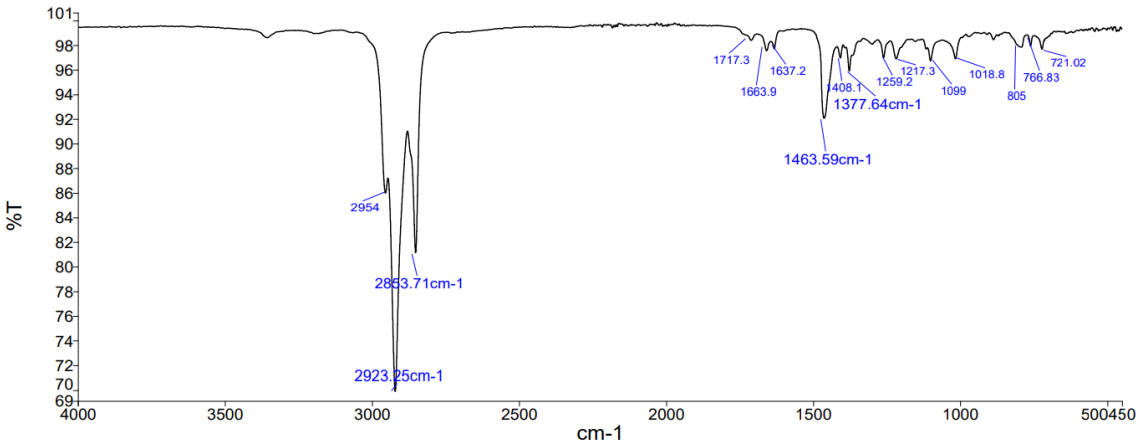


**Figure 6.39** – IR spectrum 1,3-di-*tert*-butyl-2-methoxybenzene (**5**).

## Appendix 14 – 5-bromo-1,3-di-*tert*-butyl-2-methoxybenzene (6)

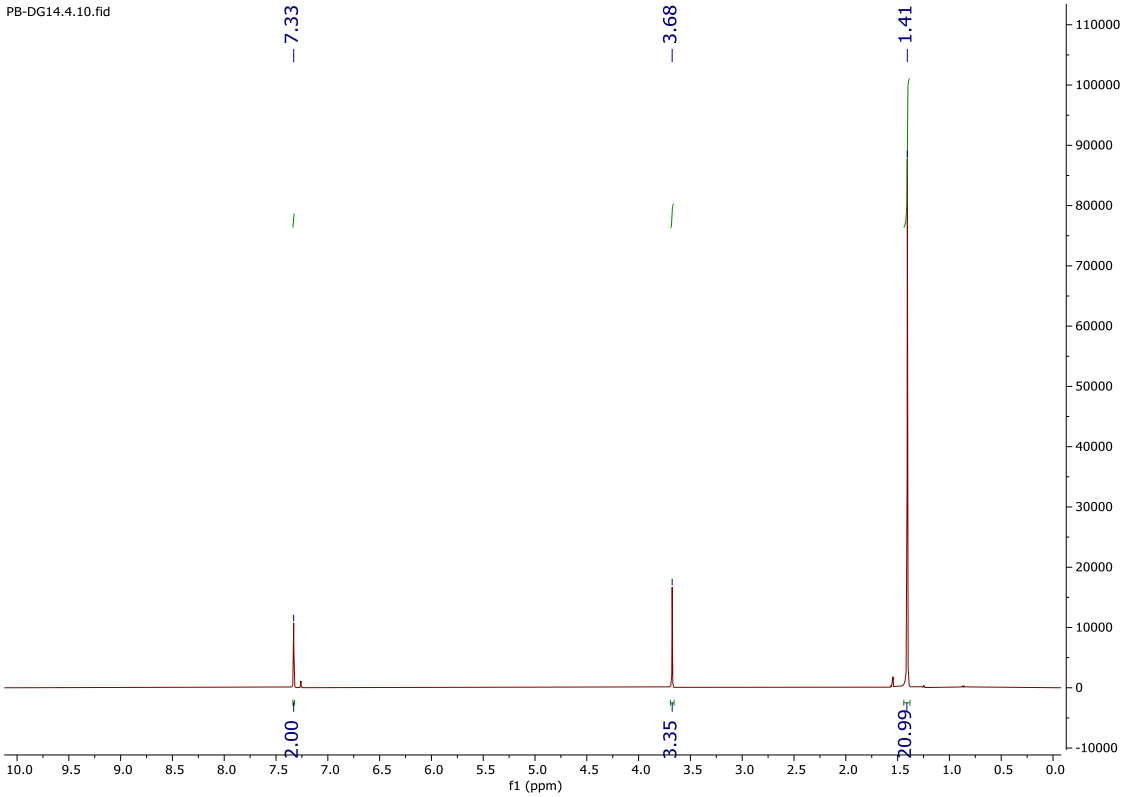


**Figure 6.40** – $^{1}H$ NMR spectrum 5-bromo-1,3-di-*tert*-butyl-2-methoxybenzene (**6**) in $CDCl_3$.

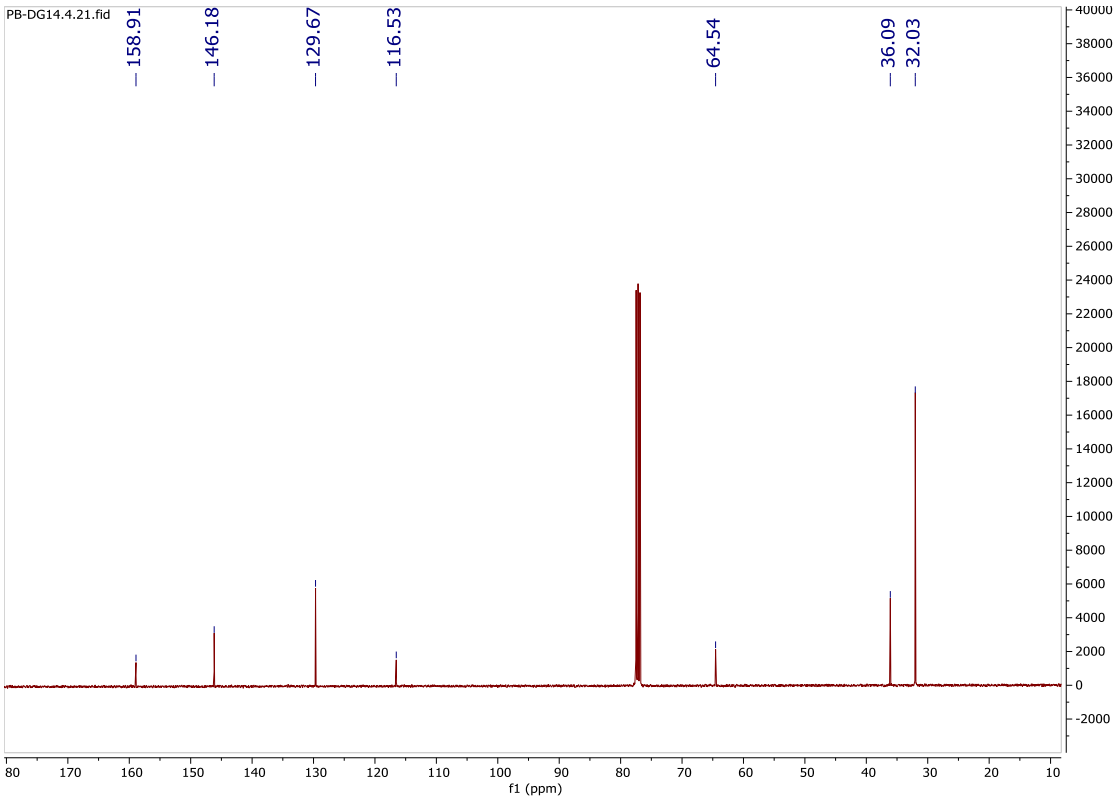


**Figure 6.41** – $^{13}C$ NMR spectrum 5-bromo-1,3-di-*tert*-butyl-2-methoxybenzene (**6**) in $CDCl_3$.

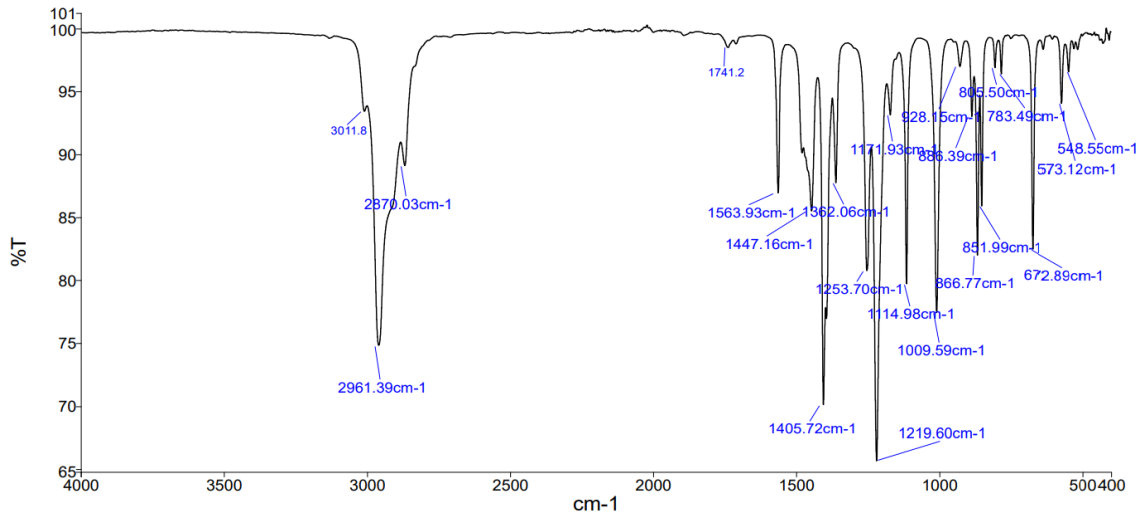


**Figure 6.42** – IR spectrum 5-bromo-1,3-di-*tert*-butyl-2-methoxybenzene (**6**).

## Appendix 15 – 2-(3,5-di-tert-butyl-4-methoxyphenyl)-4,4,5,5-tetramethyl-1,3,2-dioxaborolane (7)

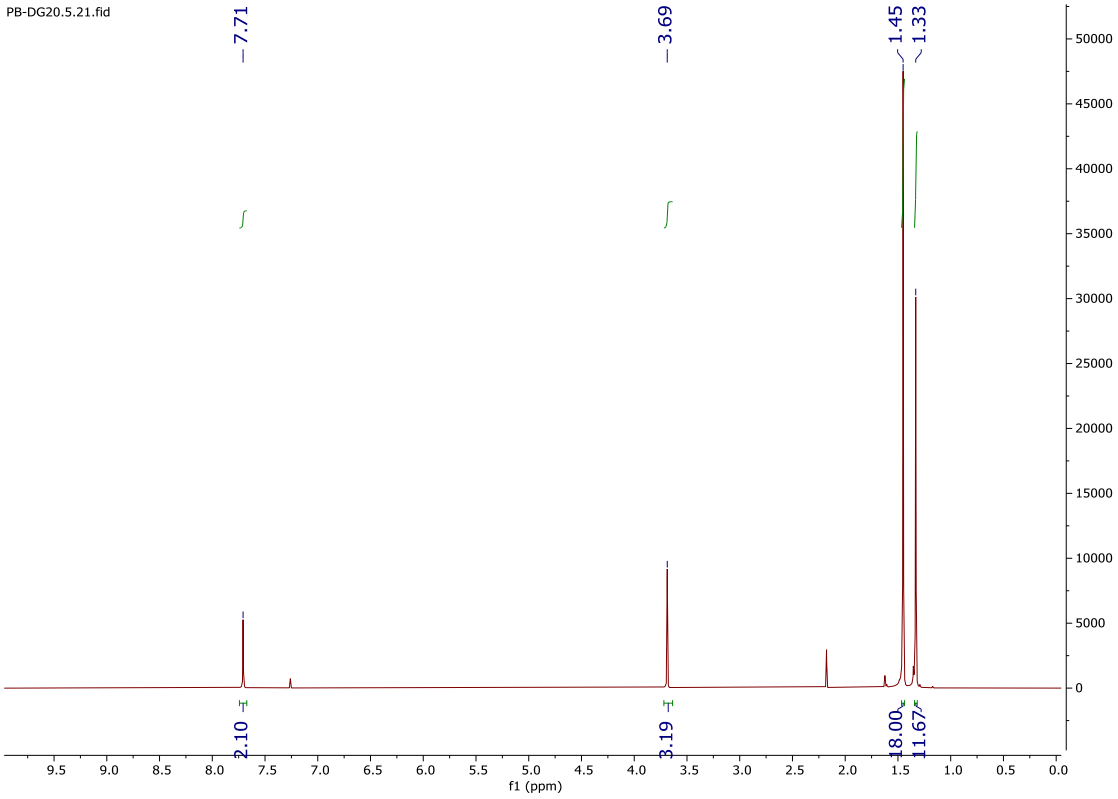


**Figure 6.43** – $^{1}H$ NMR spectrum of 2-(3,5-di-tert-butyl-4-methoxyphenyl)-4,4,5,5-tetramethyl-1,3,2-dioxaborolane (**7**) in $CDCl_3$.

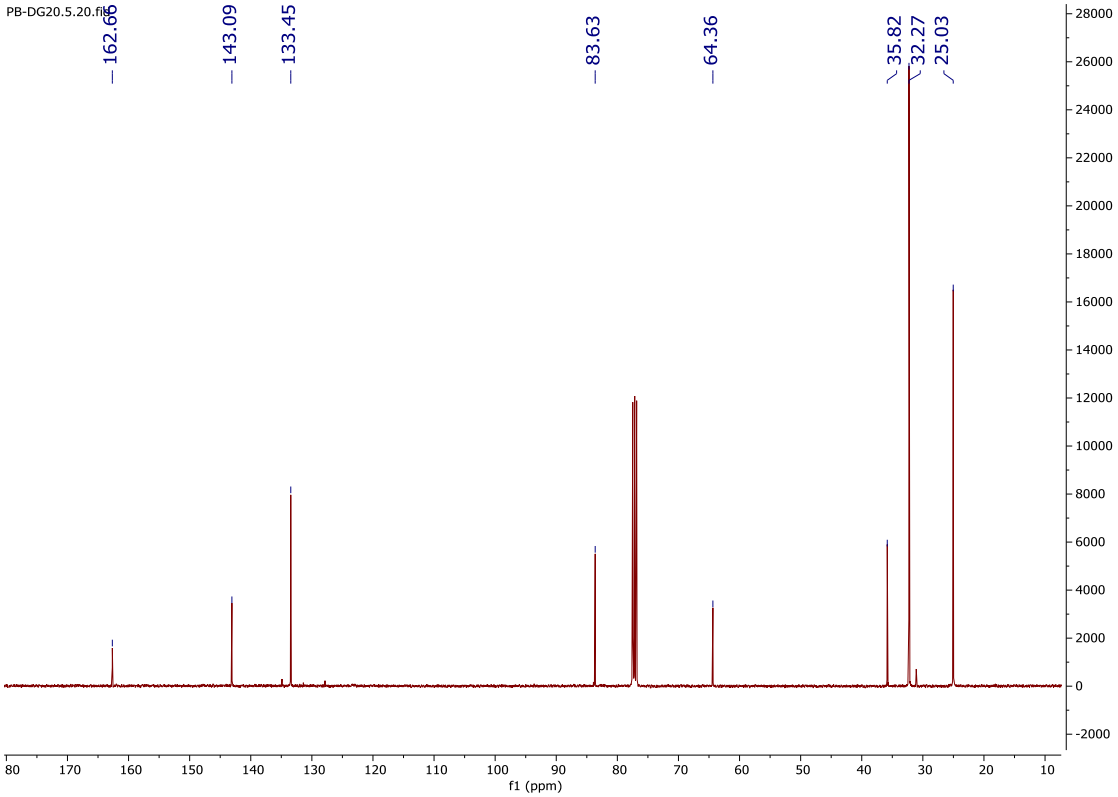


**Figure 6.44** – $^{13}C$ NMR spectrum of 2-(3,5-di-tert-butyl-4-methoxyphenyl)-4,4,5,5-tetramethyl-1,3,2-dioxaborolane (**7**) in $CDCl_3$.

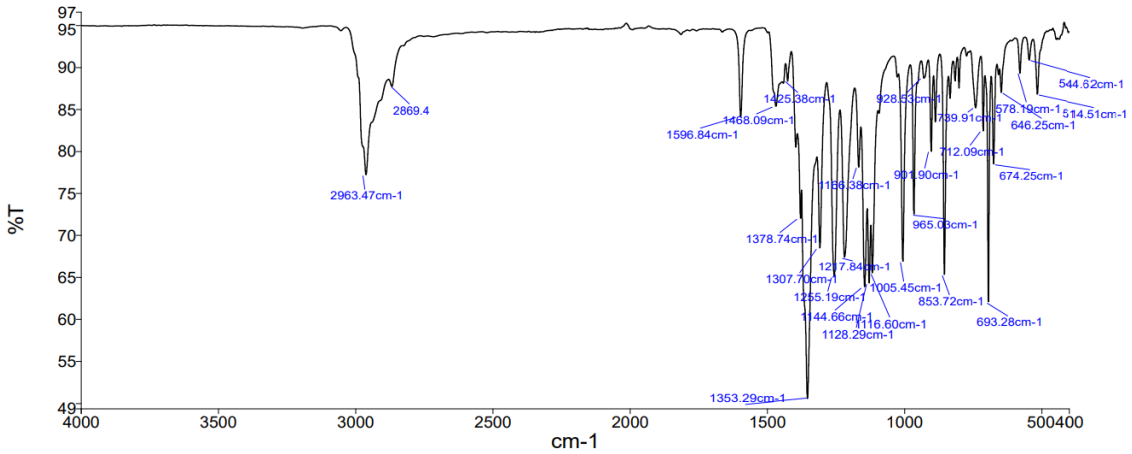


**Figure 6.45** – IR spectrum of 2-(3,5-di-tert-butyl-4-methoxyphenyl)-4,4,5,5-tetramethyl-1,3,2-dioxaborolane (**7**).

## Appendix 16 – 3,5-dimethylpyridine-1-oxide (8)

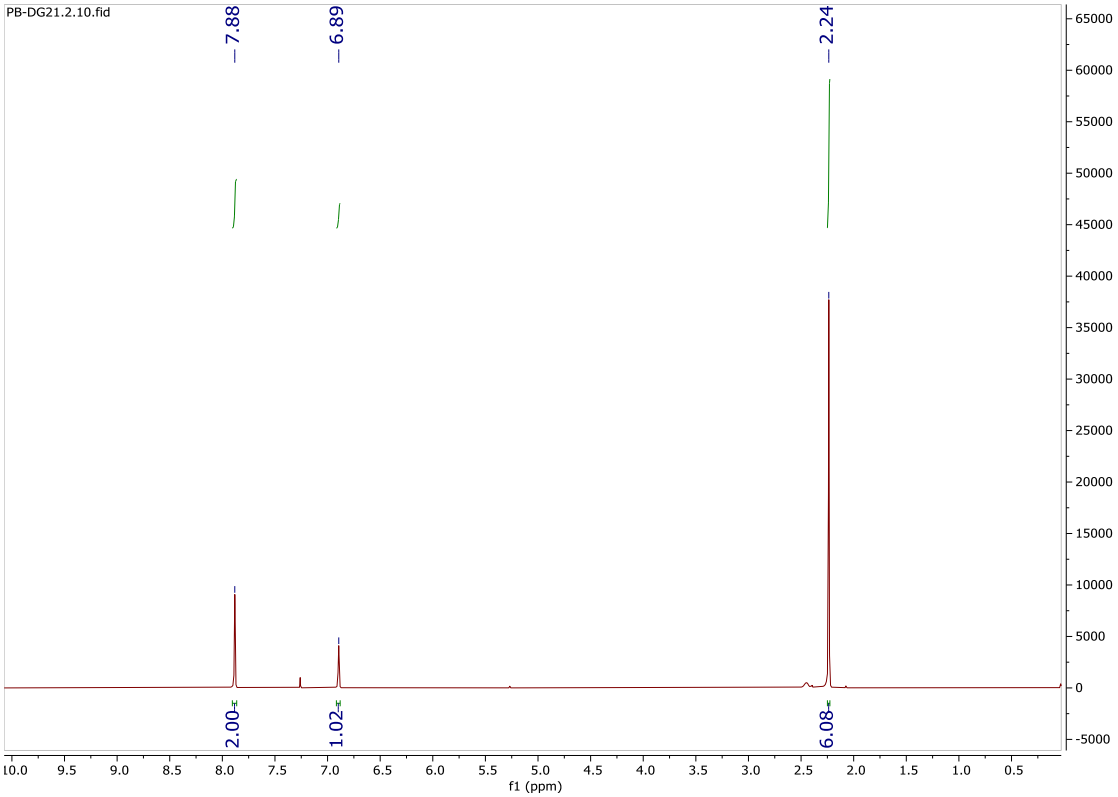


**Figure 6.46** – $^{1}H$ NMR spectrum of 3,5-dimethylpyridine-1-oxide (**8**) in $CDCl_3$.

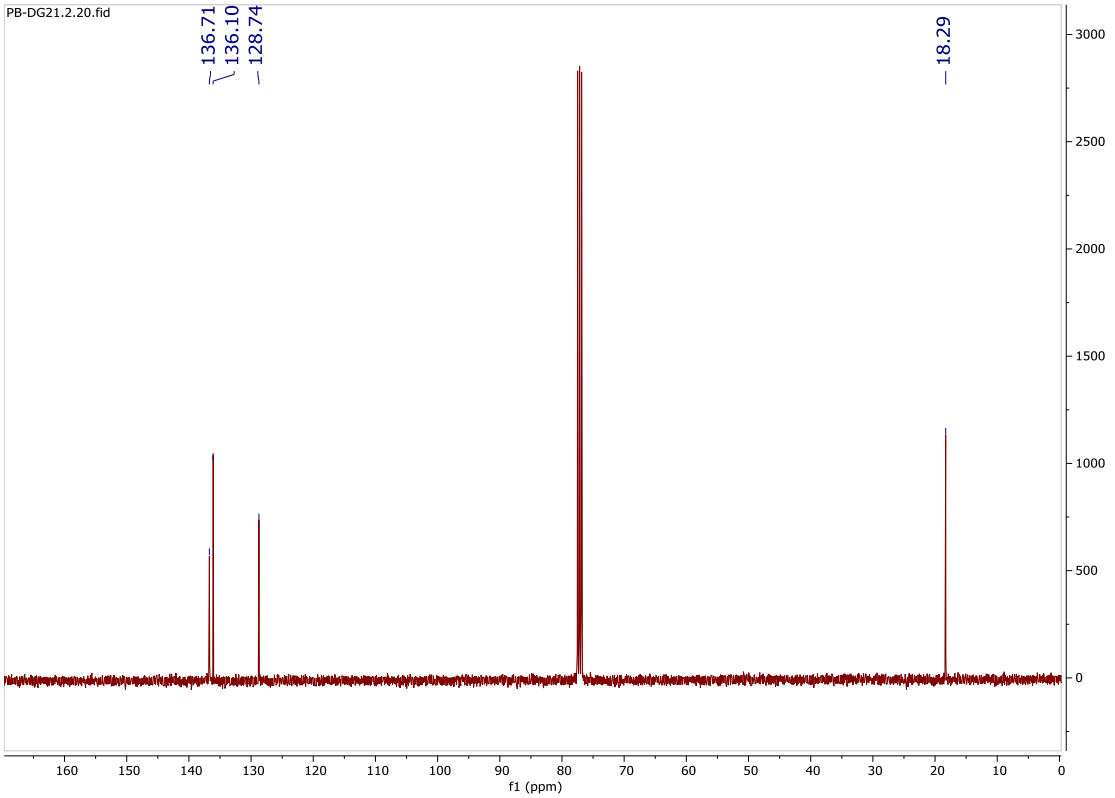


**Figure 6.47** – $^{13}C$ NMR spectrum of 3,5-dimethylpyridine-1-oxide (**8**) in $CDCl_3$.

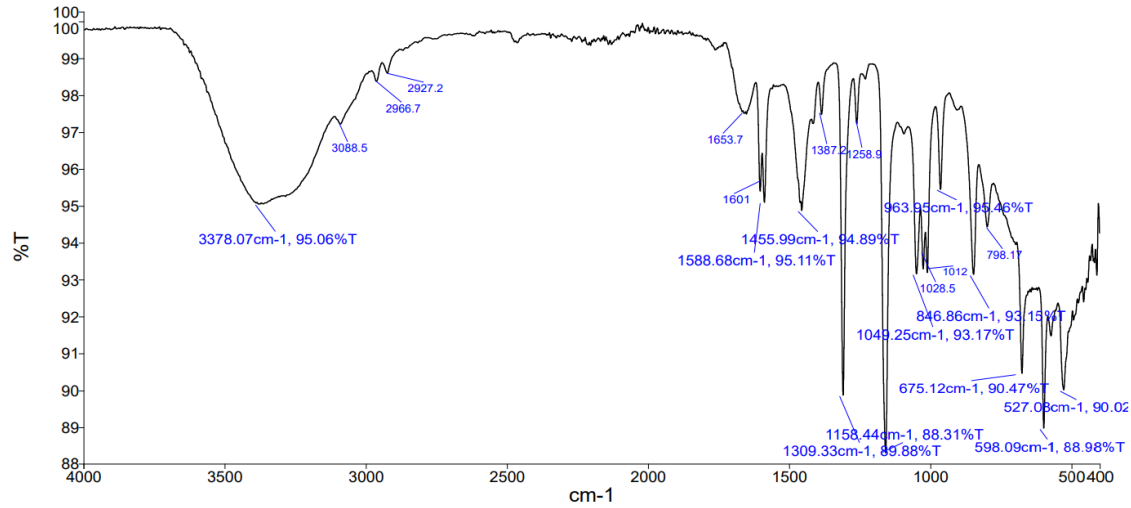


**Figure 6.48** – IR spectrum of 3,5-dimethylpyridine-1-oxide (**8**).

## Appendix 17 – 4-nitro-2,6-dimethylpyridine-1-oxide (9a)

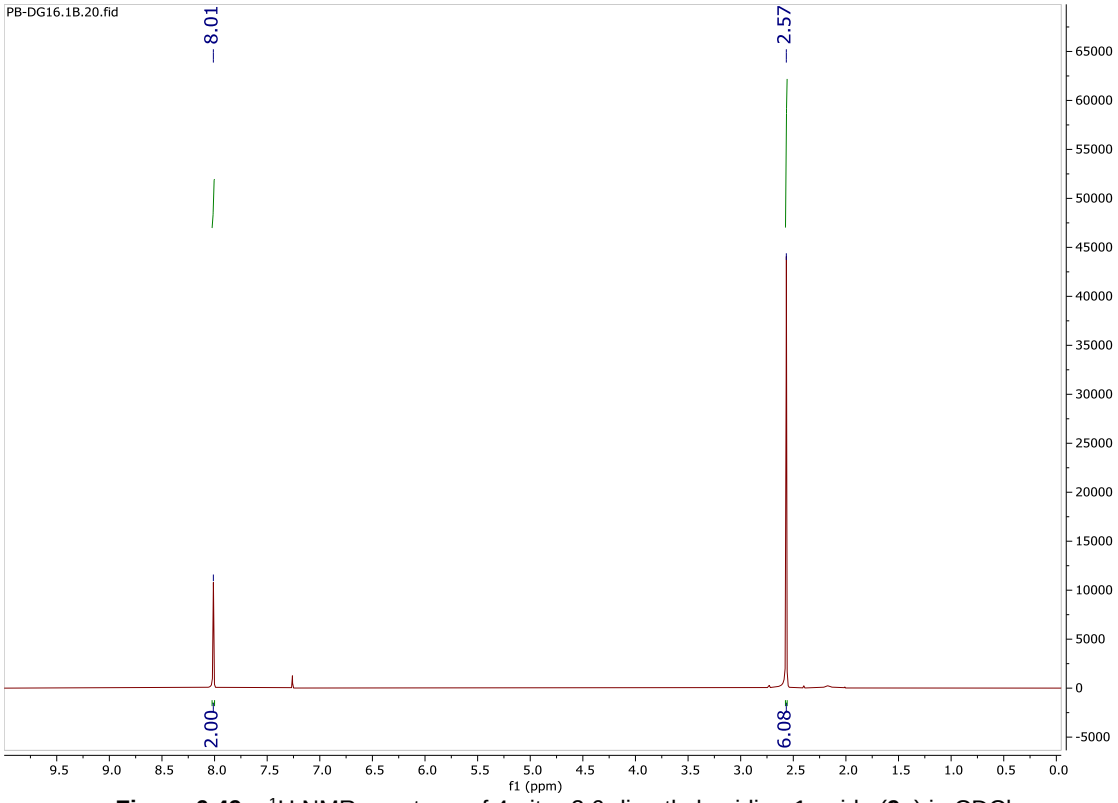


**Figure 6.49** – $^{1}H$ NMR spectrum of 4-nitro-2,6-dimethylpyridine-1-oxide (**9a**) in $CDCl_3$.

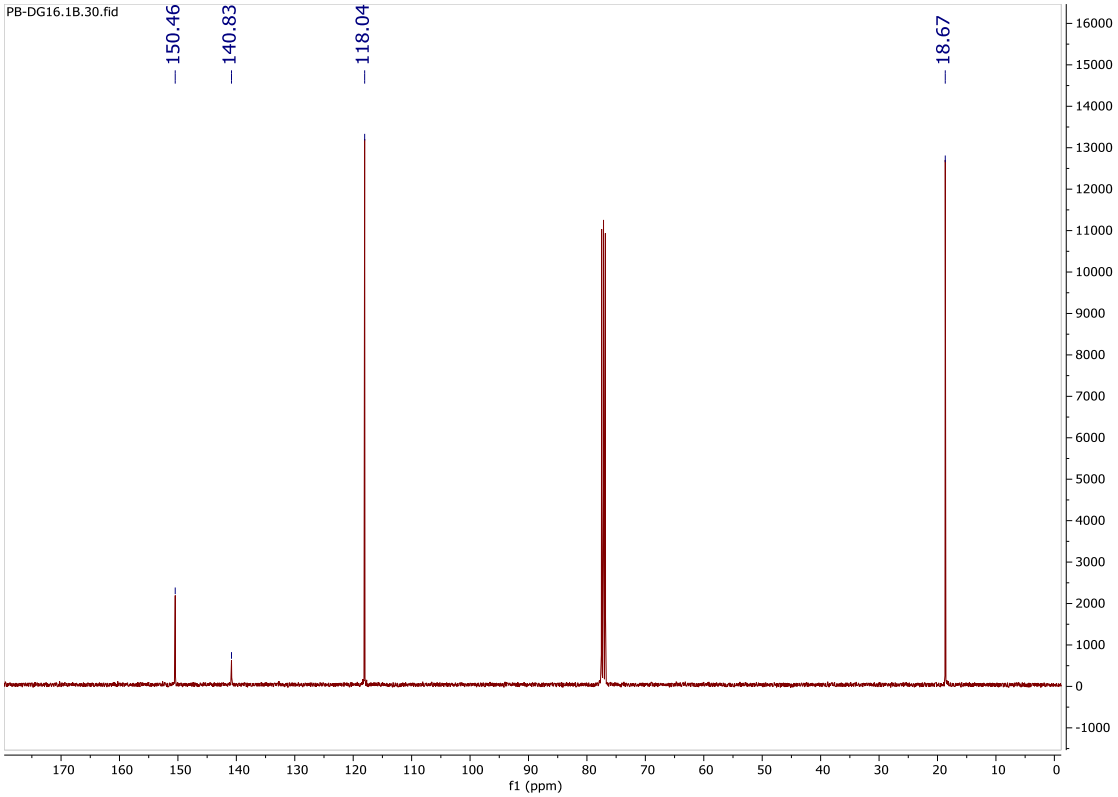


**Figure 6.50** – $^{13}C$ NMR spectrum of 4-nitro-2,6-dimethylpyridine-1-oxide (**9a**) in $CDCl_3$.

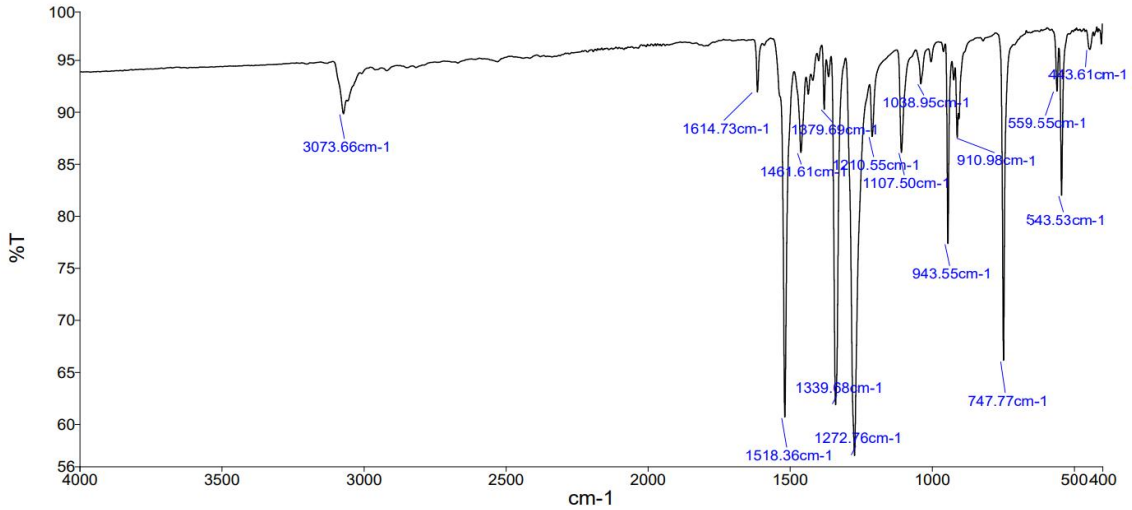


**Figure 6.51** – IR spectrum of 4-nitro-2,6-dimethylpyridine-1-oxide (**9a**).

## Appendix 18 – 4-nitro-3,5-dimethylpyridine-1-oxide (9b)

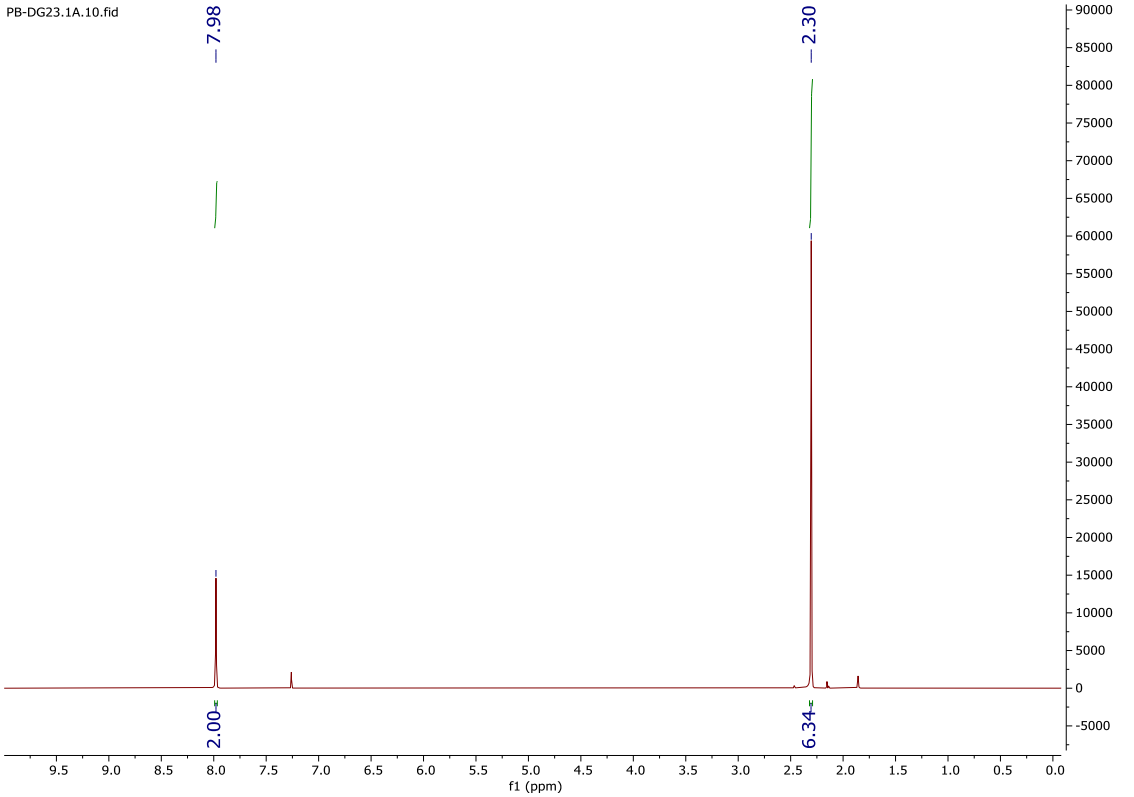


**Figure 6.52** – $^{1}H$ NMR spectrum of 4-nitro-3,5-dimethylpyridine-1-oxide (**9b**) in $CDCl_3$.

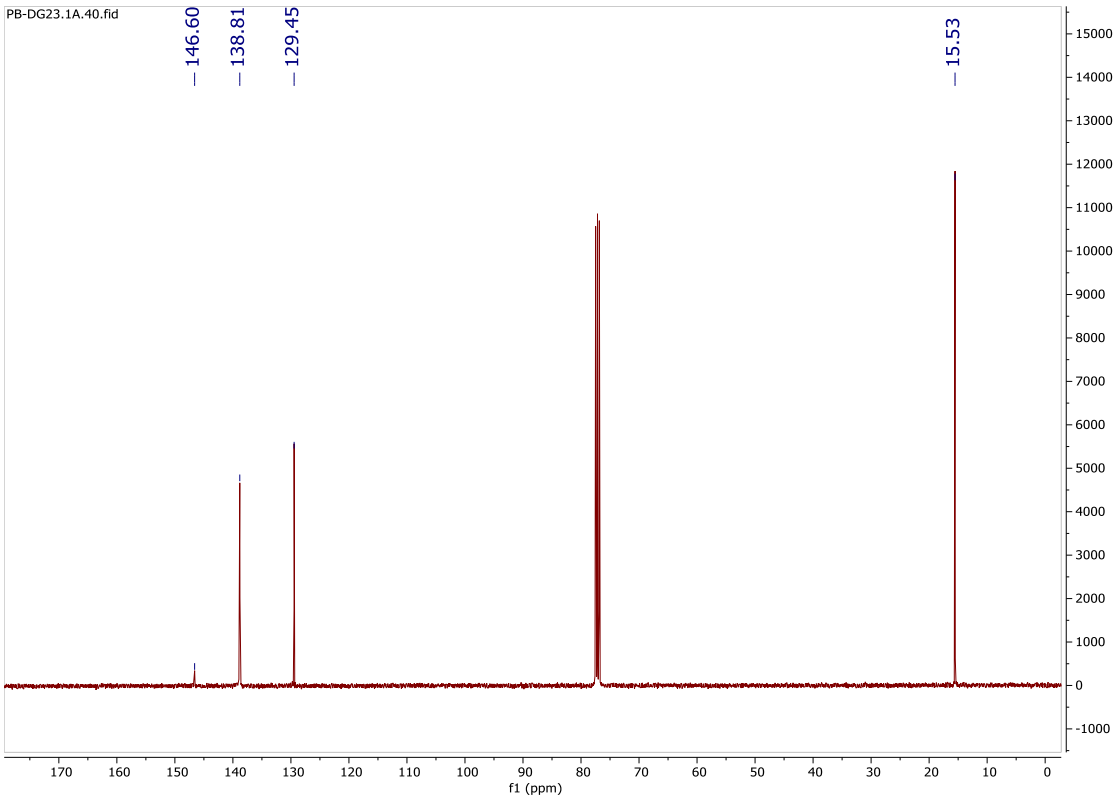


**Figure 6.53** – $^{13}C$ NMR spectrum of 4-nitro-3,5-dimethylpyridine-1-oxide (**9b**) in $CDCl_3$.

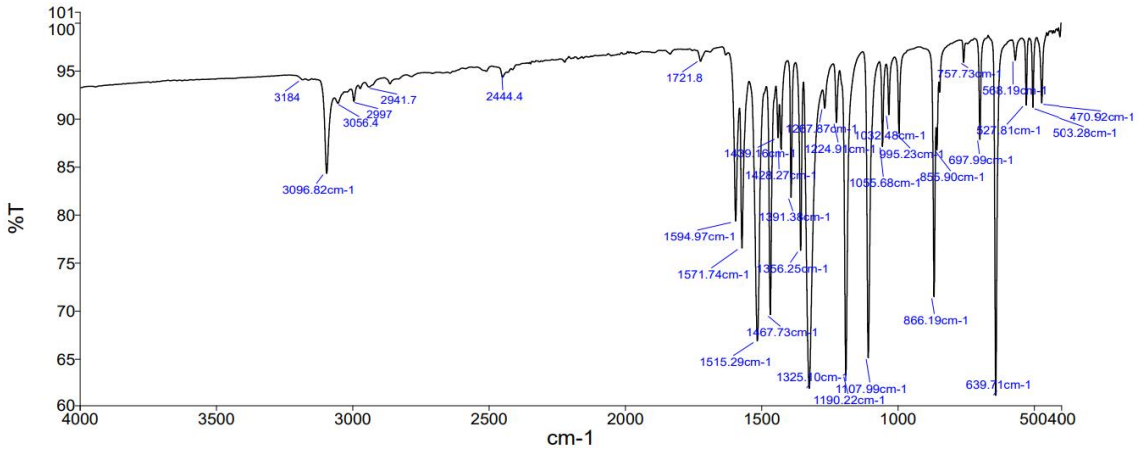


**Figure 6.54** – IR spectrum of 4-nitro-3,5-dimethylpyridine-1-oxide (**9b**).

## Appendix 19 – 4-bromo-2,6-dimethylpyridine-1-oxide (10a)

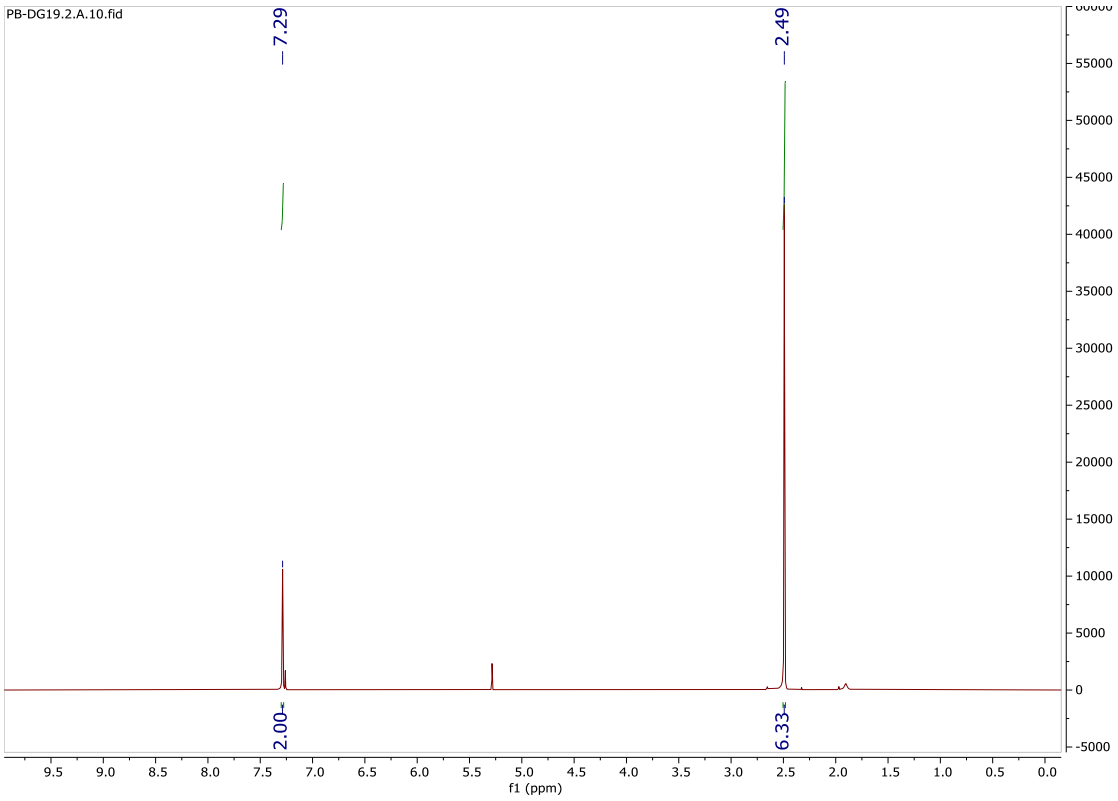


**Figure 6.55** – $^{1}H$ NMR spectrum of 4-bromo-2,6-dimethylpyridine-1-oxide (**10a**) in $CDCl_3$.

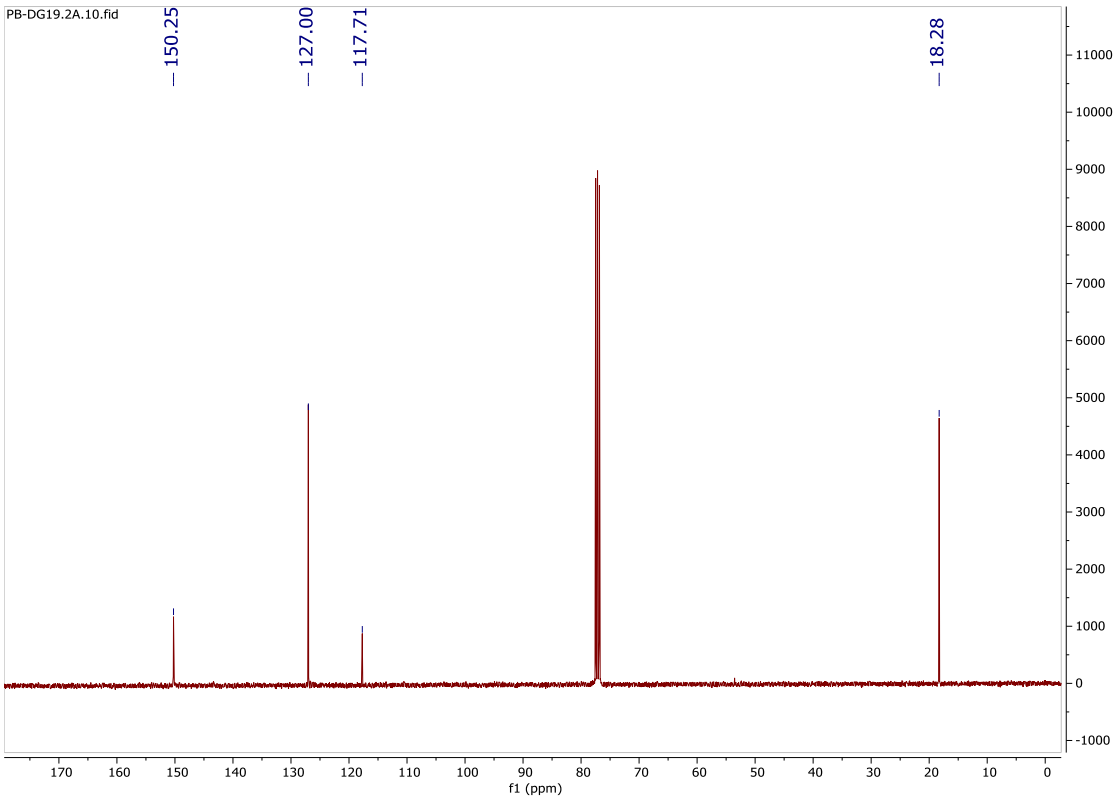


**Figure 6.56** – $^{13}C$ NMR spectrum of 4-bromo-2,6-dimethylpyridine-1-oxide (**10a**) in $CDCl_3$.

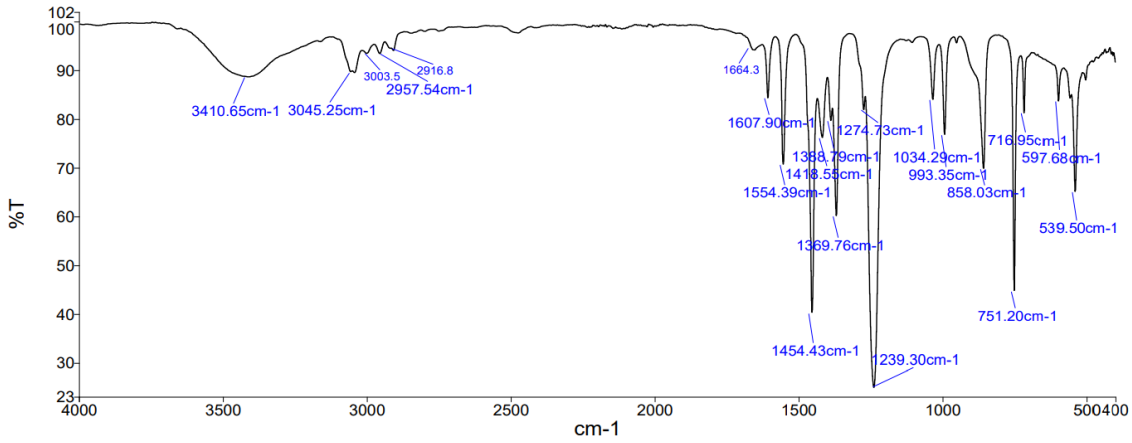


**Figure 6.57** – IR spectrum of 4-bromo-2,6-dimethylpyridine-1-oxide (**10a**).

## Appendix 20 – 4-bromo-3,5-dimethylpyridine-1-oxide (10b)

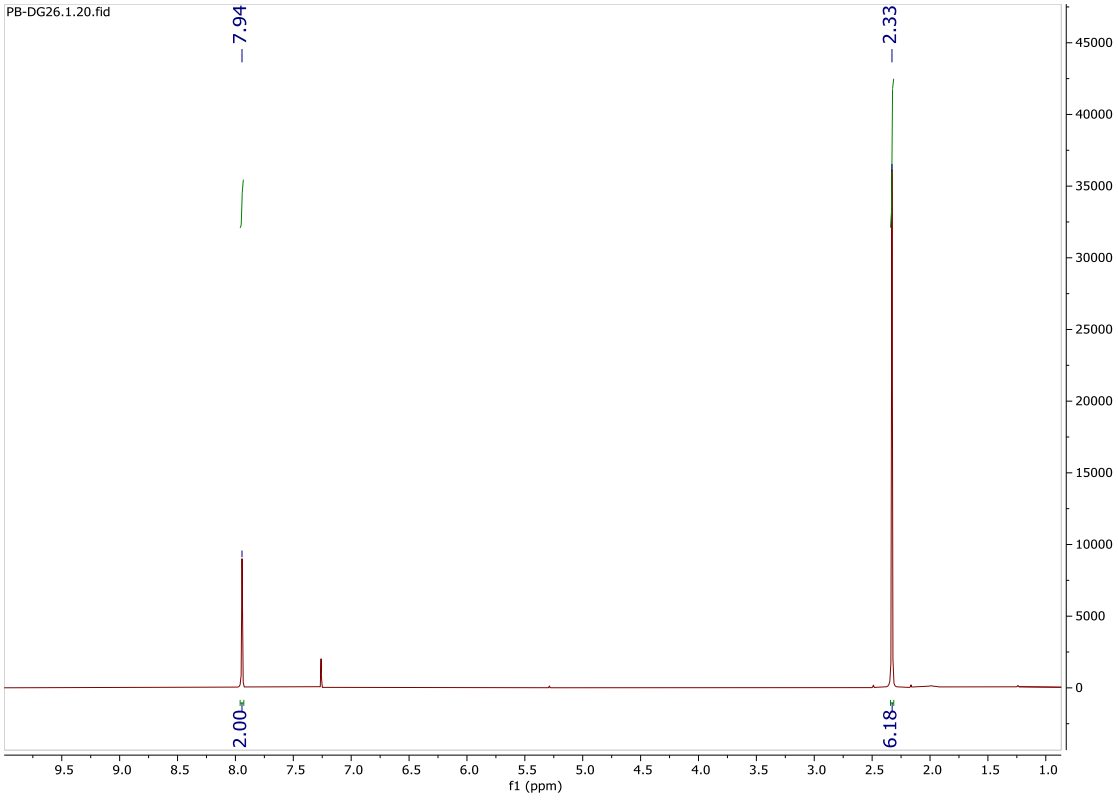


**Figure 6.58** – $^{1}$H NMR spectrum of 4-bromo-3,5-dimethylpyridine-1-oxide (**10b**) in $CDCl_3$.

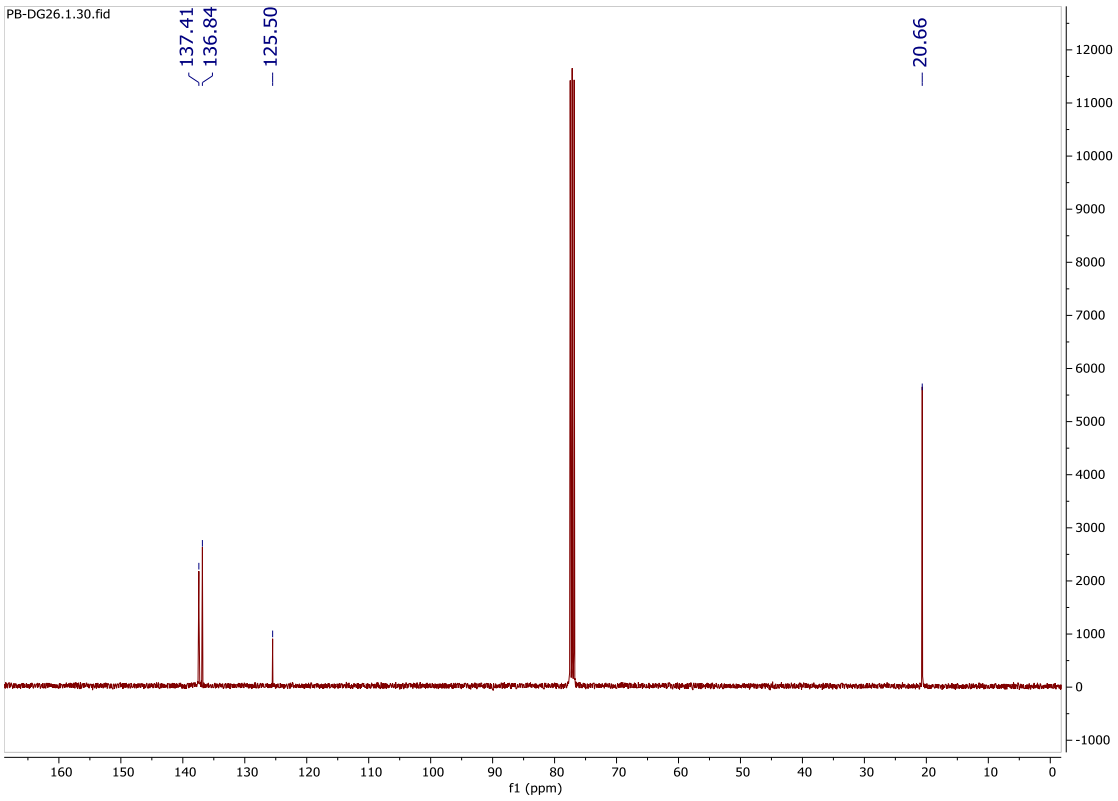


**Figure 6.59** – $^{13}C$ NMR spectrum of 4-bromo-3,5-dimethylpyridine-1-oxide (**10b**) in $CDCl_3$.

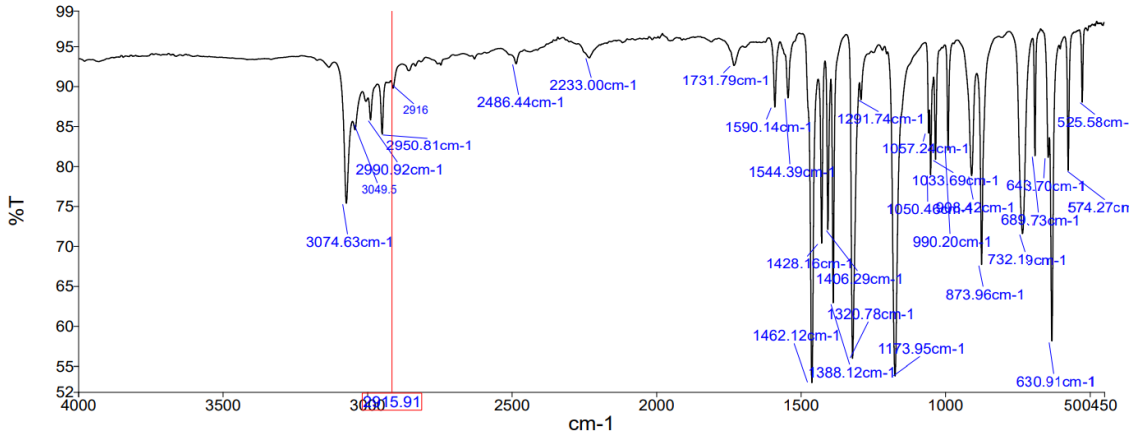


**Figure 6.60** – IR spectrum of 4-bromo-3,5-dimethylpyridine-1-oxide (**10b**).

**Appendix 21 – 4-(3,5-di-*tert*-butyl-4-methoxyphenyl)-2,6-dimethylpyridine-1-oxide (11a)**

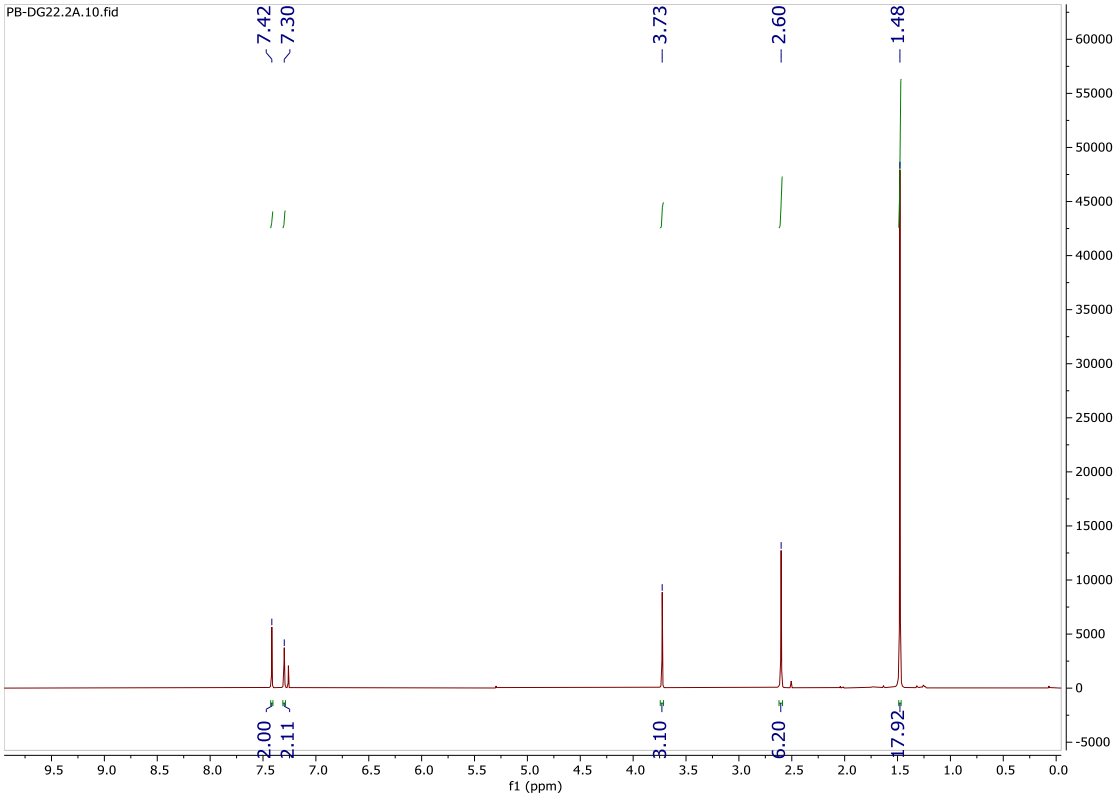


**Figure 6.61** – $^{1}H$ NMR spectrum of 4-(3,5-di-*tert*-butyl-4-methoxyphenyl)-2,6-dimethylpyridine-1-oxide (**11a**) in $CDCl_3$.

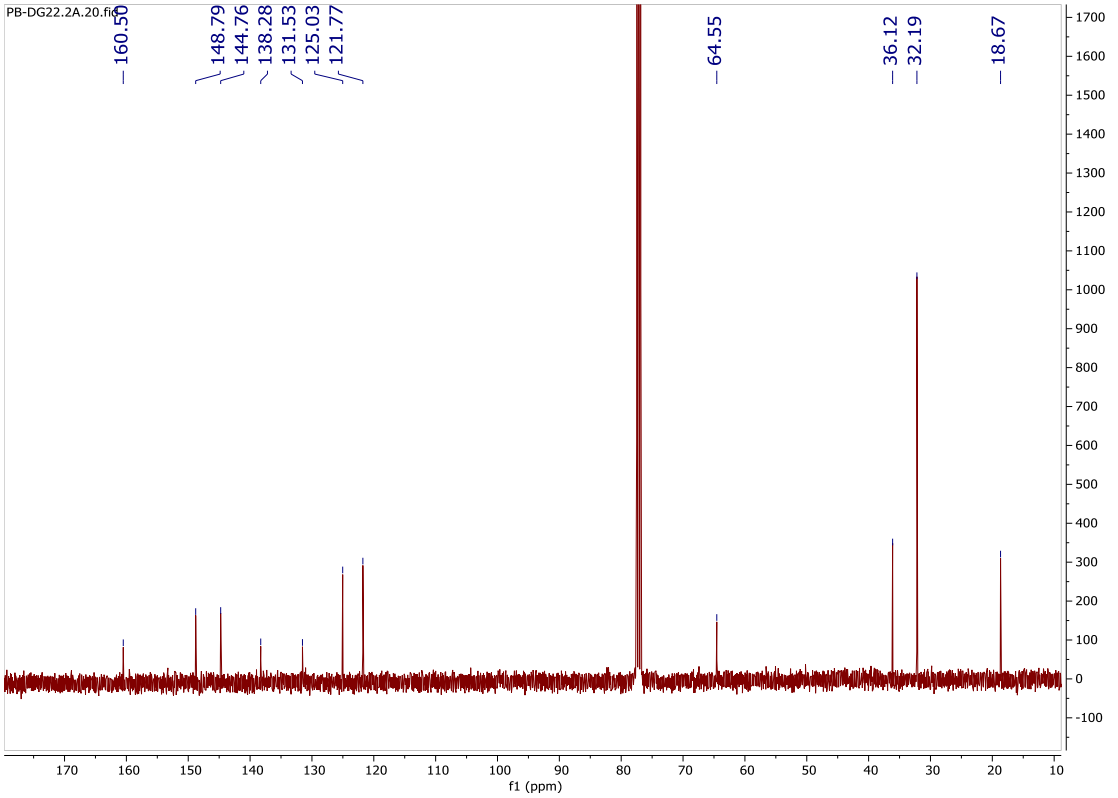


**Figure 6.62** – $^{13}C$ NMR spectrum of 4-(3,5-di-*tert*-butyl-4-methoxyphenyl)-2,6-dimethylpyridine-1-oxide (**11a**) in $CDCl_3$.

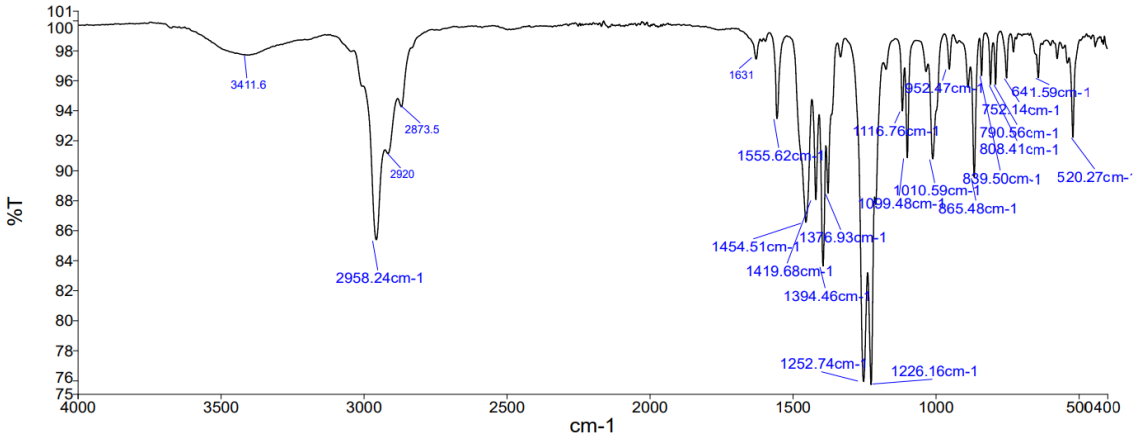


**Figure 6.63** – IR spectrum of 4-(3,5-di-*tert*-butyl-4-methoxyphenyl)-2,6-dimethylpyridine-1-oxide (**11a**).

## Appendix 22 – 4-(3,5-di-*tert*-butyl-4-methoxyphenyl)-3,5-dimethylpyridine-1-oxide (11b)

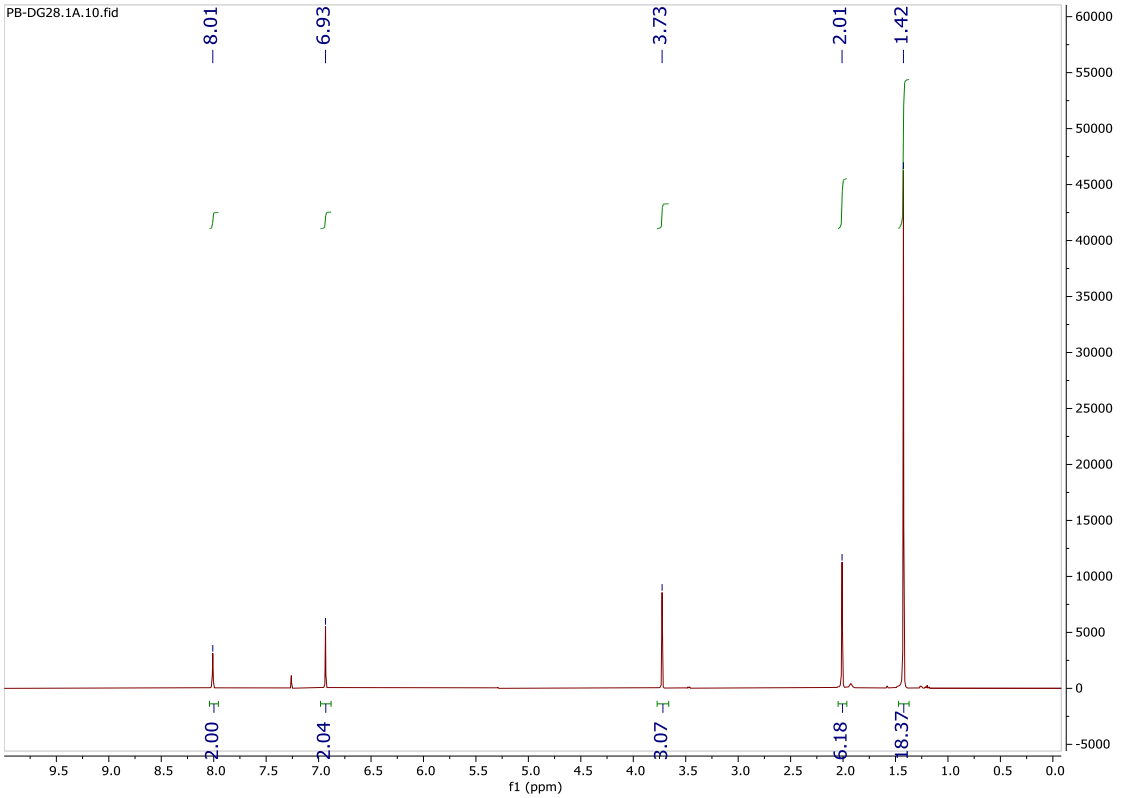


**Figure 6.64** – $^{1}$H NMR spectrum of 4-(3,5-di-*tert*-butyl-4-methoxyphenyl)-3,5-dimethylpyridine-1-oxide (**11b**) in $CDCl_3$.

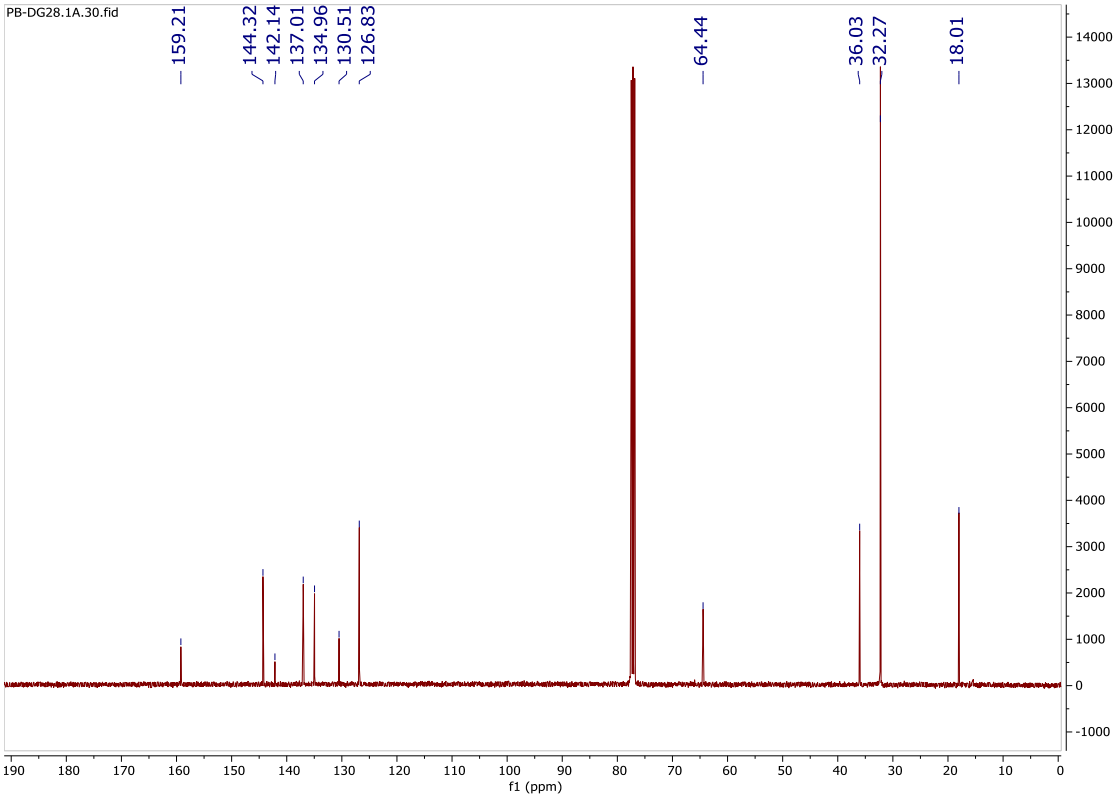


**Figure 6.65** – $^{13}C$ NMR spectrum of 4-(3,5-di-*tert*-butyl-4-methoxyphenyl)-3,5-dimethylpyridine-1-oxide (**11b**) in $CDCl_3$.

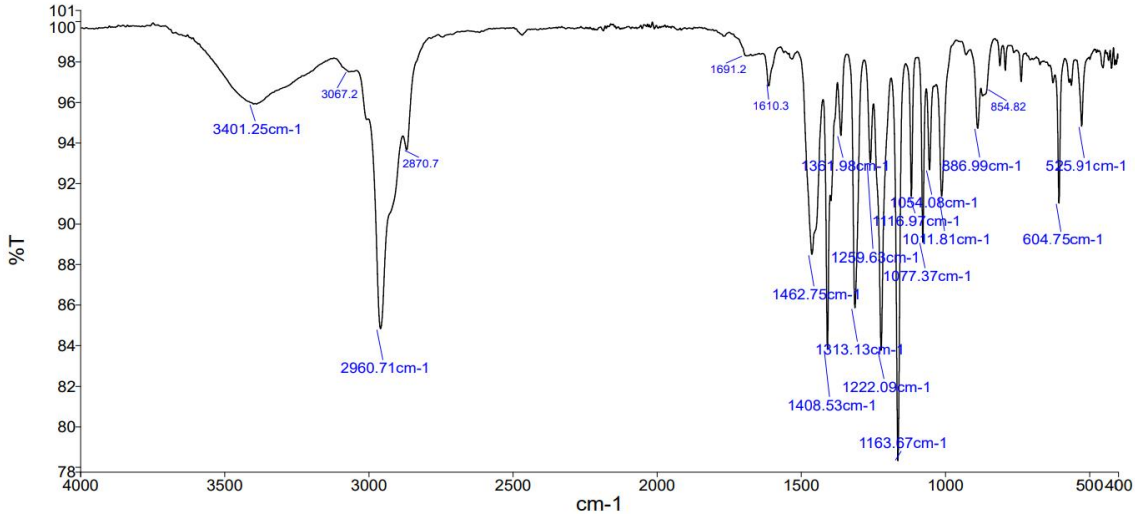


**Figure 6.66** – IR spectrum of 4-(3,5-di-*tert*-butyl-4-methoxyphenyl)-3,5-dimethylpyridine-1-oxide (**11b**).

## Appendix 23 – 4-(3,5-di-*tert*-butyl-4-methoxyphenyl)-2,6-dimethylpyridine (12)

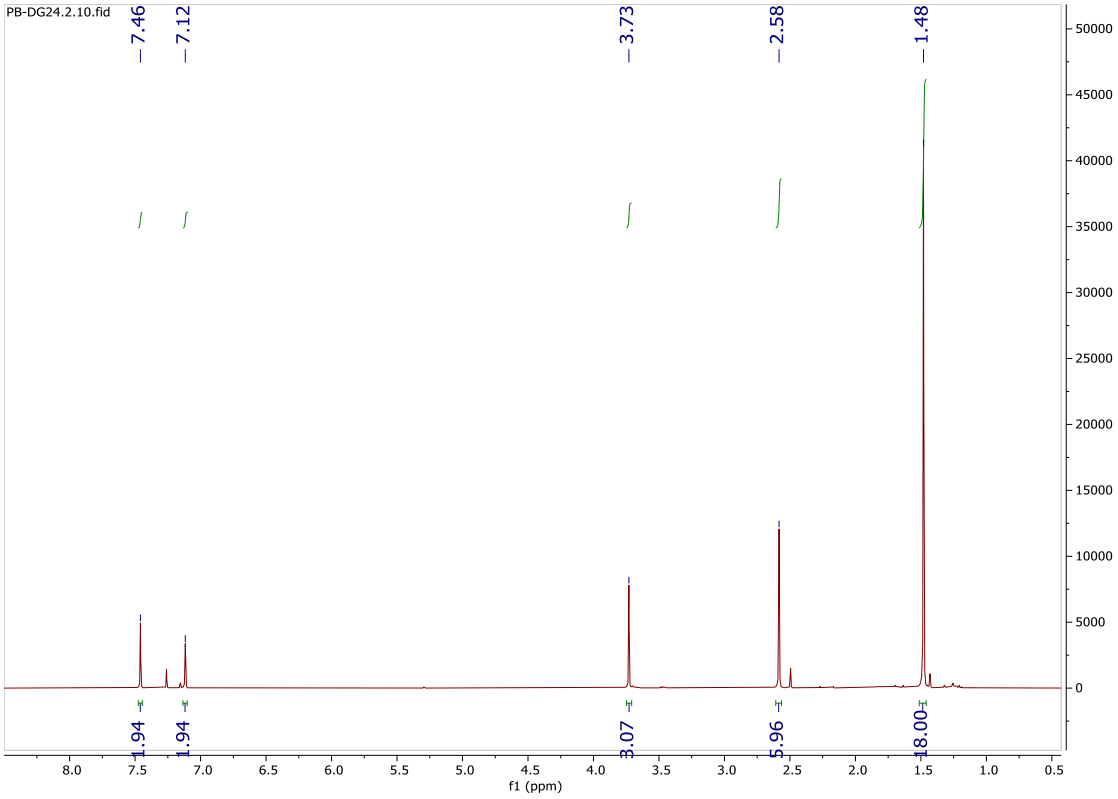


**Figure 6.67** – $^{1}$H NMR spectrum of 4-(3,5-di-*tert*-butyl-4-methoxyphenyl)-2,6-dimethylpyridine (**12**) in $CDCl_3$.

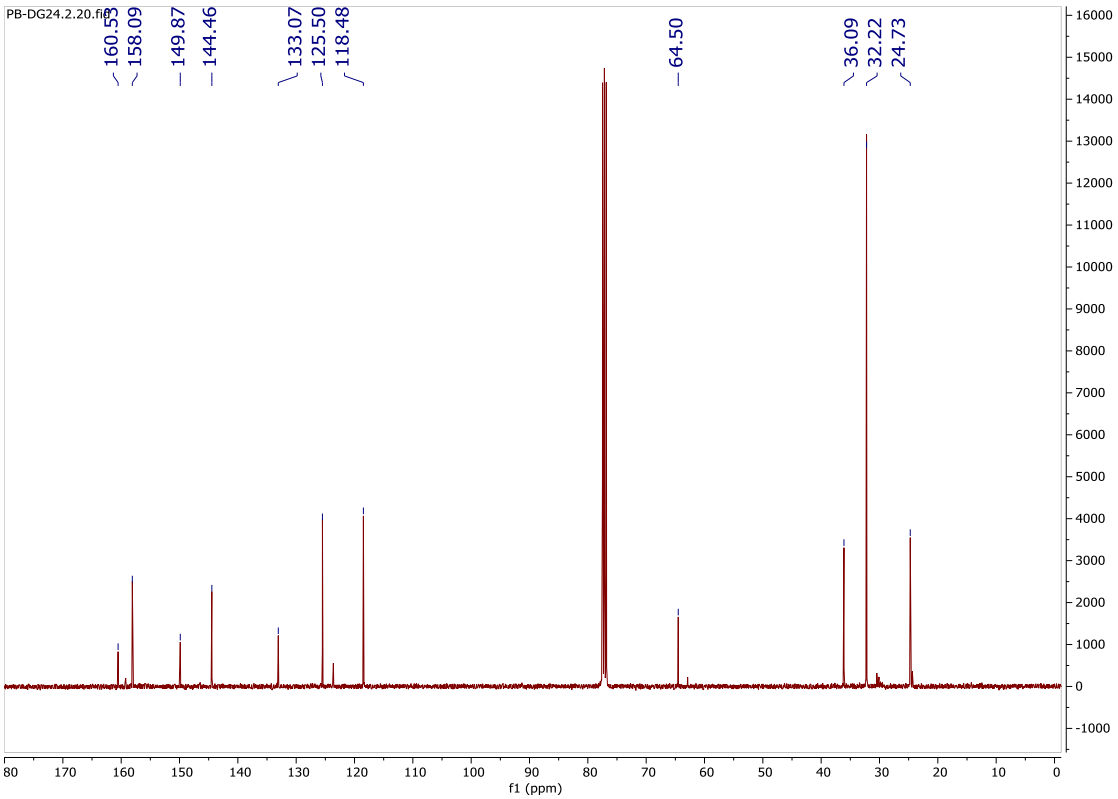


**Figure 6.68** – $^{13}$C NMR spectrum of 4-(3,5-di-*tert*-butyl-4-methoxyphenyl)-2,6-dimethylpyridine (**12**) in $CDCl_3$.

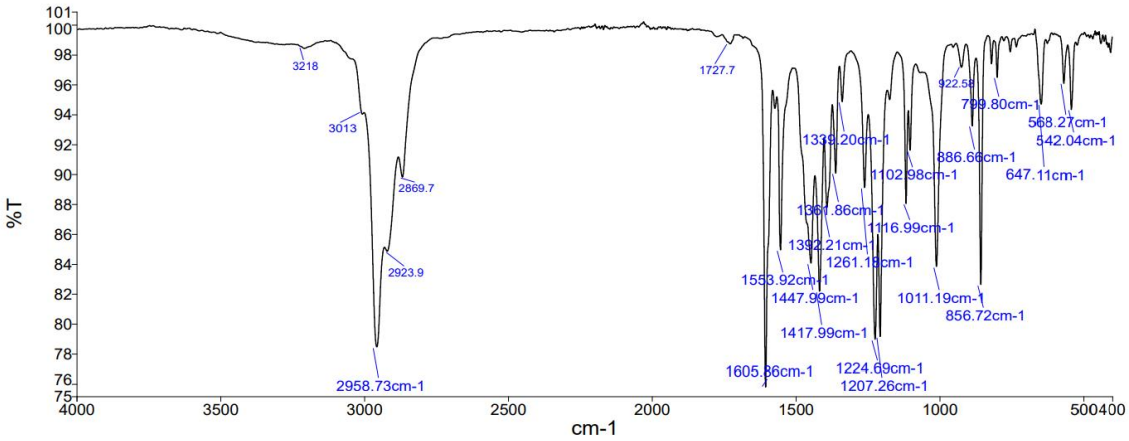


**Figure 6.69** – IR spectrum of 4-(3,5-di-*tert*-butyl-4-methoxyphenyl)-2,6-dimethylpyridine (**12**).

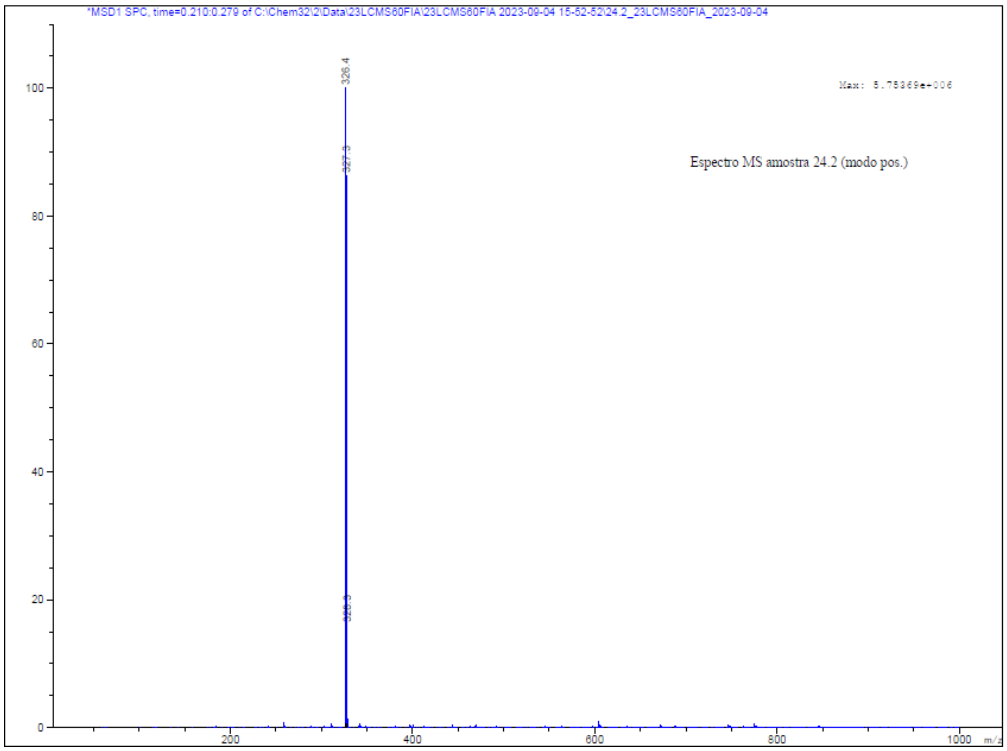


**Figure 6.70** – LCMS spectrum of 4-(3,5-di-*tert*-butyl-4-methoxyphenyl)-2,6-dimethylpyridine (**12**), in positive mode.

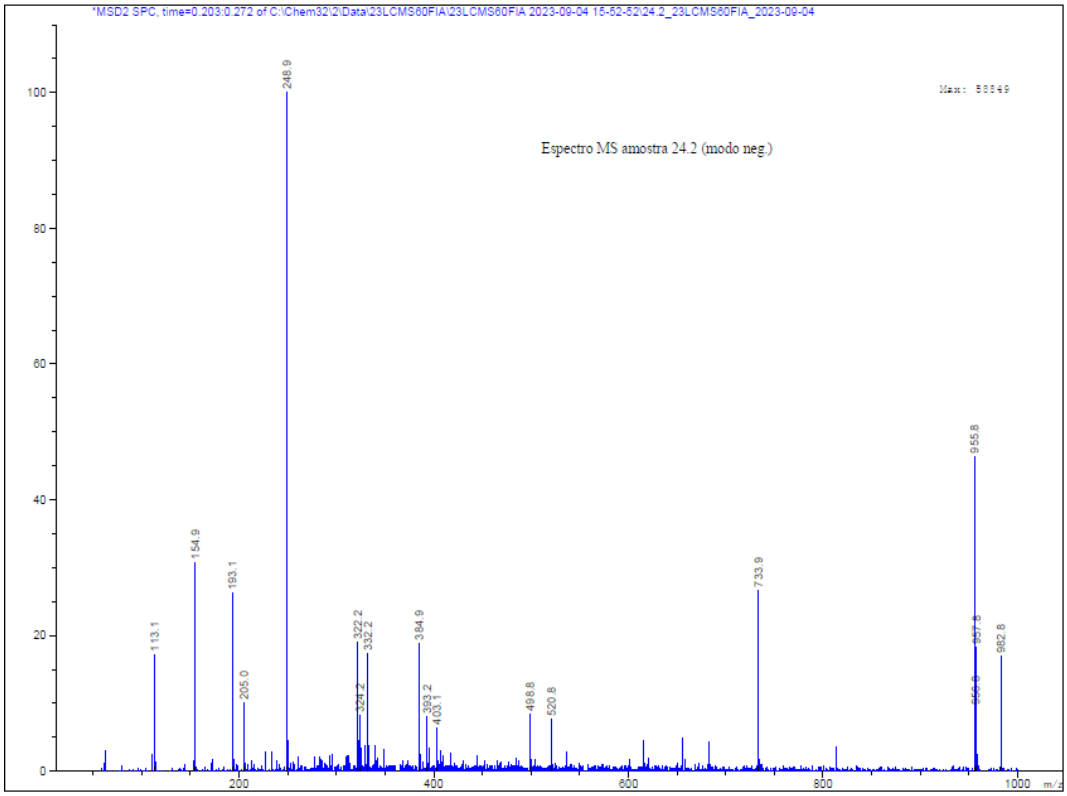


**Figure 6.71** – LCMS spectrum of 4-(3,5-di-*tert*-butyl-4-methoxyphenyl)-2,6-dimethylpyridine (**12**), in negative mode.

**Appendix 24 – 2,6-di-*tert*-butyl-4-(2,6-dimethylpyridin-4-yl)phenol (13)**

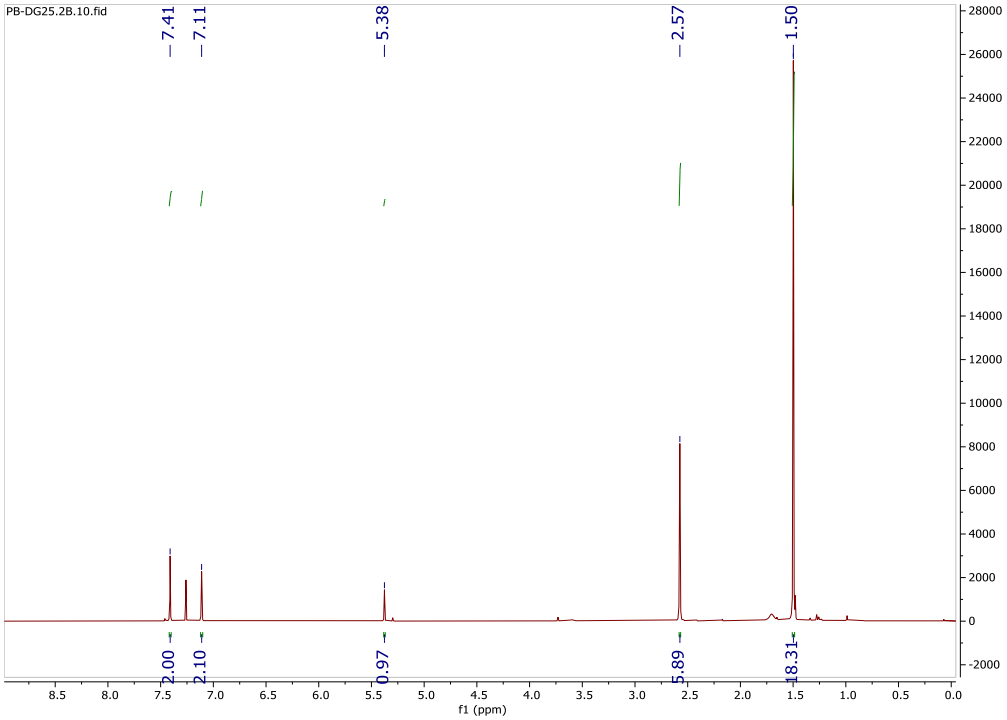


**Figure 6.72** – $^{1}$H NMR spectrum of 2,6-di-*tert*-butyl-4-(2,6-dimethylpyridin-4-yl)phenol (**13**) in $CDCl_3$.

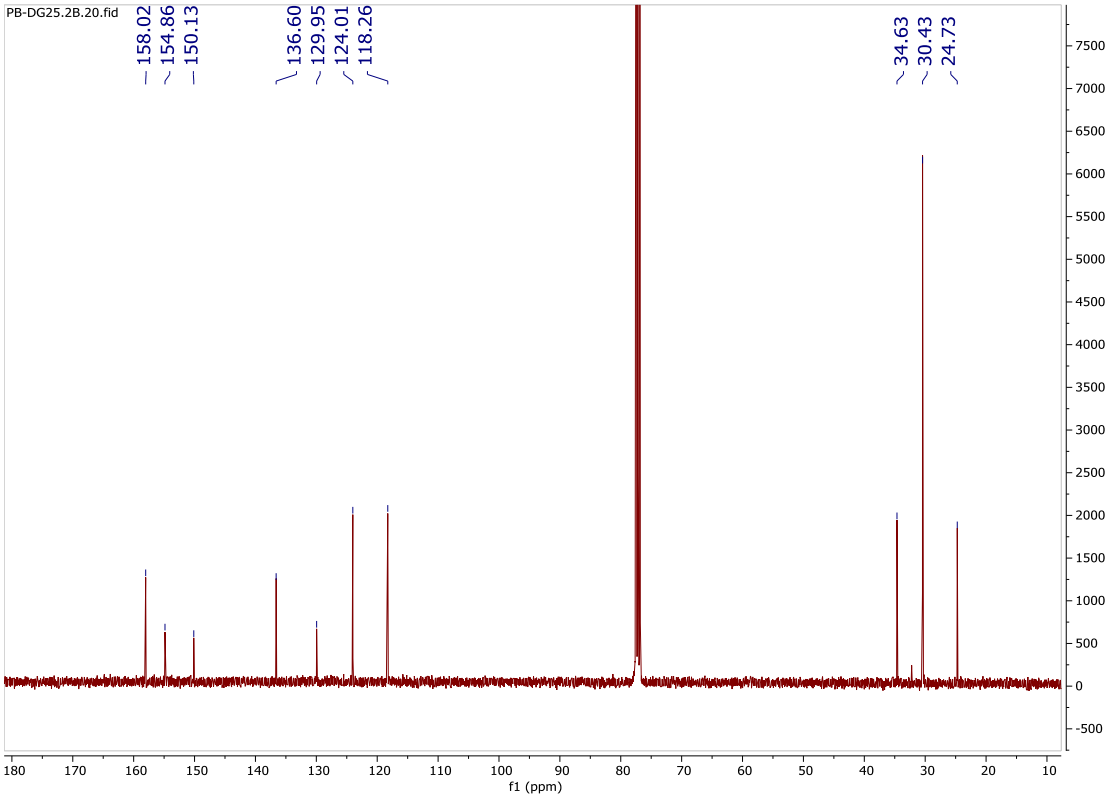


**Figure 6.73** – $^{13}C$ NMR spectrum of 2,6-di-*tert*-butyl-4-(2,6-dimethylpyridin-4-yl)phenol (**13**) in $CDCl_3$.

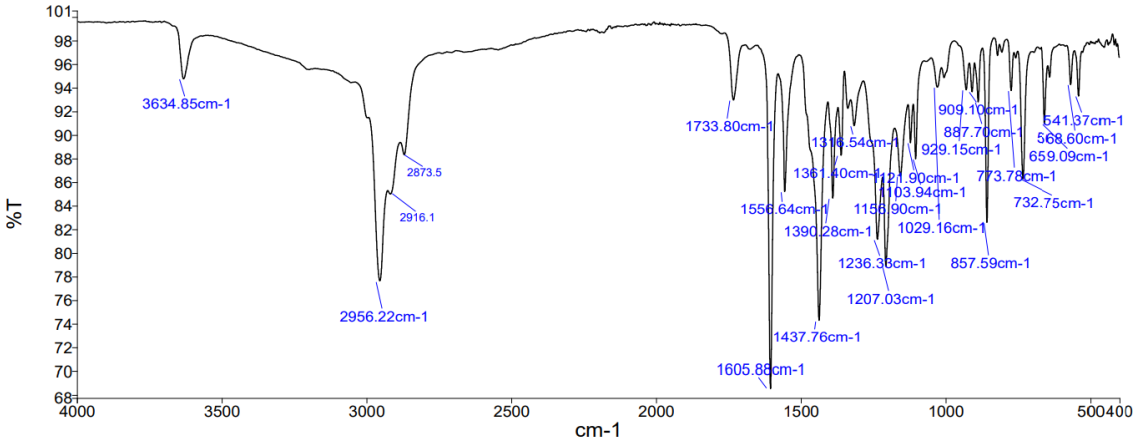


**Figure 6.74** – IR spectrum of 2,6-di-*tert*-butyl-4-(2,6-dimethylpyridin-4-yl)phenol (**13**).

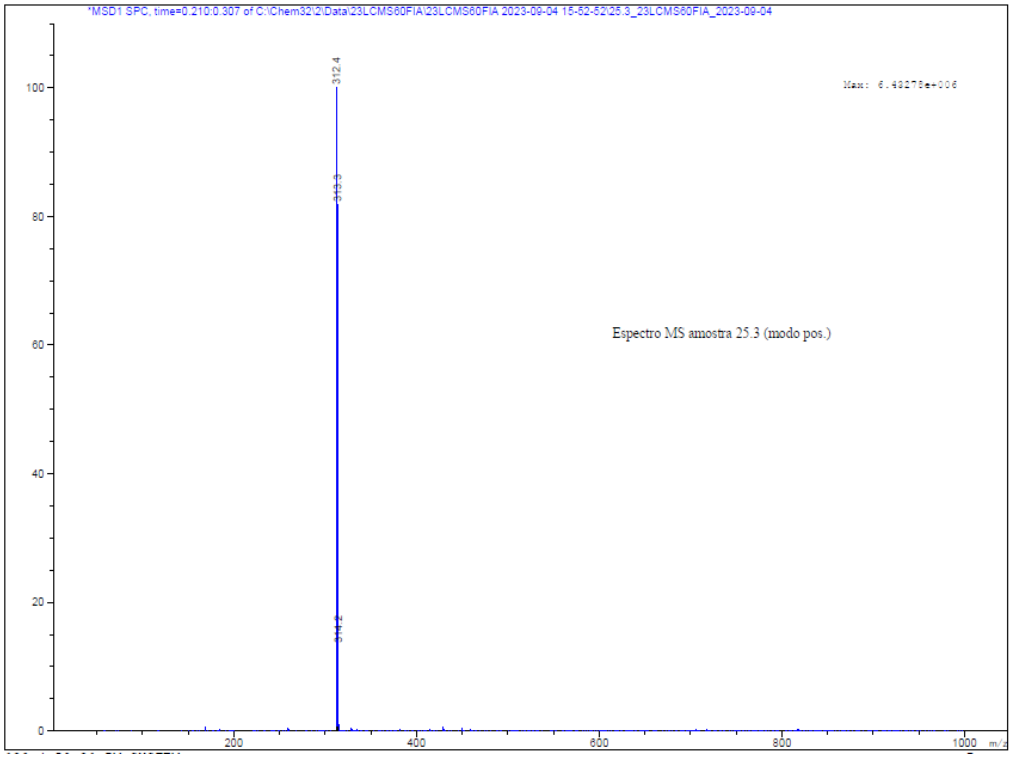


**Figure 6.75** – LCMS spectrum of 2,6-di-*tert*-butyl-4-(2,6-dimethylpyridin-4-yl)phenol (**13**), in positive mode.

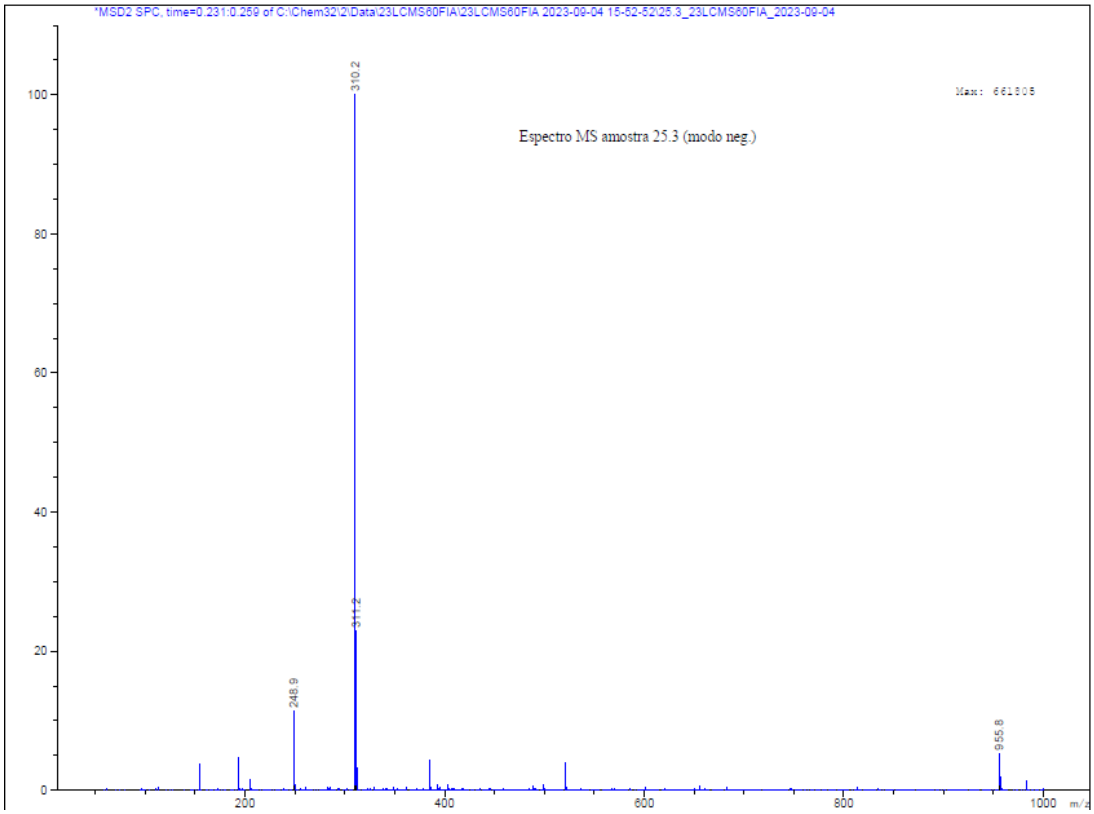


**Figure 6.76** – LCMS spectrum of 2,6-di-*tert*-butyl-4-(2,6-dimethylpyridin-4-yl)phenol (**13**), in negative mode.

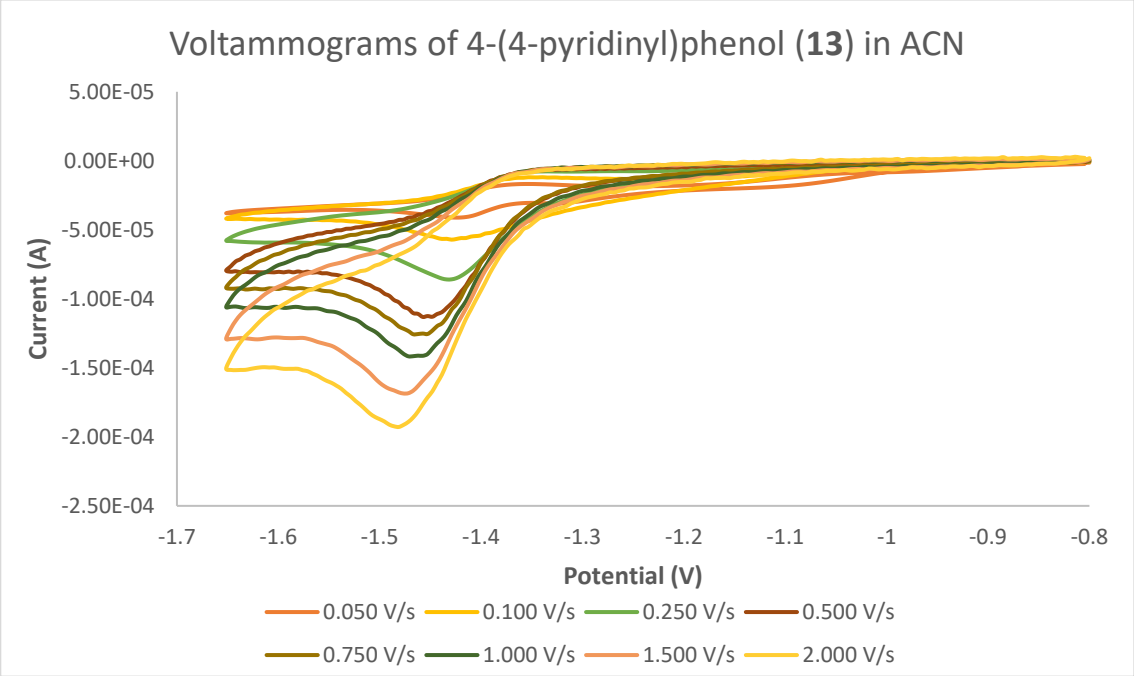


**Graphic 6.13** – Voltammograms of 2,6-di-*tert*-butyl-4-(2,6-dimethylpyridin-4-yl)phenol (**13**) in ACN, at multiple scan rates.

## Appendix 25 – 4-(3,5-di-*tert*-butyl-4-hydroxyphenyl)-1,2,6-trimethylpyridinium iodide (14)

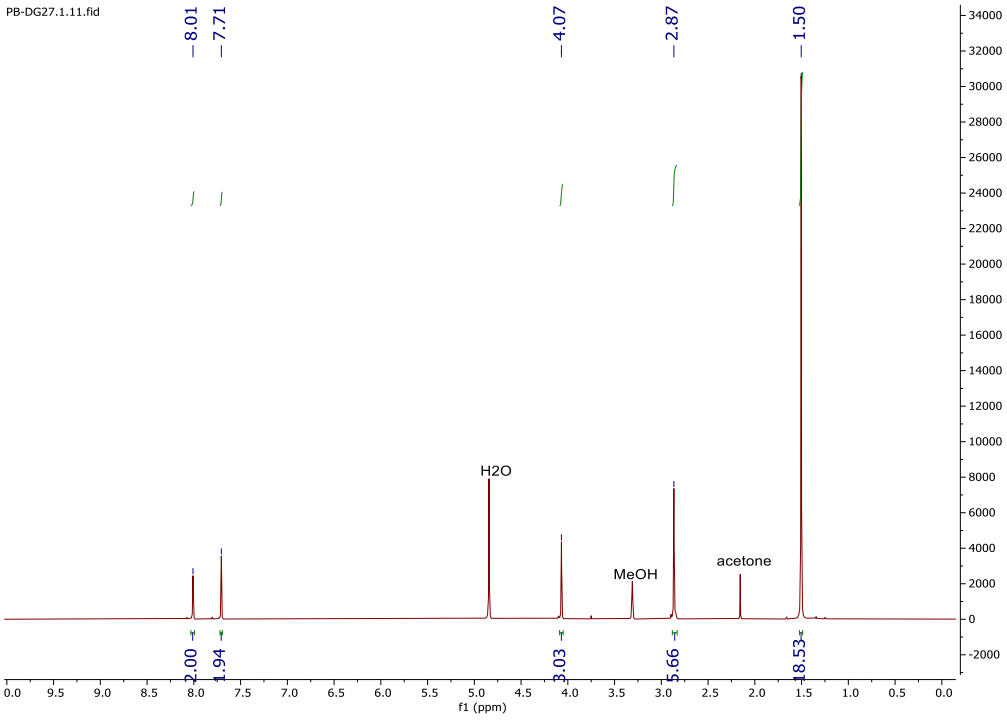


**Figure 6.77** – $^{1}$H NMR spectrum of 4-(3,5-di-*tert*-butyl-4-methoxyphenyl)-1,2,6-trimethylpyridinium iodide (**14**) in $CD_3OD$.

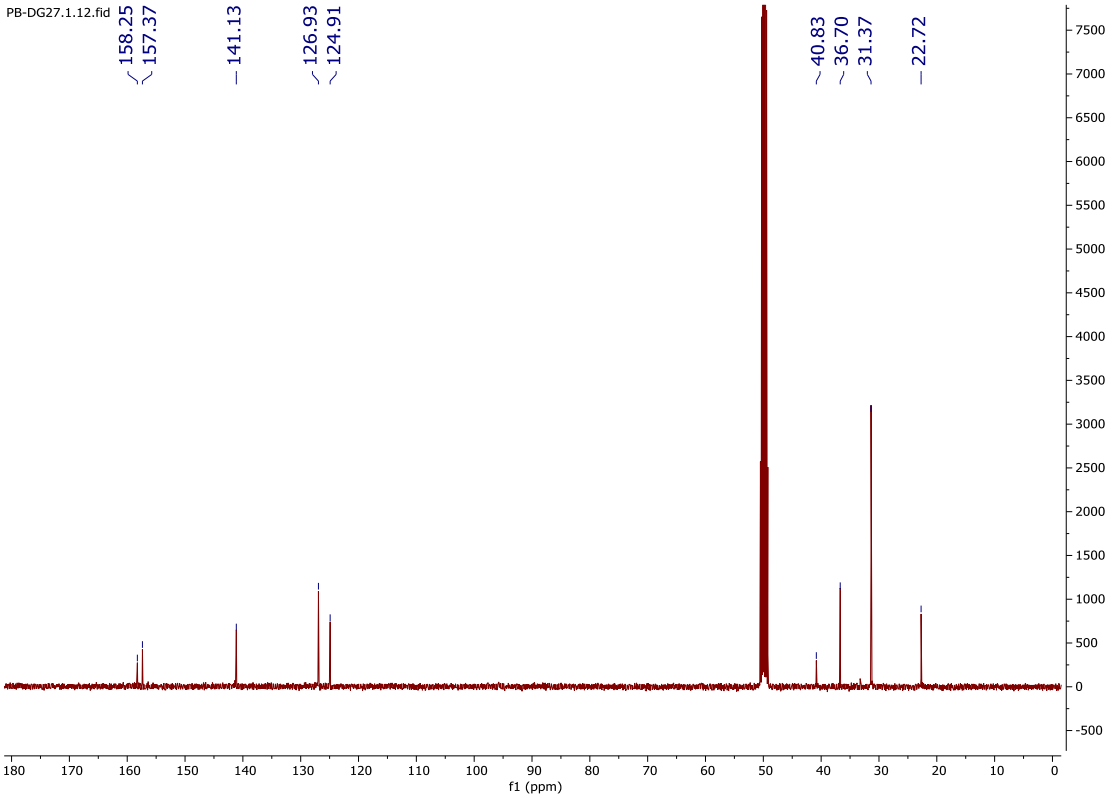


**Figure 6.78** – $^{13}C$ NMR spectrum of 4-(3,5-di-*tert*-butyl-4-methoxyphenyl)-1,2,6-trimethylpyridinium iodide (**14**) in $CD_3OD$.

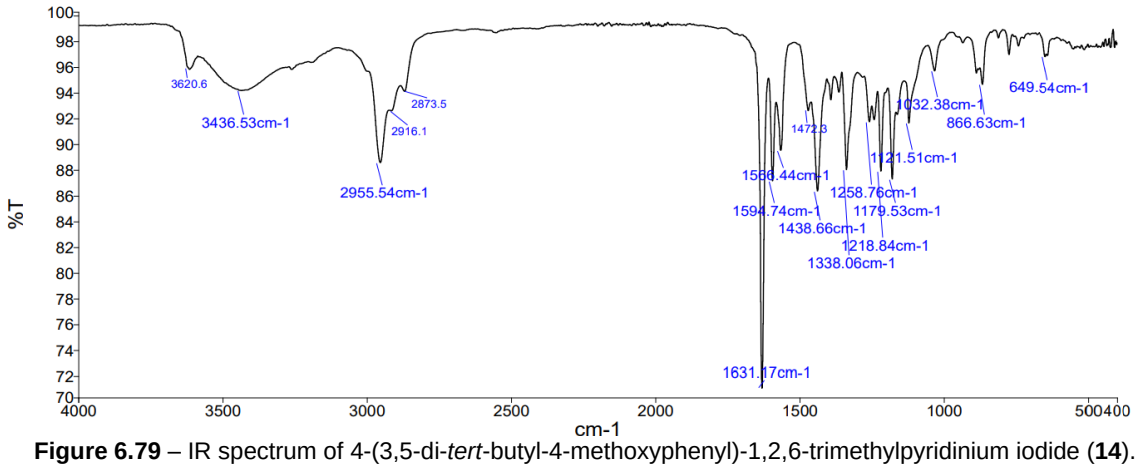


**Figure 6.79** – IR spectrum of 4-(3,5-di-*tert*-butyl-4-methoxyphenyl)-1,2,6-trimethylpyridinium iodide (**14**).

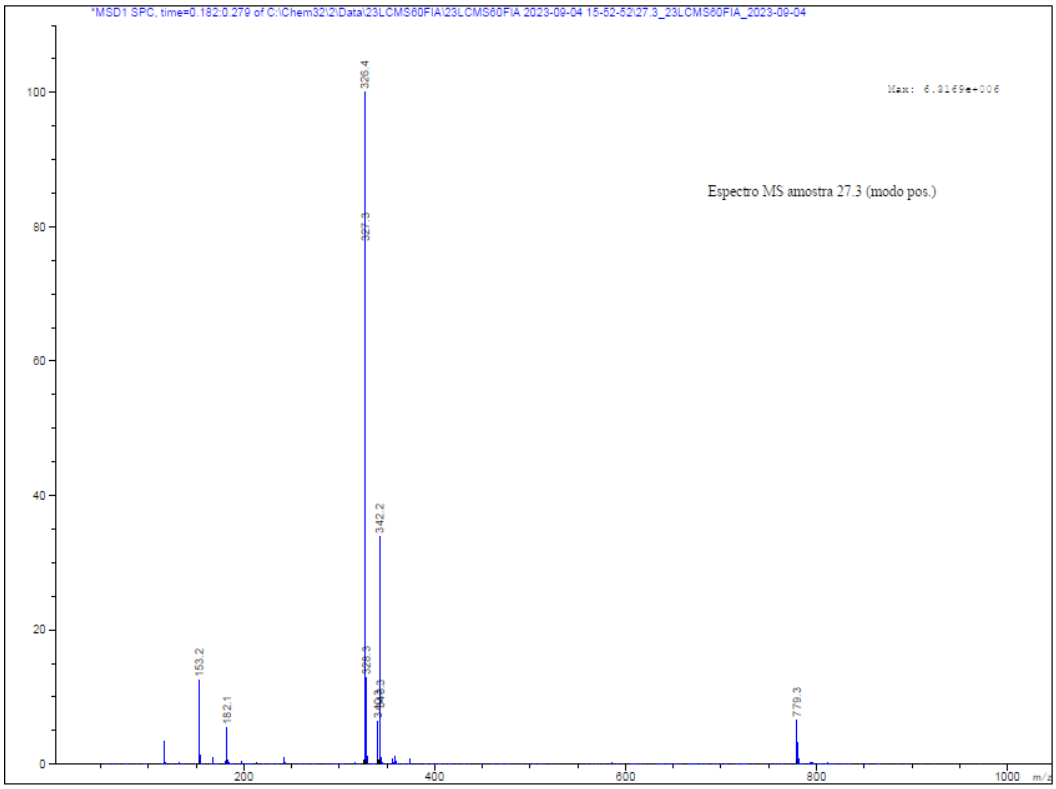


**Figure 6.80** – LCMS spectrum of 4-(3,5-di-*tert*-butyl-4-methoxyphenyl)-1,2,6-trimethylpyridinium iodide (**14**), in positive mode.

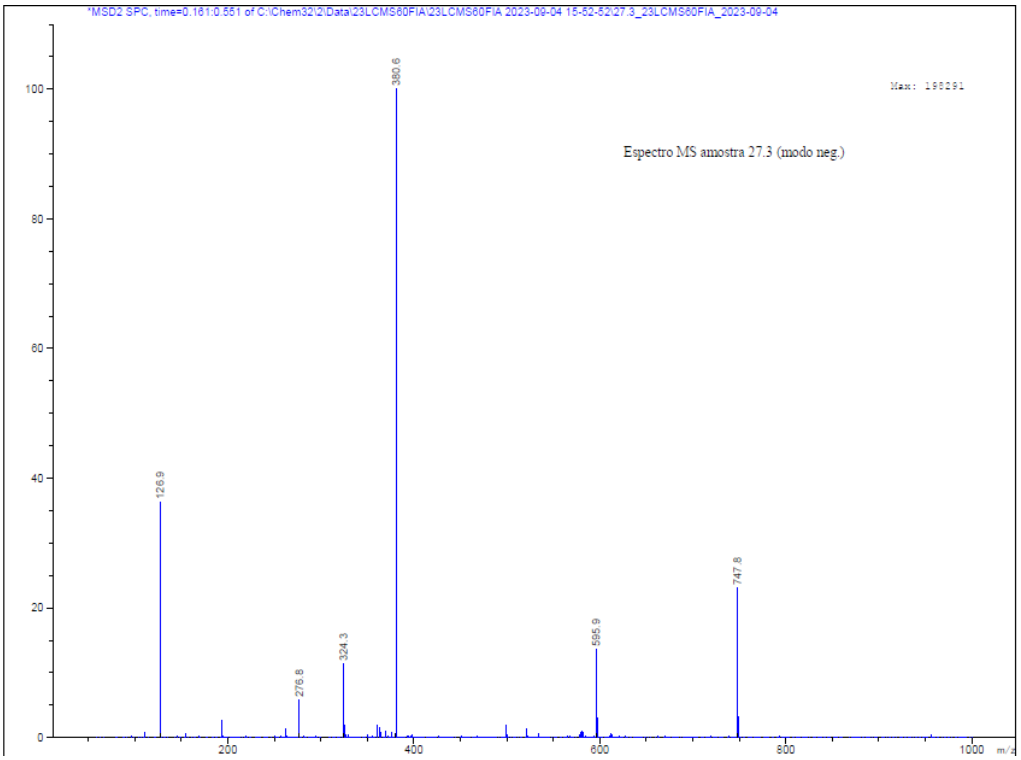


**Figure 6.81** – LCMS spectrum of 4-(3,5-di-*tert*-butyl-4-methoxyphenyl)-1,2,6-trimethylpyridinium iodide (**14**), in negative mode.

## Appendix 26 – 2,6-di-*tert*-butyl-4-(1,2,6-trimethylpyridinium-4-yl)phenolate (15)

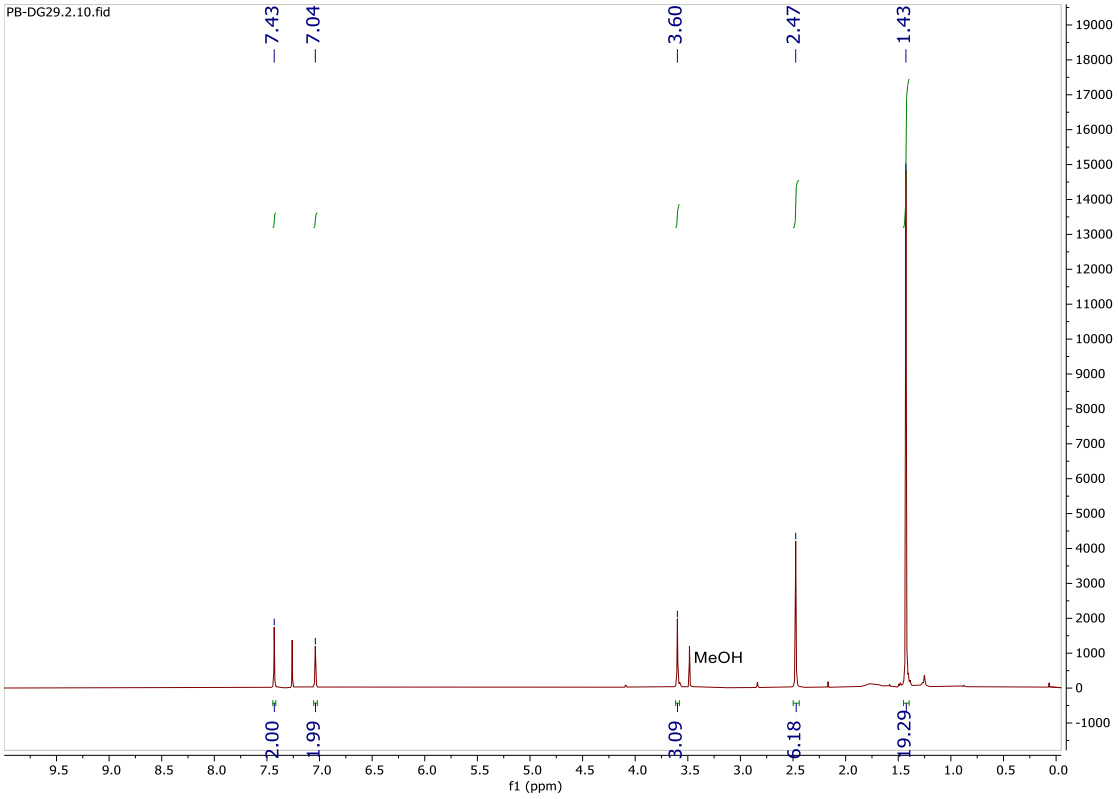


**Figure 6.82** – $^{1}$H NMR spectrum of 2,6-di-*tert*-butyl-4-(1,2,6-trimethylpyridinium-4-yl)phenolate (**15**) in $CDCl_3$.

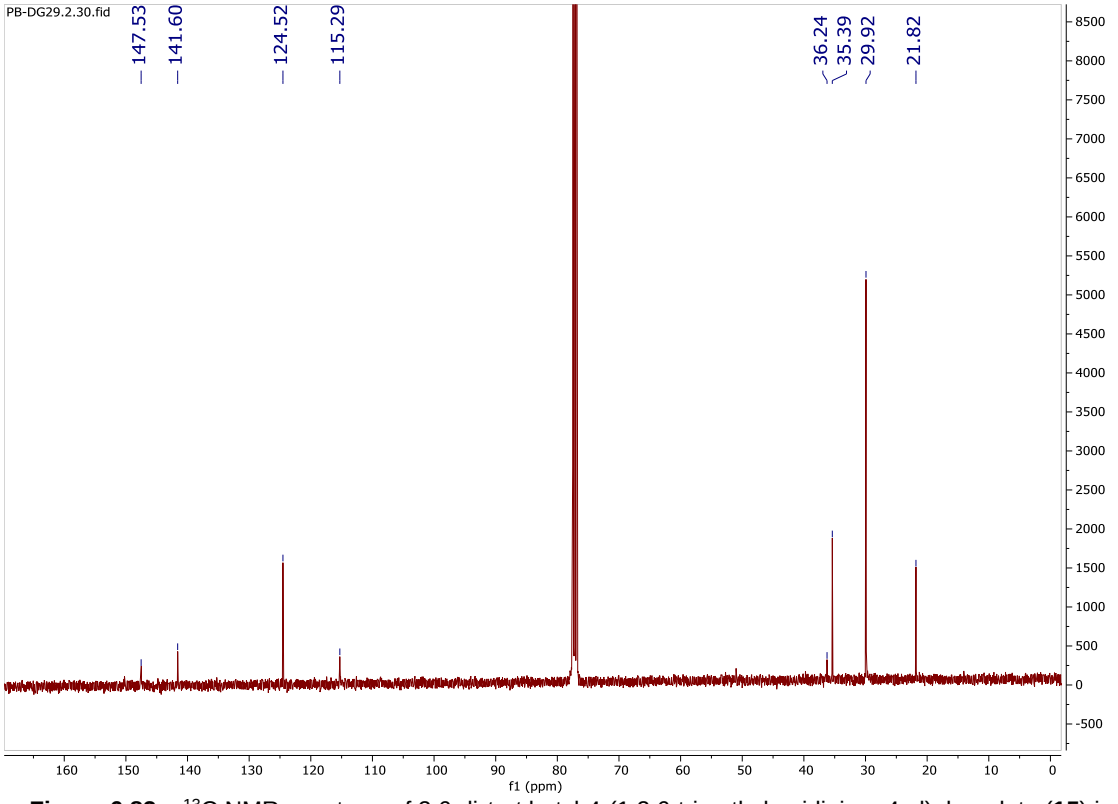


**Figure 6.83** – $^{13}$C NMR spectrum of 2,6-di-*tert*-butyl-4-(1,2,6-trimethylpyridinium-4-yl)phenolate (**15**) in $CDCl_3$.

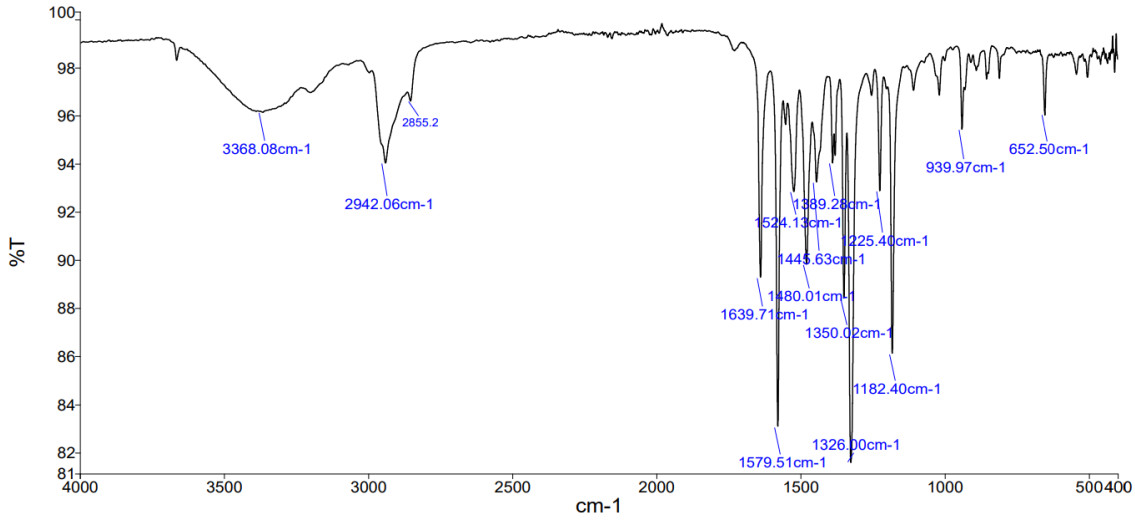


**Figure 6.84** – IR spectrum of 2,6-di-*tert*-butyl-4-(1,2,6-trimethylpyridinium-4-yl)phenolate (**15**).

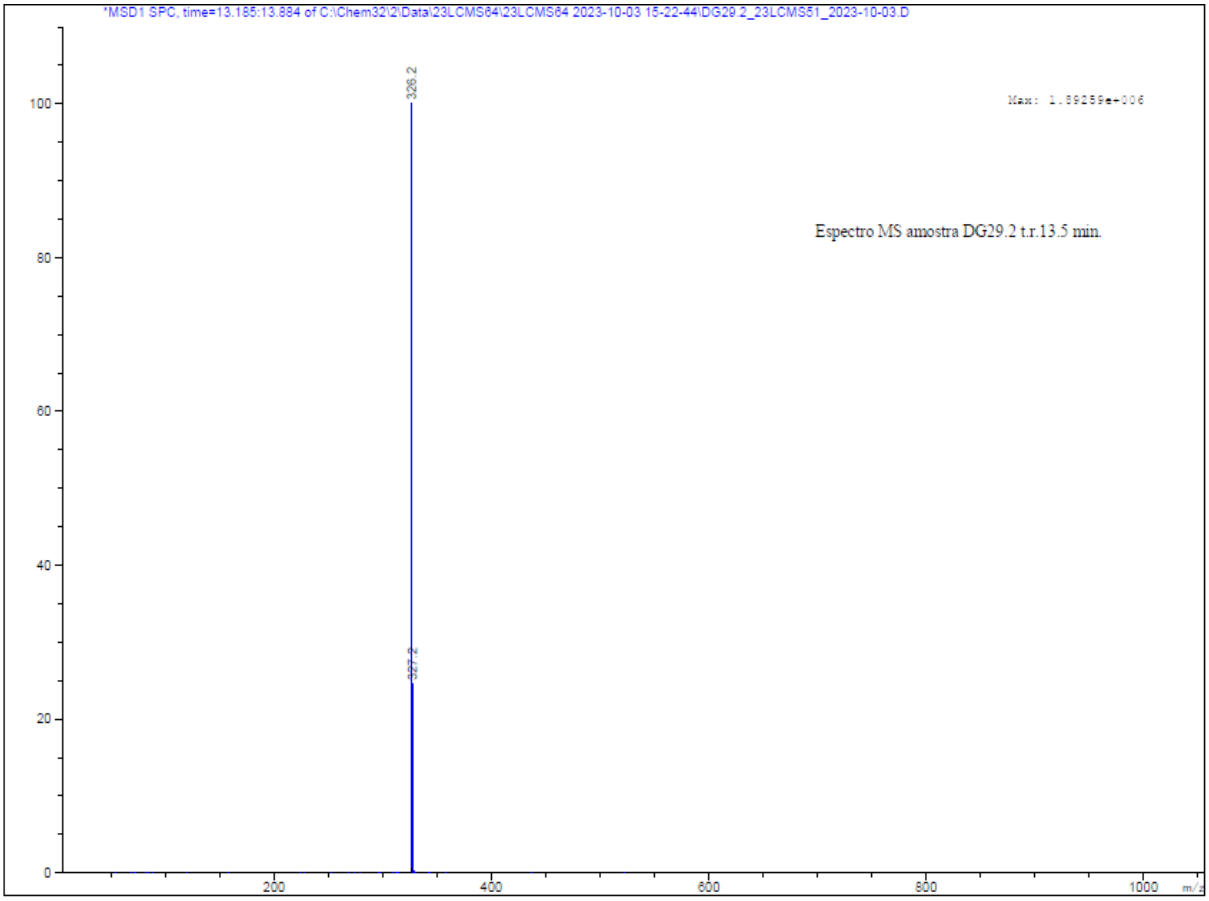


**Figure 6.85** – LCMS spectrum of 2,6-di-*tert*-butyl-4-(1,2,6-trimethylpyridinium-4-yl)phenolate (**15**), in positive mode.

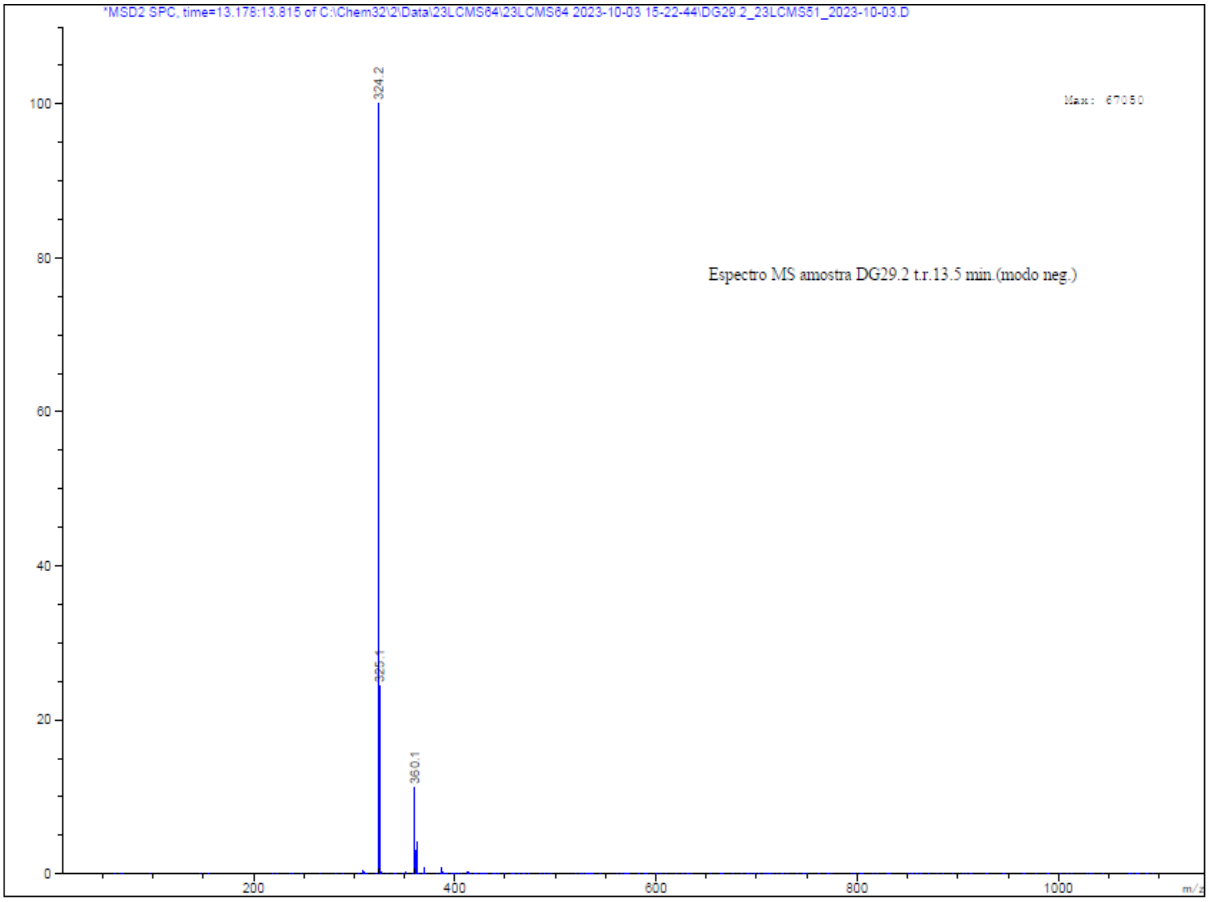


**Figure 6.86** – LCMS spectrum of 2,6-di-*tert*-butyl-4-(1,2,6-trimethylpyridinium-4-yl)phenolate (**15**), in negative mode.

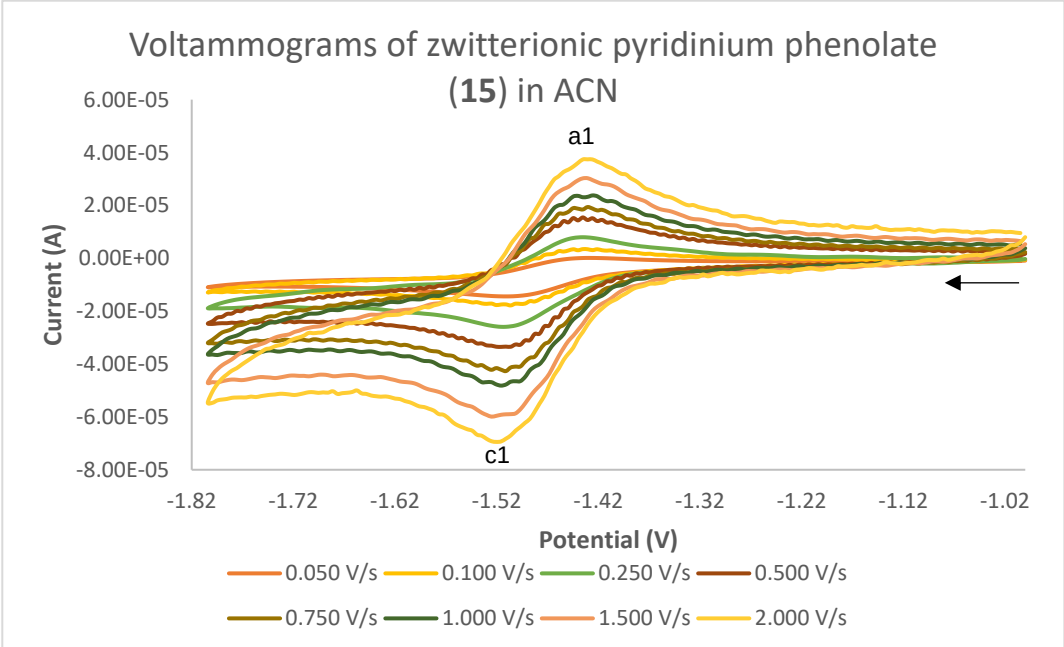


**Graphic 6.14** – Voltammograms of 2,6-di-*tert*-butyl-4-(1,2,6-trimethylpyridinium-4-yl)phenolate (**15**) in ACN, at multiple scan rates.

## Appendix 27 – 4-(3,5-di-*tert*-butyl-4-hydroxyphenyl)-1,2,6-trimethylpyridinium triflate (16)

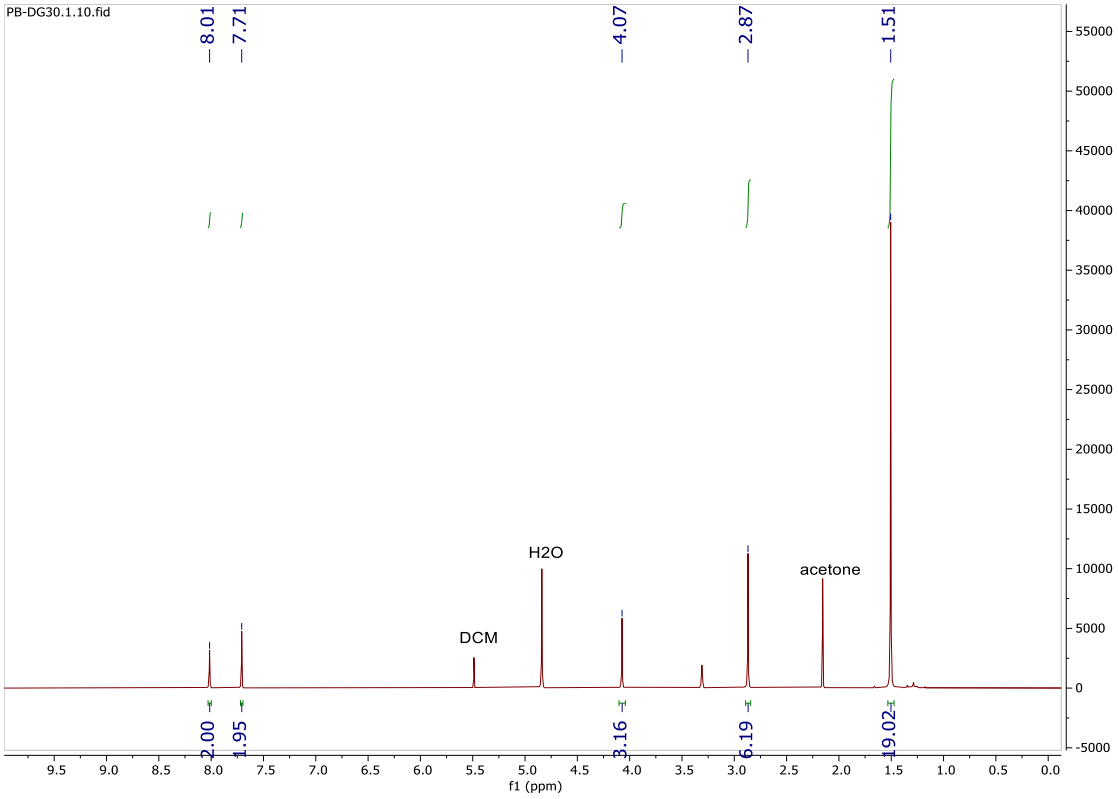


**Figure 6.87** – $^{1}H$ NMR spectrum of 4-(3,5-di-*tert*-butyl-4-hydroxyphenyl)-1,2,6-trimethylpyridinium triflate (**16**) in $CD_3OD$.

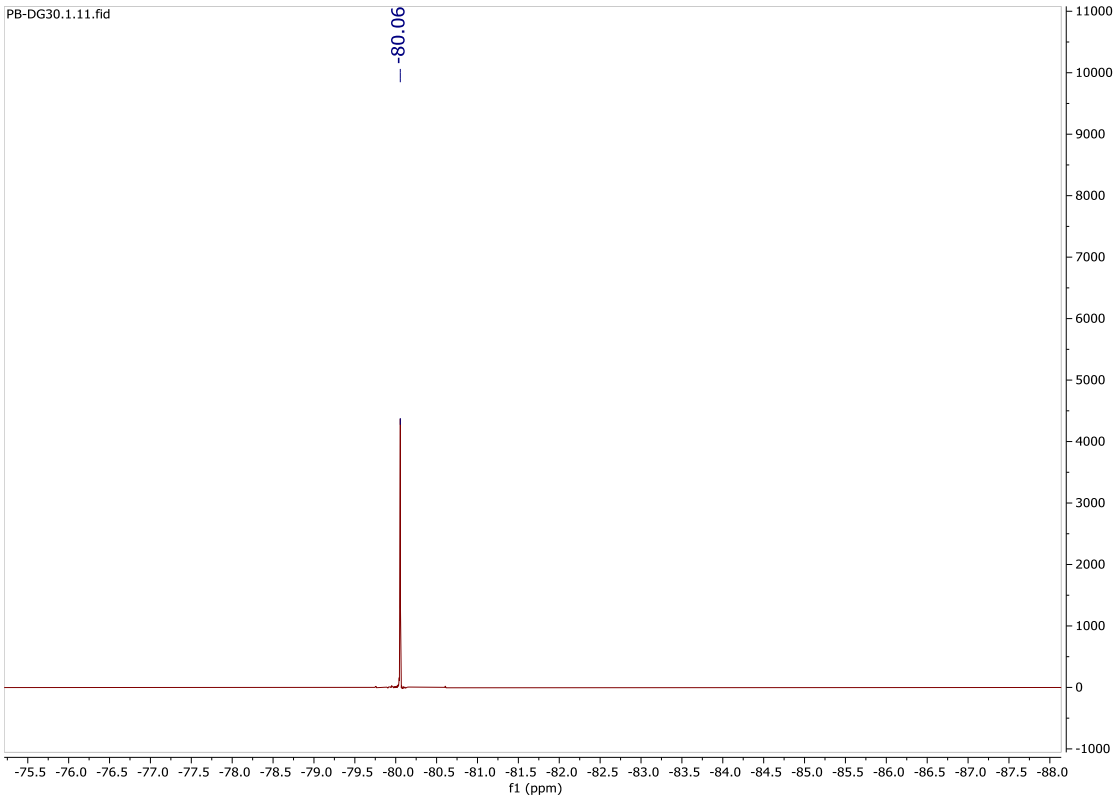


**Figure 6.88** – $^{19}F$ NMR spectrum of 4-(3,5-di-*tert*-butyl-4-hydroxyphenyl)-1,2,6-trimethylpyridinium triflate (**16**) in $CD_3OD$.

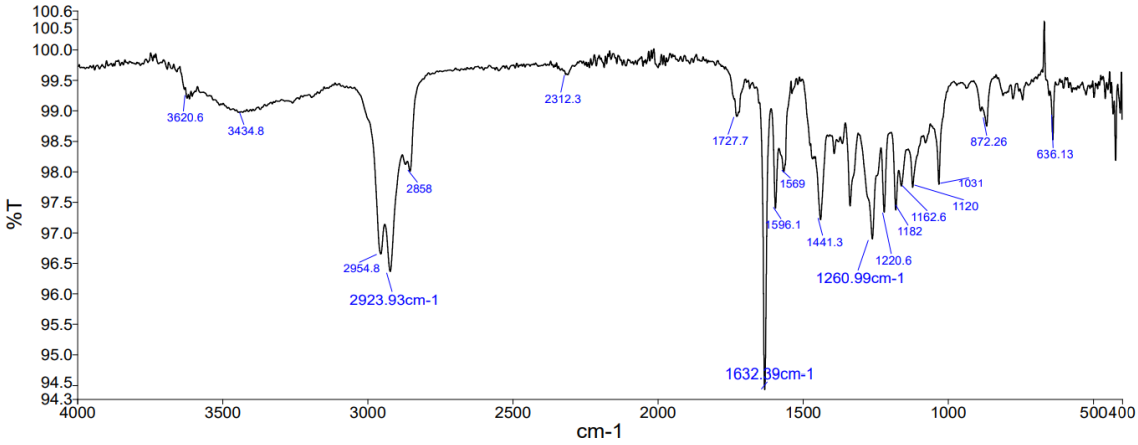


**Figure 6.89** – IR spectrum of 4-(3,5-di-tert-butyl-4-hydroxyphenyl)-1,2,6-trimethylpyridinium triflate (**16**).

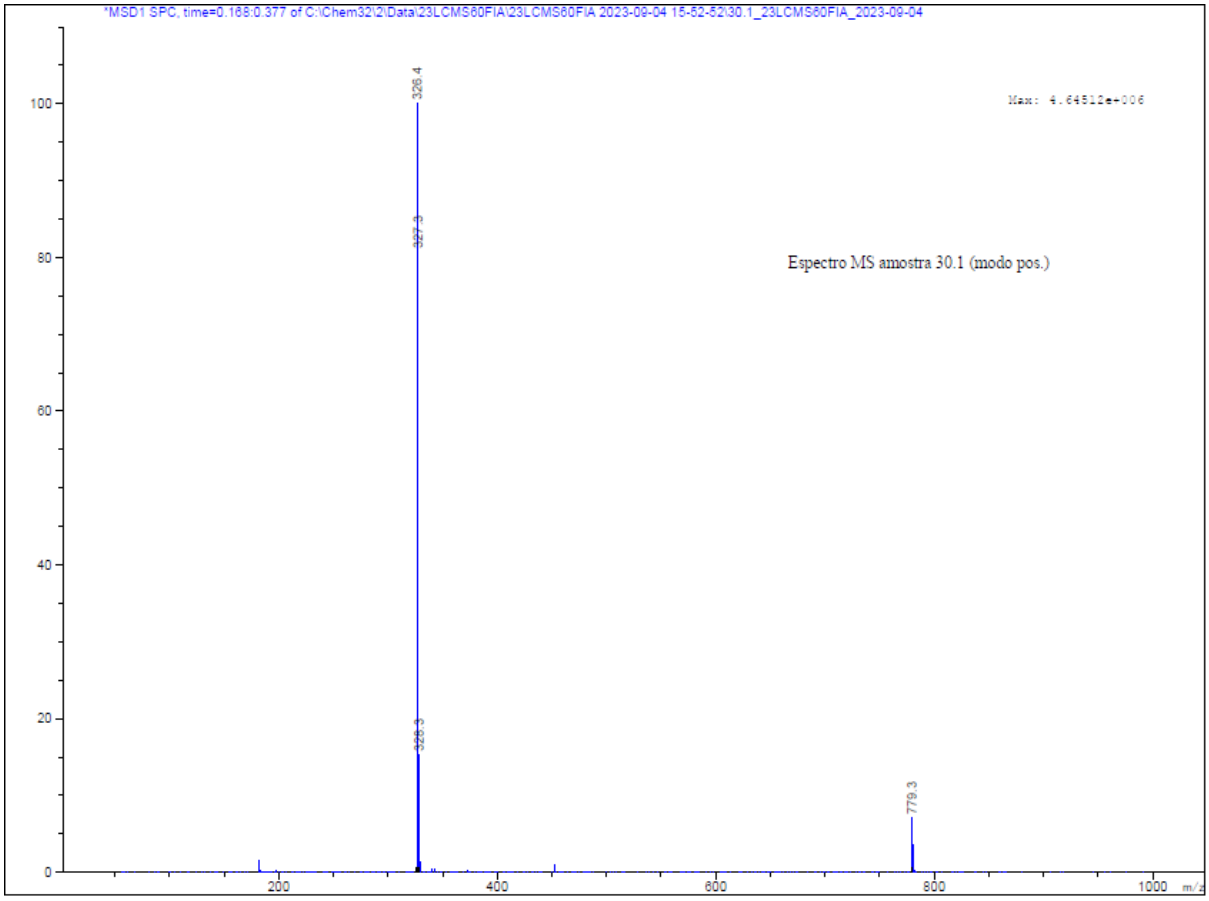


**Figure 6.90** – LCMS spectrum of 4-(3,5-di-tert-butyl-4-hydroxyphenyl)-1,2,6-trimethylpyridinium triflate (**16**), in positive mode.

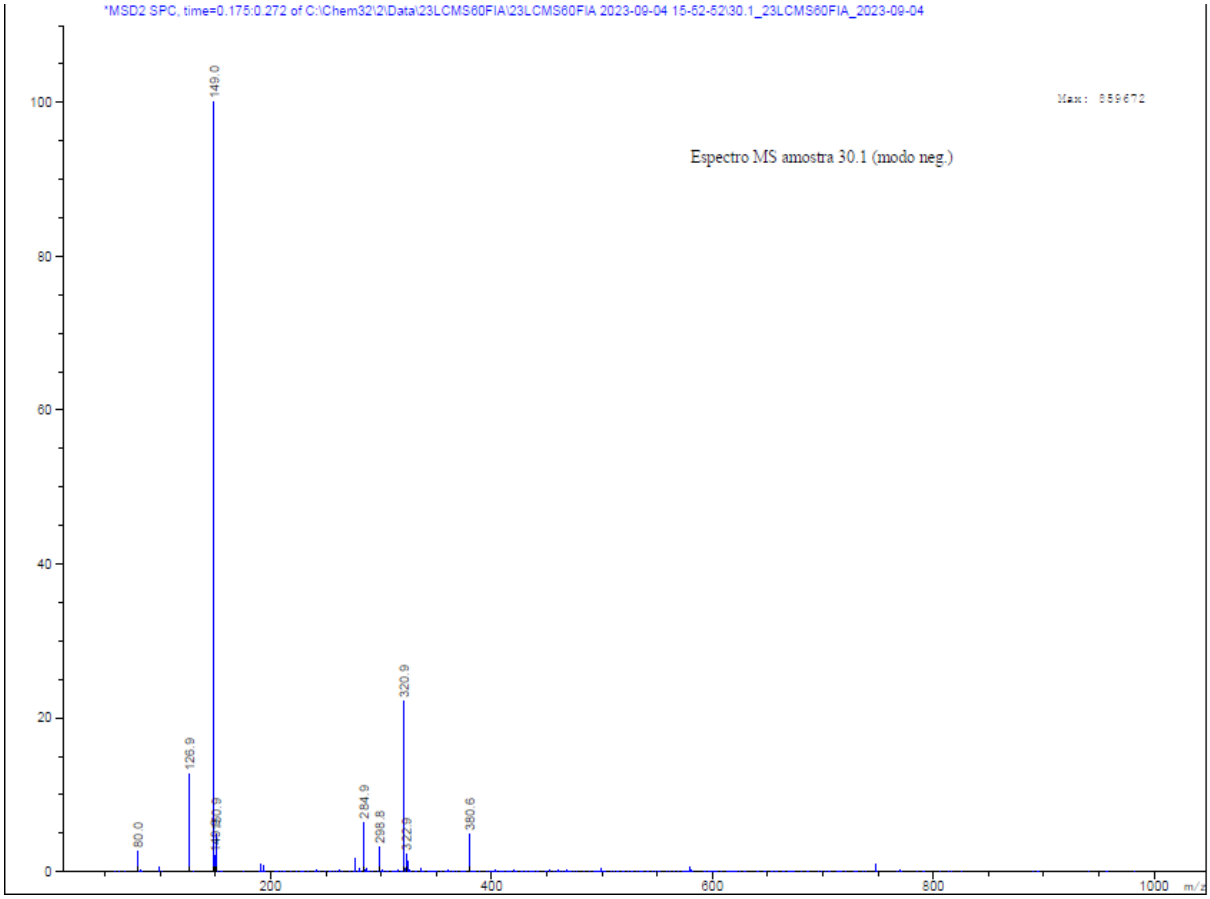


**Figure 6.91** – LCMS spectrum of 4-(3,5-di-tert-butyl-4-hydroxyphenyl)-1,2,6-trimethylpyridinium triflate (**16**), in negative mode.

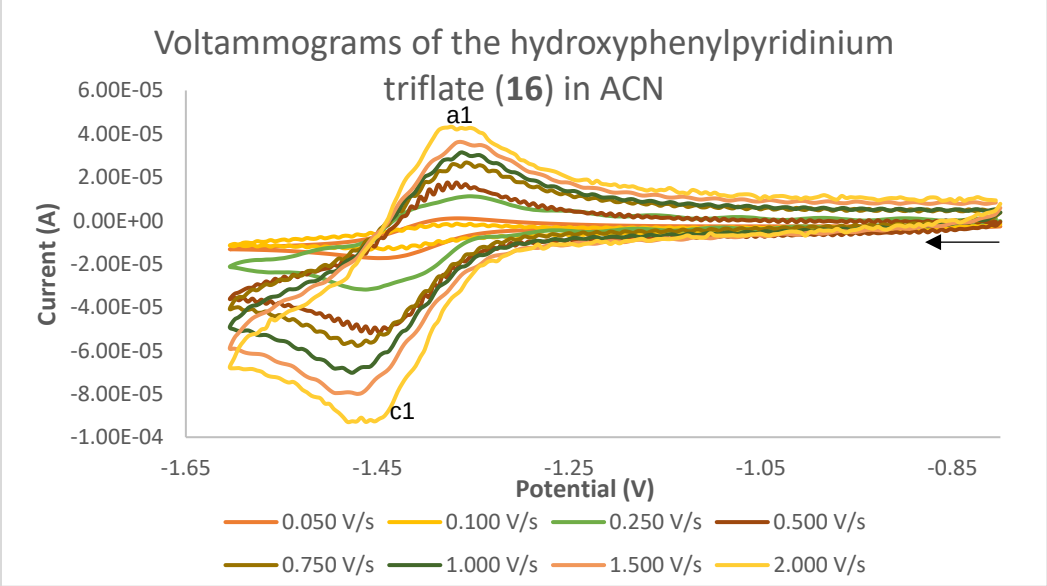


**Graphic 6.15** – Voltammograms of 4-(3,5-di-tert-butyl-4-hydroxyphenyl)-1,2,6-trimethylpyridinium triflate (**16**) in ACN, at multiple scan rates.